

BMSAP

BULLETINS ET MÉMOIRES
DE LA SOCIÉTÉ D'ANTHROPOLOGIE DE PARIS

Indexée dans SCOPUS, Google Scholar, Academic OneFile, Anthropological Index Online, Anthropological Literature, Biological Abstracts, BIOSIS, ERIH PLUS, GeoRef, OCLC, SCImago, Summon by ProQuest.

Chaque auteur recevra la version électronique définitive de son article pour usage privé uniquement.

Lavoisier

Sommaire

Volume 31 · Numéro 1-2 · Avril 2019

DOSSIER

LA VARIABILITÉ MORPHOLOGIQUE EN PALÉOANTHROPOLOGIE : DE NOUVELLES APPROCHES, DE NOUVEAUX ENJEUX ?

INTRODUCTION

La variabilité morphologique en paléoanthropologie : de nouvelles approches, de nouveaux enjeux ? (*en anglais*)
G. Daver, A. Balzeau, G. Berillon, F. Guy

1

NOTE

Taille des choanes et de la face : modèles d'échelles des voies aériennes crâniennes chez les hommes modernes et les grands singes africains. Signification pour l'évolution du massif facial chez les hominines du milieu et de la fin du Pléistocène (*en anglais*)
M. Bastir

5

ARTICLE

Variation de la pneumatisation paranasale des hominines du Pléistocène moyen finale (*en anglais*)
L.T. Buck, C.B. Stringer, A.M. MacLarnon, T.C. Rae

14

NOTES

Le rôle de l'intégration spatiale dans la morphologie du labyrinthe osseux chez les humains modernes (*en anglais*)
A. Le Maître

34

Analyse de la micro-architecture trabéculaire de la métaphyse distale du radius pendant l'acquisition de la marche bipède chez l'enfant : étude préliminaire (*en anglais*)
A. Colombo, N. B. Stephens, Z. J. Tsegai, M. Bettuzzi, M. P. Morigi, M. G. Belcastro, J.-J. Hublin

43

Distribution 3D de l'email : la répartition de l'email est-elle moins uniforme sur les secondes molaires supérieures des hominoides durophages ? (*en anglais*)
G. Thierry, F. Guy, V. Lazzari

52

Apport de la reconstruction de deux dyades mère-enfant et conséquences obstétricales de la Transition Mesolithique-Néolithique : étude de cas des sites de Vlasac et de Lepenski Vir (Serbie) (*en anglais*)
J. Jovanović, P. Frémondière, S. Stefanović

60

ARTICLES

Qu'est-ce que la taille de la cavité nasale nous dit sur les voies aériennes nasales ? (*en anglais*)
Y. Heuzé

69

BMSAP

BULLETINS ET MÉMOIRES
DE LA SOCIÉTÉ D'ANTHROPOLOGIE DE PARIS

Caractérisation sociale de la population médiévale
et moderne de Joué-lès-Tours (France) : apports de l'état
sanitaire bucco-dentaire et de l'alimentation (*en anglais*)

V. Miclon, M. Gaultier, C. Genies, O. Cotté, F. Yvernault, E. Herrscher

77

THÈSES

Liste des thèses et habilitations à diriger les recherches (HDR)
en anthropologie soutenues en 2018

93

NOTE DE LECTURE

*Les espaces funéraires de l'habitat groupé des Ruelles
à Serris (Seine et Marne)*, Frédérique Blaizot, Thanat'Os,
Maison des Sciences de l'Homme de Bordeaux, 2017, 573 p.

B. Bizot

95

NÉCROLOGIE

Jean-Pierre Bocquet-Appel (1949-2018)

J.-J. Hublin

99



Composé et imprimé par Jouve, 1, rue du Docteur Sauvé, 53100 Mayenne
Vol. 31 - N° 1-2 - Dépot légal : Avril 2019

BMSAP

BULLETINS ET MÉMOIRES
DE LA SOCIÉTÉ D'ANTHROPOLOGIE DE PARIS

Indexed in SCOPUS, Google Scholar, Academic OneFile, Anthropological Index Online, Anthropological Literature, Biological Abstracts, BIOSIS, ERIH PLUS, GeoRef, OCLC, SCImago, Summon by ProQuest.

Each corresponding author will receive the final electronic version of his article for personal use only.

Lavoisier

Table of contents

THEMATIC FILE

MORPHOLOGICAL VARIABILITY

IN PALEOANTHROPOLOGY:

NEW APPROACHES, NEW ISSUES?

INTRODUCTION

Morphological Variability in Paleoanthropology:
New Approaches, New Issues? (*In English*)

G. Daver, A. Balzeau, G. Berillon, F. Guy

1

NOTE

Big Choanae, Larger Face: Scaling Patterns
Between Cranial Airways in Modern Humans and African
Apes and Their Significance in Middle and Late
Pleistocene Hominin Facial Evolution (*In English*)

M. Bastir

5

ARTICLE

Variation in Paranasal Pneumatisation between Mid-Late
Pleistocene Hominins (*In English*)

L.T. Buck, C.B. Stringer, A.M. MacLarnon, T.C. Rae

14

NOTES

Role of Spatial Integration in the Morphology of the Bony
Labyrinth in Modern Humans (*In English*)

A. Le Maître

34

Trabecular Analysis of the Distal Radial Metaphysis
during the Acquisition of Crawling and Bipedal Walking
in Childhood: A Preliminary Study (*In English*)

A. Colombo, N. B. Stephens, Z. J. Tsegai, M. Bettuzzi, M. P. Morigi,
M. G. Belcastro, J.-J. Hublin

43

Enamel Distribution in 3D: Is Enamel Thickness More
Uneven in the Upper Second Molars of Durophagous
Hominoids? (*In English*)

G. Thiery, F. Guy, V. Lazzari

52

Reconstruction of Two Mother-Infant Dyads
and Obstetrical Consequences of the Mesolithic-Neolithic
Transition: A Case Study from Lepenski Vir and Vlasac
(Serbia) (*In English*)

J. Jovanović, P. Frémondière, S. Stefanović

60

ARTICLES

What Does Nasal Cavity Size Tell us about Functional
Nasal Airways? (*In English*)

Y. Heuzé

69

BMSAP

BULLETINS ET MÉMOIRES
DE LA SOCIÉTÉ D'ANTHROPOLOGIE DE PARIS

Table of contents

Social Characterization of the Medieval and Modern Population from Joué-lès-Tours (France): Contribution of Oral Health and Diet (*In English*)

V. Miclon, M. Gaultier, C. Genies, O. Cotté, F. Yvernault, E. Herrscher **77**

THESES

List of PhD dissertations in Anthropology defended in 2018 **93**

LECTURE NOTE

Les espaces funéraires de l'habitat groupé des Ruelles à Serris (Seine et Marne), Frédérique Blaizot Thanat'Os, Maison des Sciences de l'Homme de Bordeaux, 2017, 573 p.

B. Bizot **95**

NECROLOGY

Jean-Pierre Bocquet-Appel (1949-2018)
J.-J. Hublin

99

 *Lavoisier*

Morphological Variability in Paleoanthropology: New Approaches, New Issues?

La variabilité morphologique en paléoanthropologie : de nouvelles approches, de nouveaux enjeux ?

G. Daver · A. Balzeau · G. Berillon · F. Guy

Reçu le 11 janvier 2019 ; accepté le 8 mars 2019
© Société d'Anthropologie de Paris et Lavoisier SAS 2019

Since Darwin's seminal works, variability—from which selection acts—is considered as being specific to populations. Variability or the propensity to vary differs from variation, which represents 'the actually realised differences between individuals' in a population/sample, or between species in a clade [1, p. 967]. Hence, variability is more complex to quantify than variation, and in general, biological anthropologists focus their efforts primarily on variation *sensu stricto*. In human and non-human primates, as in all other living organisms, the potential causes of morphological variation have multiple sources. However, two main types can be identified: genetic and environmental. Genetic sources of variation are produced via mutations, sexual reproduction, epigenetics or gene flow. Environmental sources include, for instance, the prenatal environment, nutrition, quality of life and health care, culture and climate. Other sources of variation are more specifically considered in evolutionary anthropology as exemplified by diachronic or phylogenetic variations. For example, over the last decade, palaeoanthropology has yielded several new hominin taxa/groups based on morphological and genetic data (e.g. Denisova hominins [2], *Homo gautengensis* [3], *Australopithecus sediba* [4], new early representatives of the genus *Homo* [5], *Homo naledi* [6] and *Australopithecus deyiremeda* [7]).

Taken as a whole, the above-mentioned sources of variation illustrate the need to take variations of a distinctive nature (genotypic, phenotypic) into account at varying scales of organisation (from a simple anatomical structure to an integrated system), within and among clades (i.e. extant and extinct taxa).

Despite this increasingly well-documented variation and numerous conceptual and methodological developments, anthropologists seem to be inevitably confronted with the difficulty of interpreting, and even compiling, such very large amounts of data. This is why we wanted to explore this topic in a special session of the 1843rd SAP meeting, held in Poitiers, at the Espace Mendès-France, from 24 to 26 January 2018. Our guest speaker, Prof M. Bastir, introduced the special session and 21 papers were given, including 17 podium presentations and four poster displays. The six articles published in this issue of the BMSAP illustrate the diversity of the topics addressed during this session [8-13].

Five podium presentations and one poster display considered variation/variability in complex biological systems as a whole in terms of their different levels of organisation: introducing the session, Prof Bastir explored Neanderthal cranio-facial morphology from the hierarchical and organism perspectives by integrating masticatory and respiratory biomechanics, ontogenetics and evolutionary morphological interactions between the central nervous system and the respiratory system, showing that integrative approaches yield a further understanding of the biological significance of specific features in hominin skeletal morphology [14]. For obvious reasons, such covariation analyses are still frequently applied to extant humans. For example, Albessard et al. highlighted similar spatial patterns of asymmetry between neurocrania and associated endocasts of 39 *Homo sapiens*, suggesting a close link between neurocranium asymmetry and brain

G. Daver (✉) · F. Guy
PALEVOPRIM : laboratoire Paléontologie,
Évolution, Paléoécosystèmes, Paléoprimatologie,
UMR 7262, CNRS, université de Poitiers, Poitiers, France
e-mail : guillaume.daver@univ-poitiers.fr

A. Balzeau · G. Berillon
Équipe PaleoFED, UMR 7194 du CNRS,
département Homme et environnement,
Muséum national d'histoire naturelle, Paris, France

A. Balzeau
Department of African Zoology,
Royal Museum for Central Africa, Tervuren, Belgium

¹ Articles relating to this specific session were produced with the associated editors (G. Daver, A. Balzeau, G. Berillon and F. Guy).

development [15]. Le Maître and Mazurier emphasised the importance for bony labyrinth growth of the spatial constraints due to the shape of the petrosal bones in the cranium, a crucial point in any attempt to interpret the variation of such a structure from an ecological perspective [16]. In an attempt to better understand the correspondence between genotype and phenotype, Romeyer-Dherbey et al. compared the impacts of coronal nonsyndromic craniosynostosis on cranial shape in children, which made it possible to draw up a severity gradient and to consider setting up such analyses in new medical protocols [17]. By extension, the need to compare human variation/variability patterns with other patterns in non-human taxa is inherent to evolutionary studies and therefore to palaeoanthropology. Neaux et al. showed how morphological integration impacts shape disparity but not rates of phenotypic evolution, by demonstrating that the basicranium and face in primates are significantly integrated structures that can nevertheless also be considered as distinct modules, since both could evolve at different rates in response to different adaptive pressures [18]. From the postcranial perspective, Domalain et al. presented a realistic biomechanical simulation of hand force capability in fossil hominins and, as an example, demonstrated that the carpometacarpal joint of the fifth digit in *Australopithecus* could have been a factor limiting their ability to maintain Lomekwian-like tools [19].

The second set of presentations (four podium presentations, one poster display) focused on unravelling the form–function relationships of specific bone structures in connection with ecological functions, in order to propose potential applications to the fossil record. The impact of locomotion was the object of particular attention in this respect. Colombo et al. presented a new method for quantifying the morphological signal associated with the acquisition of bipedalism in the trabecular architecture of the radii in children from 0 to 3 years of age [20]. Druelle et al. demonstrated that, during growth, morphological variations in the body segments of olive baboons from 0 to 8 years of age conform to a general pattern typical of catarrhine primates, but they also showed that some inertial segment properties change with the varying locomotor repertoire [21]. Apart from locomotion, masticatory functions were also discussed. Investigating relationships between the distribution of enamel thickness and diets of extant primates, Thiery et al. showed, for instance, that various morphological and behavioural strategies might have been selected in primates that consume stress-limited food [22]. Martin-Moya et al. tested the influence of environmental and cultural behaviour patterns on craniomandibular morphology, using early settlement of the Americas a framework [23]. They identified a high correlation between cranial and mandibular shapes, but also highlighted the impact of cultural diets on variation in mandibular shape. Like locomotion and diet, the functional foundations of childbirth are also of prime ecological interest.

Based on 131 extant dyads, Frémondrière and Marchal supported that rotational birth likely have occurred with the emergence of the genus *Homo*, and suggest that such a physiological process may have been accompanied by the onset of a secondary altriciality and obstetrical assistance [24].

Finally, seven podium presentations and two poster displays proposed a reappraisal of morphological variation in extinct species based on new specimens and/or new approaches. Most concerned the difficulties of working out the perimeter of morphological variation in early hominins. Beaudet explained how new methodological developments (3D modelling) show that the endocast of *Australopithecus africanus* departs from the ancestral morphotype and pointed to unexpected degrees of variation in the spatial organisation of the frontal lobes of later hominins such as *Homo erectus-ergaster* and *Homo heidelbergensis* [25]. Daver et al. described three new limb bones (i.e. phalanx, proximal radius and second metatarsal) assigned to *Paranthropus boisei* (2.12 Ma, Shungura Formation). Evidence of habitual bipedalism and a propensity for climbing supported by these remains has helped to gain a better understanding of morphofunctional variations in an as yet poorly documented hominin [26]. Cazenave presented a reappraisal of isolated postcranial bones from various South African sites classically assigned to *Paranthropus robustus*, where high-resolution computed tomography and 3D analyses identified contrasting signals between the external and inner morphology of some of these remains (e.g. patella, distal humerus) and close affinities with extant humans for others (femur) [27]. Souron and Boissarie addressed the question of the taxonomic status of the early African and Georgian representatives of the genus *Homo* [28]. Considering dentognathic remains from two populations of African bush pigs and their fossil relatives, they showed that extinct morphospecies might represent complexes of several biological species. Based on quantitative measurements of various traits of both taxonomic and adaptive interests (dental tissue proportions, topographic distribution of enamel thickness, enamel–dentine junction), Zanolli identified different morphological trends that distinguish Southeast Asian specimens (Java) from continental Middle Pleistocene humans [29]. In their exhaustive comparative analysis, Condemi et al. found that the 19 Neanderthal teeth identified at Vergisson II, like those from other Burgundian sites, share closer affinities with specimens from the Mediterranean basin and even from Northern and Western Europe than with specimens from the ‘Near East’ [30].

Two presentations focused on the recently created species *Homo naledi*, which provides a unique opportunity to assess morphological variation in a fossil human species, thanks to its exceptionally rich hypodigm. Based on a reappraisal of the endocranial and of some of their reconstructions, Balzeau and de Bruicker underlined the close morphological affinities of the species with early representatives of the genus

Homo and *Homo erectus* [31]. Voisin et al. analysed the numerous remains of clavicles and scapulae from the cave chambers of Dinaledi and Lesedi and pointed to the intriguing combination of arboreal and bipedal behaviour suggested by the shoulder architecture and lower limb morphology in this geologically recent species [32]. In their study of the footprints from Rozel (Late Pleistocene, Manche, France), Duveau et al. presented an actualistic approach that involved recording 24 humans moving barefoot at various speeds on Rozel-like substrates: the authors demonstrated that different individuals (1–1.70 m in height) could have walked on the same surface of occupation [33]. Coutinho Nogueira et al. brought new insights into variations in Near Eastern Late Pleistocene humans through a reappraisal of age at death, developmental abnormalities and descriptions of the inner structures of the craniofacial remains of the Qafzeh 9 individual [34].

To summarise, this session showed that biological anthropologists have to deal with numerous sources of variation/variability (phylogeny, development/ontogeny/growth, genetics, behaviour, ecology, environment, sexual dimorphism, geography, idiosyncratic variation) to which many different fields are contributing, including palaeontology, primatology, palaeopathology, ontogeny and biomechanics. Whatever the sources, variations in complex biological systems occur at different levels of organisation (from individual organisms, species or populations to the ecological or community level), but the transmission of variation from one level to the next is neither straightforward nor intuitive [35]. This is why any source of variation in a biological system should be investigated further from an integrative or transdisciplinary perspective. There is now, more than ever, a need for such a holistic approach, and the many fascinating presentations we heard during this SAP meeting at Poitiers testify to the vitality of current research on this topic.

References

- Wagner GP, Altenberg L (1996) Perspective: complex adaptations and the evolution of evolvability. *Evolution* 50:967–76
- Krause J, Fu Q, Good JM, et al (2010) The complete mitochondrial DNA genome of an unknown hominin from southern Siberia. *Nature* 464:894–7
- Curnoe D (2010) A review of early *Homo* in southern Africa focusing on cranial, mandibular and dental remains, with the description of a new species (*Homo gautengensis* sp. nov.). *HOMO* 61:151–77
- Berger LR, de Ruiter DJ, Churchill SE, et al (2010) *Australopithecus sediba*: a new species of *Homo*-like australopith from South Africa. *Science* 328:195–204
- Villmoare B, Kimbel WH, Seyoum C, et al (2015) Paleoanthropology. Early *Homo* at 2.8 Ma from Ledi-Geraru, Afar, Ethiopia. *Science* 347:1352–5
- Berger LR, Hawks J, de Ruiter DJ, et al (2015). *Homo naledi*, a new species of the genus *Homo* from the Dinaledi Chamber, South Africa. *Elife* 4:e09560
- Haile-Selassie Y, Gibert L, Melillo SM, et al (2015) New species from Ethiopia further expands Middle Pliocene hominin diversity. *Nature* 521:483–8
- Bastir M (2019) Big choanae, larger face: scaling patterns between cranial airways in modern humans and African apes and their significance in Middle and Late Pleistocene hominin facial evolution. *BMSAP* 31(1-2):9-13
- Buck LT, Stringer CB, MacLarnon AM, Rae TC (2019) Variation in paranasal pneumatisation between Mid-Late Pleistocene hominins. *BMSAP* 31(1-2):14-33
- Le Maître A (2019) Role of spatial integration in the morphology of the bony labyrinth in modern humans. *BMSAP* 31(1-2):34-42
- Colombo A, Stephens NB, Tsegai ZJ, et al (2019) Trabecular analysis of the distal radial metaphysis during the acquisition of crawling and bipedal walking in childhood: a preliminary study. *BMSAP* 31(1-2):43-51
- Thiery G, Guy F, Lazzari V (2019) Enamel 3D distribution: is enamel more unevenly thick in upper second molars of durophagous hominoids? *BMSAP* 31(1-2):52-9
- Jovanović J, Frémondière P, Stefanović S (2019) Reconstruction of two mother-infant dyads and obstetrical consequences of the Mesolithic-Neolithic transition: a case study from Lepenski Vir and Vlasac (Serbia). *BMSAP* 31(1-2):60-8
- Bastir M (2018) The significance of the respiratory system for cranial and postcranial skeletal morphology in Neanderthals and modern humans. *BMSAP* 30(S1):S9
- Albessard L, Kitchell L, Grimaud-Hervé D, et al (2018) Une comparaison des asymétries crâniennes et endocraniques chez *Homo sapiens*. *BMSAP* 30:S10
- Le Maître A, Mazurier A (2018) Étude préliminaire des covariations morphologiques entre le labyrinthe osseux et la base du crâne chez *Homo sapiens*. *BMSAP* 30(S1):S18-9
- Romeyer Dherbey J, Di Rocco F, Legeai-Mallet L, et al (2018) Quantification de la variation morphologique crânienne au sein d'un échantillon d'enfants atteints de craniosynostoses de la suture coronale. *BMSAP* 30(S1):S26
- Neaux D, Sansalone G, Ledogar JA, et al (2018) Basicranium and face: assessing the impact of morphological integration on primate evolution. *BMSAP* 30(S1):S22–S3
- Domalain M, Bertin A, Daver G (2018) Développement d'une simulation biomécanique des capacités de forces de préhension d'homininés fossiles et nouvelles perspectives sur l'implication du cinquième doigt. *BMSAP* 30(S1):S15
- Colombo A, Stephens N, Tsegai ZJ, Bettuzzi M, Morigi MP, Belcastro MG, Hublin J-J (2018) Analyse micro-architecturale du développement de la marche bipède chez le jeune enfant : résultats préliminaires. *BMSAP* 30(S1):S13
- Druelle F, Aerts P, D'Août K, et al (2018) Variation morphologique au cours de l'ontogenèse chez les primates actuels : modèles généraux et différences interspécifiques. *BMSAP* 30(S1):S15
- Thiery G, Lazzari V, Ramdarshan A, Guy F (2018) La distribution de l'émail permet-elle de déduire la capacité à consommer des aliments durs ? Apport de l'étude de la topographie dentaire 3d des anthropoïdes actuels. *BMSAP* 30(S1):S29
- Martin-Moya D, Galland M, Friess M (2018) Les premiers peuplements de l'Amérique, influence des facteurs environnementaux et culturels sur la variabilité morphologique mandibulaire et crânienne. *BMSAP* 30(S1):S20
- Frémondière P, Marchal F (2018) La rotation intra-pelvienne, explications obstétricales et enjeux évolutifs. *BMSAP* 30(S1):S16
- Beaudet A (2018) Comment reconstruire l'histoire évolutive du cerveau hominine à partir du registre fossile ? Limites et perspectives en paléoneurologie humaine. *BMSAP* 30(S1):S11

26. Daver G, Berillon G, Jacquier C, et al (2018) Nouveaux restes posterâniens d'Homininés de la localité OMO 323, Formation de Shungura, Basse Vallée de l'Omo, Sud-Ouest de l'Éthiopie. BMSAP 30(S1):S14–S5
27. Cazenave M (2018) Caractéristiques endostructurales du squelette postcrânien de *Paranthropus robustus*. Implications taxinomiques, fonctionnelles et paléobiologiques. BMSAP 30(S1):S13
28. Souron A, Boissière JR (2018) Est-ce que des espèces proches parentes et morphologiquement ressemblantes sont identifiables dans le registre fossile ? Implications d'une étude de la variabilité crâniomandibulaire et dentaire chez les porcs à pinceaux actuels (Mammalia: Suidae: *Potamochoerus*). BMSAP 30(S1):S28
29. Zanolli C (2018) La variation endostructurale des dents hominées d'Asie au Pléistocène inférieur et moyen. BMSAP 30(S1): S30–S1
30. Condemi S, Giuliani ME, Saliba-Serre B, et al (2018) Les dents néandertaliennes de Vergisson II. BMSAP 30(S1):S13–S4
31. Balzeau A, de Bruicker LL (2018) Paléoanthropologie et variabilité du cerveau, que dire d'*Homo naledi* ? BMSAP 30(S1):S11
32. Voisin JL, Feuerriegel EM, Churchill SE, et al (2018) La ceinture scapulaire d'*Homo naledi*. BMSAP 30(S1):S30
33. Duveau J, Berillon G, Biets C, et al (2018) Variation morphologique d'empreintes de pieds et substrat : apport de l'expérimentation à la connaissance de la biologie des hommes du Rozel (Pléistocène supérieur, Manche). BMSAP 30(S1):S16
34. Coutinho Nogueira D, Coqueugniot H, Tillier AM (2018) La micromodensitométrie, nouvel outil d'analyse de fossiles humains anciennement découverts : l'exemple de Qafzeh 9. BMSAP 30(S1):S14
35. Hallgrímsson B, Hall BK (2005) Variation and variability: Central concepts in biology. In: Hallgrímsson B, Hall BK (eds) Variation: a central concept in biology. Academic Press, Cambridge, MA, pp 1–7

Big Choanae, Larger Face: Scaling Patterns Between Cranial Airways in Modern Humans and African Apes and Their Significance in Middle and Late Pleistocene Hominin Facial Evolution

Taille des choanes et de la face : modèles d'échelles des voies aériennes crâniennes chez les hommes modernes et les grands singes africains. Signification pour l'évolution du massif facial chez les hominines du milieu et de la fin du Pléistocène

M. Bastir

Received: 15 May 2018; Accepted: 26 November 2018
© Société d'Anthropologie de Paris et Lavoisier SAS 2019

Abstract This study aimed to understand the ontogenetic and allometric relationships in scaling between the anterior and posterior openings of the cranial airways and facial size, in order to shed light on the mechanisms that might underlie the evolution of a large face and large airways in Middle Pleistocene hominins and Neandertals. Sizes were calculated from 3D landmarks measured on the facial skeleton and airway structures of 403 skulls from two ontogenetic series of *H. sapiens* and *P. troglodytes*, an adult sample of gorillas and 11 Middle Pleistocene hominins and Neandertals. RMA regression models were used to compare the patterns in scaling between the anterior and posterior airways in relation to overall facial size. Our results show that the size of the anterior airways correlates more positively with facial size than the size of the posterior airways. This ontogenetic mechanism could explain the large faces and noses in the Neandertal lineage despite the adverse effects of such a phenotype for respiratory air-conditioning in cold climates. A large facial size could be a developmentally constrained consequence of generating airways large enough to provide the necessary oxygen for high energy demand in this large-brained and heavy-bodied hominin lineage.

Keywords Facial integration · Scaling constraints · Nasal cavity

Résumé Cette étude étudie les relations d'échelles ontogénique et allométrique entre les ouvertures antérieures et postérieures des voies aériennes crâniennes et la taille du massif

facial. L'objectif est de mettre en évidence les mécanismes qui peuvent expliquer l'apparition d'un massif facial et de voies aériennes de grande taille chez les hominines du Pléistocène moyen et chez les Néandertaliens. La taille est calculée à partir de point-repères 3D positionnés sur la face et les ouvertures liées aux voies aériennes de 403 crânes provenant de deux séries ontogénétiques d'*H. sapiens* et de *P. troglodytes*, d'une série de gorilles adultes et de 11 Néandertaliens et hominines du Pléistocène moyen. Des modèles de régressions RMA sont utilisés pour comparer les modèles d'échelles des voies aériennes antérieures et postérieures avec la taille générale de la face. Les résultats montrent que la taille des voies aériennes antérieures est corrélée avec la taille de la face, de façon plus positive que celle des voies aériennes postérieures. Ce mécanisme ontogénique pourrait expliquer la taille importante des faces et ouvertures nasales au sein de la lignée néandertalienne malgré l'effet négatif que ce phénotype peut avoir sur le système respiratoire dans des conditions climatiques froides. Une taille faciale importante pourrait être une contrainte développementale, conséquence de l'apparition de voies aériennes suffisamment grandes pour obtenir l'oxygène nécessaire à une demande énergétique élevée dans cette lignée d'hominines aux cerveaux de grandes tailles.

Mots clés Intégration faciale · Contraintes d'échelle · Cavité nasale

Introduction

Neandertals have specific characteristics in body size and shape. Many anatomical features of the craniofacial and postcranial skeleton are morphologically derived. Neandertal

M. Bastir (✉)
Paleoanthropology Group, Department of Paleobiology,
Museo Nacional de Ciencias Naturales, CSIC,
J.G. Abascal, 2, 28006 Madrid, Spain
e-mail : mbastir@mncn.csic.es

characters include midfacial prognathism and projection, a large, wide nasal aperture and an elongated overall cranial shape at the craniofacial level, a short, wide torso (thorax and pelvis) and generally short postcranial limb proportions [1–8]. The midfacial morphology and body shape of Neandertals have been interpreted as functional adaptations to cold climates [5]. However, more detailed work on functional nasal anatomy has challenged these climatic interpretations [4,9,10], because modern humans adapted to extreme cold have tall, narrow nasal apertures, whereas these structures are large and wide in Neandertals [4]. In this respect, Neandertal noses are more comparable to those of modern humans adapted to hot and humid climates [4,11–13].

The stocky body shape and estimated high body mass of Neandertals are also thought to reflect adaptations to cold [5] although they inherited a basic body configuration from heavy-bodied Early and Middle Pleistocene ancestors [14–16]. This hominin lineage probably had high energetic demands and a different body economy to that of anatomically modern *H. sapiens* [16–19]. The bioenergetic heritage of Neandertals probably had functional implications for different anatomical systems, some of which directly or indirectly affected the position and morphology of the cranial airways. This is why investigating the integration and functions of the respiratory apparatus is important in human evolutionary anatomy [20].

The cranial airways connect the outer environment with the inner organs of the body. They directly support a series of functions such as respiration, olfaction, thermoregulation, phonation, deglutition and speech [21]. In the skeleton, the cranial airways consist of the nasal cavity, which is located in the centre of the facial skeleton (midface) and of the external part of the posterior cranial base as the skeletal roof of the nasopharynx [22,23]. The nasal cavity is delimited anteriorly by the piriform aperture of the maxilla and the nasal bones. The posterior airways are delimited by the choanae, formed cranially by the sphenoid, laterally by the pterygoid processes, and posteriorly by the palates and by the external part of the spheno-occipital clivus and pharyngeal tubercle, forming the roof of the nasopharynx. The internal roof of the nasal cavity is delimited anteriorly by the cribriform plate of the ethmoid and more posteriorly by the sphenoid body. The internal floor of the airways is formed by the palatine processes of the maxilla and the horizontal laminae of the palate. The lateral walls are formed by the maxilla, the lachrymal bone, the superior and medial turbinates of the ethmoid, and the vertical parts of the palate. In the midsagittal plane, the nasal cavity is divided by the nasal septum, which is an osseocartilaginous structure formed by the perpendicular lamina of the ethmoid and the vomer.

Because of this anatomical context, the cranial airways form a central functional space around which adjacent craniofacial structures are organized. The central position of the

airways is important in both the ontogenetic and evolutionary contexts (Enlow, 1990). Integration analyses in modern humans have shown differences in the patterns of covariation between facial morphology and the openings of the nasal cavity [24]. These studies indicate that the choanae and posterior areas of the airways are morphologically more independent from the face than the anterior nasal opening, which correlates more closely with facial morphology.

Such differences in correlation patterns reflect an important aspect of posterior airway function. The choanae are the last skeletal diameter determining the size of the soft tissue components of the airways within the nasopharynx: the larger the posterior airways, the greater the amount of respiratory air passing to the lungs and available for skeletal muscle work and body activity.

Variations in cranial airway space and their importance for craniofacial morphology have been proposed by Enlow [25]. Internal spatial differences are reflected morphologically in gender-specific differences between human faces [26]. In many different human populations, both absolutely and relatively larger airway proportions in males are a constant feature of sexual dimorphism [22,27,28]. Because males have greater energetic and oxygen demands than females, larger cranial airways have been interpreted as skeletal evidence for physiological components of sexual dimorphism and body function [28,29]. This evidence supports the view that the size of the choanae might act as a constraint on respiratory function and could therefore be important in the context of human evolution in a similar physiological and respiratory–energetic context. But how do the anterior and posterior airways interact with the face during growth and across different hominins and non-human primates?

The aim of this study is to investigate the ontogenetic and allometric patterns of scaling between the anterior and posterior cranial airway openings in relation to the size of the face in a wider comparative data set. I address the null hypothesis that no differences exist in patterns of scaling between the anterior and posterior cranial airway openings in relation to the face.

Material and methods

A total of 403 skulls from two ontogenetic series of geographically variable *H. sapiens* ($N = 263$) and *P. troglodytes* ($N = 83$) and an adult Gorilla sample ($N = 46$) were analysed. The data were collected at the Anthropological Institute of the University of Coimbra, the University of Cambridge and the Natural History Museum (London) (Table 1). The fossil hominin sample consisted of Neandertals ($N = 6$) and Mid-Pleistocene hominins ($N = 5$).

For this analysis, 3D landmarks were measured on external craniofacial structures related to the airways and the

Table 1 Comparative data sets, provenances and ages / Description de l'échantillon de comparaison, origine géographique et âge			
Recent data	Adults N	Subadults N	Data source
Europeans (Coimbra)	50	42	Dry skulls
Europeans (Spitalfields, NHM)		88	Dry skulls
Africans (NHM)	36		Dry skulls
Inuit (Cambridge)	12		Dry skulls
Australians (NHM)	30		Dry skulls
Fuegians (NHM)	5		Dry skulls
	133	130	Dry skulls
Pan troglodytes (NHM, Cambridge)	50	33	Dry skulls
Gorilla gorilla (NHM)	46		Dry skulls
Fossil hominins			
Kabwe			CT-reconstruction
Bodo			CT-reconstruction
Arago 21			Cast
SH5			Cast
Petalona			Cast
Forbes Quarry			CT-reconstruction
Guattari 1			CT-reconstruction
Ferrassie 1			CT-reconstruction
La Chapelle aux Saints 1			CT-reconstruction
Saccopastore 1			CT-reconstruction
Saccopastore 2			CT-reconstruction

peripheral face, using a MicroScribe G2 digitizer. Data collection and landmarks are described in detail in Bastir and Rosas [24]. In the fossil hominins, the landmark data were digitized from original fossils (Kabwe, Forbes Quarry), high-quality casts (SH5) and high-resolution 3D reconstructions of CT scans from La Chapelle aux Saints, La Ferrassie 1, Saccopastore 1, Saccopastore 2, Guattari 1, Petralona and Bodo, and a virtual reconstruction of Arago 21 by Gunz et al. [30]. Landmarks that were missing due to fragmentary preservation of the fossils were reconstructed by Morpheus et al. using a multiple multivariate regression approach [30,31].

All the craniofacial landmarks were divided into subsets quantifying overall facial size (20 lms), anterior airways (11 lms) and posterior airways (11 lms) (Table 2, Fig. 1), based on previous studies on the nasopharynx and associated skeletal structures [12,22–24]. Centroid sizes were calculated for these compartments for the comparative scaling analysis. The anterior airway opening consisted of landmarks on the piriform aperture and the anterior part of the ethmoid, while the posterior opening consisted of the choanae and the associated nasopharyngeal landmarks at the sphenoo-occipital clivus (Table 2).

Scaling patterns between the anterior and the posterior cranial airway openings in relation to overall facial size were compared using RMA regression models [32]. To test the null hypothesis postulating no scaling differences between these airway compartments and overall facial size,

95% confidence intervals of the slopes were compared using PAST permutation analysis [33]. Scaling patterns were analysed in different groups, including human and chimpanzee growth series, the entire *Homo* sample, and the full hominin and great apes data sets.

Results

Table 3 shows the slopes of the regression models and the 95% confidence intervals of their slopes. All RMA models were statistically significant at $P = 0.001$ or higher. In all comparisons, the size of the anterior openings of the airways correlated more positively with facial size than the posterior openings. This tendency was more marked in chimpanzees, where the slopes of the posterior airways were completely outside the 95% of the range of the anterior slope. In the human data set, the slope of the posterior airways was close to the lower range of the anterior airways and the slope of the anterior airways was close to the upper range of the posterior airways. In the full *Homo* data set, the anterior slope was entirely outside the range of the posterior slope and vice versa. Figure 2 shows the data for the full sample. All these results show that the size of the anterior facial opening increases more with facial size than the size of the posterior cranial airways.

Table 2 Landmarks and assignation to different facial and airway regions / Points-repères utilisés dans l'étude et leur assignation aux différentes régions faciales et aux voies aériennes

Name of landmarks	Position on the cranium
Nasion	Ant. airways
Rhinion	Ant. airways
Anterior nasal spine	Ant. airways
Left anterior ethmoid fm	Ant. airways
Left lachrymal	Ant. airways
Left distal nasomaxillary junction (at the distal suture)	Ant. airways
Left alare	Ant. airways
Right anterior ethmoid fm	Ant. airways
Right lachrymal	Ant. airways
Right distal nasomaxillary junction (at the distal suture)	Ant. airways
Right alare	Ant. airways
Left optic canal (most medial, inferior point)	Post. airways
Left choana roof (most superior point)	Post. airways
Left midturbinate base (most posterior point at choanae level)	Post. airways
Left choana base (most lateral intranasal point at the palate)	Post. airways
Right optic canal (most medial, inferior point)	Post. airways
Right choana roof (most superior point)	Post. airways
Right midturbinate base (most posterior point at choanae level)	Post. airways
Right choana base (most lateral intranasal point at the palate)	Post. airways
Staphylion	Post. airways
Vomero-sphenoid junction [26]	Post. airways
Pharyngeal tubercle (maximal projection)	Post. airways
Glabella	Peripheral face
Nasion	Peripheral face
A-point [26]	Peripheral face
Prosthion	Peripheral face
Left posterior alveolar point (post. alveolar tubercle)	Peripheral face
Right posterior alveolar point (post. alveolar tubercle)	Peripheral face
Left frontomolare orbitale	Peripheral face
Left zygomatic root (most inferior point)	Peripheral face
Left zygomatic root (most inferior point)	Peripheral face
Left zygomatic root (most inferior point)	Peripheral face
Left zygomatic root (most inferior point)	Peripheral face
Left zygomatic root (most inferior point)	Peripheral face
Right zygomatic root (most inferior point)	Peripheral face
Right zygomatic root (most inferior point)	Peripheral face
Right zygomatic root (most inferior point)	Peripheral face
Right zygomatic root (most inferior point)	Peripheral face
Right zygomatic root (most inferior point)	Peripheral face
Right zygomatic root (most inferior point)	Peripheral face
Right zygomatic root (most inferior point)	Peripheral face
Right canine alveolus (most posterior point)	Peripheral face
Left canine alveolus (most posterior point)	Peripheral face

Discussion

This study aimed to investigate the ontogenetic and evolutionary interactions between the sizes of the anterior and posterior cranial airways and the face. Specifically, I studied

ontogenetic and allometric correlations in scaling between anterior and posterior airway sizes in humans, fossil hominins and great apes. The null hypothesis predicted no differences in the sizes of the anterior and posterior airways in relation to facial size. However, the results suggest a greater

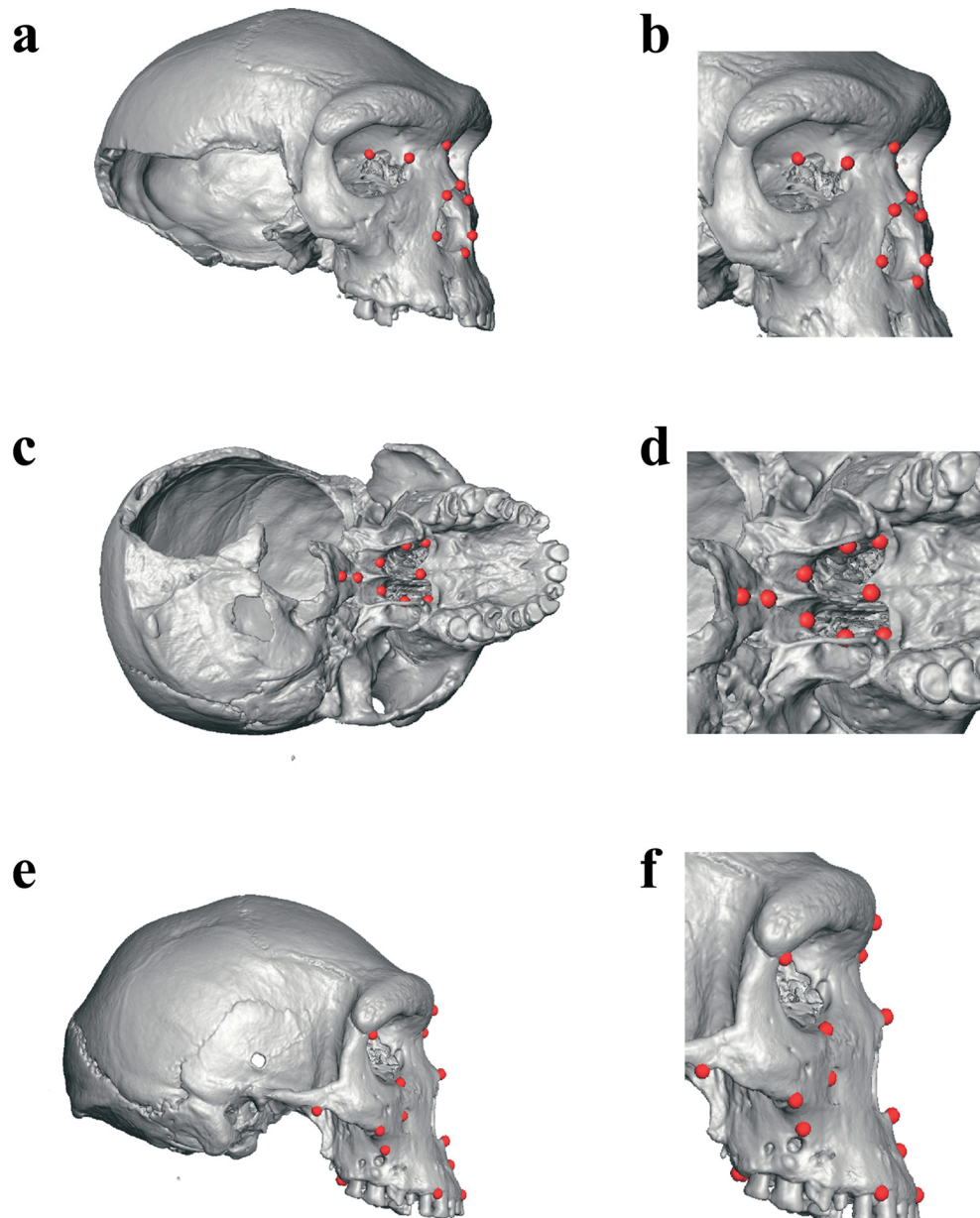


Fig. 1 Landmark sets of the different anatomical units. (a, b) show anterior airways in general context and details; (c, d) show posterior airways and (e, f) show the peripheral landmarks of the face. For definitions, see Table 2 / *Position des points-repères pour les différentes zones anatomiques*. a, b : voies aériennes antérieures, contexte général et détails ; c, d : voies aériennes postérieures ; e, f : points-repères périphériques de la face. Les points-repères sont définis dans le tableau 2

Table 3 RMA regressions, slopes plus 95% confidence intervals for the different groups / Régression RM, pente et intervalle de confiance 95 % pour les différents groupes

	Human growth	Chimpanzee growth	All hominins	Hominins and apes
Anterior airways	0.49 (0.47–0.53)	0.55 (0.52–0.57)	0.48 (0.45–0.52)	0.66 (0.63–0.69)
Posterior airways	0.46 (0.43–0.49)	0.48 (0.46–0.51)	0.42 (0.39–0.46)	0.4 (0.38–0.42)

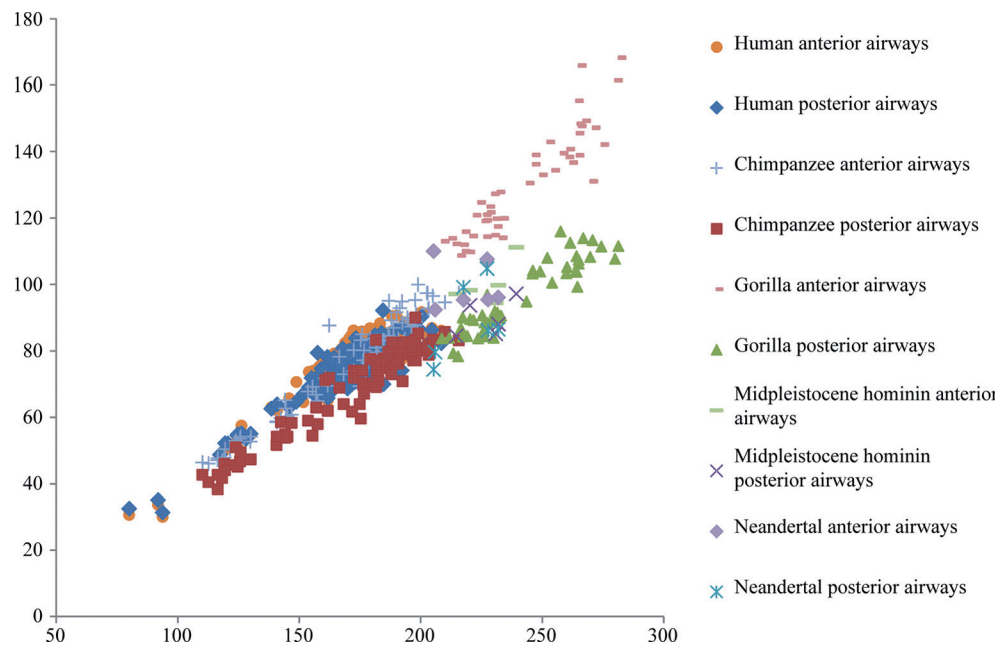


Fig. 2 Scatterplot of centroid sizes of the anterior and posterior airways (y-axis) against the centroid size of the face (x-axis). Note the divergence of the sizes of the anterior airways along facial size compared to the posterior airways. Because of these scaling relations, the differences between anterior and posterior airways is greater in larger faces / *Nuage de points des tailles centroïdes des voies aériennes antérieures et postérieures (axe y), comparé à la taille centroïde du massif facial (axe x).* Nous pouvons observer la différence entre la taille des voies antérieures par rapport à la taille du massif facial, comparés à la taille des voies postérieures par rapport à la taille du massif facial. Du fait de ces corrélations d'échelles, les différences entre les voies aériennes antérieure et postérieure sont plus importantes pour les massifs faciaux de plus grande taille

increase in the anterior airway openings relative to the face than in the posterior airways. Consequently, the null hypothesis is rejected.

The results of the ontogenetic analyses suggest that the growth mechanisms of the anterior and posterior openings of the cranial airways have similar effects in African great apes and hominins. This is surprising because postcranial changes in the nasopharyngeal area differ substantially in great apes and hominins due to different ontogenetic trends in the posterior cranial base. In humans, the base flexes antero-inferiorly, while in apes the base retroflexes [34–37]. Theoretically, this should diminish nasopharyngeal size in humans and increase this region in great apes. Yet, the posterior airways scale similarly with facial size in both groups. This could be explained by the fact that while retroflexion produces anteroposterior expansion of the nasopharyngeal space in apes, ontogenetic flexion in humans is accompanied by a lowering of the posterior base and face, which vertically expands posterior airway size. Importantly, both in human and in chimpanzee ontogeny, the posterior airways scale with a significantly lesser slope with facial size than the anterior airways. This is found in all group comparisons (Table 3, Fig. 2).

These systematic differences between anterior and posterior airway scaling patterns may explain facial morphology

and size in a functional context that could be important in Mid-Pleistocene hominins and Neandertals. As expected, due to their large faces, these hominins plot at the upper part of the modern human range (Fig. 2). Different comparative studies have shown that facial size scales positively with body size, not only in primates but also more generally in mammals [34,38–40]. However, scaling patterns are based on biological processes and should be discussed also within a functional context. The size of the airways is one functional factor that might underlie this general face–body scaling pattern [20,41,42]. This can be assumed because, for physiological reasons, body mass and the size of the respiratory organs scale isometrically and are closely correlated across mammals [43]. The results of this study could explain large facial sizes by linking energy-related factors and associated respiratory constraints with general facial growth and scaling patterns. The very large nasal apertures in Mid-Pleistocene hominins and the Neandertal lineage seem to be related to this. Body mass estimates for these hominins are higher than for anatomically modern humans [19,44]. According to Stahl [43], larger body masses require (and correlate with) larger respiratory organ sizes. Although represented only by skeletal anatomy, the large cranial airways of Neandertals correspond to their large thoracic capacities [8,45–48] and probably larger lungs [49]. These

correlations could drive the size of the face *via* functional constraints on airway size.

The airway–facial growth pattern could also have reduced its morpho-functional evolvability and possible climatic adaptations of the piriform apertures of Neandertals [4], thus accounting for the different air-conditioning strategies in Neandertals and modern humans [10]. Cold-adapted modern humans have tall, narrow anterior nasal openings [11–13], which are achieved by specific patterns of integration of the nasal cavity and the maxillary sinuses [50–52]. These narrow anterior airway openings are thought to increase turbulence, which should favour heating and moistening of the inspired air [11]. Thus, while cold-adapted modern humans have these high, narrow apertures, those of cold-adapted Neandertals are large and wide [4]. Neandertals may not have been able to evolve (and grow) narrow anterior nasal openings, as these might simply not have provided the necessary airway space [16,20,53] despite their possible advantages for airflow dynamics and turbulence induction. Instead, air-conditioning in Neandertals might have been taken over by increased air resilience time [10]. This situation illustrates how similar functional problems are resolved by different mechanisms and might shed light on evolutionary process and the importance of tinkering [54].

Increased air resilience time within the nasal cavity is probably related to the greater length of the cranial airways as part of the prognathic and projecting midface, suggesting that the entire nasofacial functional system should be considered as embedded in a specific cerebro-basicranial configuration. In Neandertals, the nasofacial functional system is related to their typical overall skull morphology. Recent analysis of basicranial and facial integration has shown that modifications at the basicranium shift the nasal cavity (and face) into a more anterior position, thereby contributing to midfacial projection and prognathism [7]. This shift could be related to encephalization and its impact on basicranial evolution, which in Neandertals differs from that of anatomically modern humans [55–57]. So, rather than a localized, independent functional adaptation to a cold climate achieved by evolving a narrow piriform aperture (through selective pressure), slight modifications among interrelated parts of systems in the organism (brain, base, face and interactions between airways), linked by ontogenetic scaling relationships (such as the link between body mass and facial size *via* the respiratory organs), could have provided effective air-conditioning *despite* nasofacial differences between the Neandertal lineage and modern humans [4,10]. Such longer and wider airways and faces may also have provided a structural solution guaranteeing a sufficient supply of oxygen to cover the high energy demands of Neandertal bodies, thus contributing to their “exaptation” to cold *via* an integrated set of organism-related anatomical features.

This could illustrate how slight modifications of integrated systems (thorax and airways in relation to body mass and encephalization) change the form and position of structures (airways, face) in which functional needs (air-conditioning) are taken over by new functional principles (resilience time due to prognathism rather than turbulence). If confirmed in future studies, this kind of tinkering could prove to be an important factor in later hominin facial evolution.

Acknowledgments I am grateful to the Société d’Anthropologie de Paris, in particular to François Marchal and Guillaume Daver, for their kind invitation to participate in the Poitiers meeting in 2018. Data and data access were provided by Chris Stringer, Fred Spoor, Rob Kruszynski and Loïse Humphrey, Maggie Bellatti, Giorgio Manzi, Roberto Machiarelli, Luca Bondiola, Alain Froment, Philippe Menecier, and Antoine Balzeau. Funding: CGL2015-63648-P (MINECO, Spain).

Conflicts of interests: Author do not have any conflict of interest to declare.

References

- Ponce de León M, Zollikofer C (2001) Neandertal cranial ontogeny and its implications for late hominid diversity. *Nature* 412:534–8
- Bastir M, O’Higgins P, Rosas A (2007) Facial ontogeny in Neandertals and modern humans. *Proc R Soc Lond [Biol]* 274:1125–32
- Gunz P, Harvati K (2007) The Neanderthal “chignon”: Variation, integration, and homology. *J Hum Evol* 53:732–46
- Holton NE, Franciscus RG (2008) The paradox of a wide nasal aperture in cold-adapted Neandertals: a causal assessment. *J Hum Evol* 55:942–51
- Weaver TD (2009) The meaning of Neandertal skeletal morphology. *Proc Natl Acad Sci U S A* 106:16028–33
- Marquez S, Pagano AS, Delson E, et al (2014) The nasal complex of Neandertals: an entry portal to their place in human ancestry. *Anat Rec* 297:2121–37
- Bastir M, Rosas A (2016) Cranial base topology and basic trends in the facial evolution of Homo. *J Hum Evol* 91:26–35
- García-Martínez D, Bastir M, Huguet R, et al (2017) The costal remains of the El Sidrón Neanderthal site (Asturias, northern Spain) and their importance for understanding Neanderthal thorax morphology. *J Hum Evol* 111:85–101
- de Azevedo S, González MF, Cintas C, et al (2017) Nasal airflow simulations suggest convergent adaptation in Neanderthals and modern humans. *Proc Natl Acad Sci U S A* 114:12442–7
- Wroe S, Parr WCH, Ledogar JA, et al (2018) Computer simulations show that Neanderthal facial morphology represents adaptation to cold and high energy demands, but not heavy biting. *Proc R Soc Lond [Biol]* 285(1876)
- Franciscus RG, Long JC (1991) Variation in Human nasal height and breadth. *Am J Phys Anthropol* 85:419–27
- Noback ML, Harvati K, Spoor F (2011) Climate-related variation of the human nasal cavity. *Am J Phys Anthropol* 145:599–614

13. Evteev A, Cardini AL, Morozova I, et al (2014) Extreme climate, rather than population history, explains mid-facial morphology of Northern Asians. *Am J Phys Anthropol* 153:449–62
14. Arsuaga JL, Carretero JM, Lorenzo C, et al (2015) Postcranial morphology of the middle Pleistocene humans from Sima de los Huesos, Spain. *Proc Natl Acad Sci U S A* 112:11524–9
15. Arsuaga JL, Lorenzo C, Carretero JM, et al (1999) A complete human pelvis from the middle pleistocene of Spain. *Nature* 399:255–8
16. Rosas A, Bastir M, Martínez-Maza C, et al (2006) Inquiries into Neanderthal crano-facial development and evolution: “accretion” vs “organismic” models. In: Harrison T, Harvati K (eds) *Neanderthals Revisited*. Springer Verlag, New York University, pp 38–69
17. Pontzer H (2017) Economy and Endurance in Human Evolution. *Curr Biol* 27:R613–R621
18. Churchill SE (2006) Bioenergetic perspectives on Neanderthal thermoregulatory and activity budgets. In: Harvati K, Harrison T (eds) *Neanderthals revisited*. Springer-Verlag, New York City, pp 113–56
19. Froehle A, Churchill SE (2009) Energetic competition between Neandertals and anatomically modern humans. *Paleoanthropology* 2009:96–116
20. Bastir M (2017) Back to basics: morphological analysis in paleoanthropology. In: Schwartz J (ed) *Biological Theory*. MIT-press, Boston, pp 205–27
21. Elad D, Wolf M, Keck T (2008) Air-conditioning in the human nasal cavity. *Respir Physiol Neurobiol* 163:121–7
22. Bastir M, Godoy P, Rosas A (2011) Common features of sexual dimorphism in the cranial airways of different human populations. *Am J Phys Anthropol* 146:414–2
23. Pagano AS, Laitman JT (2015) Three-dimensional geometric morphometric analysis of the nasopharyngeal boundaries and its functional integration with the face and external basicranium among extant hominoids. *Anat Rec* 298:85–106
24. Bastir M, Rosas A (2013) Cranial airways and the integration between the inner and outer facial skeleton in humans. *Am J Phys Anthropol* 152:287–93
25. Enlow DH (1990) *Facial Growth*, 3rd ed. W.B. Saunders Company, Philadelphia
26. Rosas A, Bastir M (2002) Thin-plate spline analysis of allometry and sexual dimorphism in the Human craniofacial complex. *Am J Phys Anthropol* 117:236–45
27. Megía I, Burgos OM, Rojas E, et al (2018) Sexual dimorphism of nasal airways in modern humans. In: Rissoch C, Nadal J., Fullola J. M., (Ed) *Geometric morphometrics Trends in biology, paleobiology and archaeology: Seminari d'Estudis i Rercherques Prehistòriques*, Universitat de Barcelona (SERP), Societat Catalana d'Arqueologia (SCA), pp 53–63
28. Holton NE, Yokley TR, Froehle AW, et al (2014) Ontogenetic scaling of the human nose in a longitudinal sample: Implications for genus *Homo* facial evolution. *Am J Phys Anthropol* 153:52–60
29. Hall RL (2005) Energetics of nose and mouth breathing, body size, body composition, and nose volume in young adult males and females. *Am J Phys Anthropol* 17:321–30
30. Gunz P, Mitteroecker P, Neubauer S, et al (2009) Principles for the virtual reconstruction of hominin crania. *J Hum Evol* 57:48–62
31. Slice DE (2000) Morphus et al: software for morphometric research (Department of Ecology and Evolution, State University, Stony Brook, New York.), Revision 01-01-2000
32. Martin RD, Barbour AD (1989) Aspects of line-fitting in bivariate allometric analyses. *Folia Primatologica* 53:65–81
33. Hammer Ø, Harper DAT, Ryan PD (2001) PAST: Paleontological statistics software package for education and data analysis. *Palaeontologia Electronica* 4:1–9
34. Biegert J (1957) Der Formwandel des Primatschädels und seine Beziehungen zur ontogenetischen Entwicklung und den phylogenetischen Spezialisierungen der Kopforgane. *Gegenbaurs Morphologisches Jahrbuch* 98:77–199
35. Lieberman DE, McCarthy RC (1999) The ontogeny of cranial base angulation in humans and chimpanzees and its implication for reconstructing pharyngeal dimensions. *J Hum Evol* 36:487–517
36. Jeffery N, Spoor F (2002) Brain size and the human cranial base: a prenatal perspective. *Am J Phys Anthropol* 118:324–40
37. Bastir M, Rosas A (2004) Facial heights: Evolutionary relevance of postnatal ontogeny for facial orientation and skull morphology in humans and chimpanzees. *J Hum Evol* 47:359–81
38. Dabelow A (1929) Über Korrelationen in der phylogenetischen Entwicklung der Schädelform I. Die Beziehungen zwischen Rumpf und Schädelform. *Gegenbaurs Morphologisches Jahrbuch* 63:1–49
39. Emerson SB, Bramble DM (1993) Scaling, allometry and skull design. In: Hanken J, Hall BK (eds) *The skull*, vol. 3: Functional and evolutionary mechanisms. University of Chicago Press, Chicago, pp 384–421
40. Cardini A, Polly D (2013) Larger mammals have longer faces because of size-related constraints on skull form. *Nat Commun* 4:2458
41. Bastir M (2004) A geometric morphometric analysis of integrative morphology and variation in human skulls with implications for the Atapuerca-SH hominids and the evolution of Neandertals. Structural and systemic factors of morphology in the hominid craniofacial system. Ph.D. Dissertation, Autonoma University of Madrid, Madrid
42. Bastir M (2008) A systems-model for the morphological analysis of integration and modularity in human craniofacial evolution. *J Anthropol Sci* 86:37–58
43. Stahl WR (1967) Scaling of respiratory variables in mammals. *J Appl Physiol* 22:453–60
44. Ruff CB, Trinkaus E, Holliday TW (1997) Body mass and encephalization in Pleistocene Homo. *Nature* 387:173–6
45. Franciscus RG, Churchill SE (2002) The costal skeleton of Shanidar 3 and a reappraisal of Neandertal thoracic morphology. *J Hum Evol* 42:303–56
46. Gómez-Olivencia A, Eaves-Johnson KL, Franciscus RG, et al (2009) Kebara 2: new insights regarding the most complete Neandertal thorax. *J Hum Evol* 57:75–90
47. García-Martínez D, Barash A, Recheis W, et al (2014) On the chest size of Kebara 2. *J Hum Evol* 70:69–72
48. Bastir M, García-Martínez D, Estalrich A, et al (2015) The relevance of the first ribs of the El Sidron site (Asturias, Spain) for the understanding of the Neandertal thorax. *J Hum Evol* 80:64–73
49. García-Martínez D, Torres-Tamayo N, Torres-Sánchez I, et al (2018) Ribcage measurements indicate greater lung capacity in Neanderthals and Lower Pleistocene hominins compared to modern humans. *Commun Biol* 1:117
50. Maddux SD, Butaric LN (2017) Zygomaticomaxillary Morphology and Maxillary Sinus Form and Function: How Spatial Constraints Influence Pneumatization Patterns among Modern Humans. *Anat Rec* 300:209–25
51. Butaric LN, Maddux SD (2016) Morphological Covariation between the Maxillary Sinus and Midfacial Skeleton among Sub-Saharan and Circumpolar Modern Humans. *Am J Phys Anthropol* 160:483–97

52. Holton N, Yokley T, Butaric L (2013) The morphological interaction between the nasal cavity and maxillary sinuses in living humans. *Anat Rec* 296:414–26
53. Yokley T, Holton NE, Franciscus RG, et al (2009) The role of body mass in the evolution of the modern human nasofacial skeleton. *Paleoanthropol Soc* 2009:A39–40
54. Lieberman DE (2011) The evolution of the human head. Belknap Press of Harvard University Press, Cambridge Massachusetts, London, England, 768 p
55. Kochiyama T, Ogihara N, Tanabe HC, et al (2018) Reconstructing the Neanderthal brain using computational anatomy. *Sci Rep* 8:6296
56. Bruner E, Manzi G, Arsuaga JL (2003) Encephalization and allometric trajectories in the genus *Homo*. Evidence from the Neandertal and modern lineages. *Proc Natl Acad Sci U S A* 100:15335–40
57. Bastir M, Rosas A, Gunz P, et al (2011) Evolution of the base of the brain in highly encephalized human species. *Nat Commun* 2:588

Variation in Paranasal Pneumatisation between Mid-Late Pleistocene Hominins

Variation de la pneumatisation paranasale des hominines du Pléistocène moyen final

L.T. Buck · C.B. Stringer · A.M. MacLarnon · T.C. Rae

Received: 23 April 2018; Accepted: 24 July 2018

© Société d'Anthropologie de Paris et Lavoisier SAS 2019

Abstract There is considerable variation in mid-late Pleistocene hominin paranasal sinuses, and in some taxa distinctive craniofacial shape has been linked to sinus size. Extreme frontal sinus size has been reported in mid-Pleistocene specimens often classified as *Homo heidelbergensis*, and Neanderthal sinuses are said to be distinctively large, explaining diagnostic Neanderthal facial shape. Here, the sinuses of fossil hominins attributed to several mid-late Pleistocene taxa were compared to those of recent *H. sapiens*. The sinuses were investigated to clarify differences in the extent of pneumatisation within this group and the relationship between sinus size and craniofacial variation in hominins from this time period. Frontal and maxillary sinus volumes were measured from CT data, and geometric morphometric methods were used to identify and analyse shape variables associated with sinus volume. Some mid-Pleistocene specimens were found to have extremely large frontal sinuses, supporting previous suggestions that this may be a diagnostic characteristic of this group. Contrary to traditional assertions, how-

ever, rather than mid-Pleistocene *Homo* or Neanderthals having large maxillary sinuses, this study shows that *H. sapiens* has distinctively small maxillary sinuses. While the causes of large sinuses in mid-Pleistocene *Homo* remain uncertain, small maxillary sinuses in *H. sapiens* most likely result from the derived craniofacial morphology that is diagnostic of our species. These conclusions build on previous studies to overturn long-standing but unfounded theories about the pneumatic influences on Neanderthal craniofacial form, whilst opening up questions about the ecological correlates of pneumatisation in hominins.

Keywords *Homo heidelbergensis* · Sinuses · Neanderthal · Pleistocene · Morphology · Hominin

Résumé Les sinus paranasaux des hominines du Pléistocène moyen final présentent une variation morphologique considérable. Chez certains taxons, la taille des sinus semble-t-être liée à une morphologie craniofaciale particulière. Les fossiles du Pléistocène moyen, souvent rattachés au taxon *H. heidelbergensis*, présentent des sinus frontaux de taille extrêmement importante. Cette caractéristique est partagée avec les Néandertaliens, chez qui une taille importante des sinus frontaux semble expliquer la forme spécifique de leur morphologie faciale. Dans cette étude, nous comparons les sinus d'hominines attribués à plusieurs taxons du Pléistocène moyen final à ceux d'*H. sapiens* récents. Les sinus ont été étudiés pour clarifier les différences dans l'étendue de la pneumatisation au sein de ce groupe et la relation entre la taille des sinus et la variation craniofaciale chez les hominines de cette période. Les volumes des sinus frontaux et maxillaires ont été mesurés à partir de données tomodensitométriques, et des méthodes de morphométrie géométrique ont été utilisées pour identifier et analyser les variables de conformation associées au volume sinusal. Certains spécimens du Pléistocène moyen ont des sinus frontaux extrêmement grands, ce qui renforce l'hypothèse précédemment suggérée selon laquelle des sinus de grandes

L.T. Buck (✉)
Department of Anthropology (Evolutionary Wing),
University of California, Davis, 1 Shield's Avenue, Davis,
California, 95616, USA
e-mail : lbuck@ucdavis.edu

L.T. Buck · T.C. Rae
Centre for Research in Evolutionary,
Social and Inter-disciplinary Anthropology,
Department of Life Sciences, University of Roehampton,
Holybourne Avenue, London, SW15 4JD, UK

L.T. Buck · C.B. Stringer
Human Origins Research Group,
Department of Earth Sciences,
Natural History Museum, Cromwell Road, London,
SW7 5BD, UK

A.M. MacLarnon
Department of Anthropology, Durham University,
Dawson Building, South Road, Durham, DH1 3LE, UK

tailles pourraient être diagnostiques de ce groupe. Cependant, et contrairement aux affirmations traditionnelles, les hominines du Pléistocène moyen et les Néandertaliens n'ont pas de grands sinus maxillaires, ce sont les *H. sapiens* qui présentent des sinus maxillaires particulièrement petits. Alors que les raisons expliquant la grande taille des sinus chez les hominines du Pléistocène moyen restent à définir, les petits sinus maxillaires des *H. sapiens* résultent très probablement de la morphologie craniofaciale dérivée de notre espèce. Ces conclusions contredisent des hypothèses anciennes, mais non fondées, sur l'influence de la pneumatisation sur la morphologie craniofaciale néandertalienne, tout en ouvrant des perspectives sur les corrélats écologiques de la pneumatisation chez les hominines.

Mots clés *Homo heidelbergensis* · Sinus · Néandertal · Pléistocène · Morphologie · Hominine

Introduction

The paranasal sinuses are air-filled cavities between the inner and outer tables of the cranial bones, lined with mucous membrane [1]. Each is recognised by the position of its ostium, the hole through which mucous drains into the nasal cavity, and each is named for the bone it most commonly pneumatises [2]. There are four types of sinus in hominins: frontal, maxillary, sphenoidal and ethmoid; maxillary and sphenoidal sinuses are present in all hominoids, whilst the frontal and ethmoid sinuses are only found in hominines [3]. The frontal and maxillary sinuses are investigated here as they are those which are most often asserted to differ between hominin taxa [4–8].

Mid-late Pleistocene taxa show high levels of variation in craniofacial shape [9]. Here, the mid-Pleistocene European and African fossils in our sample (Bodo, Broken Hill [Kabwe], Petralona, Steinheim and Ceprano) are referred to as *H. heidelbergensis*, despite disagreement in the field regarding the alpha taxonomy and indeed, the validity of this species diagnosis [10–12]. It is our intention to investigate the relationship between sinus size and craniofacial shape in these specimens, rather than to diagnose their taxonomy. Mid-Pleistocene specimens from Europe and Africa often attributed to *H. heidelbergensis* [13–19] are differentiated from *H. erectus* by an expanded upper cranial vault and increase in endocranial capacity, a vertical lateral nasal border, and reduced total facial prognathism [16,17,20]. Massive pneumatisation (hyperpneumatisation) in some *H. heidelbergensis* specimens has been linked to their craniofacial morphology [6]. For example, comparatively reduced postorbital constriction in Petralona and the anterior orientation of the upper face relative to the anterior cranial fossa in

Petralona and Broken Hill have been related to extreme frontal pneumatisation [6], though the authors do not make it explicit whether the sinuses are regarded as the cause of craniofacial shape, or vice versa. Here, associations between craniofacial morphology and sinus volume are explicitly investigated in these and other mid-Pleistocene hominins.

The complex of neurocranial features that diagnoses Neanderthals includes a large, long, low cranium, expanded nuchal region with occipital bunning [5,21] and a suprainiac fossa [22,23]. Facial characteristics include swept-back zygomatics, a great degree of mid-facial prognathism [24], double-arched supraorbital tori [22] and a large piriform aperture [22,25]. Independently, these features are not unique to Neanderthals, but they are most frequent in this taxon and, in concert, differentiate Neanderthal morphology from that of other taxa [26]. Neanderthal crania have long been characterised as being hyperpneumatised [5,27,28], and it has been asserted that these large sinuses resulted in diagnostic craniofacial shape. The large supraorbital tori of Neanderthals have been said to result from their expanded frontal sinuses [4,29], and the ‘inflated’ Neanderthal mid-face, which projects and lacks a canine fossa, has been attributed to large maxillary sinuses [4]. This supposed hyperpneumatisation has been linked to the species’ assumed adaptation to arctic conditions during the Pleistocene ‘ice ages’, suggesting that the sinuses have a thermoregulatory role [4,30]. Subsequent work, however, has demonstrated that sinus volume tends to decrease in cold temperatures [31,34], while quantification of sinus volume relative to facial size shows that relative sinus volumes in the fossil taxon are indistinguishable from those of recent European *H. sapiens* [35,36] but are substantially different from extant arctic people [37]. Research to date which has questioned the relative hyperpneumatisation of Neanderthals [35,37] has been limited by fairly small and geographically restricted samples, both of fossils and of recent *H. sapiens*. It is important therefore to test the assumption of Neanderthal hyperpneumatisation and the relationship between Neanderthal pneumatisation and craniofacial shape with a more comprehensive sample.

H. sapiens is characterised by a globular cranial vault, increased basicranial flexion, anteroposteriorly short and orthognathic face, vertical forehead, the presence of a canine fossa, and a true chin [38–44]. Suggested causes for diagnostic *H. sapiens* morphology do not usually include sinus size, yet if it is indeed a key factor governing shape in its close congeners, *H. heidelbergensis* and Neanderthals, it could also be expected to play a part in shaping *H. sapiens* craniofacial shape. These three taxa have been central to theories of hominin sinus function [4,29,30], hyperpneumatisation has been argued for both Neanderthals and *H. heidelbergensis* [6,8,16], and sinus form has been used as an explanation for Neanderthal and *H. heidelbergensis* characteristic shape

[4,6]. In the current study, the differences in frontal and maxillary sinus size between *H. heidelbergensis*, Neanderthals and *H. sapiens* are measured, and the relationship between sinus size and craniofacial shape is investigated.

Based on the literature regarding hominin sinus size, it is hypothesised that there are significant differences between sinus volumes in different taxa, namely, that either Neanderthals or *H. heidelbergensis* will be hyperpneumatised, and that these differences will be associated with taxonomically distinctive craniofacial shape. Hyperpneumatisation is clearly a relative term and when used in the literature it is not explained relative to what Neanderthals/*H. heidelbergensis* are thought to show expanded sinuses. For the purposes of this paper, hyperpneumatisation is defined as extreme sinus size in one taxon compared to the other two. If change in sinus volume causes craniofacial morphology to alter, one might expect the taxonomic differences in sinus volume to be larger than those in craniofacial morphology; if the reverse is true and the taxonomic differences in craniofacial morphology are greater than those in sinus volume, this may suggest that the differences in craniofacial morphology are proximal and drive sinus size as a secondary effect. The latter finding would have implications for our understanding of sinus function, or the lack thereof, contributing to a long-standing debate over whether the sinuses are merely evolutionary spandrels (see, [45] for review).

Previous discussions of pneumatisation [6,45,46] often assume that sinuses are a functionally and developmentally homogenous group. In fact, there is evidence that this is not necessarily the case; the number and type of sinuses present are not constant between primate species, and sinuses have been lost and regained independently on several occasions during the course of primate evolution [3,47]. This may suggest a degree of functional heterogeneity, or at least modularity. Sinus modularity is also supported by Tillier's [48] observation of a lack of covariation in sinus size between sinus types within hominin individuals. In the current study, the frontal and maxillary sinuses were considered separately to assess the case for treating paranasal pneumatisation as a single phenomenon.

Materials and methods

Materials

The sample consists of clinical and microCT data of recent *H. sapiens* from populations with a wide geographic distribution (133 from 13 populations), early *H. sapiens* (7), *H. heidelbergensis* (5) and *H. neanderthalensis* (8) (Table 1). Data collected using the two forms of CT technology were combined to provide the maximum possible sample. The higher resolution of microCT data is likely to enable a

more accurate segmentation and measurement of sinus volumes, yet comparison of measurements of the frontal and left maxillary sinuses of the Broken Hill specimen using medical and microCT shows a relatively small difference. As measured by a single observer (LTB, see [49]), the difference between measurements of frontal and left maxillary sinus volumes using medical and microCT are 4.76% and 1.20%, respectively, levels of error that were felt to be acceptable due to the importance of obtaining as large a sample as possible. It is likely that the frontal sinuses are most affected by the poorer resolution of medical CT, due to their more complex shape (particularly in the *H. heidelbergensis* sample), which may be underestimated to some extent. Thus, the level of error seen between the two measurements for Broken Hill is likely at the upper end of that for any specimen.

In the current sample, recent *H. sapiens* are defined as *H. sapiens* less than 25 ka and early *H. sapiens* are defined as *H. sapiens* from between 150 and 25 ka following the rationale of Stringer and Buck [44]. For some of the recent *H. sapiens* groups, insufficient individuals were available from one country to make a reasonable sample, and thus samples from several countries in the same region were combined if the climate, chronology and method of subsistence were comparable ([50]; Table 1). Since all the recent *H. sapiens* are combined and the goal was to capture as much as possible of global variation in recent *H. sapiens*, differences in levels of intragroup variation between different recent *H. sapiens* samples should not affect the results.

No significant differences were found between early and recent *H. sapiens* sinus volumes or sinus volume-associated craniofacial shape. Furthermore, the results presented below do not change if early *H. sapiens* are omitted from the *H. sapiens* group. Thus, early and recent *H. sapiens* are combined in the results presented here to sample the maximum possible chronological and geographical variation in *H. sapiens* and due to the small sample sizes for early *H. sapiens* in the morphological analyses. The fossils are shown separately in the graphs (Figs 3, 4) as with the other taxa for consistency and to show where the fossil specimens fall in relation to their younger conspecifics.

Despite evidence for Neanderthal introgression in the genomes of recent *H. sapiens* [51–53], Neanderthals are treated here as a separate species from *H. sapiens*: *H. neanderthalensis*. It is not uncommon for closely related species to be able to interbreed to some extent [54], and levels of morphological difference between Neanderthals and *H. sapiens* are greater than those seen between many closely related species [55–57]. *H. heidelbergensis* is a disputed category, as mentioned above. In the analyses that follow, *H. heidelbergensis* is defined following Stringer [16], as an Afro-European species.

Table 1 Sample details / Détails de l'échantillon

Specimen/ Group	Taxonomic group	Geographic location	Date	Number in sample	Medical/ microCT	Source	FVS Y/N (sample n where > 1)	FSS Y/N (sample n where > 1)	MVS Y/N (sample n where > 1)	MSS Y/N (sample n where > 1)
KNM-ER 3883	<i>H. erectus</i>	Kenya	1.5–6 Ma [96]	1	Medical	KNM	N	N	N	N
Steinheim	<i>H. heidelbergensis</i>	Germany	> 300 ka, MIS 9 [97]	1	Medical	UV	N	Y	N	N
Broken Hill	<i>H. heidelbergensis</i>	Zambia	~ 250–300 ka [98]	1	Medical	NHM	Y	Y	Y	Y
Bodo	<i>H. heidelbergensis</i>	Ethiopia	~ 600 ka [81]	1	Medical	UV	Y	N	Y	N
Petalona	<i>H. heidelbergensis</i>	Greece	~ 400 ka [75]	1	Medical	UV/UT	Y	Y	Y	Y
Ceprano	<i>H. heidelbergensis</i>	Italy	430–385 ka [99]	1	Medical	ULS	Y	N	N	N
Guattari	<i>H. neanderthalensis</i>	Italy	57–51 ka [100]	1	Medical	MNPE	Y	N	Y	N
Krapina 3	<i>H. neanderthalensis</i>	Croatia	~ 130 ka [101]	1	Medical	NESPPOS	Y	N	N	N
Tabun C1	<i>H. neanderthalensis</i>	Israel	~ 122 ka [102]	1	Medical	NHM	Y	N	N	N
Forbes' Quarry	<i>H. neanderthalensis</i>	Gibraltar	~ 50 ka [103]	1	Medical	NHM	Y	N	Y	N
La Chapelle-aux-Saints 1	<i>H. neanderthalensis</i>	France	~ 50 ka [104]	1	Medical	MH	Y	Y	Y	Y
La Ferrassie 1	<i>H. neanderthalensis</i>	France	75–60 ka [105]	1	Medical	MH	Y	Y	Y	Y
La Quina 5	<i>H. neanderthalensis</i>	France	75–48 ka [105,106]	1	Medical	MH	Y	N	N	N
Feldhofer Neanderthal	<i>H. neanderthalensis</i>	Germany	~ 40 ka [107]	1	Medical	UZ	Y	N	N	N
Skhul 5 Singa	Early <i>H. sapiens</i>	Israel Sudan	130–100 ka [108] > 131–135 ka [104]	1	Medical	NESPPOS micro	Y	N	N	N
Mladeč 1	Early <i>H. sapiens</i>	Czech Republic	~ 37.5–34.75 ka [109]	1	Medical	UV	Y	N	Y	Y
Cro-Magnon 1	Early <i>H. sapiens</i>	France	< 28 ka [110]	1	Medical	MH	Y	N	Y	N
Cro-Magnon 2	Early <i>H. sapiens</i>	France	< 28 ka [110]	1	Medical	MH	Y	Y	N	N
Cro-Magnon 3	Early <i>H. sapiens</i>	France	< 28 ka [110]	1	Medical	MH	Y	N	N	N
Ngaloba	Early <i>H. sapiens</i>	Tanzania	50–120 ka [111,112]	1	Medical	UV	Y	N	N	N
Lithuania	Recent <i>H. sapiens</i>	Lithuania	< 25 ka	14	Medical	TK	Y (11)	Y (11)	Y (11)	Y (8)
Western Africa	Recent <i>H. sapiens</i>	Angola, Liberia, Nigeria	< 25 ka	13	Medical	ORSA	Y (13)	Y (12)	Y (12)	Y (8)

(Suite page suivante)

Table 1 (suite)

Specimen/ Group	Taxonomic group	Geographic location	Date	Number in sample	Medical/ microCT	Source (sample n where > 1)	FVS Y/N (sample n where > 1)	FSS Y/N (sample n where > 1)	MVS Y/N (sample n where > 1)	MSS Y/N (sample n where > 1)
Western Europe	Recent <i>H. sapiens</i>	Germany, The Netherlands, Norway, Sweden	< 25 ka	12	Medical	NESPOS	Y (11)	Y (10)	Y (10)	Y (10)
India	Recent <i>H. sapiens</i>	India	< 25 ka	12	Medical	ORSA	Y (11)	Y (10)	Y (5)	
Greenland	Recent <i>H. sapiens</i>	Greenland	< 25 ka	7	micro	NHM	Y (7)	Y (7)	Y (7)	
Russia	Recent <i>H. sapiens</i>	Russia	< 25 ka	4	Medical	ORSA	Y (4)	Y (4)	Y (4)	
North Africa	Recent <i>H. sapiens</i>	Algeria, Morocco	< 25 ka	7	Medical	IPH	Y (7)	Y (3)	Y (2)	Y (1)
Tasmania	Recent <i>H. sapiens</i>	Tasmania	< 25 ka	8	micro	NHM	Y (8)	Y (5)	Y (8)	Y (3)
Torres Straits Islands	Recent <i>H. sapiens</i>	Torres Straits Islands	< 25 ka	15	micro	NHM	Y (12)	Y (10)	Y (12)	Y (8)
Peru	Recent <i>H. sapiens</i>	Peru	< 25 ka	10	Medical	ORSA	Y (10)	Y (10)	Y (10)	Y (10)
China	Recent <i>H. sapiens</i>	China	< 25 ka	10	Medical	ORSA	Y (9)	Y (9)	Y (10)	Y (8)
Hawaii	Recent <i>H. sapiens</i>	Hawaii	< 25 ka	11	micro	NHM	Y (11)	Y (10)	Y (10)	Y (8)
Mexico	Recent <i>H. sapiens</i>	Mexico	< 25 ka	10	Medical	ORSA	Y (10)	Y (8)	Y (9)	Y (5)

FVS: included in frontal sinus volume sample, FSS: included in frontal sinus-specific shape sample, MVS: included in maxillary sinus volume sample, MSS: included in maxillary sinus-specific shape sample. Y: included in analysis, N: not included in analysis. The sole *H. erectus* specimen, KNM-ER 3883, was not included in statistical analyses or figures, but is mentioned in the Discussion with reference to the potential phylogenetic significance of sinus size in *H. heidelbergensis*. National Museum of Kenya(NMK), (DAFFH) Digital Archive of Fossil Hominins, University of Vienna; USL: Università La Sapienza, Rome; (NHM) Natural History Museum, London; (UV) University of Vienna; AUT: Aristote University of Thessaloniki; MNPE: Museo Nazionale Preistorico Etnografico ‘Luigi Pigorini’, Rome; MHP: Musée de l’Homme, Paris; UZ: University of Zurich; Ernst-Moritz-Arndt University, Greifswald / FIVS : spécimens inclus dans l’échantillon de volume du sinus frontal, FSS : spécimens inclus dans l’échantillon de conformation cranofa-ciale spécifique au sinus frontal, MVS : spécimens inclus dans l’échantillon de volume du sinus maxillaire, MSS : spécimens inclus dans l’échantillon de conformation cranofa-ciale sinus maxillaire spécifique. Y : spécimens inclus dans l’analyse, N : spécimens non inclus dans l’analyse. Le seul spécimen d’*H. erectus*, KNM-ER 3883, n’a pas été inclus dans les analyses statistiques, mais il est discuté dans la discussion en ce qui concerne la signification phylogénétique potentielle de la taille des sinus chez *H. heidelbergensis*. National Museum of Kenya (NMK), Digital Archive of Fossil Hominins, University of Vienna (DAFFH), Università La Sapienza, Rome (USL), Natural History Museum, London (NHM), University of Vienna ; AUT : Aristotle University of Thessaloniki ; MNPE : Museo Nazionale Preistorico Etnografico « Luigi Pigorini », Rome ; MHP : Musée de l’Homme, Paris

Only adult crania were used in these analyses, and pathological crania were avoided where possible. Where no alternatives were available (i.e., the fossil sample), pathological crania were used only if the pathology did not appear to alter the regions of interest (e.g., possible pathology affecting the parietals of the early *H. sapiens* fossil Singa). Whilst each recent *H. sapiens* sample was chosen to include both males and females, it was not possible to obtain exactly equal numbers without compromising sample size. Butaric et al. [58] have shown that, at least in recent *H. sapiens*, there is no sexual dimorphism in relative maxillary sinus volumes, but this is not known for frontal sinuses. There were generally more male data available, and some populations had no reliable sex information. The sample consisted of crania only (i.e., no postcrania), and no attempt was made to sex individuals based on cranial characteristics since these are very variable between populations and, as they are largely based on levels of robusticity, decisions about sex might bias craniofacial shape analyses. The sexes of the fossils are also mostly unknown; thus even correctly inferring the sex of the recent sample would not eliminate sex as a potentially confounding variable.

Methods

Sinus volume was used to quantify sinus size [32,33, 35,36,59,60]. Sinuses were segmented manually from CT scans slice-by-slice by a single observer and their volumes measured in AVIZO versions 5–7 (FEI Visualization Sciences Group, Burlington, MA). A semi-automated method for sinus segmentation is now available [61], which may prove useful for future studies of a similar nature.

The volumes of both the right and left frontal sinuses were taken where possible (indeed, there is often no demarcation between the two), and the volume was recorded as the sum of both sides, or the only side present multiplied by two, in the instances where only one side was measurable (the Tabun C1 Neanderthal and one Western European recent *H. sapiens*). The left maxillary sinus was used if preserved and the right substituted where necessary, since there is very little bilateral asymmetry in maxillary sinuses [48].

Only crania with relatively well-preserved sinuses and surrounding craniofacial morphology were included in the study. For all samples, some of the delicate internal bones surrounding the sinuses were broken into many individuals, but by viewing the CT slices in all three planes (transverse, sagittal and coronal) in turn and also inspecting the resulting sinus volume rendered in 3D, it was possible to reconstruct the original line of these bones in AVIZO on a slice-by-slice basis (see SI, Fig. S1). Error testing (see below) suggests that this reconstruction is robust. Some fossil specimens have sediment in their sinus cavities, but a conservative approach was adopted whereby individuals were only included in the analyses if the sediment was of sufficiently

different radio densities from the bone to be clearly visually distinguished from it. Fossil specimens with sinuses rendered and shown in situ are detailed in the Supplementary Information (Fig. S2–4).

To test the precision of the method of measuring sinus volume, the two sinus types (frontal and maxillary) were sectioned out of the same recent *H. sapiens* cranial CT data five times with at least 1 day elapsing between measurements. These measurements were then compared, and error was calculated as the sum of the differences between each individual measurement and their mean, divided by the number of measurements. This error is shown below (Table 2) as a percent of the mean measurement [62].

The measurement errors (Table 2) are low for each sinus. The recent *H. sapiens* cranium used was reasonably complete and may therefore be easier to measure accurately than some of the more broken specimens (a reasonably intact specimen was chosen to enable measurements of both sinuses on the same individual). However, the medial wall of the maxillary sinus was quite broken, which is reflected in the higher level of error in the volume for that sinus. This damage resulted in the need to estimate the position of the margins of the sinus for numerous slices (SI Fig. S1), so the low level of error is reassuring. The scan is also a medical CT scan, so the level of resolution is not as high as for microCT data. For these reasons, it was felt that the error tests demonstrated the method to be sufficiently precise.

Sinus size has been shown to scale with craniofacial size in *H. sapiens* and other hominoids [36,63–65]. Therefore, to look at non-isometric differences in volume, measurements must be standardised. Centroid size is one three-dimensional measurement, appropriate for the standardisation of a volume. A centroid size's quality, however, depends on the number and distribution of landmarks used to calculate it and using enough, reasonably spatially distributed, landmarks to obtain

Table 2 Error test for sinus volume measurements. Results (mm^3) for five repetitions of sinus volume measurement (raw volume, not relative volume) and percentage error / *Test d'erreur pour les mesures de volume sinusal. Résultats (mm³) pour cinq répétitions de mesure du volume sinusal (volume brut, volume non relatif) et pourcentage d'erreur*

Replication	Frontal	Maxillary
1	7616.8	17214.2
2	7785.7	16947.0
3	7353.4	16688.7
4	7598.5	16735.8
5	7751.4	18416.8
Mean	7621.2	17200.5
Standard deviation	170.5	710.9
% error	1.8	2.9

a good measure of centroid size on fragmentary specimens is problematic. In the current sample, if only the landmarks preserved on the entire sample were used, centroid size would have to be computed using only four landmarks in the supraorbital region. This would not give a good estimate of overall craniofacial size.

To test the possibility of using a simpler metric to standardise sinus volume and thus increase sample size, relative sinus volumes calculated using a centroid size (CS) based on a low number of landmarks (see SI, Table S1, Fig. S7) were compared to relative sinus volumes calculated using a single linear measurement. A landmark set was devised to include the maximum possible sample with a minimum number of landmarks needed to capture the shape of the entire cranium (6). Despite the low number of landmarks, they are not all preserved in 75% of the fossils and 14% of the recent *H. sapiens*. In previous studies, a simple linear measurement of bi-frontomolare temporale breadth was used as a proxy for cranial size to standardise sinus volume [36,37]. The use of half this measurement (glabella to right frontomolare temporale: G-FMT) holds the same information regarding facial size and enables all crania in the current sample to be included in at least one sinus volume analysis [49]. G-FMT was measured in AVIZO, and Pearson's correlation tests were run between relative sinus volumes calculated using CS and using G-FMT. Comparison of frontal sinus volume standardisation with CS and with G-FMT produces a very strong, highly significant positive relationship ($r = 0.98, P < 0.001$). The relationship for maxillary sinus volumes, although still robust, has a smaller r -value ($r = 0.71, P < 0.001$). This is perhaps not surprising, as the maxillary region is further from the measurement. Given the number of specimens that would have to be excluded if CS

were used to measure size, however, the relationship was judged to be strong enough. It would have been possible to use different CSs for frontal and maxillary relative volumes, but this would have impaired comparisons between sinus types.

Craniofacial shape related to sinus volume was analysed using geometric morphometric methods (GMM). Preservation (particularly poor in the fossil sample) prevented the inclusion in the GMM analyses of the entire sample used to measure sinus volumes. Thus, reduced samples (Table 1) were used to analyse sinus-specific craniofacial shape, and results from the sinus-specific shape analyses on the reduced samples are inferred to apply also to the wider sinus volume samples. To maximise sample sizes, different landmark sets were designed for each sinus and are referred to as frontal/maxillary sinus-specific landmark sets (Tables 3, 4). Sinus-specific landmark sets were chosen to balance the requirements of capturing the shape of interest and including as many specimens as possible in the analyses. The intention was to capture the shape of the region of pneumatisation, but also its relationship with the rest of the cranium. For this reason, both landmark sets include a few key landmarks on the face and neurocranium outside the region of their specific sinus.

The frontal sinus-specific landmark set (Table 3) consisted of ten landmarks, mainly in the supraorbital region, allowing the inclusion of a sample of 110 specimens (Table 1). The maxillary sinus landmark set (Table 4) consisted of 13 landmarks, concentrating on the maxillary region, allowing the inclusion of 88 specimens (Table 1). These are low numbers of landmarks, but they capture shape differences between taxa and they allow the inclusion of many otherwise unusable fossils (see also [84]).

Table 3 Landmarks used in frontal sinus-specific landmark set analyses / Points repères utilisés pour l'analyse des conformations associée au volume du sinus frontal

Landmark	Definition	Number in frontal sinus-specific landmark set
Bregma	Point where coronal & sagittal sutures intersect	1
Glabella	Most anterior point on frontal bone	2
Nasion	Point of intersection of nasofrontal suture & midsagittal plane	3
C/P3	Most inferior external point between maxillary canine (C) and first pre-molar (P3)	4
Frontomolare orbitale	Point where zygomaticofrontal suture crosses orbital margin	5
Zygoorbitale	Point where zygomaticomaxillary suture intersects with inferior orbital margin	6
Frontotemporale	Point on frontal bone where temporal line reaches its most anteromedial position	7
Frontomolare temporale	Most lateral point on zygomaticofrontal suture	8
Porion	Most superior point on margin of external auditory meatus	9
Lambda	Point where sagittal & lambdoid sutures intersect	10

Table 4 Landmarks used in maxillary sinus-specific landmark set analyses / Points repères utilisés pour l'analyse des conformations associée au volume du sinus maxillaire		
Landmark	Definitions	Number in maxillary sinus-specific landmark set
Bregma	Point where coronal & sagittal sutures intersect	1
Glabella	Most anterior point on frontal bone	2
Nasion	Point of intersection of nasofrontal suture & midsagittal plane	3
Alare	Most lateral point on nasal aperture taken perpendicular to nasal height	4
C/P3	Most inferior external point between maxillary canine (C) and first pre-molar (P3)	5
Zygoorbitale	Point where zygomaticomaxillary suture intersects with inferior orbital margin	6
Zygion	Most lateral point on surface of zygomatic arch	7
Zygomaticum	Most inferoanterior point on zygomaticomaxillary suture	8
Molars pos.	Most inferoposterior point on external maxillary alveolus (posterior to M3)	9
Porion	Most superior point on margin of external auditory meatus	10
Lambda	Point where sagittal & lambdoid sutures intersect	11
Ectomolare	Most lateral point on outer surface of alveolar margin of maxilla	12
Orale	Point of intersection on palate with line tangent to posterior margins of central incisor alveoli	13

Landmarks were digitised on virtual reconstructions of crania created from CT data in AVIZO. The coordinates were exported for use in Morphologika [67] and PAST [68] software. Only one half of the cranium was digitised to remove noise from individual asymmetry. The left side was digitised where there was no difference in preservation; the right was substituted if it was better preserved and mirrored in Morphologika, this allowed larger fossil sample sizes to be included.

In Morphologika, general Procrustes analyses were performed to superimpose sinus-specific landmark coordinate data for each analysis, and then Principal Components Analyses (PCA) were run. The first seven principal components (PCs), accounting for $\geq 70\%$ of variance, were tested for correlations with the relevant relative sinus volumes from the wider sinus volume sample. The 70% variance cut-off point was based on the visualisation of scree plots and scrupu-

tiny of the eigenvalues. Pearson's correlation tests, rather than regression analyses, were used to test for relationships between shape and relative sinus volume to avoid making assumptions about dependent and independent variables as one of the questions of interest is whether sinus size drives craniofacial shape or vice versa.

PC scores from each sinus-specific analysis showing significant correlation with its respective relative sinus volume (see also [35]) were designated frontal or maxillary sinus volume shape parameters (the frontal SVSP and maxillary SVSP) and used in subsequent analyses (Table 5). Relative frontal sinus volume is correlated with PC6 (explaining 7% variance in shape between the samples from the frontal sinus-specific landmark analyses; this is a significant, negative correlation ($r^2 = -0.12$, $P = < 0.001$; remains significant with Bonferroni correction). Relative maxillary sinus volume is correlated with PC3 (explaining 11% of variance)

Table 5 Sinus volume shape parameters (SVSPs) / Paramètres de conformation associés au volume sinusal (SVSP)						
Landmark set	PC	Variance explained (%)	Direction of relationship	r^2	P	Bonferroni correction
Frontal sinus-specific	6	7	Negative	0.12	< 0.001	Yes
Maxillary sinus-specific	3	11	Positive	0.41	< 0.001	Yes

PC: principal component from frontal/maxillary sinus-specific GMM landmark analysis. Bonferroni correction: remains significant if a Bonferroni correction is applied to reduce the likelihood of type II errors / PC : composante principale de l'analyse par morphométrie géométrique des conformations crano faciales spécifiques au sinus frontal/maxillaire. Correction de Bonferroni : est significatif si une correction de Bonferroni est appliquée pour réduire la probabilité d'erreurs de type II

from the maxillary sinus-specific landmark analysis; this is a moderate, significant positive correlation ($r^2 = 0.41$, $P < 0.001$; remains significant with Bonferroni correction).

Wireframe models (Figs 1, 2) were created in Morphologika to visualise shape changes described by SVSPs. Frontal and maxillary SVSPs were used to determine sinus-related

shape differences between taxa. Since it was not the intention of this study to study total craniofacial shape differences between individuals or groups but to focus only on those aspects of shape differences that are related to sinus volume, only relevant PCs with significant relationships with sinus volume (the SVSPs, see Table 5) were analysed. These SVSPs

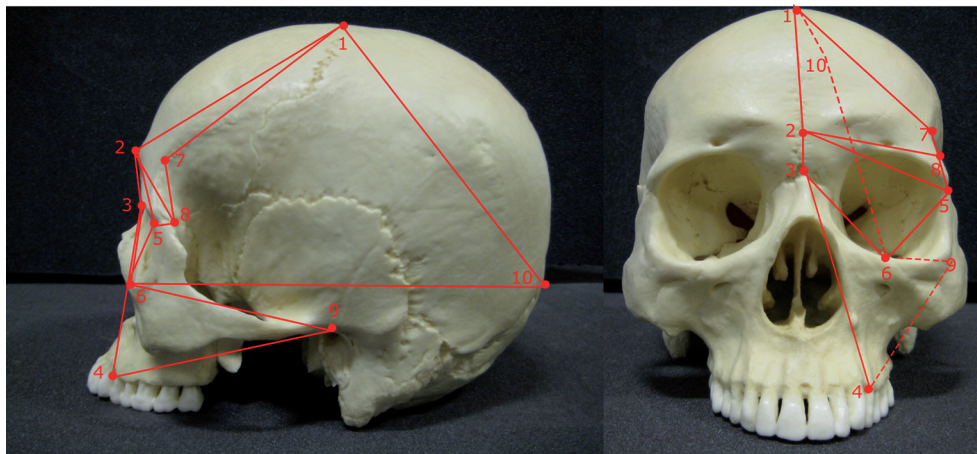


Fig. 1 Landmarks and wireframe used for frontal sinus-specific landmark set. Numbered landmarks (Table 3) of the frontal sinus-specific landmark set seen in *norma lateralis* (left) and *norma frontalis* (right). Wireframe shows which landmarks are joined to illustrate shape changes in later figures. Dashed lines indicate links between landmarks that are not visible when the cranium is shown / Points repères utilisés pour décrire la conformation associée au volume du sinus frontal. Points repères numérotés (Tableau 3) de la conformation craniofaciale spécifique au sinus frontal en *norma lateralis* (à gauche) et *norma frontalis* (à droite). Les points de repère sont reliés pour illustrer les changements de conformation dans les figures ultérieures. Les lignes pointillées indiquent les liens entre les points de repère qui ne sont pas visibles lorsque le crâne est affiché

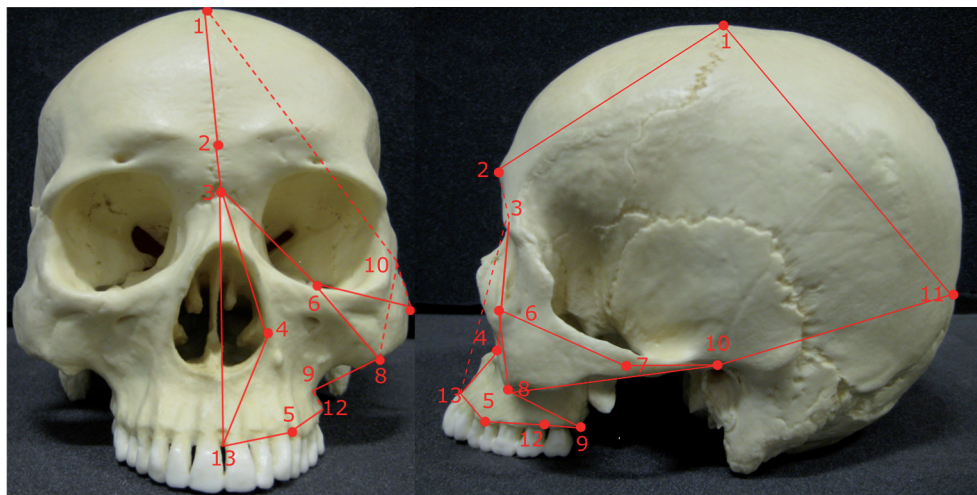


Fig. 2 Landmarks and wireframe used for maxillary sinus-specific landmark set. Numbered landmarks (Table 4) of maxillary sinus-specific landmark seen in *norma frontalis* (left) and *norma lateralis* (right). Wireframe shows which landmarks are joined to illustrate shape changes in later figures. Dashed lines indicate links between landmarks that are not visible when the cranium is shown / Points repères utilisés pour décrire la conformation associée au volume du sinus maxillaire. Points repères numérotés (Tableau 3) de la conformation craniofaciale spécifique au sinus maxillaire observés en *norma frontalis* (à gauche) et *norma lateralis* (à droite). Les points de repère sont reliés pour illustrer les changements de conformation dans les figures ultérieures. Les lignes pointillées indiquent les liens entre les points repère qui ne sont pas visibles lorsque le crâne est affiché

were analysed individually following Zollikofer et al. [35], since this method has been shown to successfully identify relationships between sinus volume and craniofacial shape.

Given the small size of the fossil samples, the distribution of variation in their sinus volumes is unknown. The very unequal size of the samples is also likely to be problematic for parametric statistics. For these reasons, non-parametric permutation tests, ANOSIMs (analysis of similarity), were performed using PAST [68] to ascertain differences in sinus volumes and SVSP (PC) scores between taxa. An ANOSIM is analogous to an ANOVA in that it compares differences within and between groups [68]. Distances are converted to ranks and the test statistic R gives a measure of relative within-group dissimilarity, with more positive numbers showing greater difference [68]. R is interpreted like a correlation coefficient and is a measure of size effect [68]. An effect size of > 0.5 is widely judged to be a large effect [69,70], a convention followed here. Euclidean distances and 9999 permutations were used for ANOSIM analyses.

Results

Sinus Volumes

There are significant differences of moderate size ($R = 0.33$, $P < 0.001$) in relative frontal sinus volumes between taxa (Fig. 3). *H. heidelbergensis* has significantly larger relative frontal sinus volumes than either *H. sapiens* or Neanderthals (Table 6).

There are large, significant differences in relative maxillary sinus volumes (Fig. 3) between taxa ($R = 0.55$, $P < 0.001$). *H. sapiens* has significantly smaller relative maxillary sinus volumes than either Neanderthals or *H. heidelbergensis* (Table 7).

Sinus-Related Shape

In the reduced sample analysed for frontal sinus-related shape (Table 1), the frontal SVSP showed a significant, negative correlation with frontal sinus volume ($r^2 = -0.12$, $P = < 0.001$; remains significant with Bonferroni correction). Craniofacial shapes associated with larger frontal sinuses, configurations with lower scores on the frontal SVSP (Fig. 4, SI Fig. S6), have relatively larger frontal and orbital regions and are taller superoinferiorly in the maxillary region (Fig. 5).

There is a moderate significant difference in frontal SVSP scores (PC scores on PC6, the frontal SVSP, which explains 7% of variation) between taxonomic groups (ANOSIM: $R = 0.45$, $P < 0.005$), due to a significantly higher scores in *H. sapiens* than *H. heidelbergensis* (Fig. 4, Table 8, SI Fig. S6). There are no significant differences in frontal SVSP scores between Neanderthals and other taxa.

In the reduced sample analysed for maxillary sinus-related shape, the maxillary SVSP (PC3, maxillary sinus-specific landmark set, which explains 11% of variation) shows a moderate, significant positive correlation with relative maxillary sinus volume ($r^2 = 0.41$, $P < 0.001$; remains significant with Bonferroni correction). Craniofacial shapes associated with relatively larger maxillary sinuses (i.e., higher scores on the maxillary SVSP, see Fig. 4, SI Fig. S7) have larger, taller, more anteriorly projecting faces relative to their neurocrania than craniofacial shapes associated with relatively smaller maxillary sinuses. The malar region appears superoinferiorly taller in high scoring configurations and the zygomatic arch appears more swept back. Higher scoring configurations also show more dolichocephalic neurocrania (Fig. 6).

There are differences between groups in maxillary sinus-related shape, *H. heidelbergensis* falls beyond the range of variation for other taxa (Fig. 4, SI Fig. S7) and Neanderthals fall at the upper extreme of the *H. sapiens* range of variation. This is reflected in the very strong, significant difference between taxonomic groups in maxillary sinus-related shape (ANOSIM: $R = 0.78$, $P < 0.001$); *H. sapiens* has significantly lower PC scores on this SVSP than either Neanderthals or *H. heidelbergensis* (Table 9).

Discussion

Paranasal hyperpneumatisation has been discussed as a characteristic of both *H. heidelbergensis* [6,8,16,35] and Neanderthals [4,5,27–29] and has been used as an explanation for craniofacial morphology in both taxa [4,6,29]. Conversely, recent research has suggested that compared to *H. sapiens*, Neanderthals are not hyperpneumatised when craniofacial size is taken into account [35–36]. The aim of this study was to determine the nature of pneumatic variation and its relationship to craniofacial shape in mid-late Pleistocene hominins, by using the largest, most representative sample to date and a more comprehensive method than previously employed. The results presented here support the suggestion that frontal hyperpneumatisation is a characteristic of at least some mid-Pleistocene hominins, yet refute the long-standing assertion that Neanderthals are hyperpneumatised. Further, if the results from the smaller craniofacial shape sample can be extended to the wider sinus volume sample, the relationship between craniofacial shape and maxillary sinus volume suggests that the distinctive small, orthognathic *H. sapiens* face has led to peculiarly small maxillary sinuses in this taxon. This may contribute to resolving long-standing arguments about sinus function [45,46].

Frontal Pneumatisation and Associated Craniofacial Shape

The picture of *H. heidelbergensis* frontal pneumatisation from prior research is complicated, in part due to the debate over

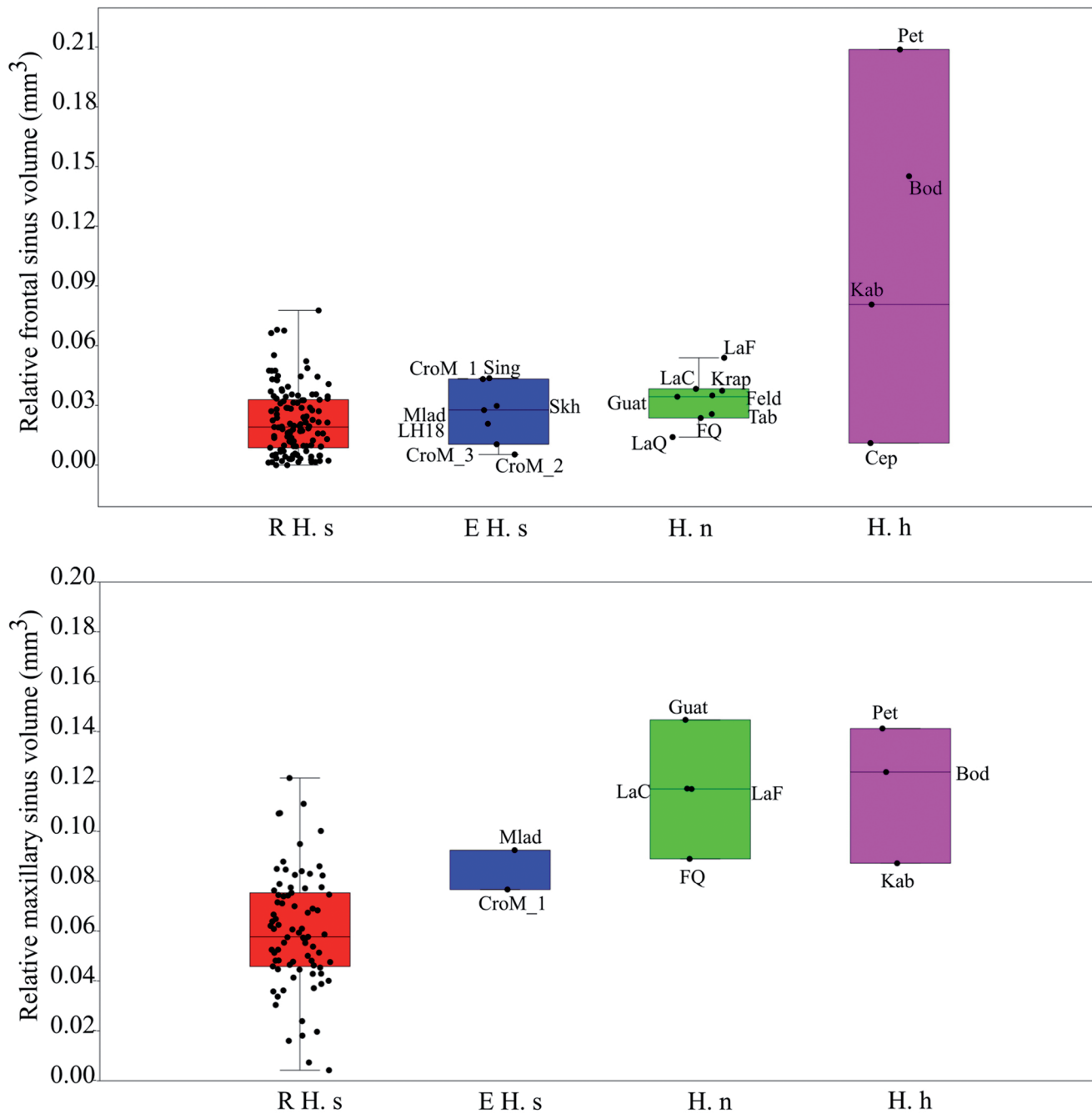


Fig. 3 Variation in sinus size in full sample. Top: relative (size-corrected) frontal sinus volume by taxon. Bottom: relative maxillary sinus volume by taxon. Red, R H. s: recent *H. sapiens*; blue, E H. s: early *H. sapiens*; green, H. n: *H. neanderthalensis*; magenta, H. h: *H. heidelbergensis*. CroM: Cro-Magnon, Sing: Singa, Mlad: Mladeč 1, Skh: Skhul, LaF: La Ferrassie, LaC: La Chapelle, Krap: Krapina, Feld: Feldhofer, Tab: Tabun C1, FQ: Forbes Quarry, LaQ: La Quina, Pet: Petralona, Bod: Bodo, Kab: Broken Hill, Cep: Ceprano. Recent and early *H. sapiens* shown separately in figure, although pooled for analyses following rationale explained in Methods / Variation de la taille des sinus dans l'échantillon complet. En haut : volume relatif du sinus frontal relatif (corrige en fonction de la taille) par taxon. En bas : volume relatif du sinus maxillaire par taxon. Rouge, R H. s: *H. sapiens* récent ; bleu, EH. s: *H. sapiens* ancien ; vert, H. n: *H. neanderthalensis* ; magenta, H. h: *H. heidelbergensis*. CroM : Cro-Magnon, Sing : Singa, Mlad : Mladeč 1, Skh : Skhul, LaF : La Ferrassie, LaC : La Chapelle, Krap : Krapina, Feld : Feldhofer, Tab : Tabun C1, FQ : Forbes Quarry, LaQ : La Quina, Pet : Petralona, Bod : Bodo, Kab : Broken Hill, Cep : Ceprano. Les *H. sapiens* récent et ancien sont montrés séparément dans la figure, mais regroupés dans les analyses suivant la justification expliquée dans la section Méthodes

Table 6 ANOSIM comparing relative frontal sinus volumes between taxa / Résultats de l'ANOSIM comparant les volumes relatifs des sinus frontaux entre les taxons

	<i>H. sapiens</i>	<i>H. neanderthalensis</i>	<i>H. heidelbergensis</i>
<i>H. sapiens</i>		0.05848	0.6914*
<i>H. neanderthalensis</i>	1		0.6930*
<i>H. heidelbergensis</i>	0.0006*	0.0186*	

The matrix is symmetrical; numbers above the trace are R values, and numbers below the trace are p values. *: significant, $\alpha < 0.05$. **Bold:** remains significant if a Bonferroni correction is applied / La matrice est symétrique ; les nombres au-dessus de la trace sont des valeurs de R , les nombres au-dessous de la trace sont des valeurs de p . * : significatif, $\alpha < 0,05$. **Gras** : est significatif si une correction de Bonferroni est appliquée

Table 7 ANOSIM of relative maxillary sinus volume differences between taxa / Résultats de l'ANOSIM comparant les volumes relatifs des sinus maxillaires entre les taxons

	<i>H. sapiens</i>	<i>H. neanderthalensis</i>	<i>H. heidelbergensis</i>
<i>H. sapiens</i>		0.6059*	0.4542*
<i>H. neanderthalensis</i>	0.0001*		-0.0714
<i>H. heidelbergensis</i>	0.0147*	0.5275	

The matrix is symmetrical ; numbers above the trace are R values, and numbers below the trace are p values; *: significant, $\alpha < 0.05$, **Bold:** remains significant if a Bonferroni correction is applied / La matrice est symétrique ; les nombres au-dessus de la trace sont des valeurs de R , les nombres au-dessous de la trace sont des valeurs de p . * : significatif, $\alpha < 0,05$. **Gras** : est significatif si une correction de Bonferroni est appliquée

which specimens should be included in the hypodigm. Petralona, Bodo and Broken Hill are all known for their large frontal sinuses [6,8,35], and similar claims have also been made for other putative *H. heidelbergensis*, such as Steinheim [8], although the current authors see little support for this latter claim based on their examination of the Steinheim CT data. Other middle Pleistocene specimens, such as Ceprano [71] and Arago 21 [48,72–74], do not necessarily show the same pattern. Arago 21 is a key fossil in the *H. heidelbergensis* hypodigm, linking the mandibular (including the type specimen) and cranial material [13,18,20]. Although Arago 21 was unavailable for inclusion in this study, there is evidence from the literature that its frontal sinuses are small [48,72–74]. They also appear to form two widely separated cells that fail to pneumatise the frontal squama [74], which is qualitatively and quantitatively different from the sinuses in Broken Hill/Bodo/Petralona, but similar those of Ceprano (Fig. 7). Interestingly, Ceprano and Arago 21 are also shown to be distinctive and closely linked in other recent morphological analyses [10], distancing them from the main Euro-African *H. heidelbergensis* hypodigm (*sensu* Rightmire and Stringer [16,20,75,76]), and supporting a link between external crano-facial shape and frontal sinus form. Thus, from the literature it appears that, despite variation, at least a core group of middle Pleistocene *Homo* from both Europe and Africa show hyperpneumatised frontal sinuses.

Given the debate surrounding the taxonomic validity of *H. heidelbergensis*, it is difficult to interpret the variation within the mid-Pleistocene sample. If these specimens constitute a single species, the results of the current study support the assertion that the frontal sinuses of *H. heidelbergensis*, relative to those of other fossil and recent hominins, are hyperpneumatised. Most, but not all, of the putative *H. heidelbergensis* individuals analysed have exceptional frontal pneumatisation, and their overall relative frontal sinus volumes are significantly greater than of the *H. sapiens* or Neanderthal samples. Although one recent *H. sapiens* has frontal pneumatisation comparable with Broken Hill, nothing in the entire sample (the largest used for a similar study to date) has frontal pneumatisation comparable with Bodo or Petralona. The shape and extension of the frontal sinuses of all the putative *H. heidelbergensis* in this study, except Ceprano (Fig. 7), appear similar and seem qualitatively different from those of the other taxa in the present study, and Ceprano has plausibly been excluded from the *H. heidelbergensis* hypodigm based on its cranofacial shape [10,14,41,71,77]. There is a high degree of variation in recent *H. sapiens* sinuses [6,78,79], and although *H. sapiens* may be a particularly variable species [80], we should expect at least some variation in *H. heidelbergensis*, particularly given the probable temporal range for the fossil specimens in the sample [75,81]. Even taking this expected

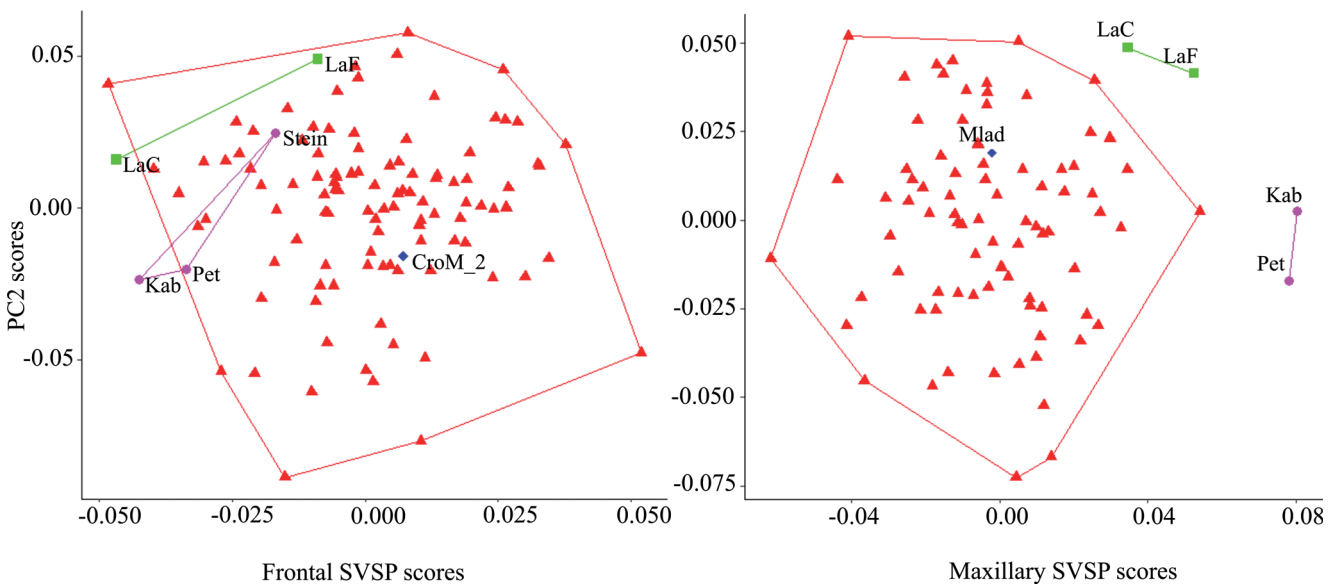


Fig. 4 Variation in sinus-specific craniofacial shape in reduced sample (Table 1). Left: PCA showing frontal sinus-related craniofacial shape (Frontal SVSP, PC6 of the frontal sinus-specific landmark set analysis explaining 7% of variance) on x-axis. Right: PCA of maxillary sinus-related craniofacial shape (Maxillary SVSP, PC3 of the maxillary sinus-specific landmark set analyses explaining 11% of variance) on x-axis. SVSPs (x-axes) are shown against PC2 on y-axes as this spreads the data more than PC1 and aids visualisation of group differences, PC2 is not correlated with frontal or maxillary sinus volume. Red triangles, R H. s: recent *H. sapiens*; blue diamonds, E. H. s: early *H. sapiens*; green squares, H. n: *H. neanderthalensis*; magenta circles, H. h: *H. heidelbergensis*. Recent and early *H. sapiens* shown separately in figure, although pooled for analyses following rationale explained in Methods. For shape changes described by frontal and maxillary SVSPs, see Fig. 5, 6. Fossil names as above / *Variation de la forme crano-faciale sinus-spécifique dans l'échantillon réduit* (Tableau 1). À gauche : ACP montrant la forme crano-faciale associée avec le sinus frontal (SVSP frontal, CP6 de l'analyse du sinus frontal) sur l'axe des x. À droite : ACP de la forme crano-faciale associée avec le sinus maxillaire (Maxillary SVSP, CP3 des analyses du sinus maxillaire) sur l'axe des x. Les SVSP (axes x) sont représentés par rapport à la CP2 sur les axes y, car cela répartit mieux les données que la CP1 et facilite la visualisation des différences entre groupes, CP2 n'est pas corrélé avec le volume sinusal frontal ou maxillaire. Triangles rouges, R H. s : *H. sapiens* récent; diamants bleus, E.H. s : *H. sapiens* ancien; carrés verts, H. n : *H. neanderthalensis* ; cercles magenta, H. h : *H. heidelbergensis*. Les *H. sapiens* récent et ancien sont montrés séparément sur la figure, mais regroupés dans les analyses suivant la justification expliquée dans la section Méthodes. Pour les changements de conformations décrits par les SVSP frontal et maxillaire, voir les figures 5, 6. Noms de fossiles comme ci-dessus

variation into account, the results from the current study suggest that either *H. heidelbergensis* as a species exhibits hyperpneumatised frontals compared to *H. sapiens* and Neanderthals, or that there is a polyphyletic group of mid-Pleistocene hominins from Europe and Africa who share hyperpneumatised frontal sinuses through convergent evolution. The latter is perhaps a more interesting question for the discussion of sinus function, as it could open interesting investigations as to which aspects of ecology (if the sinuses are functional) or craniofacial shape (if the sinuses are spandrels) these specimens share that could have led to hyperpneumatisation. Conversely, these differences in sinus morphology may be due to genetic drift, which should be the null hypothesis for any such future studies [82].

The statements above assume that hyperpneumatisation is not the primitive condition, yet based on the evidence to

date, this is uncertain, given the equivocal knowledge of sinus volume in *H. erectus*. The one *H. erectus* specimen available for sinus volume measurement in the current study (KNM-ER 3883, not included in statistical and shape analyses as the sole representative of its taxon) has a similar relative frontal sinus volume to Broken Hill. Taken alone, this would suggest that large frontal sinuses may be the primitive condition [83]. Where it is sufficiently preserved, however, the African *H. erectus* sample in fact suggests that small frontal sinuses restricted to the supraorbital region are the norm for *H. erectus* [84] and the majority of Asian *H. erectus* also have small frontal sinuses that do not extend superiorly past the glabellar region [48,72,74,85–88]. Thus, the general impression is of a small frontal sinus in *H. erectus*, with some exceptions such as KNM-ER 3833, quite different from the morphology of at least most

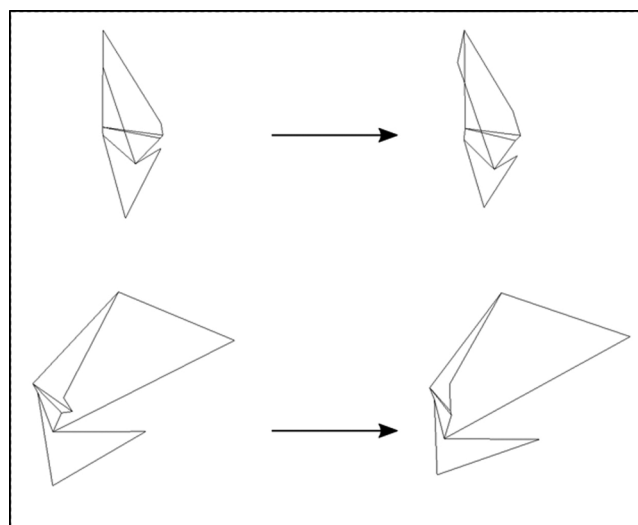


Fig. 5 Shape changes along maxillary sinus volume shape parameter (SVSP). Wireframe (Fig. 2) created in Morphologika showing shape changes in maxillary sinus-specific landmark configurations along the maxillary SVSP. Left: mean configuration warped to lowest extreme of SVSP, right: mean configuration warped to highest extreme of SVSP. Top: *norma frontalis*, middle: *norma lateralis* / *Changements de conformation du paramètre de forme du volume sinusal (SVSP) maxillaire. Configuration de landmarks spécifique des sinus maxillaires (Fig. 2) montrant les changements de conformations par rapport au SVSP maxillaire. Gauche : Conformation moyenne déformée pour l'extrême inférieure de SVSP (Fig. 4). En haut : norma frontalis, milieu : norma lateralis*

H. heidelbergensis specimens, as shown in this study. This suggests that frontal hyperpneumatisation is derived in some mid-Pleistocene hominins.

In addition to the clear difference in relative frontal sinus volumes discussed above, inter-taxonomic differences were also found in the reduced sample analysis of frontal sinus-related craniofacial shape (*H. heidelbergensis* sample: Broken Hill and Petralona). It has been argued that hyperpneumatisation is a cause of the distinctive *H. heidelbergensis*

craniofacial shape [6]. Conversely, the shape of the frontal bone [74], the orbital [35] and supraorbital regions [79] have been suggested as influences on frontal sinus form. In the reduced *H. heidelbergensis* sample, specimens show significant differences in frontal sinus-related craniofacial shape from *H. sapiens*: *H. heidelbergensis* specimens have taller supraorbital regions and deeper, taller faces than *H. sapiens*. *H. heidelbergensis* specimens often have remarkably large supraorbital tori [16] and, in common with earlier *Homo*, *H. heidelbergensis* fossils have larger faces than either *H. sapiens* or Neanderthals [17]. The particularly small, retracted face of *H. sapiens* is more derived, compared to earlier *Homo*, than the distinctive face of Neanderthals [89,90]. It is likely that the analyses of frontal sinus-related craniofacial shape in the current study reflect these differences between *H. sapiens* and *H. heidelbergensis*. The lack of a difference in this variable between *H. heidelbergensis* and Neanderthals may be caused by an insufficient number of landmarks to pick up on this relatively smaller shape difference.

The statistical difference between taxa in the frontal sinus-related shape analysis has a smaller effect size than for frontal sinus volume analysis. This could be construed as suggesting that the greater size of *H. heidelbergensis* frontal sinuses compared to *H. sapiens* is not only because of their differences in craniofacial shape (contra [3,101,107]) and could even perhaps be interpreted as supporting the idea that differences in craniofacial shape between *H. heidelbergensis* and *H. sapiens* are affected by degree of frontal pneumatisation (cf. [6,7]). However, the relatively few landmarks used in the present study could affect the quality of the shape data captured and the results may be affected by sample composition. Therefore, conclusions about the relative sizes effects in the two types of data should be made with caution pending further investigation. It seems unlikely that differences in pneumatisation lead to the differences in supraorbital form between *H. sapiens* and *H. heidelbergensis*, given that Neanderthals and *H. erectus* both have larger (although differently shaped) supraorbital

Table 8 ANOSIM of taxonomic position on the frontal SVSP / *Résultats de l'ANOSIM comparant la position taxonomique sur le SVSP frontal*

	<i>H. sapiens</i>	<i>H. neanderthalensis</i>	<i>H. heidelbergensis</i>
<i>H. sapiens</i>		0.311	0.591*
<i>H. neanderthalensis</i>	0.194		-0.25
<i>H. heidelbergensis</i>	0.015*	1	

Matrix is symmetrical; numbers above trace are *R* values, and numbers below trace are *p* values. *: significant, $\alpha < 0.05$. **Bold**: remains significant if a Bonferroni correction is applied / La matrice est symétrique ; les nombres au-dessus de la trace sont des valeurs de *R*, les nombres au-dessous de la trace sont des valeurs de *p*. *: significatif, $\alpha < 0,05$. **Gras** : est significatif si une correction de Bonferroni est appliquée

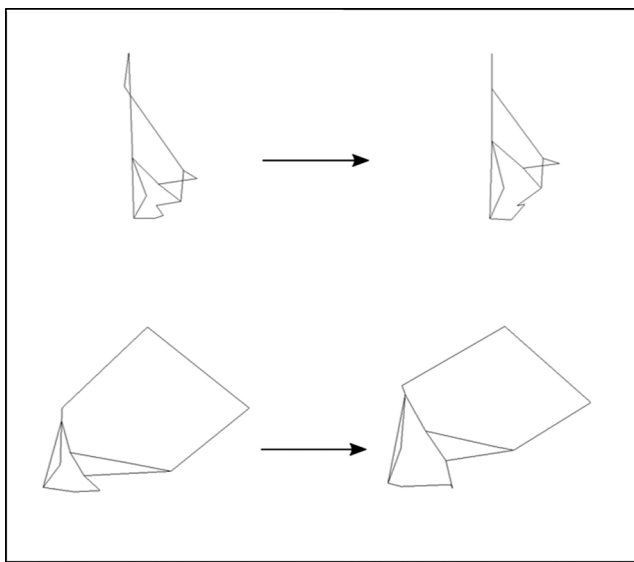


Fig. 6 Shape changes along frontal sinus volume shape parameter (SVSP). Wireframe (Fig. 1) created in Morphologika showing shape changes in frontal sinus-specific landmark configuration along the frontal SVSP. Left: mean configuration warped to lowest extreme of SVSP, right: mean configuration warped to highest extreme of SVSP (Fig. 4). Top: *norma frontalis*, middle: *norma lateralis* / *Changements de conformation du paramètre de forme du volume sinusal (SVSP) frontal. Configuration de landmarks spécifique des sinus frontaux (Fig. 1) montrant les changements de conformations par rapport au SVSP frontal. Gauche : Conformation moyenne déformée pour l'extrême inférieur de SVSP, à droite : Conformation moyenne déformée pour l'extrême supérieur de SVSP (Fig. 4). En haut : norma frontalis, milieu : norma lateralis*

tori than *H. sapiens*, yet show no relative difference in frontal sinus volume compared to *H. sapiens*.

Contrary to traditional theories regarding the cause of the supraorbital tori in Neanderthals [4,29], but in accordance with more recent findings [35–37], Neanderthal frontal sinuses were not found to be relatively larger than those of *H. sapiens*, and thus Neanderthal frontal sinuses are not

hyperpneumatised. This is despite the much greater size and geographic range of the *H. sapiens* sample in the current study compared with previous research [35–37]. Several studies, including this one, have now shown that Neanderthals do not have relatively larger frontal sinus volumes than *H. sapiens*, and there is thus no evidence that differences between *H. sapiens* and Neanderthal supraorbital shape are caused by large frontal sinuses (c.f., [9,22,105]). It seems reasonable, therefore, that this idea should be abandoned. What were asserted to be large sinuses in Neanderthals were used for many years to prop up theories that the Neanderthal face resulted from cold adaptation [4,29,30]. The lack of evidence for Neanderthal hyperpneumatisation thus also weakens the argument that their craniofacial shape is the result of hyperpolar adaptation [36,91], (but see [92]). Although these results do not necessarily rule out the possibility that relatively extreme pneumatisation was due to cold adaptation at some point in *H. heidelbergensis* evolution (depending on the location, and environmental conditions, of the origin of this taxon), experimental [34] and naturalistic [33] data from other primates/mammals strongly suggest that relative sinus size would not have increased in response to low temperatures.

Maxillary Pneumatisation and Associated Craniofacial Shape

In contrast to their frontal pneumatisation, *H. heidelbergensis* specimens in the current study do not show distinctively large maxillary sinuses compared to closely related species. However, *H. sapiens* do have significantly smaller relative maxillary sinus volumes than the other taxa (Fig. 8). This provides novel evidence that *H. sapiens* has hypopneumatised maxillary sinuses compared to its closest congeners. This is contrary to previous research, which not only suggested that *H. heidelbergensis* maxillary sinuses are distinctively large [e.g. 77], but also that maxillary hyperpneumatisation is a diagnostic feature and a cause of Neanderthal craniofacial morphology [e.g. 21].

Table 9 ANOSIM of taxonomic position on the maxillary SVSP / *Résultats de l'ANOSIM comparant la position taxonomique sur le SVSP maxillaire*

	<i>H. sapiens</i>	<i>H. neanderthalensis</i>	<i>H. heidelbergensis</i>
<i>H. sapiens</i>		0.9599*	0.6119*
<i>H. neanderthalensis</i>	0.0001*		1
<i>H. heidelbergensis</i>	0.0062*	0.3447	

Matrix is symmetrical; numbers above trace are *R* values, and numbers below trace are *p* values. *: significant, $\alpha < 0.05$, **Bold**: remains significant if a Bonferroni correction is applied / *La matrice est symétrique ; les nombres au-dessus de la trace sont des valeurs de R, les nombres au-dessous de la trace sont des valeurs de p. * : significatif, $\alpha < 0.05$. Gras : est significatif si une correction de Bonferroni est appliquée*

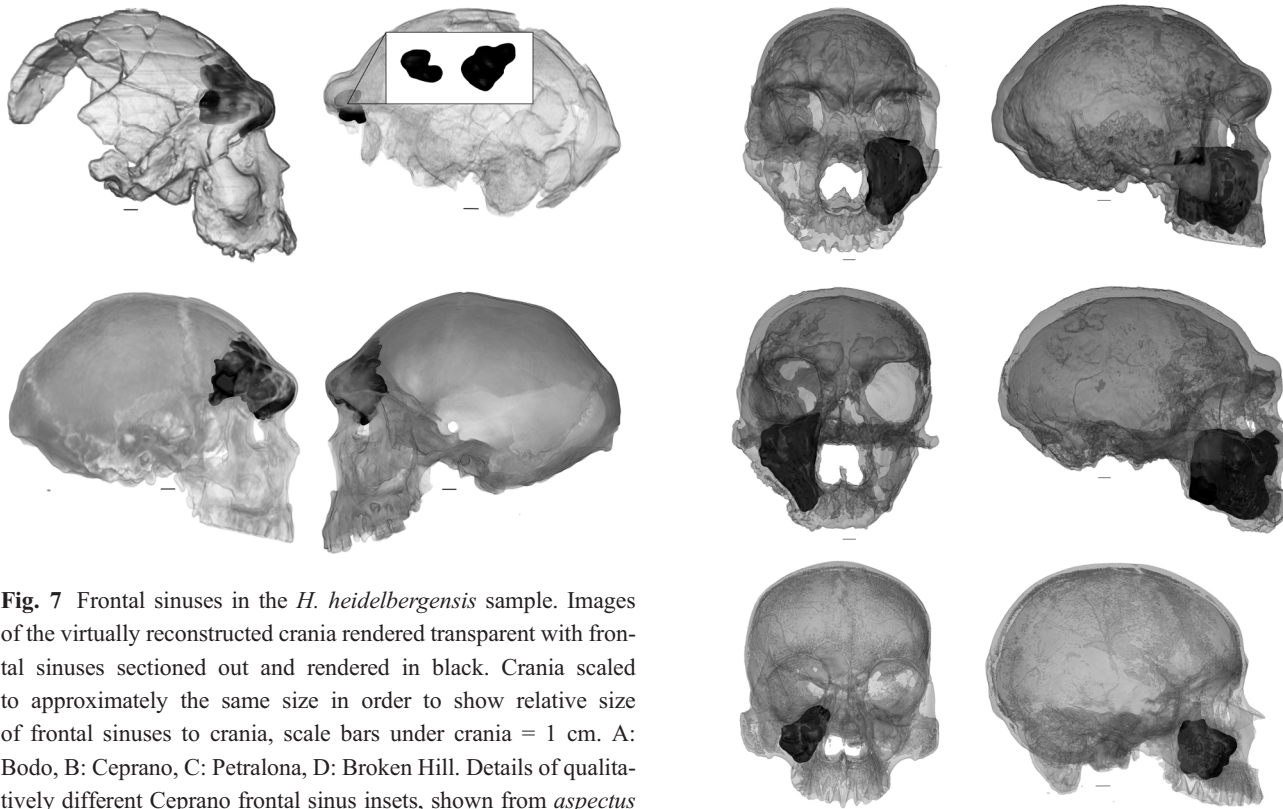


Fig. 7 Frontal sinuses in the *H. heidelbergensis* sample. Images of the virtually reconstructed crania rendered transparent with frontal sinuses sectioned out and rendered in black. Crania scaled to approximately the same size in order to show relative size of frontal sinuses to crania, scale bars under crania = 1 cm. A: Bodo, B: Ceprano, C: Petralona, D: Broken Hill. Details of qualitatively different Ceprano frontal sinus insets, shown from *aspectus superialis*. With the exception of Ceprano, all four specimens' frontal sinuses are single and continuous / *Les sinus frontaux dans l'échantillon des H. heidelbergensis. Images du crâne reconstruit montrant les sinus frontaux en noir. Les crânes ont été mis approximativement à la même échelle afin de montrer la taille relative des sinus frontaux par rapport aux crânes = 1 cm. A : Bodo, B : Ceprano, C : Petralona, D : Broken Hill. Détail de l'insert du sinus frontal de Ceprano dont la forme est différente, montré en aspectus superialis. À l'exception de Ceprano, les sinus frontaux des quatre spécimens sont continus*

In addition to differences between taxa in the full maxillary sinus volume sample, differences were also found in the reduced sample used in the maxillary sinus-related shape analyses between *H. sapiens* and the other taxa. Differences in maxillary sinus-related craniofacial shape coincide with some of the differences that are well-established as diagnosing *H. sapiens*: differences in neurocranial globularity, facial size and flatness [38–43,93]. The strength of the shape differences resulting from these derived characteristics in *H. sapiens* is demonstrated by their identification by the present analyses, despite the relatively few landmarks used and the fact that the maxillary sinus-specific shape variable does not describe the greatest shape variation in the sample (it is PC3, explaining 11% of variance). The characteristic shape of *H. sapiens* (as described by the maxillary sinus-related shape variable) is associated with smaller maxillary

Fig. 8 A comparison of maxillary sinuses between species. Virtual reconstructions of crania showing sectioned out maxillary sinuses rendered in black in (A–C) Petralona (*H. heidelbergensis*), Guattari (*H. neanderthalensis*) and a recent *H. sapiens* from Mexico. Left view: *norma frontalis*, right view: *norma lateralis*. The *norma lateralis* view for Petralona is flipped horizontally for consistency and ease of comparison, since only the left maxillary sinus is fully preserved in this fossil. Crania scaled to approximately the same size in order to show relative size of maxillary sinuses, scale bars under crania = 1 cm / *Comparaison des sinus maxillaires entre les espèces. Reconstructions virtuelles de crânes montrant les sinus maxillaires en noir (A–C) Petralona (H. heidelbergensis), Guattari (H. neanderthalensis) et un H. sapiens récent du Mexique. À gauche : norma frontalis, à droite : norma lateralis. La vue en norma lateralis pour Petralona est inversée horizontalement pour faciliter la comparaison, puisque seul le sinus maxillaire gauche est entièrement préservé chez ce fossile. Les crânes ont été mis à l'échelle pour apparaître approximativement à la même taille afin de montrer la taille relative des sinus maxillaires, les barres d'échelle sous les crânes = 1 cm*

sinuses. Despite the reduced sample size, the size effect of the difference between *H. sapiens* and Neanderthals/*H. heidelbergensis* in maxillary sinus-associated shape is much larger than that of the difference in the relative maxillary sinus volumes themselves. This offers important evidence that the derived facial shape of *H. sapiens* leads

to the distinctively small maxillary sinuses seen in our species. These results may also support theories suggesting the maxillary sinuses are in themselves functionless, their volume resulting from surrounding craniofacial form [33,58,60,94,95].

Conclusions

This study aimed to test the hypotheses that there are differences in sinus size between mid-late Pleistocene hominin taxa and that these differences are related to craniofacial shape. Sinus volume and sinus volume-associated craniofacial shape in mid-late Pleistocene hominins were compared to investigate variation in paranasal pneumatisation and its effect on craniofacial form. As construed in this study, *H. heidelbergensis* on average has a hyperpneumatised frontal compared to Neanderthals and *H. sapiens*, although it is not of homogenous size throughout the taxon as currently described. In addition to sinus volume differences, there are differences between taxa in frontal sinus-related craniofacial shape. These differences are related to supraorbital torus and facial size differences used to differentiate *H. heidelbergensis* from *H. sapiens* and Neanderthals [42,89,90]. Larger taxonomic differences in frontal sinus-related shape than in volumes themselves could be argued to offer support for the assertion that hyperpneumatisation has shaped the distinctive craniofacial shape of these specimens [6,7], but this seems implausible given the similarly sized external, but not internal, supraorbital morphology of Neanderthals and *H. erectus*. Contrary to long-standing beliefs about frontal hyperpneumatisation in Neanderthals, Neanderthals do not have larger relative frontal sinuses than *H. sapiens*. This negates the role of the frontal sinuses in the large supraorbital tori of Neanderthals and does not support theories explaining distinctive Neanderthal craniofacial form as resulting from hyperpolar adaptation via pneumatisation.

In contrast to their enlarged frontal sinuses, the maxillary sinuses of *H. heidelbergensis* are not hyperpneumatised. Conversely, it can be said that the maxillary sinuses of *H. sapiens* are hypopneumatised compared to Neanderthals /*H. heidelbergensis*. The greater size effect of the taxonomic difference in facial shape, compared to the difference in sinus size itself, suggests that this is a characteristic that can be explained partly by the distinctive craniofacial shape of our species. This finding overturns historical pneumatic explanations for Neanderthal maxillary shape, as the lack of significant difference in relative frontal sinus volumes between Neanderthals and *H. sapiens* does for Neanderthal supraorbital shape. The relationship between relative maxillary sinus volume and maxillary sinus-related craniofacial shape provides support for the hypothesised relationship between craniofacial shape and maxillary sinus

size, but suggests that it is craniofacial shape that is the driver of maxillary sinus size, rather than the converse. This may support assertions that the maxillary sinuses are functionless, but act as zones of accommodation, allowing modularity in the cranium [33,58,60,94,95]. The difference in relationship between face shape and sinus volume in frontal and maxillary sinuses within these taxa supports the assertion [48,72] that the different individual sinuses may be modular and their size governed by different stimuli.

Acknowledgements We would like to thank Antoine Balzeau and an anonymous reviewer for their constructive comments and the editor for help with French translation. LTB thanks the University of Roehampton, The Primate Society of Great Britain (Charles A. Lockwood Memorial Prize), and The Leakey Trust for funding. CBS's research is supported by the Calleva Foundation and the Human Origins Research Fund of the Natural History Museum, London. For kind permission to access specimens and help in collecting CT data, all the authors thank Robert Kruszynski, Richie Abel, Farah Ahmed, Dan Sykes, Margaret Clegg and Heather Bonney at the Natural History Museum; Janet Monge and Tom Schoenemann at the University of Pennsylvania; Phillippe Mennevier, Alain Fromment and Antoine Balzeau at the Musée de l'Homme, Paris; Thomas Koppe at the Ernst-Moritz-Arndt University, Greifswald; Christoph Zollikofer at the University of Zurich; Amelie Vialet and Henry de Lumley at the Institut de Paléontologie Humaine, Paris; Giorgio Manzi at Università La Sapienza, Rome; Gerhard Weber at the University of Vienna; George Koufos at the Aristotle University of Thessaloniki; Luca Bondioli at the Museo Nazionale Preistorico Etnografico 'Luigi Pigorini', Rome; and Andreas Pasteroors at the Neanderthal Museum, Mettmann.

Conflict of interest : The authors declare do not have any conflict of interest.

References

- Gray HG (1997) Gray's anatomy. The Promotional Reprint Company Ltd, London
- Negus SV (1957) The function of the paranasal sinuses. Arch Otolaryngol 66:430–42
- Rae TC (2008) Paranasal pneumatization in extant and fossil Cercopithecoidea. J Hum Evol 54:279–86
- Coon CS (1962) The origin of races. Alfred A. Knopf, New York
- Brose DS, Wolpoff MH (1971) Early Upper Paleolithic man and Late Middle Paleolithic tools. Am Anthropol 73:1156–94
- Seidler H, Falk D, Stringer C, et al (1997) A comparative study of stereolithographically modelled skulls of Petralona and Broken Hill: implications for future studies of middle Pleistocene hominid evolution. J Hum Evol 33:691–703
- Bookstein F, Schäfer K, Prossinger H, et al (1999) Comparing frontal cranial profiles in archaic and modern *Homo* by morphometric analysis. Anat Rec 257:217–24

8. Prossinger H, Seidler H, Wicke L, et al (2003) Electronic removal of encrustations inside the Steinheim cranium reveals paranasal sinus features and deformations, and provides a revised endocranial volume estimate. *Anat Rec* 273:132–42
9. Freidline SE, Gunz P, Harvati K, et al (2012) Middle Pleistocene human facial morphology in an evolutionary and developmental context. *J Hum Evol* 63:723–40
10. Mounier A, Caparros M (2015) The phylogenetic status of *Homo heidelbergensis* — a cladistic study of Middle Pleistocene hominins. *Bull Mem Soc Anthropol Paris* 27:110–34
11. Roksandic M, Radović P, Lindal J (2017) Revising the hypodigm of *Homo heidelbergensis*: a view from the Eastern Mediterranean. *Quat Int* 466:66–81
12. Arsuaga JL, Martínez I, Arnold LJ, et al (2014) Neandertal roots: cranial and chronological evidence from Sima de los Huesos. *Science* 344:1358–63
13. Mounier A, Marchal F, Condemi S (2009) Is *Homo heidelbergensis* a distinct species? New insight on the Mauer mandible. *J Hum Evol* 56:219–46
14. Mounier A, Condemi S, Manzi G (2011) The stem species of our species: a place for the archaic human cranium from Ceprano, Italy. *PLoS One* 6:e18821
15. Friess M (2010) Calvarial shape variation among Middle Pleistocene hominins: an application of surface scanning in palaeoanthropology. *Comptes Rendus Palevol* 9:435–43
16. Stringer C (2012) The status of *Homo heidelbergensis* (Schoetensack 1908). *Evol Anthropol* 21:101–7
17. Rightmire GP (2013) *Homo erectus* and Middle Pleistocene hominins: brain size, skull form, and species recognition. *J Hum Evol* 65:223–52
18. Buck LT, Stringer CB (2014) *Homo heidelbergensis*. *Curr Biol* 24:R214–5
19. Profico A, Di Vincenzo F, Gagliardi L, et al (2016) Filling the gap. Human cranial remains from Gombore II (Melka Kunture, Ethiopia; ca. 850 ka) and the origin of *Homo heidelbergensis*. *J Anthropol Sci* 94:1–24
20. Rightmire GP (2008) *Homo* in the middle pleistocene: Hypodigms, variation, and species recognition. *Evol Anthropol* 17:8–21
21. Vandersmeersch B (1985) The origin of the Neandertals. In: Delson E (ed) Ancestors: the hard evidence. Alan R. Liss, New York, pp 306–9
22. Tattersall I, Schwartz JH (2006) The distinctiveness and systematic context of *Homo neanderthalensis*. In: Harvati K, Harrison T (eds) Neandertals revisited: new approaches and perspectives. Springer, Berlin, pp 9–22
23. Balzeau A, Rougier H (2010) Is the suprainiac fossa a Neandertal autapomorphy? A complementary external and internal investigation. *J Hum Evol* 58:1–22
24. Delson E, Stringer C (1985) Middle Pleistocene hominid variability and the origin of late Pleistocene humans. In: Delson E (ed) Ancestors: the hard evidence. Alan R. Liss, New York, pp 289–95
25. Klein RG (1999) The human career: human biological and cultural origins, University of Chicago Press, Chicago
26. Hublin JJ (1998) Climatic changes, paleogeography and the evolution of the Neanderthals. In: Akazawa O, Aoki T, Bar-Yosef K (eds) Neanderthals and modern humans in western Asia. Plenum Press, pp 295–310
27. Busk G (1865) On a very ancient human cranium from Gibraltar. *Rep 34th Meet. Br Assoc Adv Sci Bath* 1864:91–2
28. Blake CC (1864) Climatic conditions for the last Neanderthals: herpetofaunal record of Gorham's Cave, Gibraltar. *J Anthropol Soc London* 2:cxxxix–clvii
29. Wolpoff MH (1999) Paleoanthropology. McGraw-Hill, New York
30. Churchill SE (1998) Cold adaptation, heterochrony, and Neandertals. *Evol Anthropol* 7:46–60
31. Koertvelyessy T (1972) Relationships between the frontal sinus and climatic conditions: a skeletal approach to cold adaptation. *Am J Phys Anthropol* 37:161–72
32. Shea BT (1977) Eskimo craniofacial morphology, cold stress and the maxillary sinus. *Am J Phys Anthropol* 47:289–300
33. Rae TC, Hill RA, Hamada Y, et al (2003) Clinal variation of maxillary sinus volume in Japanese macaques (*Macaca fuscata*). *Am J Primatol* 59:153–8
34. Rae TC, Vidarsdóttir US, Jeffery N, et al (2006) Developmental response to cold stress in cranial morphology of *Rattus*: implications for the interpretation of climatic adaptation in fossil hominins. *Proc R Soc London B* 273:2605–10
35. Zollikofer CPE, Ponce De León MS, Schmitz RW, et al (2008) New insights into mid-late Pleistocene fossil hominin paranasal sinus morphology. *Anat Rec* 291:1506–16
36. Rae TC, Koppe T, Stringer CB (2011) The Neanderthal face is not cold adapted. *J Hum Evol* 60:234–9
37. Noback ML, Samo E, van Leeuwen CHA, et al (2016) Paranasal sinuses: a problematic proxy for climate adaptation in Neandertals. *J Hum Evol* 97:176–9
38. Lieberman DE (1998) Neanderthal and early modern human mobility patterns: comparing archaeological and anatomical evidence. In: Akazawa O, Aoki T, Bar-Yosef, K (eds) Neanderthals and modern humans in western Asia. Plenum Press, pp 263–75
39. Lieberman DE (2002) Speculations about the selective basis for modern human craniofacial form. *Evol Anthropol* 17:55–68
40. Lieberman DE, McBratney BM, Krovitz G (2002) The evolution and development of cranial form in *Homo sapiens*. *Proc Natl Acad Sci USA* 99:1134–9
41. Stringer C (2002) Modern human origins: progress and prospects. *Philos Trans R Soc B Biol Sci* 357:563–79
42. Stringer C (2012) Evolution: what makes a modern human. *Nature* 485:33–5
43. Pearson OM (2008) Statistical and biological definitions of ‘anatomically modern’ humans: Suggestions for a unified approach to modern morphology. *Evol Anthropol* 17:38–48
44. Stringer CB, Buck LT (2014) Diagnosing *Homo sapiens* in the fossil record. *Ann Hum Biol* 41:312–22
45. Blaney S (1990) Why paranasal sinuses? *J Laryngol Otol* 104:690–3
46. Márquez S (2008) The paranasal sinuses: the last frontier in craniofacial biology. *Anat Rec* 291:1350–61
47. Rae TC, Koppe T, Spoor F, et al (2002) Ancestral loss of the maxillary sinus in Old World monkeys and independent acquisition in *Macaca*. *Am J Phys Anthropol* 117:293–6
48. Tillier AM (1975) Les sinus craniens chez les hommes actuels et fossiles: essai d'interprétation. Université de Paris-VI, Paris
49. Balzeau A, Buck LT, Grimaud-Hervé D, et al (2017) The internal cranial anatomy of the Middle Pleistocene Broken Hill 1 cranium. *PaleoAnthropol* 2017:107–38
50. Buck LT (2015) Craniofacial morphology, adaptation and paranasal sinuses in Pleistocene hominins. PhD thesis, University of Roehampton, London
51. Green RE, Krause J, Briggs AW, et al (2010) A draft sequence of the Neandertal genome. *Science* 328:710–22
52. Sánchez-Quijano F, Botigué LR, Civit S, et al (2012) North African populations carry the signature of admixture with Neandertals. *PLoS One* 7: e47765
53. Prüfer K, Racimo F, Patterson N (2014) The complete genome sequence of a Neanderthal from the Altai Mountains. *Nature* 505:43–9
54. Jolly CJ (2009) Mixed signals: Reticulation in human and primate evolution. *Evol Anthropol* 18:275–81
55. Tattersall I, Schwartz JH (1998) Morphology, Paleoanthropology and Neandertals. *Anat Rec* 253:113–7

56. Harvati K (2003) The Neanderthal taxonomic position: models of intra- and inter-specific craniofacial variation. *J Hum Evol* 44:107–32
57. Harvati K, Frost SR, McNulty KP (2004) Neanderthal taxonomy reconsidered: implications of 3D primate models of intra- and interspecific differences. *Proc Natl Acad Sci USA* 101:1147–52
58. Butaric LN, McCarthy RC, Broadfield DC (2010) A preliminary 3D computed tomography study of the human maxillary sinus and nasal cavity. *Am J Phys Anthropol* 143:426–36
59. Balzeau A, Grimaud-Hervé D (2006) Cranial base morphology and temporal bone pneumatization in Asian *Homo erectus*. *J Hum Evol* 51:350–9
60. Butaric LN, Maddux SD (2016) Morphological covariation between the maxillary sinus and midfacial skeleton among sub-Saharan and circumpolar modern humans. *Am J Phys Anthropol* 160:483–97
61. Profico A, Schlager S, Valoriani V (2018) Reproducing the internal and external anatomy of fossil bones: two new automatic digital tools. *Am J Phys Anthropol* 166:979–86
62. White TD, Folkens PA (2005) The human bone manual. Elsevier Academic Press, Burlington, MA
63. Lund VJ (1988) The maxillary sinus in the higher primates. *Acta Otolaryngol* 105:163–71
64. Koppe T, Nagai H, Rae TC (1999) Factors in the evolution of the primate paranasal sinuses. In: Koppe T, Nagai, H, Alt KW (eds) The paranasal sinuses of higher primates: development, function and evolution. Quintessence, Chicago, pp 151–75
65. Holton NE, Yokley TR, Franciscus RG (2011) Climatic adaptation and Neandertal facial evolution: a comment on Rae et al (2011). *J Hum Evol* 61:624–7, author reply 628–9
66. Schroeder L, Ackermann RR (2017) Evolutionary processes shaping diversity across the *Homo* lineage. *J Hum Evol* 111:1–17
67. O'Higgins P, Jones N (1998) Facial growth in *Cercocebus torquatus*: an application of three-dimensional geometric morphometric techniques to the study of morphological variation. *J Anat* 193:251–72
68. Hammer Ø, Harper D, Ryan P (2001) PAST: Paleontological statistics software package for education and data analysis. *Palaeontol Electronica* 4:9
69. Cohen J (1998) Statistical power analysis for the behavioural sciences. Academic Press, New York
70. Cohen J (1992) A power primer. *Psychol Bull* 112:155–9
71. Bruner E, Manzi G (2005) CT-based description and phyletic evaluation of the archaic human calvarium from Ceprano, Italy. *Anat Rec* 285:643–58
72. Tillier AM (1977) La pneumatisation du massif craniofacial chez les hommes actuels et fossiles (suite). *Bull Mem Soc Anthropol Paris* 4:287–316
73. Stringer C (1984) The definition of *Homo erectus* and the existence of the species in Africa and Europe. *Cour Forschungsunst Senckenb* 69:131–44
74. Balzeau A (2005) Spécificités des caractères morphologiques internes du squelette céphalique chez *Homo erectus*. Muséum national d'Histoire naturelle, Paris
75. Stringer CB (1983) Some further notes on the morphology and dating of the Petralona hominid. *J Hum Evol* 12:731–42
76. Lordkipanidze D, De León MSP, Margvelashvili A, et al (2013) Biology of early *Homo*. *Science* 342:326–31
77. Manzi G, Mallegni F, Ascenzi A (2001) A cranium for the earliest Europeans: phylogenetic position of the hominid from Ceprano, Italy. *Proc Natl Acad Sci USA* 98:10011–6
78. Buckland-Wright JC (2015) A radiographic examination of frontal sinuses in early British populations. *Man* 5:512–7
79. Vinyard CJ, Smith FH (1997) Morphometric relationships between the supraorbital region and frontal sinus in Melanesian crania. *Homo* 48:1–21
80. Wells JCK, Stock JT (2007) The biology of the colonizing ape. *Am J Phys Anthropol* 134:191–222
81. Clark J, de Heinzelin J, Schick K et al (1994) African *Homo erectus*: old radiometric ages and young Oldowan assemblages in the Middle Awash Valley, Ethiopia. *Science* 264:1907–10
82. Weaver TD, Roseman CC, Stringer CB (2007) Were neandertal and modern human cranial differences produced by natural selection or genetic drift? *J Hum Evol* 53:135–45
83. Sherwood RJ, Ward SC, Hill A (2002) The taxonomic status of the Chemeron temporal (KNM-BC 1). *J Hum Evol* 42:1531–84
84. Gilbert WH, Holloway RL, Kubo D, et al (2008) Tomographic analysis of the Daka calvaria. In: Gilbert WH, Asfaw B (eds) *Homo erectus: Pleistocene evidence from the Middle Awash, Ethiopia*. University of California Press, Berkeley, pp 329–48
85. Weidenreich D (1943) The skull of *Sinanthropus pekinensis*; a comparative study on a new primitive hominid skull. Geological Survey of China, Pehpei, Chungking
86. Weidenreich D (1951) Morphology of Solo Man. The American Museum of Natural History, New York
87. Wu X, Poirier FE (1995) Human evolution in China: A metric description of the fossils and a review of the sites. Oxford University Press, Oxford
88. Viallet A, Guipert G, Jianing H, et al (2010) *Homo erectus* from the Yunxian and Nankin Chinese sites: Anthropological insights using 3D virtual imaging techniques. *Comptes Rendus Palevol* 9:331–9
89. Trinkaus E (2003) Neandertal faces were not long; modern human faces are short. *Proc Natl Acad Sci USA* 100:8142–5
90. Trinkaus E (2006) Modern Human versus Neandertal Evolutionary Distinctiveness. *Curr Anthropol* 47:597–620
91. Stewart JR (2004) Neanderthal–modern human competition? A comparison between the mammals associated with Middle and Upper Palaeolithic industries in Europe during OIS 3. *Int J Osteoarchaeol* 14:178–89
92. Wroe S, Parr WCH, Ledogar JA, et al (2018) Computer simulations show that Neanderthal facial morphology represents adaptation to cold and high energy demands, but not heavy biting. *Proc R Soc B Biol Sci* 285:20180085
93. Stringer C (2016) The origin and evolution of *Homo sapiens*. *Philos Trans R Soc B Biol Sci* 371:20150237
94. Maddux SD, Butaric LN (2017) Zygomaticomaxillary morphology and maxillary sinus form and function: How spatial constraints influence pneumatization patterns among modern humans. *Anat Rec* 300:209–25
95. Ito T, Nishimura TD, Hamada Y, et al (2014) Contribution of the maxillary sinus to the modularity and variability of nasal cavity shape in Japanese macaques. *Primates* 56:11–9
96. Antón SC (2003) Natural history of *Homo erectus*. *Am J Phys Anthropol* 122:126–70
97. Street M, Terberger T, Orschiedt J (2006) A critical review of the German Paleolithic hominin record. *J Hum Evol* 51:551–79
98. Stringer C (2011) The chronological and evolutionary position of the Broken Hill cranium. *Am J Phys Anthropol* S144:287
99. Manzi G, Magri D, Milli S, et al (2010) The new chronology of the Ceprano calvarium (Italy). *J Hum Evol* 59:580–5
100. Schwarcz HP, Bietti A, Buhay WM (1991) On the reexamination of Grotta Guattari: Uranium-series and Electron-Spin-Resonance dates. *Curr Anthropol* 32:313–6
101. Rink WJ, Schwarcz HP, Smith FH, et al (1995) ESR ages for Krapina hominids. *Nature* 378:24
102. Grün R, Stringer C (2000) Tabun revisited: revised ESR chronology and new ESR and U-series analyses of dental material from Tabun C1. *J Hum Evol* 39:601–12
103. Buck LT, Stringer CB (2015) A rich locality in South Kensington: the fossil hominin collection of the Natural History Museum, London. *Geol J* 50:321–37
104. McDermott F, Stringer C, Grün R, et al (1996) New Late-Pleistocene uranium–thorium and ESR dates for the Singa hominid (Sudan). *J Hum Evol* 31:507–16

105. Pettitt P (2002) The Neanderthal dead: exploring mortuary variability in Middle Palaeolithic Eurasia. *Before Farming* 2002:1:1–26
106. Pettitt P (2011) The Palaeolithic origins of human burial. Routledge, New York
107. Schmitz RW, Serre D, Bonani G, et al (2002) The Neandertal type site revisited: interdisciplinary investigations of skeletal remains from the Neander Valley, Germany. *Proc Natl Acad Sci USA* 99:13342–7
108. Grün R, Stringer C, McDermott F, et al (2005) U-series and ESR analyses of bones and teeth relating to the human burials from Skhul. *J Hum Evol* 49:316–34
109. Douka K, Bergman CA, Hedges REM, et al (2013) Chronology of Ksar Akil (Lebanon) and implications for the colonization of Europe by anatomically modern humans. *PLoS One* 8:e72931
110. Henry-Gambier D (2002) Les fossiles de Cro-Magnon (Les Eyzies-de-Tayac, Dordogne) : nouvelles données sur leur position chronologique et leur attribution culturelle. *Bull Mem Soc Anthropol Paris* 14:89–112
111. Magori CC, Day MH (1983) Laetoli Hominid 18: an early *Homo sapiens* skull. *J Hum Evol* 12:747–53
112. Mcbrearty AS, Brooks AS (2000) The revolution that wasn't: a new interpretation of the origin of modern human behavior. *J Hum Evol* 39:453–63

Role of Spatial Integration in the Morphology of the Bony Labyrinth in Modern Humans

Le rôle de l'intégration spatiale dans la morphologie du labyrinthe osseux chez les humains modernes

A. Le Maître

Received: 9 April 2018; Accepted: 24 July 2018
© Société d'Anthropologie de Paris et Lavoisier SAS 2018

Abstract The bony labyrinth corresponds to the osseous wall of the inner ear, the hearing and balance organ located in the petrous pyramids, in the base of the cranium. The morphology of the labyrinth reflects phylogenetic and ecological signals. In hominoid primates, it is also influenced by its anatomical environment. The aim of this study is to determine whether, in the species *Homo sapiens*, the morphological relationships between the labyrinth and the skull result from geometrical constraints linked to equilibrioception, or from spatial constraints due to the inclusion of the inner ear in the petrous bone. Based on CT-scans of the skulls of adult individuals ($n=30$), two sets of 22 landmarks each were placed on the labyrinth and on the basicranium. The covariations between these two sets were investigated using two-block partial least squares (2B-PLS) analyses. The shape of the labyrinth is significantly correlated with the cranial base, but not with the isolated temporal bone. This indicates that the morphology of the labyrinth mainly results from functional constraints. However, several observations suggest that spatial constraints also have an influence, especially on the cochlea. The associated changes in shape are consistent with the ontogenetic trend, but differ slightly from the phylogenetic trend. These covariations caution against exclusively ecological interpretations of the morphology of the labyrinth.

Keywords Bony labyrinth · Petrous bone · Cranial base · Integration · Geometric morphometrics · *Homo sapiens*

Résumé Le labyrinthe osseux correspond à la paroi osseuse de l'oreille interne, organe de l'audition et de l'équilibre situé dans les pyramides pétreuses, dans la base du crâne.

A. Le Maître (✉)
ORCID (0000-0003-2690-7367)
Department of Theoretical Biology, University of Vienna,
Althanstrasse 14, A-1090 Vienna, Austria
e-mail : anne.le.maitre@univie.ac.at (or
anne.le.maitre@ens-lyon.org)

La morphologie du labyrinthe reflète des signaux écologique et phylogénétique. Chez les primates hominoïdes, elle est également influencée par son environnement anatomique. L'objectif de cette étude est de déterminer si dans l'espèce *Homo sapiens*, les relations morphologiques entre le labyrinthe et le crâne résultent de contraintes géométriques en lien avec l'équilibrionception ou de contraintes spatiales dues à l'inclusion de l'oreille interne dans le pétreux. À partir de CT-scans du crâne d'individus adultes ($n = 30$), deux ensembles de 22 points-repères sont placés sur le labyrinthe d'une part et sur le basicrâne d'autre part. Les covariations entre ces deux ensembles sont étudiées à l'aide d'analyses aux moindres carrés partiels à deux blocs (2B-PLS). La forme du labyrinthe est significativement corrélée à celle de la base du crâne, mais pas à celle de l'os temporal pris isolément, ce qui indique que la morphologie du labyrinthe résulte surtout de contraintes fonctionnelles. Cependant, certaines observations suggèrent l'influence de contraintes spatiales, notamment sur la cochlée. Les changements de forme associés sont cohérents avec la tendance ontogénétique observée chez les humains, mais diffèrent de la tendance phylogénétique. L'existence de ces covariations incite à la prudence quant aux interprétations écologiques de la morphologie du labyrinthe.

Mots clés Labyrinthe osseux · Os pétreux · Basicrâne · Intégration · Morphométrie géométrique · *Homo sapiens*

Introduction

The bony labyrinth consists of tubes and cavities embedded in the petrous part of the temporal bone, on each side of the head. It holds and roughly moulds the inner ear, which is a sensory detector for balance and hearing. In mammals, three semicircular ducts detect head rotations, two otolithic organs give the position of the head relative to the vertical axis, and

sounds are sensed by the coiled cochlea. The three semicircular canals are roughly orthogonal, the lateral semicircular canal forms an angle of 20° to 25° relative to the Frankfurt plane, so that it is nearly horizontal at rest, and the angle between the midsagittal plane of the head and the two vertical (anterior and posterior) semicircular canals is about 45° [1]. This geometry allows efficient detection of head rotations in all directions, further improved by the coupling between the labyrinths on both sides of the head [1]. The geometry of the labyrinth is remarkably conservative in mammals, suggesting strong functional constraints [2].

However, some variability exists in the morphology of the labyrinth, both across species [3] and within species [4,5]. The morphology of the bony labyrinth carries both a phylogenetic signal and an ecological signal [6-8]. For instance, the dimensions of the vestibular apparatus differ between aquatic and terrestrial mammals, and in musteloid taxa, the degree of arboreal and fossorial behaviour are reflected by the shape of the labyrinth [7,9,10]. In primates, the cochlear length and the area of the oval window, located on the base of the cochlea, reflect auditory capacities [11,12], whereas the semicircular canal sizes and geometry provide information on posture, locomotor agility and angular head velocity [4,12-15]. The spiral form of the cochlea also results from spatial packing in the petrous bone, at least in humans [16]. In primates, when the cranial base is more flexed and the posterior surface of the petrous pyramids is more vertical, the lateral semicircular canal (particularly its posterior part) tends to be tilted upwards in relation to the rest of the labyrinth [2]. Some correlations are also observed during the prenatal development of humans, but not necessarily the same ones [17]. In the first weeks of gestation, the cranial base angle increases and the petrous pyramids rotate coronally. While the orientation of the labyrinth follows the orientation of the posterior cranial base, the lateral semicircular canal tilts upwards (especially relative to the cochlea), the basal turn of the cochlea rotates coronally and the angle between the two vertical canals increases because of their greater torsion. The morphological changes in the labyrinth observed during ontogeny are associated with the orientation of the petrous bone rather than with retroflexion of the basiscranium. Because of the ossification of the otic capsule that surrounds it, the adult size and shape of the labyrinth are attained before 19 weeks of gestation [17]. In adult humans, the upward tilt of the lateral semicircular canal – combined with a smaller posterior canal – is also associated with a relatively more coronally rotated petrous bone, and hence a wider posterior cranial fossa [18].

In this study, we focus on a single species, modern humans, so that the phylogenetic and ecological signals can be ignored. In particular, the differences in locomotor behaviour and sound perception associated with the use of diverse ecological niches are considered as negligible

between individuals. The aim is to determine whether the morphological correlations between the bony labyrinth and the cranial base reflect

- 1) geometrical constraints related to efficient perception of head movements, i.e., functional constraints, or
- 2) spatial constraints linked to the restricted space within the petrous bone, as with cochlear coiling, or
- 3) both spatial and functional constraints.

To do so, we evaluated the integration between the labyrinth and its osseous surroundings, namely the petrous pyramids and, more generally, the basiscranium. When the constraints are functional (hypotheses 1 and 3), the shape of the labyrinth is linked to the orientation of the petrous pyramids in the cranial base, and hence to the shape of the basiscranium, which is not the case for spatial integration only (hypothesis 2). If there is spatial packing (hypotheses 2 and 3), the shapes of the labyrinth and the petrous pyramids are correlated, whereas they are independent in the absence of spatial constraints (hypothesis 1). In all cases, the sizes of the petrous pyramids and the bony labyrinth are likely to be influenced by the overall size of the cranial base. However, when this general effect is removed, interactions between the shapes and sizes of the labyrinth and the pyramids are to be expected in the presence of spatial constraints (hypotheses 2 and 3), but should disappear in their absence (hypothesis 1).

Materials and methods

The sample consisted of 30 humans aged 20 to 95 years from the Terry anatomical collection, an osteological collection of 1,728 individuals of known ethnic origin, sex, age and cause of death, collected in the U.S.A. in the first half of the 20th century. 18 individuals were Afro-American and 12 of European ancestry. The sex ratio is balanced. Using Amira software (Thermo Fisher Scientific), the skull and the bony labyrinth were virtually extracted from the CT-scans provided by Copes [19]. The 22 landmarks defined by Lebrun et al. [6] were positioned on the labyrinth (Fig. 1, Table 1). 22 landmarks were placed on the cranial base: 7 on the midsagittal plane and 15 on one side; of these, 9 were located on the temporal bone and more specifically on the petrous pyramids (Fig. 2, Table 2).

Statistical analyses were conducted on the landmark coordinates using MorphoJ v1.0e software [20]. The landmark coordinates were aligned, centred and scaled using Procrustes superimpositions [21,22]. They were then regressed against their log centroid size to remove allometric effects [22]. These two operations were performed independently for each set of landmark coordinates: the labyrinth (22 landmarks), the petrous part of the temporal bone (9 landmarks)

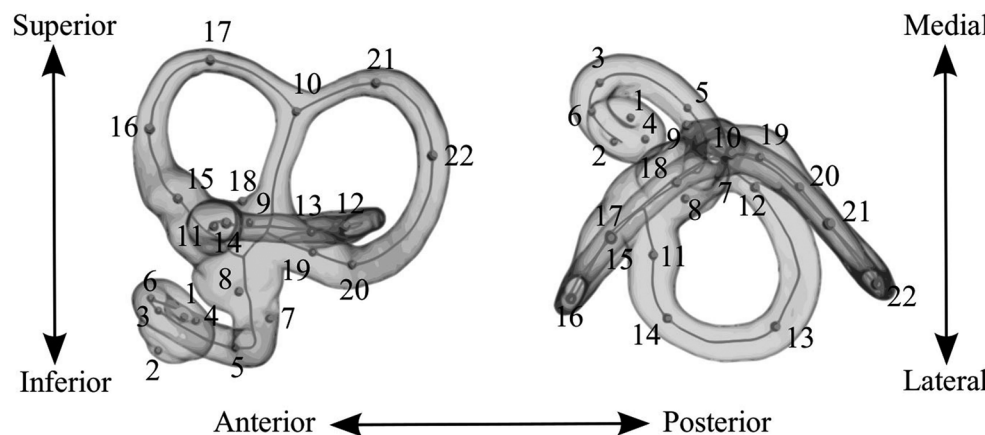


Fig. 1 Position of the 22 landmarks of the bony labyrinth. After Le Maître et al. [15] / *Position des 22 points-repères sur le labyrinthe osseux. D'après Le Maître et al. [15]*

Table 1 Definition of landmarks on the bony labyrinth [6] / <i>Définition des points-repères sur le labyrinthe osseux [6]</i>		
Number	Name	Definition
1	Helix basis	Centre of the first turn of the cochlea
2	Helix apex	Centre of the last turn of the cochlea
3	Helix anteromedial	Anteromedial-most point of the first turn of the cochlea
4	Helix posterolateral	Posterolateral-most point of the first turn of the cochlea
5	Helix inferior	Inferior-most point of the first turn of the cochlea
6	Helix superior	Superior-most point of the first turn of the cochlea
7	Fenestra cochlea	Centre of the round window
8	Fenestra vestibuli	Centre of the oval window
9	Aquaeductus vestibuli	Opening of the vestibular aqueduct in the vestibular wall
10	Crus commune apex	Bifurcation point of the common crus
11	Canalis lateralis ampulla	Centre of the ampulla of the lateral semicircular canal
12	Canalis lateralis posteromedial	Posteromedial-most point of the lateral semicircular canal
13	Canalis lateralis posterolateral	Posterolateral-most point of the lateral semicircular canal
14	Canalis lateralis anterolateral	Anterolateral-most point of the lateral semicircular canal
15	Canalis anterior ampulla	Centre of the ampulla of the anterior semicircular canal
16	Canalis anterior anterolateral	Anterolateral-most point of the anterior semicircular canal
17	Canalis anterior superior	Uppermost point of the anterior semicircular canal
18	Canalis anterior inferior	Inferior-most point of the anterior semicircular canal
19	Canalis posterior ampulla	Centre of the ampulla of the posterior semicircular canal
20	Canalis posterior inferior	Inferior-most point of the posterior semicircular canal
21	Canalis posterior superior	Uppermost point of the posterior semicircular canal
22	Canalis posterior posterolateral	Posterolateral-most point of the posterior semicircular canal

and the cranial base (22 landmarks including on the temporal bone). Finally, two-block partial least squared (2B-PLS) analyses were performed between the labyrinth and either the temporal bone or the whole cranial base, in order to assess the degree of covariation between their shapes [23]. Permutation tests against the null hypothesis of independence between the two blocks were performed with 10,000 randomization rounds. The 3D shape changes associated

with each PLS component were visualized using the rgl package in R v3.2.2 software [24,25].

In a second round of analyses, the log centroid size of the cranial base (computed with the 22 landmarks) was regressed out, in order to correct for the effect of the overall skull size on the covariation patterns between the bony labyrinth and the petrous pyramids. The regression residuals of the variables (Procrustes coordinates and / or log centroid

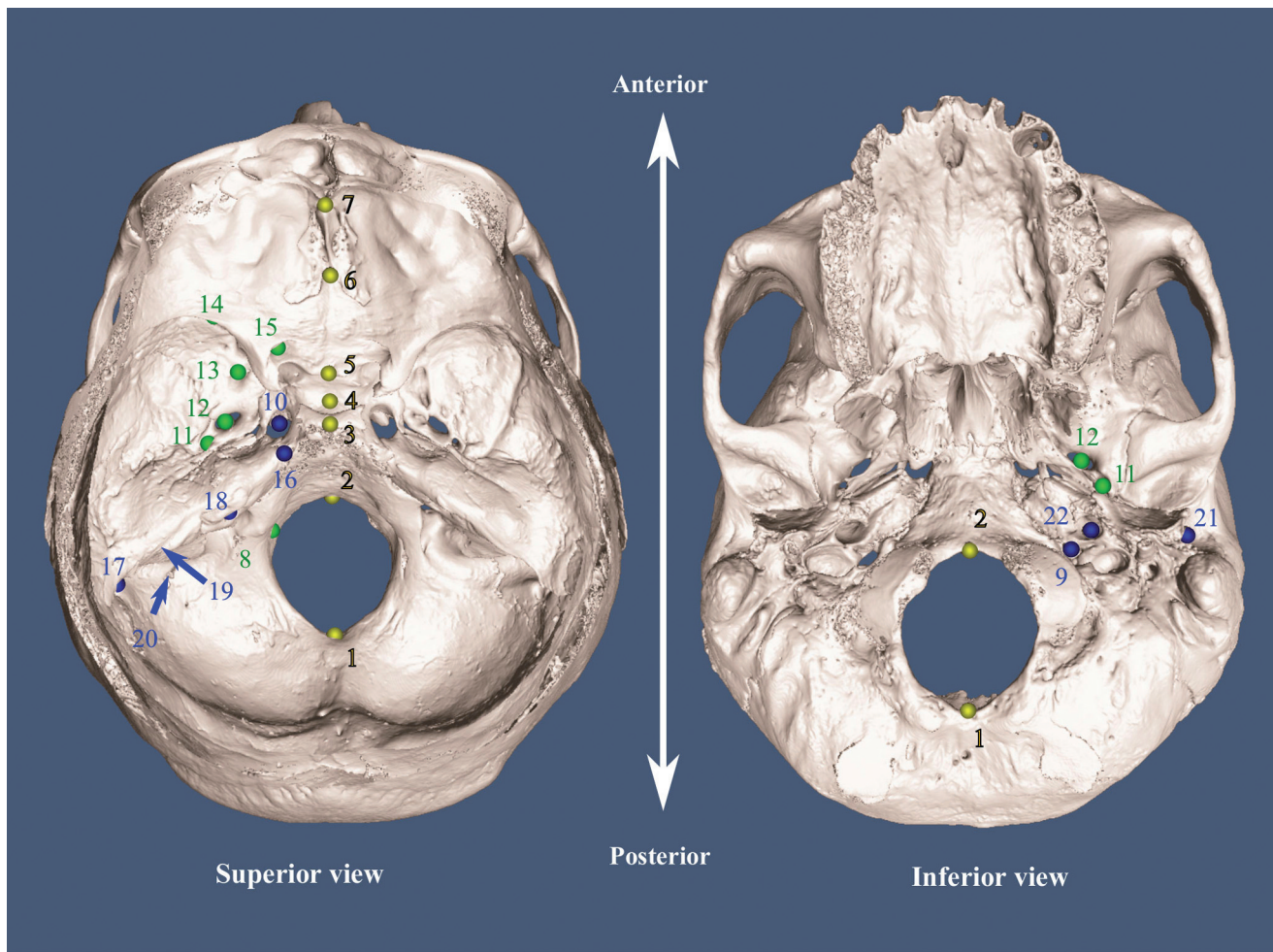


Fig. 2 Position of the 22 landmarks of the cranial base. Yellow: midsagittal plane; blue: temporal bone; green: lateral base excluding the temporal bone. The 9 landmarks in blue were used for the analyses on the temporal bone and all 22 landmarks were used for the analyses on the cranial base / *Position des 22 points-repères sur la base du crâne. Jaune, plan médio-sagittal ; bleu, os temporal ; vert, partie latérale de la base à l'exclusion de l'os temporal. Les 9 points-repères en bleu ont été utilisés pour les analyses sur l'os temporal et l'ensemble des 22 points-repères en bleu ont été utilisés pour les analyses sur la base du crâne*

size) describing these two structures were used as covariates in 2B-PLS analyses to investigate their morphological integration in terms of both size and shape.

Results

The overall correlation between the shapes of the labyrinth and the petrous part of the temporal bone is very low and not significant ($RV=0.3726$, $P=0.4928$). According to the scree plot, the first four PLS components carry the main signal for the correlations and account for 70.9% of the total squared covariance. For each PLS component, the pairwise correlation coefficient is higher than the overall correlation between the two blocks, but all values remain below 0.6 except for

PLS 3 with $r^2 = 0.759$ (Table 3). The first PLS component ($r^2=0.593$) accounts for 25.7% of the total squared covariance. High values correspond to comparatively high, short and narrow petrous pyramids (Fig. 3). Relative to the upper ridge of the petrous bone, the inferior part of the pyramid (that is, the segment linking the jugular and the mastoid foramina) is sagittally rotated. The associated changes in labyrinth shape are a downward translation of the posterior semicircular canal with a shortening of the common crus, a sagittal rotation of the lateral semicircular canal in the horizontal plane, a tightening of the cochlear spiral and the rotation of its basal turn relatively to the semicircular canal system, clockwise when seen from the left side of the head.

The shape of the labyrinth is significantly correlated with the shape of the cranial base ($RV = 0.5327$, $P < 0.05$).

Table 2 Definition of landmarks on the cranial base. The landmarks positioned on the temporal bone are highlighted with a star (*) /
Définition des points-repères sur la base du crâne. Les points-repères positionnés sur l'os temporal sont marqués d'une étoile ()*

Number	Temporal	Name	Notes
1		Opisthion	Posterior-most point of the foramen magnum
2		Basion	Anterior-most point of the foramen magnum
3		Dorsum sellae	Posterior-most point
4		Fossa hypophysialis	Inferior-most point
5		Tuberculum sellae	Posterior-most point
6		Cribriform plate	Posterior-most point
7		Foramen caecum	
8		Hypoglossal canal	
9	*	Jugular foramen	Anterior-most point
10	*	Foramen lacerum	
11		Foramen spinosum	
12		Foramen ovale	
13		Foramen rotundum	
14		Superior orbital fissure	Anterolateral-most point
15		Optic foramen	
16	*	Apex of the petrous pyramid	
17	*	Base of the petrous pyramid	
18	*	Internal acoustic meatus	
19	*	Aquaeductus vestibuli	
20	*	Mastoid foramen	
21	*	External acoustic meatus	
22	*	Carotid canal	

The main signal is conveyed by the first five PLS components (76.0 % of the total squared covariance) for the association with the cranial base. All five pairwise correlation coefficients are above 0.6 and even above 0.7 for PLS 1, 2 and 3 (Tab. 3). The correlation is higher for PLS 1 ($r^2=0.754$), which accounts for 22.0 % of the total squared covariance. Compared to the lower values, high PLS 1 values correspond to an overall shortening, widening and increase in height of the cranial base, with a lateral projection of the middle and posterior fossae and a lengthening of the clivus and its surrounding area, producing a narrower angle with the foramen magnum (Fig. 4a). The morphological changes in the petrous pyramids are similar to the features observed for PLS1 in the previous 2B-PLS analysis on the petrous bone only. The associated changes in labyrinth shape also correspond to PLS1 in the previous analysis, except for the absence of rotation of the lateral semicircular canal in the horizontal plane. PLS 2 accounts for 15.0 % of the total squared covariance ($r^2 = 0.725$). Relatively to the lowest values, the highest correspond to a reduction of the basicranial flexure and an upward rotation of the posterior part of the cranial base, together with the sagittal rotation of the lateral part of the skull, producing a long, low and narrow cranial base (Fig. 4b). These changes in shape are associated

with the rotation of the labyrinth around the lateral semicircular canal, clockwise when observed from the left side of the head. The angle between the two vertical canals is more obtuse and the lateral semicircular canal is more projected along the anteroposterior axis.

The log centroid size of the cranial base significantly ($P<0.005$) predicts 48.9% of the log centroid size of the petrous pyramids and 36.6 % of the log centroid size of the bony labyrinth. Conversely, only a small proportion of the shape of the petrous pyramids (4.2%) and the bony labyrinth (3.4%) are predicted by the log centroid size of the cranial base, and these relationships are not significant ($P=0.2665$ and $P=0.4980$, respectively). When the effect of the overall size of the basicranium is removed, none of the associations between the labyrinth and the petrous pyramids is statistically significant. The correlation between their log centroid sizes is very low ($r^2=0.0462$, $P=0.2541$), as is the association between the shape of the labyrinth and the size of the petrous pyramids ($RV=0.1554$, $P=0.2480$) and between the size of the labyrinth and the shape of the petrous pyramids ($RV=0.0363$, $P=0.9738$). The overall association between the shapes of the labyrinth and the petrous pyramids is not statistically significant ($P= 0.4439$), with a RV coefficient as low as 0.3761 (Tab. 3). The first four components (69.9% of

Table 3 Results of the 2B-PLS analyses between the labyrinth and the temporal bone or the cranial base. The RV-coefficients measure the overall association between the two blocks of variables and the r^2 measure the pairwise association for each PLS component (only the first five components are shown, with the % of total squared covariance described). The star (*) indicates $P<0.05$ / *Résultats des analyses aux moindres carrés à deux blocs entre le labyrinthe et l'os temporal ou le basicrâne. Les coefficients RV mesurent l'association globale entre les deux blocs de variables et les r^2 mesurent l'association entre les deux axes de chaque composante de l'analyse aux moindres carrés (seules les cinq premières composantes sont mentionnées, avec le % du total des carrés des covariances décrit par chacune). L'étoile (*) indique que $P < 0,05$.*

	Cranial base		Petrosal bone		Petrosal bone - size base regressed out	
	r^2	% tot. cov 2	r^2	% tot. cov 2	r^2	% tot. cov 2
RV-coefficient	0.5327*	-	0.3726	-	0.3761	-
PLS1	0.754	22.0 %	0.593	25.7%	0.622	25.8%
PLS2	0.725	15.0 %	0.587	17.9%	0.684	17.9%
PLS3	0.724	12.6 %	0.759	16.1%	0.618	15.4%
PLS4	0.632	10.4 %	0.576	11.2%	0.576	10.7%
PLS5	0.637	8.0 %	0.551	6.8%	0.666	6.3%

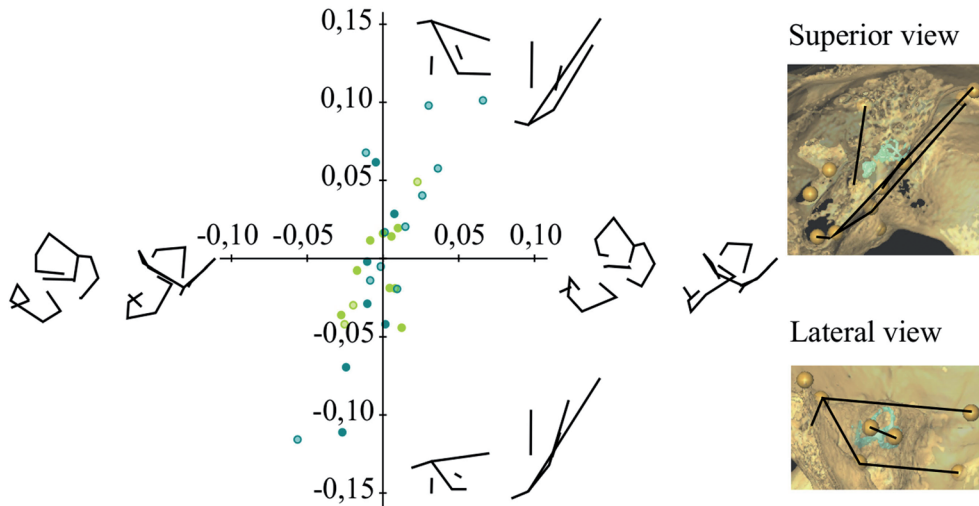


Fig. 3 Scatter plots of the first PLS axes describing 25.7 % of the total squared covariance between the shape of the labyrinth and the shape of the temporal bone. Blue circles: Afro-Americans; green circles: European ancestry; dark filling: men; light filling: women. Wireframes show the shape changes along each axis. Left: lateral view; right: superior view / *Nuage de points pour les premiers axes de la PLS décrivant 25,7 % du total des carrés des covariances entre la forme du labyrinthe et celle de l'os temporal. Cercles bleus : Afro-Américains, cercles verts : individus d'origine européenne ; remplissage sombre : hommes ; remplissage clair : femmes. Les points reliés par des segments représentent les changements de forme le long de chaque axe. À gauche, vue latérale ; à droite, vue de dessus*

the total squared covariance) carry most of the signal. For each PLS component, the proportion of total squared covariance accounted for is very similar to the results of the previous 2B-PLS analysis between the shapes of the labyrinth and the petrosal pyramids, in which the log centroid size of the latter had been regressed out instead of the log centroid size of the cranial base (Tab. 3). Here, the pairwise correlations are slightly higher than previously except for PLS3, but all coefficients remain below 0.7.

Discussion

The correlation between the shape of the labyrinth and the shape of the cranial base suggests that geometrical constraints linked to equilibrium are involved in the morphology of the labyrinth. Along the main axis of covariation, the linear changes in length, width or height of the cranial base do not modify the semicircular canal system, except the translation of one canal and the shortening of the common

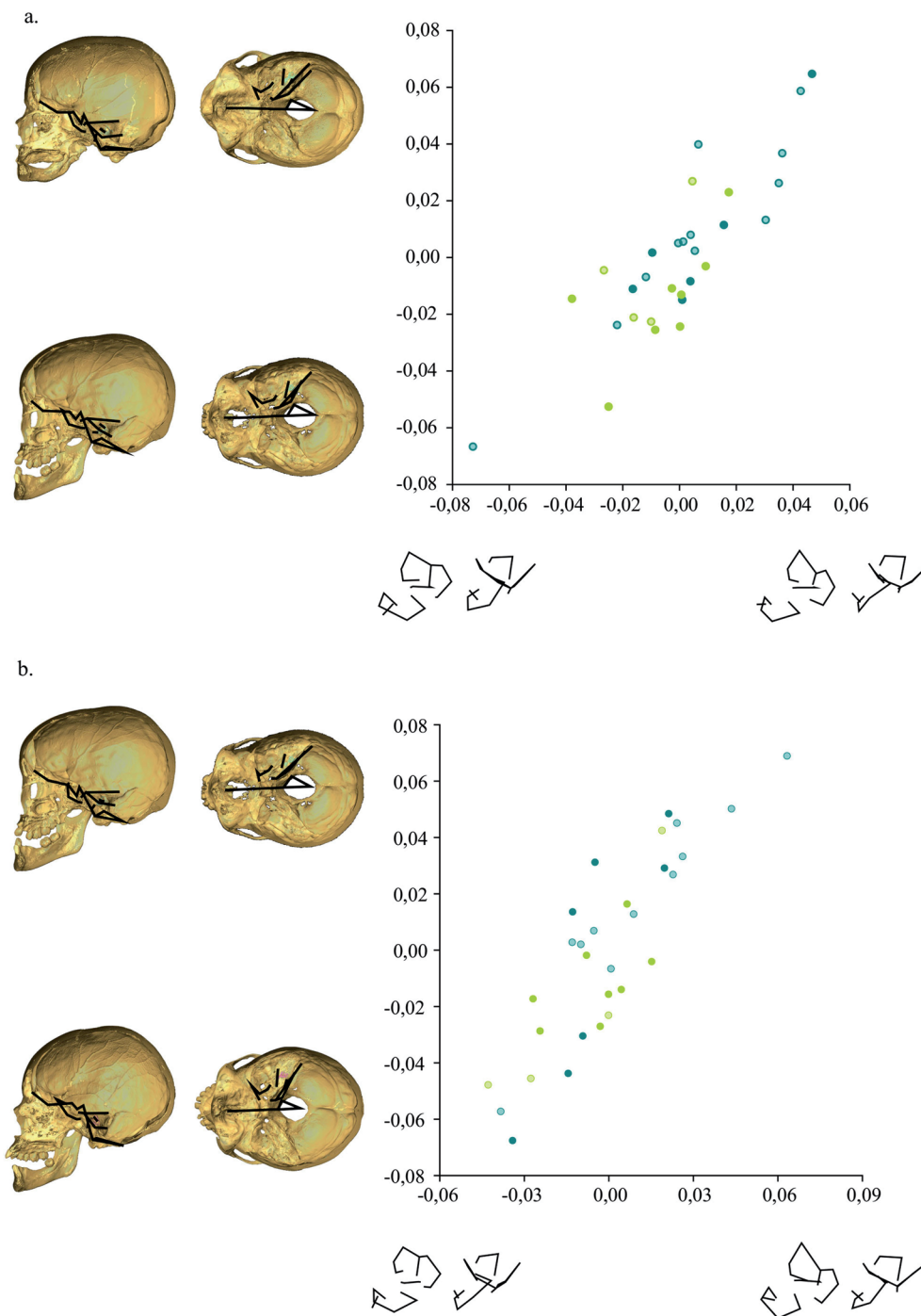


Fig. 4 Scatter plots of (a) PLS 1 and (b) PLS 2 axes describing 22.0% and 15.0% of the total squared covariance between the shape of the labyrinth and the shape of the cranial base. Blue circles: Afro-Americans; green circles: European ancestry; dark filling: men; light filling: women. Wireframes show the shape changes along each axis. Left: lateral view; right: superior view / *Nuage de points pour (a) PLS 1 et (b) PLS 2 décrivant respectivement 22,0 % et 15,0 % du total des carrés des covariances entre la forme du labyrinthe et celle de la base du crâne. Cercles bleus : Afro-Américains ; cercles verts : individus d'origine européenne ; remplissage sombre : hommes ; remplissage clair : femmes. Les points reliés par des segments représentent les changements de forme le long de chaque axe. À gauche, vue latérale ; à droite, vue de dessus*

crus (Fig. 4a), which have no influence on the parameters that matter for the detection of head movements [26]. By contrast, in the second axis of covariation, the rotations of the petrous pyramid are associated with changes in the geometry of the semicircular canal system (Fig. 4b). The rotation of the petrous pyramid linked to the basicranial flexion is correlated with the rotation of the lateral semicircular canal, in the same direction relatively to the rest of the labyrinth. The sagittal rotation of the petrous pyramids corresponds to the anteroposterior elongation of the labyrinth, with a wider angle between the anterior and the posterior canals. According to biophysical models, the sensitivity of a semicircular duct depends on arc size, cross-sectional area and eccentricity [27-29] and, as the three semicircular ducts are coupled in the mammalian inner ear, their relative angles and dimensions also play a role in the detection of head movements [30]. In both rotations, the angles between the semicircular canals and their dimensions change, and hence the sensitivity of the system. However, these morphological changes tend to maintain the overall orientation of the semicircular canals in the skull: the vertical canals remain symmetrical in relation to the midsagittal plane and the lateral semicircular canal follows the orientation of the posterior cranial base, and hence of the foramen magnum. The correlation between the orientation of the lateral canal and the posterior cranial base is consistent with both the phylogenetic trend in primates [2] and the ontogenetic trend in humans [17]. The association between the width of the posterior basicranial fossa and the translation of a smaller posterior semicircular canal (because of the shorter common crus) also broadly corresponds to the main covariation axis found in a previous study conducted on adult humans, except for the rotation of the petrous bone [18]. This small difference could be due to the use of semi-landmarks that capture shape more finely.

After correction for the overall effect of skull size, there is no correlation between the labyrinth and the petrous bone when size is involved, and the overall correlations between their shapes are not significant. However, spatial constraints could have an effect on the shape of the labyrinth, because the pairwise correlation coefficients for individual PLS components are not too low (r^2 around 0.6 for the five first components) and the associated changes in shape are consistent with spatial integration, since the rotations of the basal turn of the cochlea and of the posterior surface of the petrous pyramid are similar and the sagittal rotation of the lateral semicircular canal follows the rotation of the petrous pyramid (Fig. 3). Some morphological associations revealed when the cranial base is considered also suggest that spatial constraints have an influence: for the first component, the rotation of the cochlea corresponds to the rotation of the petrous pyramid on the head and, as in correlations with the temporal bone, the downward translation of the posterior

semicircular canal follows the increase in height of the posterior surface of the petrous pyramid (Fig. 4a). The association between the orientation of the cochlea and the orientation of the petrous pyramids is similar to the human ontogenetic trend [17] and, together with the changes in coiling shape, consistent with the spatial packing observed for the cochlea in humans [16].

Compared to chimpanzees, our closest relatives, humans have a more flexed cranial base [31] and their petrous pyramids have a more coronal orientation [32]. These features roughly correspond to the changes in shape observed along PLS 2 (Fig. 4b) for the analysis with the whole cranial base, with chimpanzees having morphologies closer to the highest values for humans. Compared to great apes, the lateral semicircular canal in humans is coronally rotated and less posteriorly projected, and the labyrinth overall is rotated around this canal [2,15]. Except for the projection of the lateral canal, this morphology is not consistent with the changes in shape associated with the cranial base for PLS 2, suggesting that the phylogenetic trend might be slightly different to the ontogenetic and intraspecies trends in humans.

Conclusion

It has been known since the early 2000s that the labyrinth and the cranial base are morphologically correlated in primates and during human foetal development. This study shows that this is also the case within adult variability in our species. The shape of the semicircular canals depends on geometrical constraints linked to equilibrioception. The morphological correlation with the petrous pyramids is not significant; however, the shape associations observed could be a sign of some spatial packing of the cochlea in the temporal bone. The patterns observed in adults are consistent with the ontogenetic trend reported previously in humans.

Despite some similarities, the intraspecies covariation pattern in humans is not the same as the phylogenetic pattern in hominoids, suggesting that the intraspecies trend might be different across species. It would be interesting to perform the same study for chimpanzees or gorillas, to determine whether the correlation pattern found in humans is specific to this species or represents a general trend in hominoids. Humans are characterized by very large brains compared to other primates, which induce morphological constraints on the skull as a whole that result in its peculiar basicranial shape. The spatial packing induced by this large brain could be a much stronger determinant of the shape of the labyrinth than ecology, as observed for the semicircular canals of birds [33].

Acknowledgments The author is grateful to Lynn Copes for providing the CT-scans of the skulls from the Terry

anatomical skeletal collection, curated in the Smithsonian Natural Museum of Natural History, and to Philipp Mitteröcker for useful advice about the analyses. This research study was funded by the Austrian Science Foundation (FWF, project grant P29397).

Conflict of interest: The author do not have any conflict of interest to declare.

References

- Graf W, Klam F (2006) Le système vestibulaire : anatomie fonctionnelle et comparée, évolution et développement. *C R Palevol* 5:637–55
- Spoor F, Zonneveld F (1998) Comparative review of the human bony labyrinth. *Am J Phys Anthropol* 107:211–51
- Berlin JC, Kirk EC, Rowe TB (2013) Functional Implications of Ubiquitous Semicircular Canal Non-Orthogonality in Mammals. *PLoS ONE* 8:e79585
- Perier A, Lebrun R, Marivaux L (2016) Different level of intra-specific variability of the bony labyrinth morphology in slow-versus fast-moving primates. *J Mammalian Evol* 23(4):353–8
- Ponce de León MS, Koesbardiati T, Weissmann JD, et al (2018) Human bony labyrinth is an indicator of population history and dispersal from Africa. *Proc Nat Acad Sci* 201717873
- Lebrun R, Ponce de León MS, Tafforeau P, et al (2010) Deep evolutionary roots of strepsirrhine primate labyrinthine morphology. *J Anat* 216:368–80
- Grohé C, Tseng ZJ, Lebrun R, et al (2015) Bony labyrinth shape variation in extant Carnivora: a case study of Musteloidea. *J Anat* 228:366–83
- Ekdale EG (2016) Form and function of the mammalian inner ear. *J Anat* 228:324–37
- Spoor F, Bajpai S, Hussain ST, et al (2002) Vestibular evidence for the evolution of aquatic behaviour in early cetaceans. *Nature* 417(6885):163–6
- Ekdale EG (2013) Comparative anatomy of the bony labyrinth (inner ear) of placental mammals. *PLoS One* 8(6):e66624
- Coleman MN, Boyer DM (2012) Inner ear evolution in primates through the Cenozoic: implications for the evolution of hearing. *Anat Rec* 295:615–31
- Bernardi M, Couette S (2017) Eocene Paleoenvironment of *Adapis parisiensis* (Primate, Adapidae): From Inner Ear to Lifestyle. *Anat Rec* 300:1576–88
- Spoor F, Garland T, Krovitz G, et al (2007) The primate semicircular canal system and locomotion. *Proc Natl Acad Sci* 104:10808–12
- Malinzak MD, Kay RF, Hullar TE (2012) Locomotor head movements and semicircular canal morphology in primates. *Proc Natl Acad Sci* 109:17914–9
- Le Maître A, Schuetz P, Vignaud P, et al (2017) New data about semicircular canal morphology and locomotion in modern hominoids. *J Anat* 231:95–109
- Pietsch M, Dávila LA, Erfurt P, et al (2017) Spiral Form of the Human Cochlea Results from Spatial Constraints. *Sci Rep* 7 (1):7500
- Jeffery N, Spoor F (2004) Prenatal growth and development of the modern human labyrinth. *J Anat* 204:71–92
- Gunz P, Stoessel A, Neubauer S, et al (2013) Morphological integration of the bony labyrinth and the cranial base in modern humans and Neandertals (abstract). *Europ Soc Hum Evol* 104
- Copes L (2012) Comparative and experimental investigations of cranial robusticity in Mid-Pleistocene Hominins. Arizona State University, Arizona
- Klingenberg CP (2011) MorphoJ: an integrated software package for geometric morphometrics. *Mol Ecol Resour* 11:353–7
- Rohlf FJ, Slice D (1990) Extensions of the Procrustes method for the optimal superimposition of landmarks. *Syst Zool* 39:40–59
- Bookstein FL (1991) Morphometric tools for landmark data: geometry and biology. Cambridge: Cambridge University Press
- Rohlf FJ, Corti M (2000) Use of two-block partial least-squares to study covariation in shape. *Syst Biol* 49:740–53
- Adler D, Murdoch D, et al (2018) rgl: 3D Visualization Using OpenGL
- R Development Core Team (2008) R: A language and environment for statistical computing. Vienna, Austria
- Muller M, Verhagen JHG (2002) Optimization of the mechanical performance of a two-duct semicircular duct system – Part 2: Excitation of endolymph movements. *J Theor Biol* 216:425–42
- Jones GM, Spells K (1963) A theoretical and comparative study of the functional dependence of the semicircular canal upon its physical dimensions. *Proc R Soc Lond B Biol Sci* 157:403–19
- McVean A (1999) Are the semicircular canals of the European mole, *Talpa europaea*, adapted to a subterranean habitat? *Comp Biochem Physiol A Mol Integr Physiol* 123:173–8
- Muller M (1999) Size limitations in semicircular duct systems. *J Theor Biol* 198:405–437
- Muller M, Verhagen JHG (1988) A new quantitative model of total endolymph flow in the system of semicircular ducts. *J Theor Biol* 134:473–501
- Lieberman DE, Ross CF, Ravosa MJ (2000) The primate cranial base: ontogeny, function, and integration. *Am J Phys Anthropol* 119:117–69
- Jeffery N, Spoor F (2002) Brain size and the human cranial base: A prenatal perspective. *Am J Phys Anthropol* 118:324–40
- Benson RBJ, Starmer-Jones E, Close RA, et al (2017) Comparative analysis of vestibular ecomorphology in birds. *J Anat* 231:990–1018

Trabecular Analysis of the Distal Radial Metaphysis during the Acquisition of Crawling and Bipedal Walking in Childhood: A Preliminary Study

Analyse de la micro-architecture trabéculaire de la métaphyse distale du radius pendant l'acquisition de la marche bipède chez l'enfant : étude préliminaire

A. Colombo · N. B. Stephens · Z. J. Tsegai · M. Bettuzzi · M. P. Morigi · M. G. Belcastro · J.-J. Hublin

Received: 01 May 2018; Accepted: 26 November 2018
© Société d'Anthropologie de Paris et Lavoisier SAS 2018

Abstract In modern day populations, children following a normal pattern of development acquire independent bipedal locomotion between the ages of 9 and 18 months. Variability in the timing of this psychomotor developmental milestone depends on various factors, including cultural influences. It is well known that trabecular bone adapts to changes in biomechanical loading and that this can be influenced by alternative locomotor modes, such as crawling, which may be adopted before the acquisition of bipedal locomotion. With the onset of crawling, increased loading of the distal metaphysis of the radius, a component of the wrist, may lead to

changes in trabecular bone architecture. To test this hypothesis, eight distal metaphyses of the radius of non-pathological children aged 0 to 3 years from the Bologna collection of identified skeletons were μ CT-scanned at a resolution of 10.7 μ m. The microarchitectural parameters of the trabecular bone (trabecular bone volume fraction, trabecular thickness, trabecular spacing, and trabecular ellipsoid factor) were quantified for the entire metaphysis and 3D morphometric maps of the distribution of the bone volume fraction were generated. Analysis of these microarchitectural parameters and the 3D morphometric maps show changes in the trabecular bone structure between 6 and 15 months, the period during which both crawling and bipedalism are acquired. This preliminary study analyzed the trabecular structure of the growing radius in three dimensions for the first time, and suggests that ontogenetic changes in the trabecular structure of the radial metaphysis may be related to changes in the biomechanical loading of the wrist during early locomotor transitions, *i.e.* the onset of crawling. Moreover, microarchitectural analysis could supply important information on the developmental timing of locomotor transitions, which would facilitate interpretations of locomotor development in past populations.

A. Colombo (✉)
Ecole pratique des Hautes études, PSL University Paris, Chaire d'anthropologie biologique Paul Broca
e-mail : antony.colombo@ephe.psl.eu

UMR 5199 PACEA, University of Bordeaux, CNRS, MCC ;
LabEx Sciences archéologiques de Bordeaux,
n°ANR-10-LABX-52, bât. B8, allée Geoffroy Saint Hilaire,
CS50023, F-33615 Pessac, France

A. Colombo · N. B. Stephens · Z. J. Tsegai · J.-J. Hublin
Max Planck Institute for Evolutionary Anthropology,
Department of Human Evolution, Deutscher Platz 6,
D-04103 Leipzig, Germany

M. Bettuzzi · M. P. Morigi
University of Bologna, DIFA - Department of Physics and
Astronomy, viale Berti Pichat 6/2, I-40127 Bologna, Italy

M. Bettuzzi · M. P. Morigi · M. G. Belcastro
Centro Fermi, Piazza Del Viminale 1, I-00184 Roma, Italy

M. G. Belcastro
University of Bologna, BiGeA - Department of Biological,
Geological, and Environmental sciences,
Piazza di Porta San Donato, 1, I-40126 Bologna, Italy

UMR 7268 ADES, Aix Marseille University, CNRS, EFS, bât. A,
Bd Pierre Dramard, F-13344 Marseille, France

Keywords Trabecular bone microarchitecture · Ontogeny · Bipedal walking · Biomechanics · Cancellous bone

Résumé Dans les populations actuelles, les enfants présentant un développement normal acquièrent une marche bipède autonome entre les âges de 9 et 18 mois. La variabilité dans le rythme de l'acquisition de cette étape clé du développement psychomoteur dépend aussi de divers facteurs culturels. Il est bien connu que l'os trabéculaire réagit aux changements biomécaniques et que les modes de locomotion alternatifs adoptés avant l'acquisition de la bipédie (*e.g.* marche à quatre pattes) peuvent influencer la structure de l'os trabéculaire.

Une augmentation de la charge sur la métaphyse distale du radius, l'une des composantes de l'articulation du poignet, très sollicitée pendant la marche à quatre pattes, pourrait entraîner des changements micro-architecturaux trabéculaires associés. Pour tester cette hypothèse, huit métaphyses de radius d'enfants ne présentant aucun signe pathologique, d'âges compris entre 0 et 3 ans, provenant de la collection ostéologique de référence de Bologne, ont été microscannés à une résolution de 10,7 µm. Les paramètres microarchitecturaux de l'os trabéculaire (la fraction volumique d'os trabéculaire, l'épaisseur trabéculaire, l'espacement trabéculaire, et le facteur ellipsoïdal trabéculaire) ont été quantifiés sur l'ensemble de la métaphyse et des cartographies morphométriques 3D de la distribution de la fraction volumique d'os trabéculaire ont été générées. L'analyse de paramètre microarchitecturaux et des cartes morphométriques 3D a montré des changements importants dans la structure osseuse trabéculaire entre 6 et 15 mois, période pendant laquelle locomotion alternative et marche bipède sont acquises. Cette étude préliminaire a analysé pour la première fois la structure trabéculaire tridimensionnelle de radius en croissance et suggère que les changements ontogéniques de la structure trabéculaire de la métaphyse radiale pourraient être reliés aux changements biomécaniques spécifiques à l'utilisation du poignet pendant les transitions locomotrices précoces. De plus, l'analyse microarchitecturale pourrait fournir des informations importantes sur les rythmes de développement de l'acquisition locomotrice de l'enfant, ce qui permettrait d'interpréter leur développement psychomoteur dans les populations du passé.

Mots clés Micro-architecture osseuse trabéculaire · Ontogénie · Bipédie · Biomécanique

Introduction

The acquisition of bipedal locomotion is a complex psychomotor process, requiring development of both postural (*e.g.* standing) and dynamic (*e.g.* walking) motor skills. The timing of this process is influenced by both biological and cultural factors. The development of bipedal locomotion is dependent on the maturation of the central nervous system [1,2], since it relies on improved motor coordination in response to stimuli from the vestibular and proprioceptive systems and, especially, the visual system. Visual information is essential for the development of postural control [3, 4], and its absence causes substantial delays in locomotor development [5]. In addition to maturation of the nervous system, motor skills improve as both muscular tone and strength increase, which, along with changes in the distribution of muscle mass, facilitate independent postural and locomotor coordination [3].

Locomotor development can be divided into a sequence of steps observed in all children [6]. An innate reflex stepping phase is the first stage in locomotor development. The subsequent stages are: head support; chest raising; sitting with and then without support; acquisition of an alternative autonomous locomotor mode (*i.e.* crawling); standing independently; moving with support; and, finally, independent bipedalism [6]. Provided their development is normal, children in present-day populations are able to walk independently between the age of 9 and 18 months [3,6]. A mature, adult-like gait usually develops around the age of 6 [3], although there is a great deal of both intra- and inter-individual variability in the developmental timing of locomotor transitions [7], in part due to differences among socio-cultural groups [2,5,8-10]. Child-rearing strategies differ between socio-cultural contexts, with the acquisition of independent bipedal locomotion representing the beginning of an individual's autonomy [2]. Thus, interactions with family and friends, especially with the mother [11], the quality of emotional exchanges, the degree of encouragement to walk [3], and the learning provided [2,9] are all important factors contributing to variability in the developmental timing of locomotor acquisition.

It has been well established that trabecular bone responds to changes in biomechanical loading by modifying its structure to optimize stress resistance [12,13]. Signals of locomotor behaviour can thus be identified from the variability of the trabecular microarchitecture [14-16]. Differences between individuals at different ages, and most likely at different stages of locomotor development, could therefore lead to a more complete understanding of the impact of loading on bone development.

During foetal development, the femur and humerus have a similar trabecular structure [17], most likely because prenatal bone morphology is under stricter genetic regulation. Subsequently, during ontogeny, the trabecular structure of the humerus and femur begins to diverge as they adopt different functional roles and experience a very different biomechanical environment. This partly accounts for the wide microarchitectural variations observed between different anatomical locations in adulthood [17-21]: remodelling of the trabecular structure occurs at a rapid rate during development, and especially during the first few years of life [22]. During growth, locomotor changes lead to morphological adaptations of the bone tissue of the lower limb, with especially pronounced changes in the bony morphology of the proximal femur [23]. In contrast, the rate of change of the trabecular structure of the proximal humerus is slower than in the proximal femur and, once bipedal locomotion is acquired, the upper limb switches from assistance during locomotion to working in conjunction with the hand during complex manipulation [21,24]. However, during the developmental stages preceding independent bipedalism, especially during crawling and

standing, the distribution of loads between the limbs changes. This is especially the case for the wrist, a joint predominantly used when a child crawls [3]. The wrist is likely to experience relatively large biomechanical loads during crawling, which are lessened with the acquisition of bipedal locomotion as the upper limb is no longer used to support the weight of the body.

Considering these different factors, this preliminary study investigates the trabecular structure of the wrist, specifically that of the distal radius, to test whether its trabecular micro-architecture could reflect this biomechanical shift from crawling to independent bipedal locomotion. We hypothesize that the trabecular structure of the distal radius will be more robust as crawling begins and loading increases, while a reduction in bone robustness will be observed after the transition to bipedal locomotion, due to the subsequent decrease in locomotor loading of the upper limb.

Materials and Methods

This preliminary study analyzed the distal metaphysis of the radius, as a component of the wrist. Its growth cartilage contributes to 75% of the total bone length [25], and it is therefore likely to retain a record of osteological changes to the trabecular structure during the locomotor transition from crawling to independent bipedalism.

The sample included in this preliminary study includes the distal radial metaphysis of 8 children of known age and sex, aged between 0 and 3 years (Table 1), from the Bologna collection of identified skeletons [26]. The age of the individuals was chosen to encompass the period which, in European populations, spans the developmental milestones that lead to independent bipedalism. This skeletal collection is unique in that the occupation of 94% of the individuals more than 15 years of age is known, so that the socio-economic group to which they belonged can be inferred. The majority of the women were housewives, domestic workers or farmers, while most of the men were farmers, labourers, masons, woodworkers or soldiers [26]. Accordingly, the individuals selected are considered to be from a homogeneous low-to-middle socio-economic group. The left radii were analyzed for this study. However, although absolute bilateral asymmetry has been identified for the human proximal humerus during ontogeny, the asymmetry is not directional [27]. Moreover, during this period of development, it is likely that the left and right wrist joints are equally loaded. The skeletons of the individuals selected did not show any macroscopic pathological signs.

Microcomputed tomography (μ CT), a non-destructive X-ray imaging technique, was used to analyze the radii; all were positioned and oriented in a uniform manner inside the μ CT-scanner, with the Z-axis of acquisition parallel to the

Table 1 Sample composition and μ CT acquisition parameters / *Composition de l'échantillon étudié et paramètres d'acquisition microtomodensitométrique*

Sample composition		
Sex	n	Ages (in months)
M	4	0, 15, 17, 36
F	4	6, 8, 11, 24
μCT acquisition parameters		
Voltage		130 kV
Current		32 μ A
Filter		0.5 mmAl
Exposure time		2250 ms
Frames averaged		32
Projections		1200
Angle		360°
Pixel size		18 μ m
Source-detector distance		228.5 mm
Source-object distance		135.5 mm
Magnification		1.69
Scanning time		20 hours
Voxel size		10.7 μ m

long axis of the bone. As bone is initially deposited in a grid-like structure, the most recently formed trabecular bone, located directly below the metaphyseal surface, is the least influenced by biomechanical stresses; this region was therefore excluded from scanning. The μ CT-scanned area began at 5% of the bone length and stopped at 15% of its maximum length, representing a section 5 to 10mm in thickness depending on the length of the bone. Acquisitions were performed with a laboratory system¹ (Figure 1a) at the Department of Physics and Astronomy of Bologna University (Table 1) at an isometric voxel size of 10.7 μ m. Tomographic reconstruction was performed with IMAGEREC research software, implementing the Filtered Back Projection algorithm in cone-beam geometry [28].

1. The μ CT protocol was set to obtain the best quality from the 3D reconstruction of the volume. Thus, the Kevex microfocus X-ray tube (PSX-10 65W) was operated at its lowest power (4W) to reduce the focal spot size to the minimum (6 μ m). The X-ray detector was a CCD camera produced by Photonic Science. The CCD sensor (Kodak KAI 1100) counts 4000 x 2600 square pixels with a pixel size of 9 μ m. This was coupled to a scintillator layer by means of a fibre optic plate. The CCD camera was double-cooled with a Peltier cell and liquid circulation for maximum efficiency and stability in long-term measurements. To reduce the fairly high noise, due to CCD and electronics construction at full resolution, a 2x2 binning mode (actual pixel size of 18 μ m) was used. Furthermore, 32-frame averaging was used to increase the signal-to-noise ratio and obtain the best image contrast. The magnification factor in cone beam geometry was 1.69.

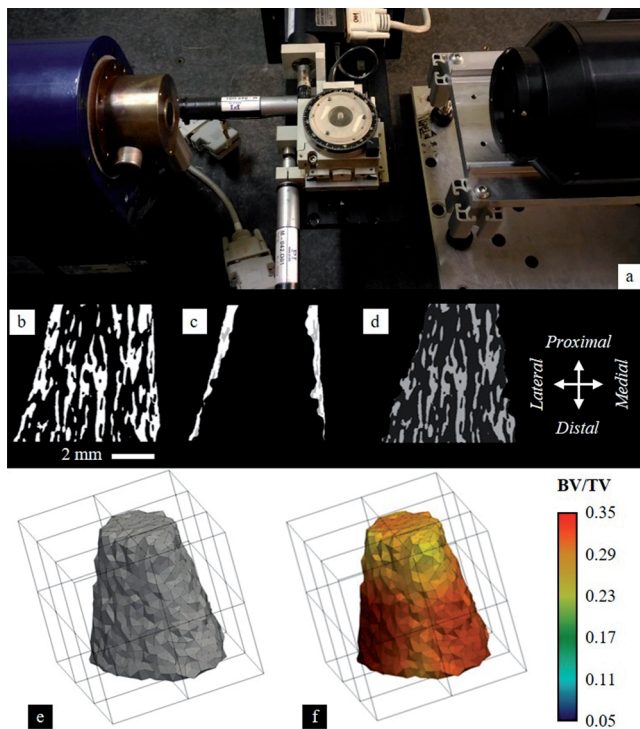


Fig. 1 Methods used to analyze the trabecular structure of the radial distal metaphysis. (a) The μ CT system at the Department of Physics and Astronomy of Bologna University; (b-f) Processing stages to analyze trabecular bone structure: Mid-plane images of (b) the segmented radial metaphysis, (c) removed cortical bone, (d) inner region with trabecular bone and non-bone grey values, (e) 3D mesh with superimposed grid, (f) mesh with interpolated BV/TV / Méthodes d'analyses de la micro-architecture osseuse trabéculaire de la métaphyshe distale du radius. (a) Système microtomodensitométrique hébergé au Département de Physique et d'Astronomie de l'université de Bologne ; (b-f) Etapes d'analyses de la micro-architecture trabéculaire : coupes centrales (b) de la métaphyshe radiale segmentée, (c) de l'os cortical extrait, (d) sans l'os cortical, région interne avec l'os trabéculaire et les espaces non osseux, (e) maillage 3D avec grille surimposée, (f) maillage avec les valeurs de BV/TV interpolées

The reconstructed scans of the distal radius were segmented into bone and non-bone components with the Ray Casting Algorithm [29]. From the segmented scans, the trabecular and cortical tissues were separated using an in-house script for medtool v4.0 (<http://www.dr-pahr.at>) [30]. Here, the voxels are defined by four grey values (*i.e.* 0-3), corresponding to external non-bone, cortical bone, trabecular bone, and internal non-bone (Figure 1d-f). Segmentation of these regions enabled analysis of trabecular bone throughout the entire metaphysis (Figure 1).

Quantitative analyses were performed on the entire inner region of the metaphysis (*i.e.* only voxels representing the trabeculae and internal non-bone). The trabecular bone vol-

ume fraction (BV/TV: trabecular bone volume/total volume) was quantified by superimposing a 2.5 mm grid onto the voxel data (Figure 1e), then calculating BV/TV from within a 5 mm spherical volume of interest (VOI) at each node of the grid. To visualize BV/TV distribution, the VOI results were interpolated onto a 3D tetrahedral mesh of the inner region, which was generated from the voxel data using CGAL v4.11 [31]. Colour maps were then created and displayed in Paraview 4.3 [32] (Figure 1f).

Trabecular bone variables were quantified for the entire inner region of the metaphysis, and are described in Table 2. Mean trabecular thickness (Tb.Th) and mean trabecular spacing (Tb.Sp) were quantified using medtool v4.0, following the sphere fitting method [33]. The ellipsoid factor (Tb.EF) was quantified to characterize the mean shape of the trabecular struts (*i.e.* along a continuum: -1 = oblate (*i.e.* plate-like), 0 = sphere (*i.e.* intermediate trabecular strut shape), 1 = prolate (*i.e.* rod-like) [34, 35]), using the BoneJ 1.4.2 plugin [36] for Image J 1.50 [37].

Results and Discussion

This preliminary study quantified the trabecular structure of the distal radius in individuals from birth to 3 years of age. Although each age is represented by a single individual in this cross-sectional sample, some trends were identified that demonstrate the high potential of trabecular bone analysis for reconstructing locomotor transitions.

In general, the distal metaphysis of the radius shows differences between ages in its trabecular structure during the period from birth to 3 years of age, which includes the bipedal acquisition stage, and a general trend can be observed. Specifically, BV/TV decreases during this period from 26.5% to 11.1%, Tb.Th increases from 0.108mm to 0.118mm, and Tb.Sp increases from 0.261mm to 0.583mm. As a result of the increased Tb.Sp, the trabecular network becomes less dense with increasing age, despite the increase in trabecular thickness. This pattern of change during ontogeny suggests that the trabecular structure reflects biomechanical changes. Of particular interest is the reversal of this trend for all parameters between 6 and 15 months of age (Figure 2). In present-day European populations, this age range encompasses the period during which infants begin to sit both with and without support, at 5 and 9 months old respectively; stand with the help of the hands; enter the crawling phase, at around 11 months; and finally become independently bipedal, before 15 months of age [3].

The youngest individual, a neonate (0 months old), has a higher BV/TV than all the older individuals (Figure 2), with trabecular bone distributed homogeneously throughout the metaphysis (Figure 3). Tb.Sp is lower than in all the older individuals and Tb.EF is close to 0, reflecting an imperfectly

Table 2 Definition of trabecular variables quantified in the distal radial metaphysis / Définitions des paramètres micro-architecturaux trabéculaire mesurés au niveau de la métaphyshe distale du radius.

Variable	Abbreviation	Units	
Bone volume fraction <i>Fraction volumique d'os trabéculaire</i>	BV/TV	-	Bone volume / total volume <i>Volume osseux trabéculaire / Volume total</i>
Trabecular thickness <i>Epaisseur trabéculaire</i>	Tb.Th	mm	Mean thickness of trabeculae <i>Epaisseur moyenne des trabécules</i>
Trabecular spacing <i>Espacement trabéculaire</i>	Tb.Sp	mm	Mean spacing between trabeculae <i>Espace moyen entre les trabécules</i>
Ellipsoid factor <i>Facteur ellipsoïde</i>	Tb.EF	-	Mean trabecular shape where -1 is plate-like and 1 is rod-like <i>Forme des trabécules, allant de -1 (en forme de plateau) à 1 (en forme de tube)</i>

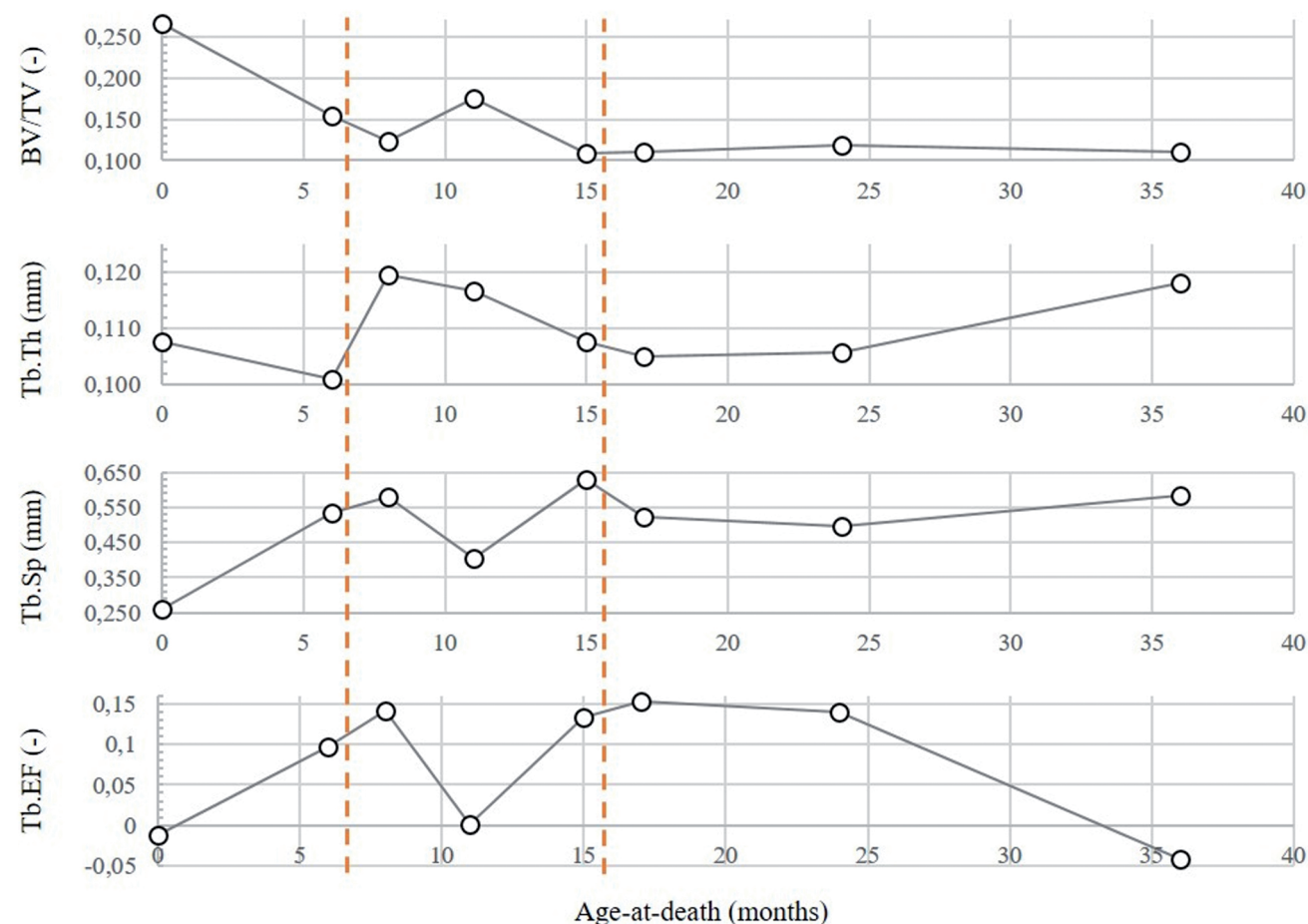


Fig. 2 Variations of TBMA parameters according to the age of individuals (Tb.EF - ellipsoid factor, Tb.Sp - trabecular spacing, Tb.Th - trabecular thickness, BV/TV-trabecular bone volume fraction, red dashed lines highlight an important period of variation) / Variations des paramètres micro-architecturaux en fonction de l'âge des individus (Tb.EF - facteur ellipsoïde, Tb.Sp – espacement trabéculaire, Tb.Th - épaisseur trabéculaire, BV/TV - fraction volumique d'os trabéculaire, les lignes pointillées rouges mettent en évidence une période importante de variation)

defined trabecular strut shape (Figure 2). At birth, individuals are growing rapidly and a high volume of unspecialized trabecular bone is produced [18].

For individuals aged from 6 to 8 months, the trabecular structure of the radial metaphyses still has a homogeneous BV/TV distribution (Figure 3) but, despite a higher Tb.Th from 0.101 to 0.120mm than in the youngest individual, their BV/TV values subsequently decrease with increasing age. This is likely to be attributable to a smaller trabecular number with a larger Tb.Sp and the proliferation of more rod-like structures, as shown by the increase in Tb.EF (Figure 2) with age. These observations could reflect significant remodelling of the trabecular structure to reduce a biomechanically unnecessary amount of bone. This suggests that the thicker - or more biomechanically useful - trabeculae are preserved and reinforced in response to the initial changes in the loading environment, the most notable change resulting from the need to distribute and transfer body mass [38].

In the 11-month-old individual, BV/TV distribution is fairly heterogeneous. The regions with the highest BV/TV are located close to the cortex and to the growth plate, and BV/TV is relatively lower towards the centre of the metaphysis (Figure 3). In this case, compared to younger individuals, there is an increase in BV/TV, a decrease in Tb.Sp, a higher Tb.Th (Figure 2), while Tb.EF decreases to nearly 0. At this age, children are usually very mobile but not yet able to walk

independently [6]. The wrists are used in both static positions (*i.e.* sitting or standing) and dynamic movement (*i.e.* crawling). The concentric organization of BV/TV could potentially reflect a reinforcement of the metaphyseal trabecular structure through the production of trabeculae of undifferentiated shape. These structural changes could highlight the capacity of bone to adapt to both support and mechanical resistance functions, and would show adaptation to a changing pattern of loading, as has been previously demonstrated [38].

Compared to younger individuals, the 15-month-old shows more heterogeneously distributed BV/TV, with the region of highest BV/TV on the medial side (Figure 3). BV/TV decreases again and Tb.Sp reaches its highest values, while Tb.Th decreases and the values for Tb.EF indicate a larger number of rod-like trabeculae as age increases (Figure 2). The microarchitectural pattern observed at this age – when independent bipedalism usually begins – could mark the potential hyper-specialization of trabecular bone within the radial metaphysis, which may be an adaptation to the biomechanical demands of crawling.

Among the three older individuals (17, 24 and 36 months of age), the regions with the highest BV/TV are localized and the overall distribution is highly heterogeneous (Figure 3), while BV/TV remains relatively low in comparison with the younger individuals and stable among these three. Tb.Sp is lower than in younger individuals and becomes quite stable between these three (Figure 2). Reduced biomechanical

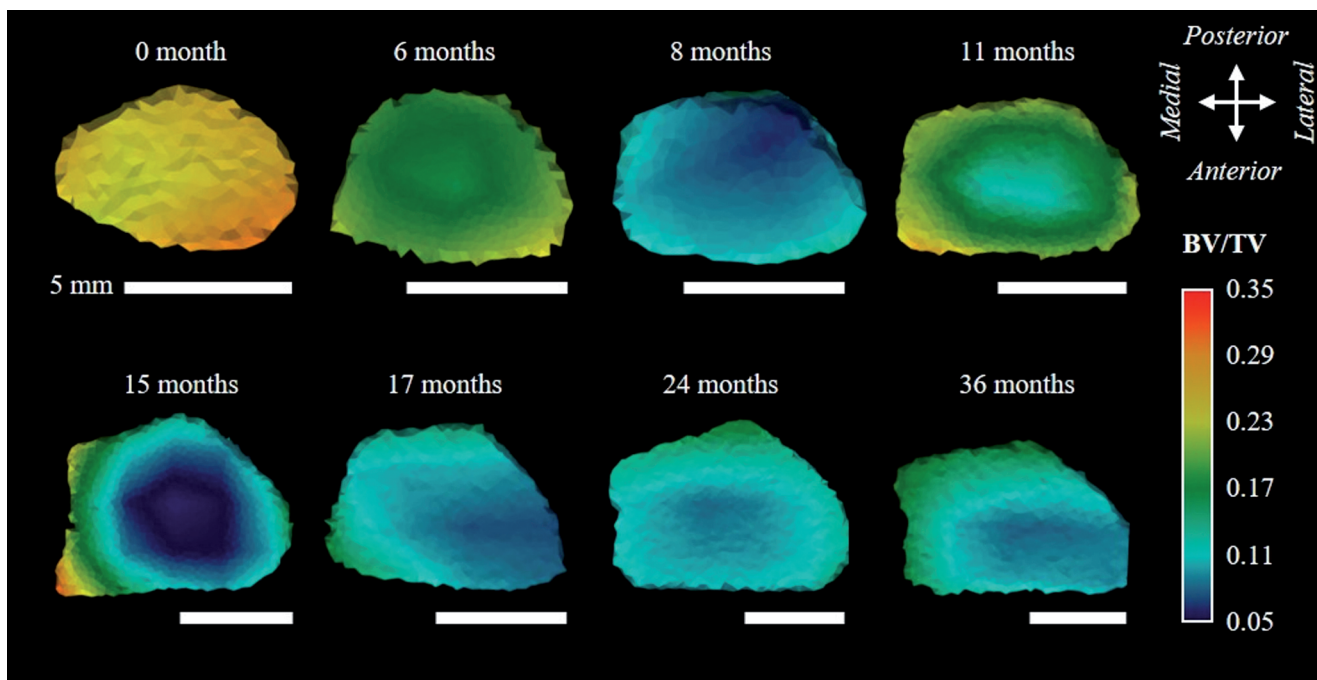


Fig. 3 Distal view of 3D maps of BV/TV distribution inside the radial metaphysis of each individual / Vue distale des cartographies 3D de la distribution des valeurs de BV/TV de la métaphyse du radius pour chaque individu analysé

loading of the wrist with the onset of bipedalism may be reflected in the BV/TV of these older individuals. The upper limb is increasingly free of locomotor constraints and becomes specialized for other functions [24], which are likely to exert smaller loads on the wrist compared to locomotion. However, the 36-month-old individual has a slightly higher Tb.Th and a Tb.EF close to 0 (Figure 2) compared to younger individuals. This may reflect a new phase of adaptation, with changes in the use of the wrist that may be linked to changes in hand use, such as improved hand dexterity and more precise manual manipulation.

Trabecular bone may reflect locomotor behaviour [15] by responding to changes in biomechanical loading [12,13,38], for example reflecting the refinement of bipedalism with ontogenetic changes in trabecular anisotropy within the distal tibial metaphysis [20]. Therefore, we suggest that the observed differences in trabecular structure of the distal radius between individuals of different ages could reflect an ontogenetic pattern resulting from biomechanical changes initiated by the acquisition and subsequent reduction of a transitional locomotor mode (*i.e.* crawling) that occurs between 6 and 15 months of age.

In anthropology, previous analyses of trabecular bone ontogeny in humans have focused on the lower limb, either on the proximal femur or the proximal and distal tibia [*e.g.* 20,21], and three studies have analyzed the proximal humerus [18,28,39]. These studies identified a common pattern of trabecular architectural change in both the forelimb and hindlimb during ontogeny, whereby the trabecular structure is very robust at birth, with robustness decreasing until around 1-2 years of age, then increasing to reach adult-like levels during adolescence. Biomedical studies have previously explored the trabecular ontogeny of the distal radius, but due to the methodologies applied and the period of development investigated, the results cannot be directly compared with those of the present study [*e.g.* 40-42]. The preliminary results of this study suggest that the pattern of trabecular ontogeny of the distal radius may differ from that of other skeletal sites. The robustness of the trabecular structure decreases after birth, but peaks again (*i.e.* high BV/TV and high Tb.Th) between the ages of 6 and 15 months. This distinct ontogenetic pattern suggests that this anatomical region may record a locomotor signal of crawling.

It should be kept in mind that these are preliminary results and that additional research is needed to confirm these findings. In order to assess the degree of variability at each developmental stage, a larger sample would further clarify the signal identified here. Although skeletal collections including individuals of known age are relatively rare, these results would be further strengthened by including individuals from other populations. Because trabecular bone structure may be influenced by numerous factors other than direct biomechani-

cal loading of a localized joint, this analysis would benefit from a comparison with a different anatomical site. For example, comparisons between parts of the forelimb and hindlimb, using comparable methodologies, could reflect the different loading regimes of the forelimb and hindlimb at this developmental stage. Moreover, trabecular bone analysis is often limited by the absence of a skeletal site that can be used as a control, because identifying a region of the skeleton that does not undergo biomechanical changes is a challenge. We suggest that including the cranial vault or a skeletal element from the axial skeleton, a rib or a vertebra for instance, may improve the identification of trabecular structural changes that are triggered by a changing biomechanical environment. A few biomedical studies exist on the ontogeny of the trabecular bone microarchitecture of vertebrae [43,44] and ribs [45,46] but they cannot be used for comparison with our results because the methodologies applied and the period of development investigated are different. Comparisons of trabecular ontogeny between humans and extant apes may also reveal different ontogenetic trajectories that can be related to locomotor transitions.

We predicted that trabecular structure would reflect behavioural changes related to the acquisition of bipedal locomotion, and therefore selected individuals of known age from the transitional stage prior to crawling and independent bipedalism. Our results suggest that this approach could help to detect differences in trabecular bone microarchitecture between individuals, related to biomechanical changes caused by the locomotor transition. Although males and females differ slightly in the timing of these developmental stages [6], it is generally accepted that before adolescence, there are no significant differences in trabecular structure between the sexes [18,19]. The skeletons of the individuals analyzed here showed no pathological signs of abnormal growth or dietary deficiency (*e.g.* vitamin D, iron) that could have affected their physical and psychomotor development [47,48]. Furthermore, the provenance of the individuals in the study sample is constrained both chronologically (all died in 1901) and geographically (city of Bologna, Italy), so that the sample is from a single biologically and culturally homogeneous population [26].

Child care is socially and culturally defined, and the socio-cultural environment during childhood has a major effect on the timing of psychomotor development [6]. Daily stimulation and increased social interaction, with parents and other individuals, accelerates psychomotor development, as has been shown in Malian and Korean populations in which children are able to walk at the mean age of 9 months [10]. Moreover, the influence of this socio-cultural context is dominant whether in rural or urban areas, with consequences for early independent bipedalism across different African countries [49] even if the nutritional status is unfavorable [8].

Conclusions

This preliminary study has quantified, for the first time, the trabecular structure of the human distal radius during the first years of development, a time during which there are notable changes in biomechanical loading. Morphometric maps of bone distribution were generated for the first time for an ontogenetic series of human individuals of known age. Although further investigations are necessary to confirm the findings presented here, the results suggest that the trabecular structure of the distal radial metaphysis holds potential for the identification of signals of locomotor transitions during growth. As the age of acquisition of bipedalism in a normal developmental context (*i.e.* good health status, adequate nutrition and absence of developmental stressors) is largely influenced by cultural factors, trabecular bone analysis may provide important insights into the developmental timing of locomotor changes during early locomotor transitions and support interpretations of psychomotor development in past populations. For example, Neolithization led to significant changes in lifestyle (from nomadism to sedentism, from hunter-gatherers to farmers), redefining human cultures and certainly affecting the timing of developmental changes. Trabecular analysis would thus make it possible to understand the impacts of cultural practices on the biology of the individual. Finally, the analysis of microarchitectural signals of locomotor changes in young extant primates, together with studies on brain evolution, could potentially inform cultural interpretations concerning modern humans and provide additional insights into ontogenetic processes and their patterns during hominid evolution.

Acknowledgments AC would like to thank the Fyssen Foundation for funding this project. The research was funded by the Max Planck Society (AC, NBS, ZJT, JJH). Thanks to two anonymous reviewers and the editor, Aurélien Mounier, for their comments, which have greatly improved the clarity of the manuscript.

Conflict of interest : authors do not have any conflict of interest to declare.

References

- He M, Walle EA, Campos JJ (2015) A cross-national investigation of the relationship between infant walking and language development. *Infancy* 20(3):283–305
- Sylla M, Sidibé T, Traoré B, et al (2007) Développement psychomoteur des nourrissons de 0 à 12 mois dans le district de Bamako. *J Pédiatr Puéric* 20(6): 233–7
- Barbe V, Tourrette C (1999) Tous les enfants présentent-ils le même profil de développement psychomoteur dans la petite enfance? *J Pédiatr Puéric* 12(1):35–49
- Lee DN, Aronson E (1974) Visual proprioceptive control of standing in human infants. *Percept Psychophys* 15(3):529–32
- Levtzion-Korach O, Tennenbaum A, Schnitzer R, et al (2000) Early motor development of blind children. *J Paediatr Child Health* 36(3): 226–9
- Adolph KE, Karasik LB, Tamis-Lemonda CS (2009) Motor skill. In: Bornstein MH (ed), *Handbook of cultural developmental science*, Taylor and Francis Press, New York, pp 61–88
- Sutherland D (1997) The development of mature gait. *Gait and Posture* 6(2):163–170
- Angulo-Barroso RM, Schapiro L, Liang W, et al (2011) Motor development in 9-month-old infants in relation to cultural differences and iron status. *Dev Psychobiol* 53(2):196–210
- Berger SE, Theuring C, Adolph KE (2007) How and when infants learn to climb stairs. *Infant Behav Dev* 30(1):36–49
- Bril B (1997) Culture et premières acquisitions motrices: enfants d'Europe, d'Asie, d'Afrique. *J Pédiatr Puéric* 10(5):302–14
- Clearfield MW (2011) Learning to walk changes infants' social interactions. *Infant Behav Dev* 34(1):15–25
- Frost HM (1990) Skeletal structural adaptations to mechanical usage (SATMU): 1. Redefining Wolff's law: The bone modeling problem. *Anat Rec* 226(4):403–13
- Frost HM (1990) Skeletal structural adaptations to mechanical usage (SATMU): 2. Redefining Wolff's law: The remodeling problem. *Anat Rec* 226(4):414–22
- Fajardo RJ, Müller R, Ketcham RA et al (2007) Nonhuman anthropoid primate femoral neck trabecular architecture and its relationship to locomotor mode. *Anat Rec* 290(4):422–36
- Ryan TM, Shaw CN (2012) Unique suites of trabecular bone features characterize locomotor behavior in human and non-human anthropoid primates. *PLoS ONE* 7(7):e41037
- Shaw CN, Ryan TM (2012) Does skeletal anatomy reflect adaptation to locomotor patterns? Cortical and trabecular architecture in human and nonhuman anthropoids. *Am J Phys Anthropol* 147 (2):187–200
- Reissis D, Abel RL (2012) Development of fetal trabecular micro-architecture in the humerus and femur. *J Anat* 220 (5):496–503
- Colombo A (2014) La Micro-Architecture Trabéculaire de l'os en Croissance: Variabilité Tridimensionnelle Normale et Pathologique Analysée par Microtomodensitométrie. Doctoral Dissertation, Bordeaux University, 286 p
- Kirmani S, Christen D, Van Lenthe GH et al (2009) Bone structure at the distal radius during adolescent growth. *J Bone Miner Res* 24(6):1033–42
- Raichlen DA, Gordon AD, Foster AD, et al (2015) An ontogenetic framework linking locomotion and trabecular bone architecture with applications for reconstructing hominin life history. *J Hum Evol* 81:1–12
- Ryan TM, Krovitz GE (2006) Trabecular bone ontogeny in the human proximal femur. *J Hum Evol* 51:591–602
- Valentin J, Streffer C (2002) Basic anatomical and physiological data for use in radiological protection: Reference values. *Ann ICRP* 32(3-4):1–265
- Tardieu C (1999) Ontogeny and phylogeny of femoro-tibial characters in humans and hominid fossils: Functional influence and genetic determinism. *Am J Phys Anthropol* 110(3):365–77
- Stephens NB, Kivell TL, Gross T, et al (2016) Trabecular architecture in the thumb of *Pan* and *Homo*: implications for investigating hand use, loading, and hand preference in the fossil record. *Am J Phys Anthropol* 161(4):603–19
- Pritchett JW (1991) Growth plate activity in the upper extremity. *Clin Orthop Relat Res* 268:235–42
- Belcastro MG, Bonfiglioli B, Pedrosi ME, et al (2017) The history and composition of the identified human skeletal collection

- of the Certosa Cemetery (Bologna, Italy, 19th–20th Century). *Int J Osteoarcheol* 27(5):912–25
27. Perchalski B, Placke A, Sukhdeo SM, et al (2018) Asymmetry in the cortical and trabecular bone of the human humerus during development. *Anat Rec* 301(6):1012–25
 28. Feldkamp LA, Davis LC, Kress JW (1984) Practical cone-beam algorithm. *J Opt Soc Am A* 1(6):612–9
 29. Scherf H, Tilgner R (2009) A new high-resolution computed tomography (CT) segmentation method for trabecular bone architectural analysis. *Am J Phys Anthropol* 140:39–51
 30. Gross T, Kivell TL, Skinner MM, et al (2014) A CT-image-based framework for the holistic analysis of cortical and trabecular bone morphology. *Palaeontol Electron* 17(3):1–13
 31. The CGAL Project (2018) CGAL User and Reference Manual. CGAL Editorial Board, 4.12 ed
 32. Ayachit U, Geveci B, Avila L (2015) The ParaView Guide. Kitware, Los Alamos 254 p.
 33. Hildebrand T, Rüegsegger P (1997) A new method for the model-independent assessment of thickness in three-dimensional images. *J Microsc* 185(1):67–75
 34. Doube M (2015) The ellipsoid factor for quantification of rods, plates, and intermediate forms in 3D geometries. *Front Endocrinol* 6:15
 35. Salmon PL, Ohlsson C, Shefelbine SJ, et al (2015) Structure model index does not measure rods and plates in trabecular bone. *Front Endocrinol* 6:162
 36. Doube M, Kłosowski MM, Arganda-Carreras I, et al (2010) BoneJ: Free and extensible bone image analysis in ImageJ. *Bone* 47(6):1076–9
 37. Schneider CA, Rasband WS, Eliceiri KW (2012) NIH Image to ImageJ: 25 years of Image Analysis. *Nat methods* 9(7):671–5
 38. Schulte FA, Ruffoni D, Lambers FM, et al (2013) Local mechanical stimuli regulate bone formation and resorption in mice at the tissue level. *PLoS ONE* 8:e62172
 39. Ryan TM, Raichlen DA, Gosman JH (2017) Structural and mechanical changes in trabecular bone during early development in the human femur and humerus. In: Percival CJ, Richtsmeier JT (eds) *Building bones: Bone formation and development in anthropology*. Cambridge University Press, Cambridge, pp 254–80
 40. Erlandson MC, Kontulainen SA, Baxter-Jones ADG (2011) Pre-competitive and recreational gymnasts have greater bone density, mass, and estimated strength at the distal radius in young childhood. *Osteoporosis Int* 22(1):75–84
 41. Gabel L, Macdonald HM, Nettlefold L, et al (2017) Physical Activity, Sedentary Time, and Bone Strength From Childhood to Early Adulthood: A Mixed Longitudinal HR-pQCT study. *J Bone Miner Res* 32(7):1525–36
 42. Wang Q, Ghasem-Zadeh A, Wang XF, et al (2011) Trabecular bone of growth plate origin influences both trabecular and cortical morphology in adulthood. *J Bone Miner Res* 26(7):1577–83
 43. Acquaah F, Robson Brown KA, Ahmed F, et al (2015) Early trabecular development in human vertebrae: Overproduction, constructive regression, and refinement. *Front Endocrinol* 6(May):67
 44. Nuzzo S, Meneghini C, Braillon P, et al (2003) Microarchitectural and physical changes during fetal growth in human vertebral bone. *J Bone Miner Res* 18(4):760–8
 45. Byers S, Moore AJ, Byard RW, et al (2000) Quantitative histomorphometric analysis of the human growth plate from birth to adolescence. *Bone* 27(4):495–501
 46. Fazzalari NL, Moore AJ, Byers S, et al (1997) Quantitative analysis of trabecular morphogenesis in the human costochondral junction during the postnatal period in normal subjects. *Anat Rec* 248(1):1–12
 47. Morales E, Guxens M, Llop S, et al (2012) Circulating 25-hydroxyvitamin D3 in pregnancy and infant neuropsychological development. *Pediatrics* 130(4):e913–e920
 48. Pala E, Erguvan M, Guven S, et al (2010) Psychomotor development in children with iron deficiency and iron-deficiency anemia. *Food Nutr Bull* 31(3):431–5
 49. Geber M (1973) L'environnement et le développement des enfants africains. *Enfance* 26(3–4):145–74

Enamel Distribution in 3D: Is Enamel Thickness More Uneven in the Upper Second Molars of Durophagous Hominoids?

Distribution 3D de l'émail : la répartition de l'émail est-elle moins uniforme sur les secondes molaires supérieures des hominoides durophages ?

G. Thiery · F. Guy · V. Lazzari

Received: 31 August 2018; Accepted: 04 March 2019
© Société d'Anthropologie de Paris et Lavoisier SAS 2019

Abstract Enamel thickness is not uniform across the dental crown of primates. It has been suggested that enamel distribution could be used in taxonomy or for ecological inferences. For instance, the thickness of molar enamel in mammals consuming hard food is expected to be uneven, despite differing reports on extant and extinct apes. Overall estimations of average and relative enamel thickness may mask the details of enamel distribution in complex teeth such as molars. Investigating enamel distribution and its purported relationship with ecology or phylogeny would require more detailed assessments. This paper aims to assess whether apes that consume hard foods on a regular basis, such as *Pongo pygmaeus*, can be characterized by the evenness or unevenness of enamel thickness. To do so, we combined topographic maps and distribution histograms of enamel thickness with cumulative profiles of its variation, or “pachymetric profiles”. We investigated a sample of 25 unworn hominoid upper second molars scanned by X-ray microtomography, and further compared this to a sample of 32 cercopithecines and colobines. Topographic maps show uniformly thin enamel for *Gorilla gorilla* and *Hylobates* sp., unevenly thin enamel for *Pan paniscus* and *Pan troglodytes*, and unevenly thick enamel for *Pongo pygmaeus*. The skewness of enamel distribution does not distinguish between ape species, but does separate apes from Old World monkeys. Contrary to previous reports on Old World monkeys, the slope of enamel thickness profiles, or pachymetric slope, does not predict the diet of extant apes. However, it does separate the *Pan* genus,

which is characterized by a higher pachymetric slope indicating more uneven enamel distribution compared to other apes. The uneven thickness of enamel distribution observed on topographic maps for *P. pygmaeus* is not supported by its low pachymetric slope, which instead indicates uniform enamel distribution. This discrepancy in the results obtained for *P. pygmaeus* can be interpreted as an evolutionary trade-off between fine-scale versus overall enamel distribution. On the one hand, unevenly thick enamel at a fine scale, combined with strongly decussated enamel as observed in *P. pygmaeus*, is expected to increase local resistance to crack propagation. On the other hand, uniformly thick enamel at the overall scale would improve the overall resilience of the enamel in coping with challenging food on a daily basis. Although understanding the effects of ecology on enamel distribution in apes requires further investigation, the results presented in this paper confirm the interest of enamel distribution for taxonomy and phylogeny.

Keywords Apes · Ecology · Enamel thickness · Pachymetric profiles · Phylogeny

Résumé L'épaisseur de l'émail n'est pas constante au sein de la couronne dentaire des primates. Il a été suggéré que la distribution de l'émail pouvait être utilisée en taxonomie ou pour faire des inférences écologiques. Par exemple, il est attendu que l'émail des molaires de mammifères consommant des aliments durs soit non uniformément épais, malgré des observations contradictoires chez les grands singes actuels et fossiles. Les variables estimant l'épaisseur de l'émail moyenne et relative peuvent dissimuler des variations plus subtiles dans la distribution de l'épaisseur de l'émail, notamment pour des dents complexes telles que les molaires. C'est pourquoi l'étude de la distribution de l'émail et ses possibles interactions avec l'écologie et la phylogénie peut nécessiter des estimateurs à la résolution plus fine. Cette étude a pour objectif de déterminer si les grands singes qui

G. Thiery (✉)
School of Sociology and Anthropology, 135 Xingang West Road,
Sun Yat-Sen University, 510275 Guangzhou, China
e-mail : ghislain.thiery@ntymail.com

G. Thiery · F. Guy · V. Lazzari
PALEVOPRIM UMR 7262 CNRS,
Université de Poitiers, Bât B35 – TSA 51106,
6 rue Michel Brunet, 86073 Poitiers, France

consomment des aliments plus résistants, comme *Pongo pygmaeus*, présentent un émail uniformément épais ou non uniformément épais. Pour ce faire, nous avons combiné les cartes topographiques et les histogrammes de distribution de l'épaisseur de l'émail avec les profils cumulés de la variation en épaisseur de l'émail, ou « profils pachymétriques ». Nous avons étudié un échantillon de 25 molaires supérieures non usées d'hominoides actuels, scannées par microtomographie à rayons X. Cet échantillon a ensuite été comparé à un échantillon de 32 cercopithèques et colobes. Les cartes topographiques indiquent que l'émail de *Gorilla gorilla* et d'*Hylobates* sp. est uniformément fin; que celui de *Pan paniscus* et *Pan troglodytes* est non uniformément fin; et que celui de *P. pygmaeus* est non uniformément épais. L'asymétrie de la distribution de l'émail ne permet pas de distinguer les grands singes entre eux, mais elle permet de distinguer des singes de l'Ancien Monde. Contrairement à ce qui a pu être observé chez ces derniers, la pente des profils d'épaisseur de l'émail, ou pente pachymétrique, ne permet pas d'estimer le régime alimentaire des grands singes actuels. En revanche, elle permet de distinguer le genre *Pan*, dont la pente du profil pachymétrique est significativement plus grande que chez les autres grands singes, ce qui traduit une distribution moins uniforme. La distribution non uniforme observée sur les cartes topographiques n'est pas détectée chez *P. pygmaeus*, dont les profils pachymétriques ont une pente plus faible qui indique au contraire une distribution uniforme de l'émail. Les résultats contradictoires obtenus pour *P. pygmaeus* peuvent être interprétés comme un compromis évolutif entre la distribution fine de l'émail et sa distribution globale. D'une part, une distribution non uniforme à fine échelle, combinée à l'émail fortement décussé observé chez *P. pygmaeus*, augmenterait la résistance locale à la propagation des fractures de l'émail. D'autre part, un émail uniformément épais à une échelle plus globale augmenterait la résilience de la dent lorsqu'elle est confrontée à des aliments résistants quotidiennement. En résumé, comprendre l'influence de l'écologie sur la distribution de l'émail chez les grands singes nécessite de plus amples recherches. Cependant, l'ensemble des résultats obtenus confirment l'intérêt de la distribution de l'émail en taxonomie et en phylogénie.

Mots clés Écologie · Épaisseur de l'émail · Grands singes · Phylogénie · Profils pachymétriques

Introduction

The multifactor origins of enamel thickness

Because of its widely accepted taxonomic and phylogenetic value, enamel thickness is an important measurement in

anthropology [1]. But because thicker enamel lessens deformation due to strain, thus improving resistance to tooth fracture, enamel thickness is also influenced by natural selection and may thus inform about the ecology of our extinct relatives [2]. Average enamel thickness (AET) seems to correlate with life expectancy in anthropoid primates [3]. Different estimates of relative enamel thickness (RET) have been made on the teeth of primates to infer diet and physical properties of food, mostly its hardness [1,4,5] and abrasiveness [6,7,8]. Thicker enamel could have also been selected in some extinct primates as a morphological response to the consumption of tough foods such as tubers or sedges [9,10].

Besides phylogeny and natural selection, enamel thickness is affected by physiological, developmental or environmental factors [11], which may explain regional differences reported within the same genus [12]. Ultimately, thick enamel could result from a wide array of factors, and it may be necessary to combine AET or RET with other enamel features such as its distribution in order to interpret enamel thickness.

Enamel distribution as an estimator of tooth function?

While AET and RET are convenient overall estimators of enamel thickness, enamel is usually not evenly distributed over the tooth surface. This is especially true for complex teeth such as premolars and molars, which have multiple cusps with different ranges of enamel thickness. For instance, in hominoids, enamel is significantly thicker on the upper molar lingual cusps and on the lower molar buccal cusps, which undergo more stress during mastication and have consequently been termed “functional cusps” [13-15]. In primates in general, function may play a major role in enamel distribution and it has been suggested that enamel distribution could be used to infer either the phylogeny or the ecology of extinct species, for instance when no differences in AET or RET have been observed [14,16]. Regarding ecological inferences, two different hypotheses have been put forward.

First, Lucas et al. [2] expected the enamel of mammals consuming hard food to be unevenly thick i.e., thicker at the molar cusp tips before they start wearing out. Their hypothesis is based on the assumption that unevenly distributed enamel would increase its resistance by inhibiting the extension of cracks where hard food comes into contact with the outer enamel surface. Conversely, evenly distributed enamel would promote the extension of cracks and make the molars more sensitive to challenging hard food. They also predicted that enamel decussation i.e., crossed sets of enamel prisms that increase resistance to crack propagation [17,18], would be found throughout the enamel cap in consumers of hard food.

In contrast, Olejniczak et al. observed on topographic maps of lower molar enamel thickness that *Gigantopithecus blacki*

and, to a lesser extent, *Pongo pygmaeus* were characterized by more evenly thick enamel than extant African apes, resulting in broader and flatter occlusal surfaces in *G. Blacki* and *P. pygmaeus* [19]. Since *P. pygmaeus* is a consumer of hard and tough foods [20], they subsequently hypothesized that more uniformly thick enamel, combined with short dentine horn height, might be explained by “hyper-masticatory” adaptation. However, this hypothesis is yet to be compared with the predictions of Lucas et al.[2].

Measuring enamel distribution

Most studies investigating enamel distribution are based on qualitative observations, either from three-dimensional (3D) topographic maps [19] or from two-dimensional (2D) sections that can be located on mesial, distal, lingual or buccal sections [21], at regular intervals along the molar row [22] or along the complete dental row [23]. From such 2D sections, enamel distribution can be quantified using linear measurements, for instance the minimum enamel thickness of the occlusal fovea or the maximum thickness of the lateral surface [16]. Assuming that enamel growth time is known, linear measurements can even be used to compute the daily enamel growth rate for different enamel regions [24]. Alternatively, enamel distribution can be measured by comparing AET and RET [21,22], lateral AET and lateral RET [25], relative enamel content [27] or relative enamel area [26] between slices made at different locations of the enamel crown.

Enamel distribution can also be quantified in 3D using AET and RET on well-defined dental regions of the enamel cap, such as the occlusal fovea versus the lateral surface, or the cuspal region versus the cervical region [16,28]. However, delimiting dental regions at a finer scale can be highly subjective. Alternatively, enamel distribution can be assessed from 3D models (in fact polygonal meshes) of the outer enamel surface (OES) and of the underlying enamel dentine junction (EDJ). In this case, the enamel thickness corresponds to the shortest normal distance from the OES to the EDJ surface [29]. In a later study, Thiery et al. [30] used within-model variation of this enamel-dentine distance to quantify enamel distribution in upper second molars of extant anthropoids. They reported a more uneven enamel distribution in Old World monkeys consuming hard food. This study is an extension of the Thiery *et al.* study [30] using the same methods.

Objectives

The aim of this study was to investigate whether the enamel of upper second molars in hard food specialist hominoids is uniformly thick, as suggested by the results of Olejniczak et al. [20] or unevenly thick, as predicted by Lucas et al. [2]. To do

so, we combined qualitative assessments from topographic maps of enamel distribution with quantitative assessments from within-model (intramesh) variations in enamel-dentine distance, as described by Guy et al. [29,30]. Since *Pongo pygmaeus* consumes more challenging hard food than other apes [20,32], the thickness of its enamel is expected to be more uneven [2,30].

Methods

Material

We collected 57 upper second molars from the following institutions: the University of Poitiers PALEVOPRIM collections, France, the Muséum national d’Histoire naturelle in Paris, France, the Royal Museum of Central Africa in Tervuren, Belgium and the Senckenberg Museum in Frankfurt, Germany (Table S1). We included 25 teeth of apes (Hominoidea), as well as 32 teeth of Old World monkeys (Cercopithecoidea) for extra-group comparison. No living animal was involved in this work, and no animal was killed specifically for this study. Only juvenile specimens and sub-adults were selected, so that the enamel was minimally worn *i.e.*, score of 1-2 using Scott’s dental wear scoring system [33].

Acquisition of Dental 3D Meshes

In order to investigate enamel thickness without damaging valuable museum specimens of juvenile primates, the teeth were scanned using high-resolution X-ray micro-computed tomography (HR- μ CT) at the Microtomography Centre in Poitiers, France. The scans were acquired using an EasyTom HR-microtomograph. Isovoxel resolution ranged from 15 to 30 μ m depending on tooth size. The resulting array of 2D slices was stacked to build 3D reconstructions of the teeth, which were segmented using Avizo following Guy *et al* [29,35]. We extracted models (polygonal 3D meshes) from both OES and EDJ. Using Geomagic Studio, these models were re-tessellated to 55,000 triangles of normalized area, which removed scaling effects on triangle geometry [34].

Following Guy et al. [35], the OES and EDJ surfaces were paired together and their orientation was standardized. Both OES and EDJ models were cropped occlusally *i.e.*, we retained only the occlusal basins and discarded the polygons below a plane parallel to the occlusal plane (xy) and passing through the lowermost point of (i), the enamel occlusal fovea and (ii), the dentine occlusal fovea.

Enamel-dentine distance and thickness maps

Following Guy et al. [29], enamel-dentine distances (EDD) were computed as the shortest Euclidean distance to the EDJ

surface. All computations were made in R 3.3.0 [36]. Surfaces were opened out as 3D meshes, and from the resulting array of polygon-based values, topographic maps of enamel thickness were plotted using the Rvcg package [37] (Fig. 1A). It is worth noting that our EDD maps are very

similar to Kono et al.'s thickness maps or *T-maps*, which picture the minimum distance to EDJ from OES pixels [15,16]. Both 3D AET and 3D RET values have already been published in another paper, so they are not reported here [30].

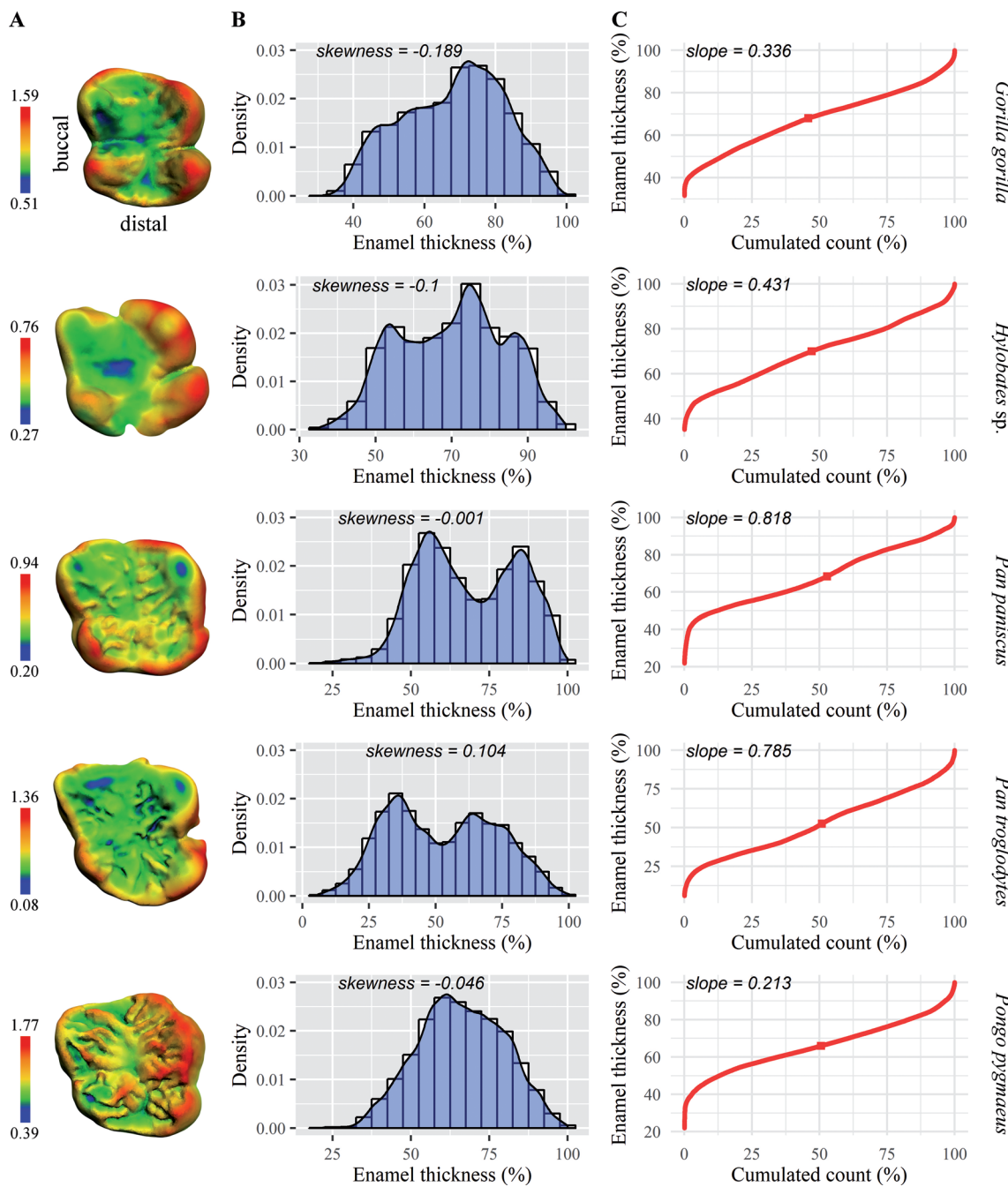


Fig. 1 Enamel distribution on the second upper molars of five extant ape species. The dental surfaces were cropped above the lowermost point of the occlusal surface. A: topographic maps of enamel-dentine distance (EDD), in mm; B: histograms of EDD distribution and density curves; C: pachymetric profiles. The red square corresponds to average enamel thickness / Distribution de l'émail de la deuxième molaire supérieure de cinq espèces actuelles de grands singes. Les surfaces dentaires ont été recadrées au-dessus du point le plus bas de la surface occlusale. A : carte topographique de la distance émail-dentine (EDD) en mm ; B : histogrammes de la distribution d'EDD et des courbes de densité ; profile pachymétrique. Les carrés rouges correspondent à l'épaisseur moyenne de l'émail

Within-model distribution of enamel-dentine distance

For every 3D tooth model, the range of EDD values was used to plot distribution histograms (Fig. 1B; Fig. S2). Two kinds of information could be retrieved from these figures. First, the major distribution modes were isolated. Second, we computed Pearson's skewness of the EDD distribution curves. Skewness is an estimation of a distribution's asymmetry: the skewness of a perfectly symmetrical distribution is zero, a negative value usually indicates asymmetry towards higher values and a positive value indicates asymmetry towards lower values. The higher the absolute skewness, the more asymmetrical the distribution of EDD values will be. The reverse is not true, however, because low skewness might also be due to a long tail somewhat compensated by a short but strong tail on the other side of the distribution curve.

Pachymetric profiles

Cumulative profiles of enamel thickness, or “pachymetric profiles” [30] (from the Greek *pachys-/παχυς-* “thick” and *métron-/μέτρον* “a measure”), are meant to represent the rate of change in the thickness of an object and draw on the cumulative profiles of ground elevation (hypso-metric profiles) used in traditional topography [31], with EDD replacing elevation. These profiles are built from EDD (in percentage of maximum EDD) plotted against the accumulated polygon count for each EDD value (as a percentage of the total number of polygons) (Fig. 1C).

The pachymetric slope is defined as the average slope of the pachymetric profile at average EDD. It is an estimate of the unevenness of enamel thickness: the steeper the slope, the more abrupt the thickness profile, and the less gradual the change in enamel thickness [30].

Results

Topographic maps

Occlusal enamel was found to be thinner than lateral enamel in *Gorilla gorilla*, *Hylobates* sp., *Pan paniscus* and *Pan troglodytes*, although it was especially marked in the genus *Pan*. Topographic maps of upper second molars show that the enamel of the occlusal fovea is evenly thin in *G. gorilla* and *Hylobates* sp., with relatively thicker enamel on the buccal side. (Fig. 1A; Fig. S2). Several *G. gorilla* teeth have thinner enamel on the protocone tip, although this might result from slight apical wear (Fig. S2). Both *P. paniscus* and *P. troglodytes* have an unevenly thin enamel distribution on the occlusal surface, which is characterized by local thickening in the enamel crenulations and by a thinner protocone tip, but again this might result from slight apical wear

(Fig. 1A; see also Kono 2004). The upper second molars of *Pongo pygmaeus* have unevenly thick enamel, characterized by local thickening not only on enamel crenulations, but also on the protocone and hypocone tips (Fig. 1A).

Within-model enamel distribution

Most *P. paniscus* and *P. troglodytes* specimens have a clear bimodal and sometimes multimodal EDD distribution (Fig. 1B; Fig. S2). In contrast, the second mode is less marked or completely absent in *G. gorilla* and *P. pygmaeus* specimens. No difference in distribution asymmetry could be detected between hominoid species (Kruskal-Wallis chi-squared = 3.872, df = 3, p-value = 0.275). Skewness scores for hominoids are close to zero and never below -0.50 (Fig. 2). In contrast, Old World monkeys have skewness scores as low as -1.25 (Fig. 3).

Pachymetric slope

The hard food specialist *P. pygmaeus* and the soft but tough food specialist *G. gorilla* have similar pachymetric slopes (Fig. 2). In contrast, both *P. paniscus* and *P. troglodytes* have significantly higher pachymetric slope scores (Wilcoxon rank sum test, W = 145, p-value < 0,001). Moreover, for a given skewness of EDD distribution, panines always have a steeper pachymetric slope and therefore a more uneven enamel distribution than any other extant ape (Fig. 2).

Discussion

Using topographic maps of EDD, we observed that the crenulations on the surface of *Pongo pygmaeus* upper second

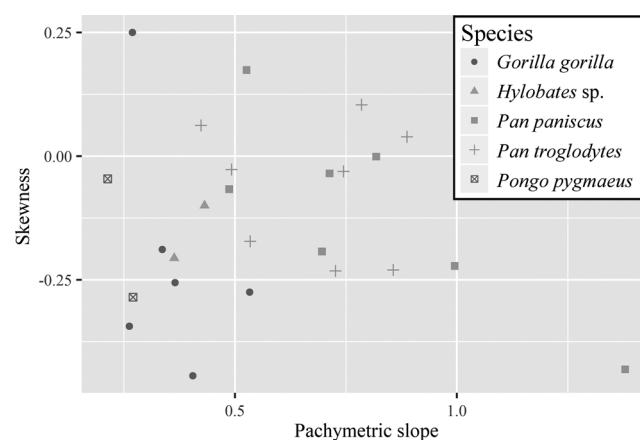


Fig. 2 Skewness of EDD distribution versus pachymetric slope in apes. Both variables are dimensionless / Asymétrie de la distribution de l'EDD comparée aux pentes pachymétriques chez les grands singes. Les deux variables n'ont pas de dimension

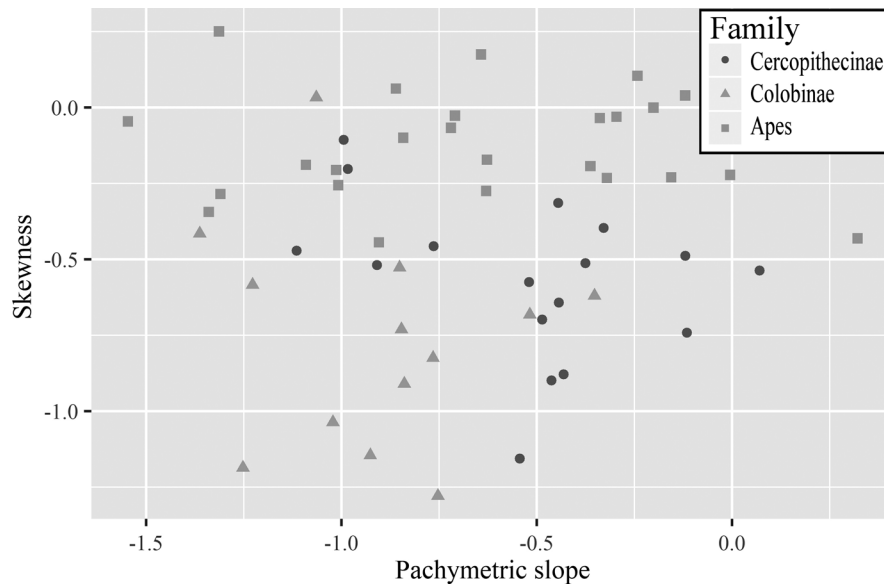


Fig. 3 Skewness of EDD distribution versus pachymetric slope in apes and Old World monkeys combined. Both variables are dimensionless / Asymétrie de la distribution de l'EDD comparée aux pentes pachymétriques chez les singes de l'ancien monde et les grands singes combinés. Les deux variables n'ont pas de dimension

molars result in uneven enamel thickness (Fig. 1A; Fig. S2). The enamel is locally thicker on the edge of the crenulations and at the tip of the functional cusps i.e., the protocone and the hypocone. To a lesser extent, this is also the case for the crenulated molars of *P. paniscus* and *P. troglodytes* (Fig. 1; Fig. S2). These observations contrast with the results of Olejniczak et al. [19] and tend to support the hypothesis of Lucas et al., who expected enamel to be unevenly thick in primates consuming hard food, such as *P. pygmaeus* [2]. Together with data on the enamel microstructure, which suggest that enamel decussation is more marked in *P. pygmaeus* than in any other extant ape [38], the predictions of Lucas et al. match what is observed in hominoids.

Nevertheless, this qualitative observation is not supported by the quantitative measurements reported in this paper, especially the slope of the cumulative enamel thickness profile (pachymetric slope). The upper second molars of *P. pygmaeus* are indeed characterized by a relatively low pachymetric slope, comparable to that of the upper second molars of the soft but tough food consumer *Gorilla gorilla* (Fig. 1C). This contradicts our expectations, as the pachymetric slope was significantly steeper for the hard food consuming species of Old World monkeys [30]. In contrast, the upper second molars of *P. paniscus* and *P. troglodytes* were characterized by steep pachymetric slopes, which probably result from unevenly thin occlusal enamel (Fig. 1C). These observations support the hypothesis of Olejniczak et al., who expected the enamel of *P. pygmaeus* to be more uniformly thick than in other apes [19].

These contrasting results can be explained by the fact that fine morphological details of enamel distribution, which are observable on thickness maps (Fig. 1A; Fig. S2), are concealed in the overall value calculated from pachymetric profiles (Fig. 1C; Fig. S2). This could result from an adaptive trade-off between better resistance to small-scale crack propagation, as suggested by Lucas et al. [2] and a large, thickly enamelled occlusal surface which is resilient to repetitive chewing of challenging food, as suggested by Olejniczak et al. [19]. However, it is not clear whether this trade-off might be linked to enamel crenulations or not. While crenulations of the enamel are observed in many seed-eating primates, their adaptive function is still in debate [39,20].

Because our sample is limited to unworn upper second molars, several questions remain unanswered. On the one hand, it is not known whether the methods presented here would produce the same results when applied to other tooth positions i.e., third molars, first molars and premolars. In hominoids, enamel thickness tends to increase along the dental row, but the putative effect of this gradient on enamel distribution is unknown [23,40]. On the other hand, there might be differences in enamel distribution between upper and lower molars. Furthermore, the hypothesis of unevenly thick enamel in hominoids adapted to hyper-mastication was formulated not from upper molars, but from lower molars [19].

In addition, enamel distribution is expected to be strongly affected by dental wear. We predict that the removal of occlusal enamel would increase the influence of the thick,

unworn lateral enamel on the distribution curves (Fig. 1A), resulting in greater asymmetry of EDD distribution and a steeper pachymetric slope as the tooth wears down. Most specimens of extinct hominoids are characterized by dental wear, and investigating the distribution of enamel across different wear stages may be a useful addition to other approaches, for example on lateral enamel [25].

Another factor that was not taken into account here is sexual dimorphism, especially in *P. pygmaeus*. Female orangutans have significantly higher AET and RET scores than males in both *P. pygmaeus* and *P. abelli* [40]. While this difference has been related to a significantly larger dentine core in males, a larger EDJ surface may also affect enamel distribution. Both specimens of *P. pygmaeus* used in this study are subadults, but their RET scores fall outside the range for males, suggesting that they could be females [40,30]. Including male specimens in future comparisons would help to understand how enamel distribution in *P. pygmaeus* is affected by sexual dimorphism and by dentine core size in general.

This study nevertheless shows that enamel distribution requires further investigation as it may convey both ecological and phylogenetic information. As regards the latter, one unexpected result was the difference in EDD distribution skewness between Old World monkeys and apes (Fig. 3). This result is unlikely to reflect more asymmetrical molars in Old World monkeys because the range of pachymetric profiles is actually wider in apes [30]. However, EDD skewness is close to zero in apes whereas it is almost entirely negative in Old World monkeys. This indicates that the EDD asymmetry shifts towards high EDD values in Old World monkeys. In apes however, this asymmetry may come from lower EDD values as well, as seen in the unevenly thin enamel of *P. paniscus* and *P. troglodytes* (Fig. 1A-B).

Another important phylogenetic application that emerges from this study is the identification of extinct hominoids from their enamel distribution. Several authors have proposed differences in enamel distribution as diagnostic features [9, 14, 19]. In this study, extant panines were characterized by steeper pachymetric slopes compared to other extant apes. We also observed that the enamel of the occlusal fovea is visibly thinner than lateral enamel, but this feature has been related to the ripe fruit dependent diet of the genus *Pan* [16,28,41]. Nevertheless, we suggest that a highly uneven enamel distribution in upper second molars, combined with thin occlusal enamel, could be diagnostic of the genus *Pan*. Fossil panines would therefore be expected to have a steep pachymetric slope, at least for unworn upper second molars [42]. This is consistent with evidence that genes involved in the regulation of enamel secretion underwent stronger selection in the genus *Pan* than in other extant apes [43].

Acknowledgments This study was supported by the French National Research Agency (*Agence nationale de la Recherche*, ANR-09-BLAN-0238 and ANR-17-CE02-0010-01), the Ministry for Education, Higher Education and Research (*ministère de l'Education nationale, de l'Enseignement supérieur et de la Recherche*), the Poitou-Charentes Region (*Conventions Région* #07/RPC-R-100 and #12/RPC-013) and by a research grant from the International Primatological Society. Many thanks to J. Cuisin from the *Muséum national d'Histoire naturelle* (Paris, France), E. Gilissen from the Royal Museum of Central Africa (Tervuren, Belgium) and K. Krohmann from the Senckenberg Museum (Frankfurt-am-Main, Germany) for granting us access to many of the specimens used for our work. We are greatly indebted to A. Mazurier (IC2MP), A. Euriat (PALEVOPRIM) and J. Surault (PALEVOPRIM) for their help with data acquisition.

Conflict of interest: The authors do not have any conflict of interest to declare.

References

1. Martin L (1985) Significance of enamel thickness in hominoid evolution. *Nature*, 314(6008):260–3
2. Lucas PW, Constantino P, Wood B, Lawn B (2008) Dental enamel as a dietary indicator in mammals. *BioEssays*, 30(4):374–85
3. Pampush JD, Duque AC, Burrows BR, et al (2013) Homoplasny and thick enamel in primates. *J Hum Evol*, 64(3):216–24
4. Kay RF (1981) The nut-crackers – a new theory of the adaptations of the Ramapithecinae. *Am J Phys Anthropol*, 55(2):141–51
5. Daegling DJ, McGraw WS, Ungar PS, et al (2011) Hard-Object Feeding in Sooty Mangabeys (*Cercocebus atys*) and Interpretation of Early Hominin Feeding Ecology. *PLoS ONE*, 6(8), e23095
6. Maas MC (1991) Enamel structure and microwear: An experimental study of the response of enamel to shearing force. *Am J Phys Anthropol*, 85(1):31–49
7. Teaford MF, Maas MC, Simons EL (1996) Dental microwear and microstructure in early oligocene primates from the Fayum, Egypt: Implications for diet. *Am J Phys Anthropol*, 101(4):527–43
8. Rabenold D, Pearson OM (2011) Abrasive, silica phytoliths and the evolution of thick molar enamel in primates, with implications for the diet of *Paranthropus boisei*. *PLoS ONE*, 6(12): e28379
9. Olejniczak AJ, Smith TM, Skinner MM, et al (2008) Three-dimensional molar enamel distribution and thickness in *Australopithecus* and *Paranthropus*. *Biol Lett*, 4(4):406–10
10. Ungar PS, Hlusko LJ (2016) The evolutionary path of least resistance. *Science*, 353(6294):29–30
11. Żądzińska E, Kurek M, Borowska-Strugińska B, et al (2013) The effect of the season of birth and of selected maternal factors on linear enamel thickness in modern human deciduous incisors. *Arch Oral Biol*, 58(8):951–63
12. Kato A, Tang N, Borries C, et al (2014) Intra- and interspecific variation in macaque molar enamel thickness. *Am J Phys Anthropol*, 155(3):447–59
13. Macho GA, Berner ME (1993) Enamel thickness of human maxillary molars reconsidered. *Am J Phys Anthropol*, 92(2):189–200

14. Schwartz GT (2000) Taxonomic and functional aspects of the patterning of enamel thickness distribution in extant large-bodied hominoids. *Am J Phys Anthropol*, 111(2):221–24
15. Kono RT, Suwa G, Tanijiri T (2002) A three-dimensional analysis of enamel distribution patterns in human permanent first molars. *Arch Oral Biol*, 47(12):867–75
16. Kono RT (2004) Molar enamel thickness and distribution patterns in extant great apes and humans: new insights based on a 3-dimensional whole crown perspective. *Anthropol Sci*, 112 (2):121–46
17. Koenigswald W, Rensberger JM, Pretzschner HU (1987) Changes in the tooth enamel of early Paleocene mammals allowing increased diet diversity. *Nature*, 328(6126):150–152
18. Bajaj D, Arola DD (2009) On the R-curve behavior of human tooth enamel. *Biomaterials*, 30(23–24):4037–46
19. Olejniczak AJ, Smith TM, Wang W, et al (2008) Molar enamel thickness and dentine horn height in *Gigantopithecus blacki*. *Am J Phys Anthropol*, 135(1):85–91
20. Vogel ER, van Woerden JT, Lucas PW, et al (2008) Functional ecology and evolution of hominoid molar enamel thickness: *Pan troglodytes schweinfurthii* and *Pongo pygmaeus wurmbii*. *J Hum Evol*, 55(1):60–74
21. Macchiarelli R, Mazurier A, Illerhaus B, Zanolli C (2009) *Orrorin tugenensis* (Mammalia, Primates, Hominoidea): virtual reconstruction and 3D analysis of a juvenile mandibular dentition (RPI-82 and RPI-83). *Geodiversitas*, 31(4):851–63
22. Smith TM, Olejniczak AJ, Martin LB, Reid DJ (2005) Variation in hominoid molar enamel thickness. *J Hum Evol*, 48(6):575–92
23. Smith TM, Olejniczak AJ, Reh S, et al (2008) Brief communication: Enamel thickness trends in the dental arcade of humans and chimpanzees. *Am J Phys Anthropol*, 136(2):237–41
24. Zanolli C, Dean C, Rook L, et al (2016) Enamel thickness and enamel growth in *Oreopithecus*: Combining microtomographic and histological evidence. *CR Palevol*, 15(1):209–26
25. Zanolli C, Bayle P, Bondioli L, et al (2017) Is the deciduous/permanent molar enamel thickness ratio a taxon-specific indicator in extant and extinct hominids? *CR Palevol*, 16(5):702–14
26. Engelsch LM, Kostrzewa K, Kopke S, et al (2017) Uneven distribution of enamel, dentine and cementum in cheek teeth of domestic horses (*Equus caballus*): A micro computed tomography study. *PLOS ONE*, 12(8):e0183220
27. Winkler DE, Kaiser TM (2015) Structural Morphology of Molars in Large Mammalian Herbivores: Enamel Content Varies between Tooth Positions. *PLOS ONE*, 10(8):e0135716
28. Kono RT, Suwa G (2008) Enamel Distribution Patterns of Extant Human and Hominoid Molars: Occlusal versus lateral enamel thickness. *Bull Natl Mus Natl Sci, Ser D*, 34:1–9
29. Guy F, Gouvard F, Boistel R, et al (2013) Prospective in (primate) dental analysis through tooth 3D topographical quantification. *PLoS ONE*, 8(6):e66142
30. Thiery G, Lazzari V, Ramdarshan A, Guy F (2017) Beyond the map: enamel distribution characterized from 3D dental topography. *Front Physiol*, 8:524
31. Strahler AN (1952) Hypsometric (area-altitude) analysis of erosional topography. *GSA Bulletin*, 63(11):1117–42
32. Lucas PW, Gaskins JT, Lowrey TK, et al (2012) Evolutionary optimization of material properties of a tropical seed. *J Roy Soc Interface*, 9(66):34–42
33. Scott EC (1979) Dental wear scoring technique. *American Journal of Physical Anthropology*, 51(2):213–17
34. Lazzari V, Guy F (2014) Quantitative three-dimensional topography in taxonomy applied to the dental morphology of catarrhines. *Bull Mém Soc Anthropol Paris*, 26(3–4):140–6
35. Guy F, Lazzari V, Gilissen E, Thiery G (2015) To what extent is primate second molar enamel occlusal morphology shaped by the enamel-dentine junction? *PLoS ONE*, 10(9):e0138802
36. R Core Team (2016) R: A language and environment for statistical computing. Vienna, Austria, R Foundation for Statistical Computing
37. Schlager S (2017) Morpho and Rvcg – Shape Analysis in R. In: Zheng G, Li S, Szekely G (eds), *Statistical Shape and Deformation Analysis*. Academic Press, pp 217–56
38. Macho GA, Jiang Y, Spears IR (2003) Enamel microstructure—a truly three-dimensional structure. *J Hum Evol*, 45(1):81–90
39. Lucas PW, Teaford MF (1994) Functional morphology of colobine teeth. In: Davies G, Oates J (eds) Colobine monkeys: their ecology, behaviour and evolution. Cambridge, Cambridge University Press, pp 173–203
40. Smith TM, Kupczik K, Machanda Z, et al (2012) Enamel thickness in Bornean and Sumatran orangutan dentitions. *Am J Phys Anthropol*, 147(3):417–26
41. Suwa G, Kono RT, Simpson SW, et al (2009) Paleobiological Implications of the *Ardipithecus ramidus* Dentition. *Science*, 326(69):94–9
42. McBrearty S, Jablonski NG (2005) First fossil chimpanzee. *Nature*, 437(7055):105–8
43. Horvath JE, Ramachandran GL, Fedrigo O, et al (2014) Genetic Comparisons Yield Insight into the Evolution of Enamel Thickness during Human Evolution. *J Hum Evol* 73:75–87

Reconstruction of Two Mother-Infant Dyads and Obstetrical Consequences of the Mesolithic-Neolithic Transition: A Case Study from Lepenski Vir and Vlasac (Serbia)

Apport de la reconstruction de deux dyades mère-enfant et conséquences obstétricales de la Transition Méolithique-Néolithique : étude de cas des sites de Vlasac et de Lepenski Vir (Serbie)

J. Jovanović · P. Frémondière · S. Stefanović

Received: 7 May 2018; Accepted: 8 October 2018
© Société d'Anthropologie de Paris et Lavoisier SAS 2018

Abstract The current world population of approximately seven billion people shows that despite the complexities of human birthing, the human species is thriving. Changes in human pelvic morphology resulting from bipedalism and encephalisation, often described as the “obstetric dilemma”, have made the birthing process extremely difficult and risky for both mothers and neonates. The major Mesolithic-Neolithic shift in lifestyle could have had important obstetric consequences. It is often hypothesised that the shift to an agricultural diet, with a lower protein content and higher glycaemic loading than the hunter-gatherer diet, could have led to a decrease in maternal height and an increase in neonatal birth weight, brain size and foetal-pelvic strain, which may have exacerbated the obstetric dilemma. The Mesolithic-Neolithic osteological collection from the Danube Gorges (7400-5500 cal BC, Balkans) provides material (2 pelvises and a neonate skull) to test this hypothesis by virtually reconstructing the

fossil dyads and their foetal-pelvic relationship. We compared these dyads with a large obstetrical sample of mother-child dyads with a known birthing history, conducting a linear-discriminant analysis in order to predict the most probable delivery outcomes for the prehistoric dyads. The results suggest that delivery was dystocic for the Mesolithic mother-child dyad and eutocic for the Neolithic mother-child dyad; obstetrically, the former is notably more efficient. However, due to the small sample size, further research is required with a larger series in order to determine whether the development of obstetrically efficient pelvic bones in the Neolithic was widespread and whether it had an impact on the birthing process and thus potentially contributed to the increasing size of the population.

Keywords Mesolithic-Neolithic · Balkans · Pelvis · Neonates · Birth

J. Jovanović (✉)
Laboratory for Bioarchaeology, Faculty of Philosophy,
University of Belgrade, Čika Ljubina 18-20, 11000 Belgrade,
Serbia; Biosense Institute, University of Novi Sad, Bulevar
Zorana Đindjića 1, 21000 Novi Sad, Serbia
e-mail : jelena.jovanovic@bioarch.rs

P. Frémondière (✉)
UMR 7268 AdéS, Aix-Marseille Université, CNRS,
Faculté de Médecine de Marseille, Secteur Nord,
Batiment A-CS80011, Marseille cedex 15, France
e-mail : pierrefremondiere@yahoo.fr

S. Stefanović (✉)
Biosense Institute, University of Novi Sad,
Bulevar Zorana Đindjića 1, 21000 Novi Sad, Serbia;
Laboratory for Bioarchaeology, Faculty of Philosophy,
University of Belgrade, Čika Ljubina 18-20,
11000 Belgrade, Serbia
e-mail : sofija.Stefanović@biosens.rs

Résumé La population actuelle, d'environ 7 milliards d'individus, est la preuve que l'humanité a pu prospérer malgré la complexité de la mécanique obstétricale qui la caractérise. Les changements de la morphologie pelvienne issus du « dilemme obstétrical » impliquent le processus d'encéphalisation et de bipédie. L'accouchement humain est supposé risqué et dystocique. Celui-ci pourrait être impacté au moment de la transition mésolithique – néolithique : le changement de l'alimentation vers un régime incluant de nouvelles ressources cultivées avec un apport plus riche en glucide, et pauvre en protéine, pourrait augmenter le poids et les dimensions cérébrales néonatales, diminuer la stature maternelle et augmenter la contrainte foeto-pelvienne. Les collections ostéologiques des gorges du Danube (7400-5500 BC) offrent l'opportunité de reconstruire deux dyades virtuelles fossiles (2 bassins et 1 crâne de nouveau-né) et d'étudier leur contrainte foeto-pelvienne. Basés sur une analyse discriminante linéaire, et sur des

données cliniques, nos résultats suggèrent que la dyade mésolithique est dystocique, tandis que la dyade néolithique est eutocique. Cependant la taille de l'échantillon étudié incite à reproduire ces analyses sur d'autres séries afin de déterminer si l'émergence d'un bassin plus eutocique fut un phénomène global au Néolithique qui aurait potentiellement pu affecter le déroulement des naissances et peut être influencé ainsi l'accroissement de la population.

Mots clés Mésolithique-Néolithique · Les Balkans · Bassin · Nouveau-nés · Naissance

Introduction

In modern humans, giving birth is a more difficult, dangerous and painful process than in other primates. However, the current world population of more than seven billion people shows that human reproduction is successful despite the complexities of birthing. The human pelvis is an extraordinary structure and is of critical importance for bipedal locomotion, thermoregulation and childbirth. The shift to bipedalism affected the shape of human pelvis [1], which became narrower due to the need to balance the body on one foot and to keep the leg and pelvis joints close to the centre of gravity. The distance between the promontory of the sacrum and the hip joint therefore decreased, improving stability between the legs, the pelvis and the vertebral column and increasing locomotor efficiency. It also influenced the size and shape of the birth canal, making it relatively narrow along the anterior-posterior plane [2]. Additional changes in pelvic morphology occurred during the Middle Pleistocene with the increase in brain size in hominines [3]. The heads of the more encephalised neonates could barely fit into the narrow birth canal, making the passage very difficult [4]. If the head, which is the largest part of the foetal anatomy, is too voluminous to pass through the pelvis, labour is obstructed or dystocic, and the cephalic pole lies above the inlet (this is known as CPD, or cephalopelvic disproportion). Because of these changes, the birth mechanism also changed, requiring neonates to rotate in order to push their heads through the narrow birth canal [5]. The interaction of the two opposed evolutionary pressures of bipedalism and encephalisation is often described as the “obstetric dilemma” [6,7]. According to WHO reports¹, prolonged or obstructed labour directly accounts for about 8% of maternal deaths globally.

The evolution of human parturition is not easily studied because pelvic bones and their specific parts, which are

crucial for the reconstruction of the birth canal, are often badly preserved in the archaeological record. Despite extensive work undertaken to further our understanding of the evolution of the birthing process in humans [2,4,6-10] and in the ancestor species of modern humans [e.g.11-14], there are no studies focusing on the Mesolithic-Neolithic transitional period, which saw not only the first large increase in the human population [15], but also significant changes in lifestyle, including the beginning of a fully sedentary life and the domestication of animals and plants. The shift to an agricultural diet, with a lower protein content and higher glycaemic load than a hunter-gatherer diet, could have increased neonatal birth weight and brain size, decreased maternal size and increased the foetal-pelvic constraint, thus exacerbating the obstetric dilemma [6,10,16]. On the other hand, an agricultural diet could have had important obstetric consequences for the skeletal morphology of mothers and babies, leading to higher fertility rates in the Neolithic period. In order to investigate and predict the most probable delivery outcomes during the Mesolithic-Neolithic transition, we reconstructed virtual dyads and their foetal-pelvic relationship from the Danube Gorges Mesolithic-Neolithic osteological collection (7400-5500 calBC, Balkans).

The human skeletal remains analysed are from the Late Mesolithic site of Vlasac and the Mesolithic-Neolithic site of Lepenski Vir (Fig. 1), in the Balkans in south-eastern Europe. The two sites are ~3 km apart along the Serbian-Romanian border in the Danube Gorges region. Due to the exceptional continuity of life in this region (9500-5500 calBC) [17]², these sites are central to our understanding of the nature of the Mesolithic-Neolithic transition in this part of Europe. Different kinds of evidence from these settlements suggest that the Mesolithic hunter/fisher/gatherers adopted a sedentary way of life prior to and independently of their adoption of animal and plant husbandry [17,18]. Although the Neolithic way of life (farming of crops and animals, appearance of polished stone tools and pottery) arrived in the area around 6300 BC [19,20], as well as people from the Aegean carrying a different genome [21], the Mesolithic traditions persisted [17].

Materials and Methods

For this study, we carried out morphometric analyses and a virtual reconstruction of two female pelvic bones (one

2. Stratigraphically and chronologically, the Mesolithic and Neolithic sequences in the Danube Gorges are divided into Early Mesolithic (9500-7400 calBC); Late Mesolithic (7400-6300 calBC), Transformational/Early Neolithic (6200-6000/5950 calBC) and Early/Middle Neolithic (5900-5500 calBC) phases [21].

1. World Health Organization (2005) The World Health report- Make every mother and child count. Geneva, p. 230.

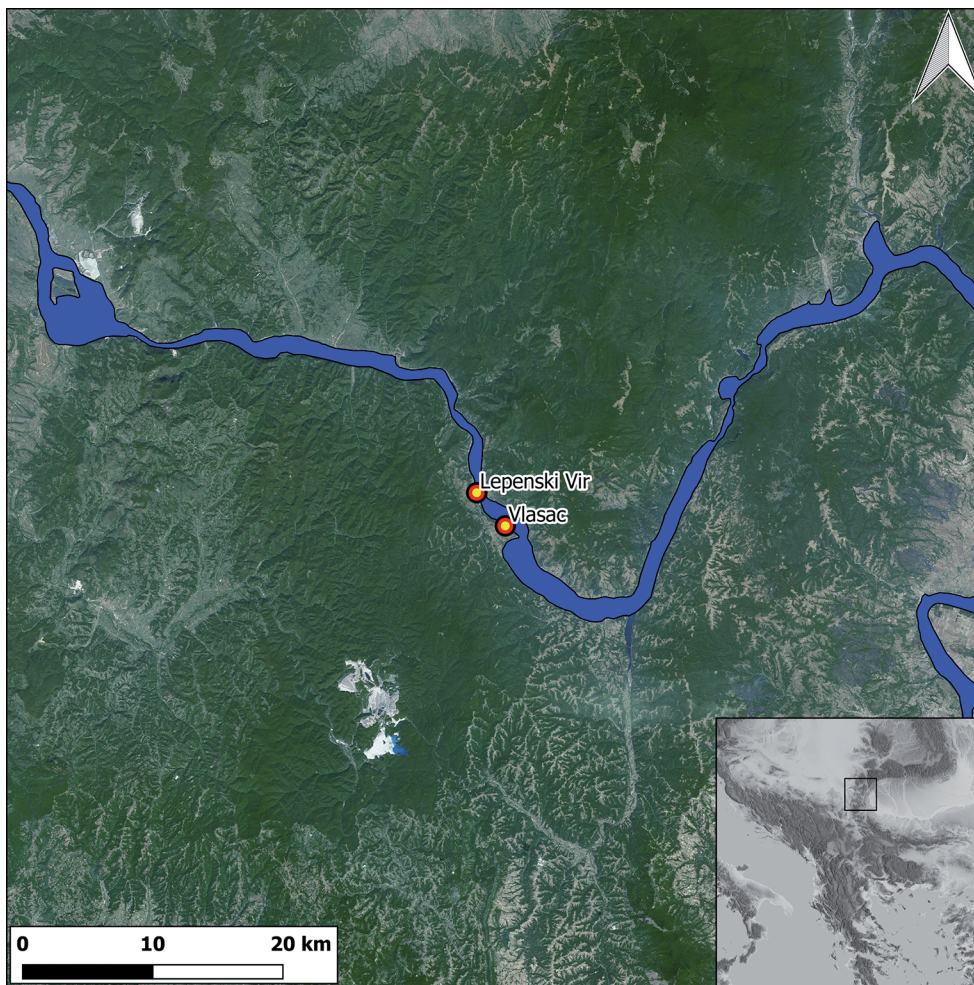


Fig. 1 Map of the research area with sites from which the samples in this study originate / *Carte de la zone de recherche avec les sites dont est issu l'échantillon de cette étude*

Mesolithic and one Neolithic) and one neonate head (from the Mesolithic-Neolithic transitional period). The study involved analysing the variability of the foetal-pelvic relationship from an anatomical perspective and its consequences on clinical outcomes (*i.e.* dystocic or eutocic labour). This analysis indicates whether the Mesolithic/Neolithic dyads were eutocic or dystocic. All bones were scanned to 0.15 mm resolution with a Range Vision Pro 3D scanner. We compared our mother-child dyads and their foetal-pelvic relationships with a large obstetrical sample of mother-child dyads from a previous study [22], with known birth histories, by conducting partial linear-discriminant analysis (LDA) to predict the most probable delivery outcomes for the prehistoric dyads. The sex of the two females was determined using a morphological approach [23] and a probabilistic morphometric approach [24], both based on the pelvic bones. By combining these two methods, we minimised observer error [24] and maximised the number of sex determinations [23]. Their age was estimated from the auricular surface and the pubic symphysis [25,26]. The sex of

the neonate was determined by DNA analysis [27], while the age was estimated from long bone measurements [28].

Reconstruction of the Vlasac79 pelvis

The pelvis belongs to a female aged over 60 and 171.3 cm in stature, found in Burial 79 at the Late Mesolithic site of Vlasac (7400-6200 calBC) [29]. The pelvis, noted in this study as "Vlasac79", consists of a fragment from the first sacral vertebra, a partial right ilium and an almost complete right superior pubic ramus. Reconstruction of the pelvis was possible at the level of the arcuate line of the ilium and the pectenial line of the pubis because they are well preserved. The reconstruction of the iliopectenial line and the inlet allows a plausible estimation of the risk of obstructed labour. The reconstruction involved rotation and translation of the preserved parts of the pelvis. This adjustment produced the best fitting position between each preserved part of the pelvis: for example, the sacrum and ilium are well adjusted

when the auricular surface of the sacrum is superimposed on the auricular surface of the ilium. We did not reconstruct missing parts with interpolation methods such as kriging [30] or thin-plate spline [31], as the shape of the complete modern pelvis could strongly influence the shape of the fossils.

The right ilium and the right superior pubic ramus were adjusted by observing three rules:

- 1) Medially, the arcuate line of the ilium and the pectineal line should be in the same plane (*i.e.* the inlet plane);
- 2) Frontally, the anterior and superior part of the acetabulum of the right superior pubic ramus should align with the posterior part of the acetabulum of the right ilium;
- 3) When viewed superiorly, the iliopectineal line should describe a plausible curve compatible with the position of the symphyseal surface in the sagittal plane.

We were able to adjust the right ilium and the sacrum thanks to the well-preserved superior and anterior part of the auricular surface of the ilium, which fitted well with the well-preserved superior and anterior part of the right auricular surface of the sacrum. The sagittal plane was created with the posterior-most mid-sagittal point of the superior endplate of the first sacral vertebra, the promontory, and the mid-sagittal inferior and anterior point of the vertebral body. This sagittal plane enabled us to mirror-image the right ilium and the right superior pubic ramus, and to reconstruct the inlet of the pelvis.

Reconstruction of the Lvir19 pelvis

This pelvis belongs to a female aged 25-39 and 159.7 cm in stature, found in Burial 19 in the Early Neolithic layer at Lepenski Vir (5984-5752 calBC) [29]. The pelvis, noted in this study as “Lvir19”, is composed of almost complete left parts of the first and second sacral vertebra, part of the left ilium and a large part of the left superior pubic ramus. The left ilium, left superior pubic ramus and the sacrum were adjusted by observing the same three rules as for Vlasac79. The same mirror-imaging methodology was used. The sagittal plane was created with the mid-sagittal posterior-most point of the superior endplate of the first sacral vertebra, the promontory, and the mid-sagittal inferior and anterior point of the 2nd vertebral body. The translation and rotation were performed with Avizo v.7.0.

Reconstruction of neonate skull Lvir98

The skull belongs to a female neonate determined to have reached 35-37 gestational weeks, found in Burial 98 in the Mesolithic-Neolithic transitional layer (6200-5950 cal BC) at Lepenski Vir [28]. The reconstruction of this neonatal skull, noted here as “Lvir98”, is based on the left frontal

bone, a partial left section of the parietal bone, and a fragment of the occipital bone. The reconstruction was performed in two stages:

- 1) the frontal, parietal and occipital bones were adjusted to the 3D model of a modern neonate skull: this was necessary because the connections between the three parts are missing;
- 2) the modern neonate skull was scaled to fit the size and curvature of the frontal, occipital and parietal bones.

Measurement of foetal-pelvic variables

The foetal-pelvic variables were measured to identify the most probable delivery outcomes for the “Vlasac79-Lvir98” and “Lvir19-Lvir98” virtual mother-child dyads. Different delivery outcomes could be considered, such as the arrest of labour [22] and the arrest of descent during the 2nd stage of labour [22]. Here we decided to focus on the risk of arrest of labour because the pelvis reconstruction enabled us to analyse only the inlet plane. The neonatal and pelvic variables used are those described by Frémondrière et al. [22] (Fig. 2).

A previous study [22] was conducted with a large sample of modern females and their neonates. Eighteen neonatal measurements and 43 pelvic variables were taken from the modern dyads, and the delivery outcomes (*i.e.* presence/absence of the arrest of labour, also called foetal-pelvic disproportion) was taken from the medical record. The LDA of the variables available for the fossil dyads (*i.e.* cephalic and inlet variables) enabled us to distinguish two groups, *i.e.* eutocia versus dystocia, to add further dyads to the analysis (here “Vlasac79-Lvir98” dyad and “Lvir19-Lvir98”) and to predict the most probable delivery outcomes.

Results

The reconstructions of the Lvir98 neonate and the Vlasac79 and Lvir19 pelvises are shown in Figure 3 and the measurements of the dyads are given in Table 1. The measurements reflect the variability of the modern obstetrical sample. The prediction of the most probable delivery outcome, based on the LDA, is shown in Figure 4. The “Vlasac79-Lvir98” dyad was attributed to the dystocic delivery group (characterised by the arrest of labour and foetal-pelvic disproportion) with a probability of 96%, and the “Lvir19-Lvir98” dyad to the eutocic group with a probability of 99%.

Discussion

The results suggest that the Mesolithic dyad “Vlasac79-Lvir98” is more dystocic and would have a greater chance of a difficult birth than the “Lvir19-Lvir98” Neolithic

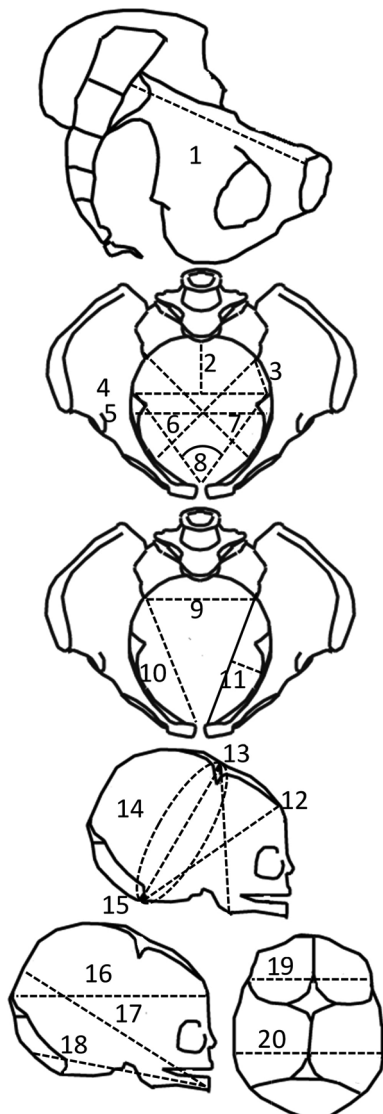


Fig. 2 Foetal-pelvic variables: 1: Inlet antero-posterior, 2: Sagittal posterior inlet, 3: Left inlet posterior space, 4: Maximal transverse inlet, 5: Medial transverse inlet, 6: Left oblique inlet, 7: Right oblique inlet, 8: Pectineal angle, 9: Sacral breadth, 10: Right ilio-pectineal chord length, 11: Left iliopectineal chord subtense, 12: suboccipitofrontal, 13:submentobregmatic, 14:suboccipitobregmatic circumference, 15: suboccipitobregmatic, 16: occipitofrontal, 17: mentovertical, 18: mentooccipital, 19: bitemporal, 20: biparietal / Variables foeto-pelviennes : 1 : antéro-postérieur du détroit supérieur; 2 : Sagittal postérieur du détroit supérieur; 3 : Espace postérieur gauche du détroit supérieur; 4 : Transverse maximum, 5 : Transverse médian du détroit supérieur; 6 : Oblique gauche du détroit supérieur; 7 : Oblique droit du détroit supérieur; 8 : Angle de l'arc antérieur; 9 : Largeur sacrée, 10 : Corde ilio-pectinée droite, 11 : Flèche ilio-pectinée gauche, 12 : Sous-occipito-frontal, 13 : Sous-mento-bregmatique, 14 : Circonference sous-occipito-bregmatique, 15 : Sous-occipito-bregmatique, 16 : Occipito-frontal, 17 : Sincipito-mentonnier, 18 : Occipito-mentonnier, 19 : Bitemporal, 20 : Bipariétal.

dyad, for which a “normal” childbirth would be expected. This is surprising given the large dimensions of the Vlasac79 pelvis compared to Lvir19. However, Lvir19 has a more rounded inlet, which is assumed to be more obstetrically efficient [22,32]. This result could be explained by the circular shape of the inlet (gynaecoid shape): the pectineal angle, the sagittal posterior inlet, and the iliopectineal chord subtense are larger in Lvir19 than in Vlasac79.

Given that our findings are based on a limited sample (*i.e.* only one pelvis for the two periods considered), the results from our analyses should be considered with caution. This limitation is common in palaeo-obstetrical studies. For example, only one [33,34] or two [35,36] reconstructions of the pelvis showed that Australopithecines experienced eutocic birth [33], dystocic birth [34,35] or non rotational birth [34,36]. To compensate for this limitation, we chose to consider only the best-preserved pelvises and to limit our reconstruction to the pelvis inlet. We also show two dyads based on neonatal reconstruction, which is rare in palaeo-obstetrical studies (see Ponce de Léon *et al.*, 2008 for a Neanderthal dyad reconstruction).

The observed difference in obstetrical efficiency can be examined in the light of the major dietary change during the Mesolithic-Neolithic transition. In a review, Roy [16] underlines that childbirth among hunter-gatherers in Africa and Australia seems to have been remarkably easy compared to agricultural societies. The development of agriculture during the Mesolithic-Neolithic transition triggered profound changes in both diet and population densities. It has been hypothesised that the shift from a protein-based diet to a diet dominated by carbohydrates with a higher glycaemic load may have led to a decrease in maternal stature and an increase in foetal weight [37,38]: many studies have shown that mothers of short stature (<155cm) have a higher risk of Caesarean delivery and adverse outcomes of pregnancy [39,40]. These changes could have caused more obstructed labour in the Neolithic. However, stable isotope analysis showed that, in the Danube Gorges, there was no abrupt shift in the diet as seen in other European Mesolithic-Neolithic communities because, in the Gorges, many Neolithic individuals relied on wild (aquatic) food [17]. For instance, the Neolithic female from Burial 19 at Lepenski Vir had a diet based on animal protein and aquatic resources, similar to the Mesolithic woman buried in Burial 79 at Vlasac. Furthermore, both of the females had an aquatic diet rich in vitamin D and neither shows evidence of rickets (*i.e.* vitamin D deficiency), which is often connected with a higher risk of obstructed labour and indicative distortion of the pelvis shape [41].

Since diet was not the cause of the different pelvic morphologies, the age of the Mesolithic woman needs to be considered (*i.e.* over 60). A study by Huseynov *et al.* [8] showed that the female pelvis has the most adequate

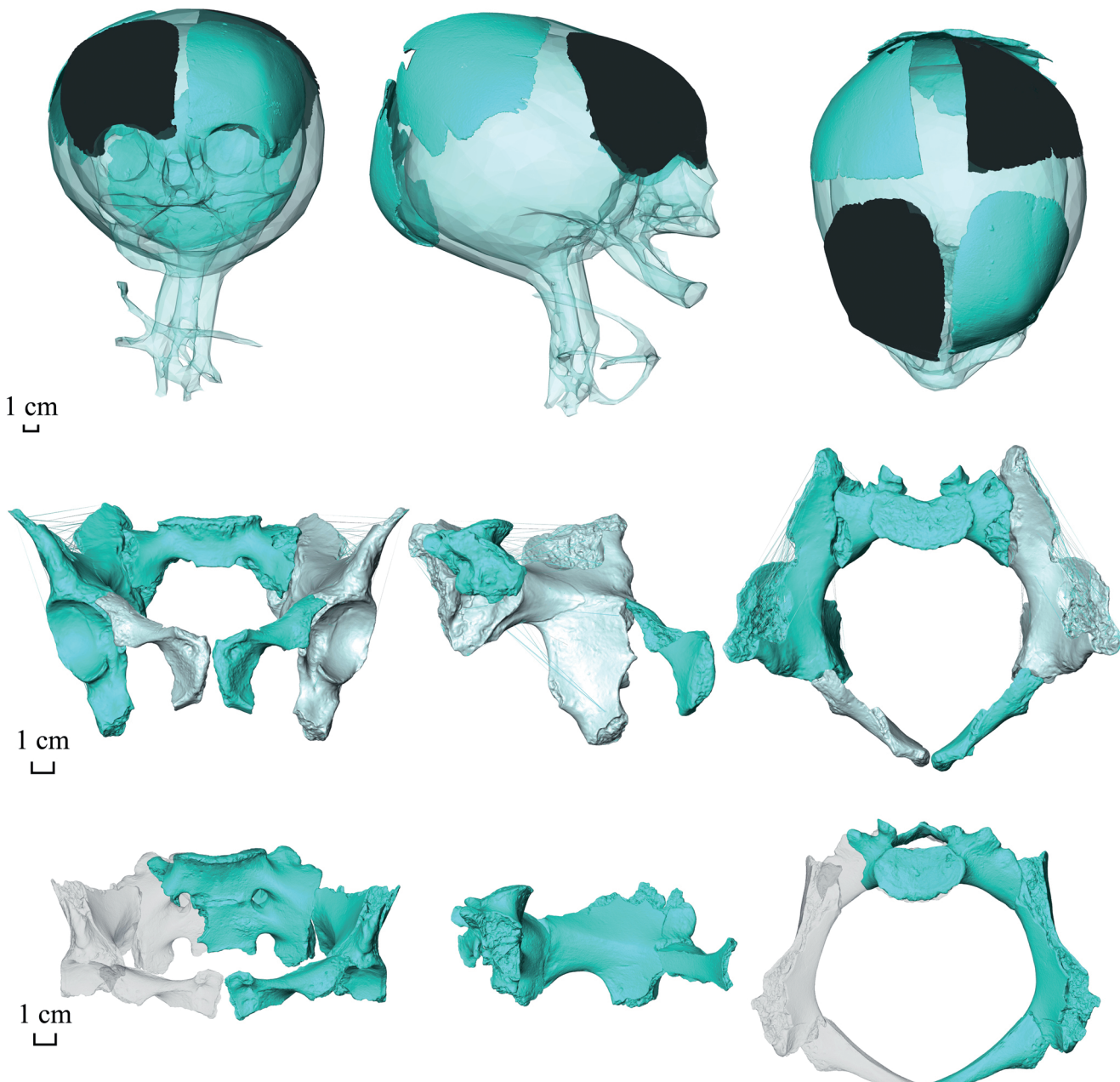


Fig. 3 Reconstruction of neonate Lvir98 (top row), and pelvises Vlasac79 (middle row) and Lvir19 (bottom row) / La reconstruction du nouveau-né Lvir98 (en haut), et des bassins Vlasac79 (au milieu) et Lvir19 (en bas)

morphology during the reproductive period, but that it may change later to a pattern of development similar to that of males, which can reduce the dimensions of the birth canal. Some modifications in pelvis morphology could be linked to hormonal changes during puberty, when the shape of the pelvis is adjusting to the needs of the birthing process [8]. During puberty, the female pelvis starts to diverge from the male pelvis, with obstetrically relevant pelvic dimensions expanding rapidly up to 25–30 years of age. This change is mostly related to the pubertal rise in the oestrogen hormone

oestradiol, resulting in the obstetrically most adequate pelvic morphology during the period of maximum female fertility. From 40 years of age onwards, oestradiol levels begin to fall, which results in a reduction of the obstetric dimensions. Although morphological changes associated with aging are possible, the sexual dimorphism expressed by the pelvis is considered as having a greater impact on the overall morphology of the bone.

Individual age may be one of the reasons for the observed variations in the obstetric characteristics of the pelvis, but the

Table 1 Measurements of the “Vlasac79-Lvir98” and “Lvir19-Lvir98” dyads / <i>Les mesures des dyades “Vlasac79-Lvir98” et » Lvir19-Lvir98”</i>				
	Lvir19	Vlasac79	Modern obstetrical sample of females and their neonates	
Pelvises			Mean	Standard deviation
Inlet antero-posterior diameter	112.8	136.0	124.5	9.3
Medial transverse diameter	123.2	124.3	121.5	7.8
Maximum transverse diameter	123.8	130.8	127.3	8.0
Right iliopectineal chord length	111.3	126.1	118.8	6.6
Left iliopectineal chord subtense	31.4	28.7	32.0	8.1
Right oblique diameter	119.1	125.5	126.0	6.5
Left oblique diameter	119.1	125.5	125.5	7.0
Left inlet posterior space	44.5	54.6	97.4	5.5
Sagittal posterior space	55.0	54.8	50.7	7.2
Pectineal angle	90.8	76.2	80.9	5.7
Inlet sacral breadth	95.7	104.3	103.2	8.6
Lvir98				
Submentobregmatic	91.3		97.3	5.7
Suboccipitofrontal	97.1		104.8	4.3
Mentooccipital	126.5		134.0	5.5
Suboccipitobregmatic	84.0		95.6	3.9
Bitemporal	76.5		74.7	4.4
Suboccipitobregmatic circumference	290.0		325.6	11.4
Biparietal	92.4		94.4	3.9
Mentovertical	119.5		127.4	6.4
Occipitofrontal	113.5		114.4	3.9

Probability of eutocic delivery

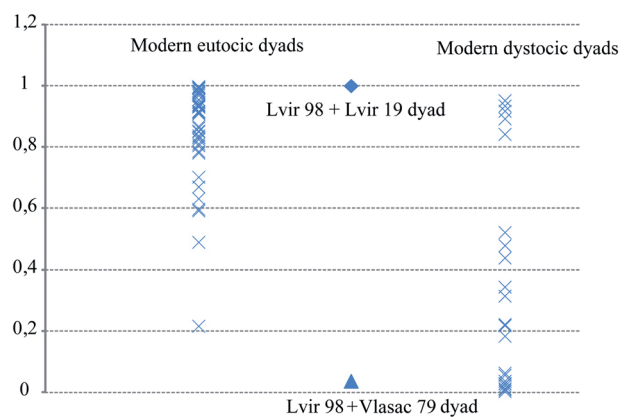


Fig. 4 Prediction of the most probable delivery outcome for the “Lvir 98-Vlasac79” dyad and “Lvir98-Lvir19” dyad, based on the LDA / *Prédiction de la modalité d'accouchement la plus probable pour les dyades “Lvir98-Vlasac79” et “Lvir98-Lvir19”, basée sur l'ADL*

different genetic background of the Mesolithic and Neolithic females could also have played a role. A recent DNA study [21] showed that these two females probably had different genetic origins. Even though there is no genetic data available for the Mesolithic female analysed here, all other individuals from Vlasac for which DNA was analysed showed that this was an isolated hunter-gatherer population, whereas at Lepenski Vir, incorporation of individuals from the Aegean (presumably farmers) was detected [21]. The Neolithic female (Lvir19) has a farmer gene (K1b1a) and certainly belongs to a different population from the one at Vlasac. The different genetic origin could be one of the reasons for the different obstetrical measurements. The anatomically narrow modern pelvis with a more circular birth canal appeared some 200 000 years ago in Africa and the Middle East [2]. It can be hypothesised that the Neolithic female's pelvis, which is the most common shape among females today, was better suited to the birthing process due to the long, gradual genetic adaptation that took place in the Near East, although we need more samples in order to confirm this hypothesis. Of the various adaptations, the circular shape of

the inlet may have had a critical impact on the success of reproduction.

Another explanation could be the difference in body size: the Neolithic woman (159.7cm) was shorter than the Mesolithic woman (171.3cm). A study of a modern human sample shows that short females with an increased risk of cephalopelvic mismatch have a round inlet, which is obstetrically beneficial [42]. Our study based on the reconstruction of one Mesolithic woman, who was taller with a triangular inlet, and one Neolithic woman, who was shorter with a more rounded inlet, produced results similar to those of the modern cohort study mentioned above. It could be hypothesised that the Mesolithic-Neolithic population followed this pattern of anatomical development in relation to childbirth. However, given the small sample size, more research needs to be done on this topic.

Conclusion

This study indicates that with the onset of the Neolithic way of life in the central Balkan region around 8000 years ago, various changes may have occurred in the shape and size of female pelvic bones. These changes could have been influenced by the arrival of Neolithic populations from the Aegean region, with a different genetic background. Although this is just a case study and the sample is limited, our results suggest that the pelvic birth canal of the Neolithic individual analysed in this study was more adequate obstetrically than that of the Mesolithic individual.

The potential pattern of covariation detected could reflect ease of childbirth and may have evolved in response to strong selection, although some studies suggest that the emergence of agriculture may have exacerbated the obstetric dilemma (*via* a decrease in maternal stature and an increase in neonatal growth and obesity) due to changes in the diet and in population density. At the same time, these factors could have promoted a larger offspring size through both plastic and genetic mechanisms.

Furthermore, our results may support the idea of the Neolithic Demographic Transition formulated by Bocquet-Appel [15], since the abrupt population increase detected in the Neolithic could be due to long-term selective pressure resulting from obstetric requirements. However, given the small sample used in this study, our data should be interpreted with caution. More extensive research is required in order to test these observations and establish whether the wider pelvic bones in the Neolithic were a widespread development, and whether and how they influenced the birthing process and, potentially, the increasing size of the population. Nevertheless, our findings are important because they demonstrate that prehistoric skeletons of mothers and babies can

be used to shed light on important aspects of the history of the human population.

Acknowledgements The authors are grateful to Jugoslav Pendić for his help with Figure 1 and to Camille de Becdelièvre for helpful comments on earlier drafts of the manuscript. We would also like to thank the two anonymous reviewers whose comments significantly improved the manuscript. This research is a result of the project “BIRTH: Births, mothers and babies: prehistoric fertility in the Balkans between 10000-5000 BC”, funded by the European Research Council (Grant Agreement No. 640557).

Conflict of interest: The authors do not have any conflict of interest to declare.

References

1. Grabowski M, Roseman CC (2015) Complex and changing patterns of natural selection explain the evolution of the human hip. *J Hum Evol* 85:94–10
2. Gruss LT, Schmitt D (2015) The evolution of the human pelvis: changing adaptations to bipedalism, obstetrics and thermoregulation. *Phil Trans R Soc B* 370: 20140063
3. Rightmire GP (2004) Brain size and encephalization in early to Mid- Pleistocene Homo. *Am J Phys Anthropol* 124:109–23
4. Rosenberg KR, Trevathan W (2002) Birth, obstetrics and human evolution. *BJOG* 109: 1199–206
5. Trevathan W, Rosenberg KR (2000) The shoulders follow the head: postcranial constraints on human childbirth. *J Hum Evol* 39: 583–6
6. Wells JCK, Desilva JM, Stock JT (2012) “The obstetric dilemma: An ancient game of Russian roulette, or a variable dilemma sensitive to ecology?”. *Am J Phy Anthropol* 149: 40–71
7. Washburn SL (1960) Tools and human evolution. *Sci Am* 203:63–75
8. Huseynov A, Zollikofer CPE, Coudyzer W, et al (2016) Developmental evidence for obstetric adaptation of the human female pelvis. *PNAS* 113 (19): 5227–32
9. Wittman AB, Wall LL (2007) The Evolutionary Origins of Obstructed Labor: Bipedalism, Encephalization, and the Human Obstetric Dilemma. *Obstet Gynecol Surv* 62 (11): 739–48
10. Betti L (2017) Human Variation in Pelvic Shape and the Effects of Climate and Past Population History. *Anat Rec* 300:687–97
11. Dunsworth H, Eccleston L (2015) The evolution of difficult childbirth and helpless hominin infants. *Annu Rev Anthropol* 44 (1):55–69
12. Ponce de Leon M, Golovanova L, Doronichev V, et al (2008) Neanderthal brain size at birth provides insights into the evolution of human life history. *PNAS* 105:13764–8
13. Ruff CB (1995) Biomechanics of the hip and birth in early *Homo*. *Am J Phys Anthropol* 98:527–74
14. Weawer TD, Hublin JJ (2009) Neandertal birth canal shape and the evolution of human childbirth. *PNAS* 106 (20): 8151–6
15. Bocquet-Appel JP (2011) When the world’s population took off: the springboard of the Neolithic Demographic Transition. *Science* 333: 560–1
16. Roy RP (2003) A Darwinian view of obstructed labor. *Obstet Gynecol* 101 (2): 397–01

17. Borić D (2011) Adaptations and transformations of the Danube Gorges foragers c. 13,000-5500 cal. BC: An overview. In: Krauß R (ed) Beginnings - New Research in the Appearance of the Neolithic between Northwest Anatolia and the Carpathian Basin. Rahden/Westfalen: Verlag Marie Leidorf GmbH, pp 157-203
18. Dimitrijević V, Živaljević I, Stefanović S (2016) Becoming sedentary? The seasonality of food resource exploitation in the Mesolithic-Neolithic Danube Gorges. *Doc Praehist* 43: 103–22
19. Borić D, Dimitrijević V (2007) When did the 'Neolithic package' reach Lepenski Vir? Radiometric and faunal evidence. *Doc Praehist* 34: 53–72
20. Filipović D, Jovanović J, Rančić D (2017) In search of plants in the diet of Mesolithic-Neolithic communities in the Iron Gates. In: Mărgărit M, Boroneanț A (eds) From Hunter-Gatherers to Farmers: Human Adaptations at the End of the Pleistocene and the first Part of the holocene: Papers in Honour of Clive Bonsall. Editura Cetatea de Scaun, Targoviște, pp 93-11
21. Hofmanová Z (2016) Palaeogenomic and Biostatistical Analysis of Ancient DNA Data from Mesolithic and Neolithic Skeletal Remains, PhD Thesis, University of Mainz, 182 p
22. Frémondière P, Thollon L, Adalian P, Delotte J, Marchal F (2017) Which foetal-pelvic variables are useful for predicting caesarean section and instrumental assistance? *Med Princ Pract* 26:359–67
23. Bruzek J (2002) A method for visual determination of sex using the human hip bone. *Am J Phys Anthropol* 117: 157–68
24. Murail P, Bruzek J, Houët F, et al (2005) DSP: a tool for probabilistic sex diagnosis using worldwide variability in hip-bone measurements. *BMSAP* 17: 167–76
25. Schmitt A (2002) Estimation de l'âge au décès des sujets adultes à partir du squelette: des raisons d'espérer. *BMSAP* 14:51–73
26. Schmit A (2005) Une nouvelle méthode pour estimer l'âge au décès des adultes à partir de la surface sacropelvienne iliaque. *BMSAP* 17:89–101
27. Čuljković B, Stefanović S, Romac S (2008) DNA-based sex identification of the infant remains from Lepenski Vir. In Bonsall C. et al (eds.) The Iron Gates in Prehistory: New perspectives (BAR International Series 1893). Archaeopress, Oxford, pp 170–4
28. Borić D, Stefanović S (2004) Birth and death: infant burials from Vlasac and Lepenski Vir. *Antiquity* 78:582–01
29. Jovanović J (2017) The diet and health status of the Early Neolithic communities of the Central Balkans (6200-5200 BC). PhD thesis, University of Belgrade, 422 p
30. Frémondière P (2015) L'évolution de l'accouchement dans la lignée humaine. Estimation de la contrainte foeto-pelvienne par deux méthodes complémentaires: la simulation numérique de l'accouchement et l'analyse discriminante des modalités d'accouchement au sein d'un échantillon obstétrical, PhD thesis, Aix-Marseille University, 268 p
31. Meyer V (2013) Apport de la reconstruction virtuelle du bassin Regourdou 1 (Dordogne, France) à la connaissance de l'obstétrique néandertalienne. PhD thesis, University of Bordeaux, 371 p
32. Caldwell WE, Moloy HC (1933) Anatomical variations in the female pelvis and their effect in labor with a suggested classification. *Am J Obstet Gynecol* 26:479–05
33. Berge C, Orbansegebarth R, Schmid, P (1984) Obstetrical Interpretation of the Australopithecine Pelvic Cavity. *J Hum Evol* 13:573–87
34. Tague R.G, Lovejoy C.O. (1986) The obstetric Pelvis of A.L. 288-1 (Lucy). *J Hum Evol* 15:237–55
35. Häusler M, Schmid, P (1995) Comparison of the Pelves of Sts-14 and AL-288-1. Implications for birth and sexual Dimorphism in Australopithecines. *J Hum Evol* 29:363–83
36. Abitbol M.M (1995) Reconstruction of the Sts-14 (*Australopithecus africanus*) pelvis. *Am J Phys Anthropol* 96:143–58
37. Moses RG, Luebcke M, Davis WS, et al (2006) Effect of a low-glycemic index diet during pregnancy on obstetric outcomes. *Am J Clin Nutr* 84:807–12
38. Scholl TO, Chen X, Khoo CS, et al (2004) The dietary glycemic index during pregnancy: influence on infant birth weight, fetal growth, and biomarkers of carbohydrate metabolism. *Am J Epidemiol* 159:467–74
39. Mahomed K, Muchini B, Mudzamiri S, et al (1995) Maternal height—how high is the risk of short stature? *J Obstet Gynaecol* 15 (2):76–80
40. Kirchengast S, Hartmann B (2007) Short Stature Is Associated with an Increased Risk of Caesarean Deliveries in Low Risk Population. *Acta Med Litu* 14(1):1–6
41. Merewood A, Mehta SD, Chen TC, et al (2009) Association between vitamin D deficiency and primary cesarean section. *J Clin Endocrinol Metab* 94:940–5
42. Fischer B, Mitteroecker P (2015) Covariation between pelvis, stature, and head size alleviates the obstetric dilemma. *PNAS* 112 (18): 5655–60

What Does Nasal Cavity Size Tell us about Functional Nasal Airways?

Qu'est-ce que la taille de la cavité nasale nous dit sur les voies aériennes nasales ?

Y. Heuzé

Received: 8 February 2017; Accepted: 6 December 2017
© Société d'Anthropologie de Paris et Lavoisier SAS 2018

Abstract Studies on dry human skulls have shown that nasal cavity (NC) morphology varies with eco-geographic factors. These findings have been used by some authors to interpret the facial morphology of Neanderthals. However, respiratory and air-conditioning functions are primarily carried out by the nasal airways (NA), which are delimited by mucosa. The aims of this study were to test whether: (1) NC volume (V) and surface-area-to-volume ratio (SA/V) are proportional to NA counterparts; (2) measurements for male NC and NA are larger than in females; (3) the centroid size (CS) of a set of landmarks measured on NC provides a reliable proxy for NC V. Head CT (computed tomography) images of adult patients ($N = 30$) at the University Hospital of Bordeaux were selected retrospectively. NA were defined by segmenting the lumen corresponding to the functional volume. NC was defined by adding to NA the soft tissues delimited by the bones forming the NC. The coordinates of 16 landmarks measured on NC bones were recorded. A rather low correlation was found between NA and NC V while NA SA/V and NC SA/V were not correlated. No significant differences were found between male and female NA and NC measurements. A rather low correlation was found between NC V and NC CS. If these preliminary results were to be confirmed by future studies, results using NC as a proxy for NA focusing on air-conditioning and respiratory energetics might need to be re-interpreted.

Keywords Air conditioning · Respiratory energetics · Computed tomography · *in vivo*

Résumé Plusieurs études sur des crânes secs humains ont révélé que la morphologie de la cavité nasale (NC) varie selon des facteurs écogéographiques. Ces résultats ont été utilisés par certains auteurs pour interpréter la morphologie faciale des Néandertaliens. Cependant, les fonctions respiratoires et le conditionnement de l'air sont assurés en premier lieu par les voies aériennes nasales (NA) qui sont délimitées par une muqueuse. Les buts de cette étude étaient de tester si : 1) le volume (V) et le rapport de l'aire surfacique sur le volume (NA/V) de NC sont proportionnels à ceux de NA ; 2) NC et NA sont plus grandes chez les hommes ; 3) la taille centroïde (CS) représente un indicateur fiable du V de NC. Des images tomographiques d'individus adultes ($N = 30$) du CHU de Bordeaux ont été sélectionnées de manière rétrospective. NA étaient définies par la segmentation du lumen correspondant au volume fonctionnel. NC était défini en ajoutant à NA les tissus mous délimités par les os formant NC. Les coordonnées de 16 landmarks mesurés sur les os de NC ont été enregistrées. Une faible corrélation a été trouvée entre les V de NA et NC tandis qu'aucune n'a été identifiée entre NA SA/V et NC SA/V. Aucune différence significative entre hommes et femmes n'a été trouvée. Une corrélation relativement faible a été identifiée entre NC V et NC CS. Si ces résultats préliminaires venaient à être confirmés par de futures études, les résultats utilisant NC comme un proxy pour NA pour l'étude des capacités respiratoires et du conditionnement de l'air devraient être réinterprétés.

Mots clés Conditionnement de l'air · Dimension énergétique de la respiration · Tomographie · *in vivo*

Y. Heuzé (✉)
CNRS, Univ. Bordeaux, MCC, PACEA, UMR 5199, Bordeaux archaeological sciences cluster of excellence, Pessac, France
e-mail : yann.heuze@u-bordeaux.fr, yannheuze@gmail.com

1. Y. Heuzé is supported by the French National Research Agency (ANR) under its LaScArBx research program and its “Investments for the Future” program [ANR-10-LABX-52]

Introduction

Several studies on dry skull materials of different human populations from different latitudes have shown that nasal cavity (NC) morphology varies with eco-geographic factors such as temperature and humidity. Historically, the relationship between climate and NC size and proportions was

established by studies focusing primarily on the dimensions of the nose and the nasal aperture [1–7]. Later on, studies taking the entire NC into account confirmed this relationship, particularly for populations living in extremely cold climates [8–11]. Populations living in cold climates tend to display a narrower nasal aperture, a sagittally enlarged NC and a larger surface-area-to-volume ratio (SA/V) of the NC, resulting in greater air-conditioning capacity [9,12–16]. On the other hand, a recent paper by Maddux et al. [17] indicates that the internal nasal fossa is the only component of the nasal complex (i.e., external pyramid, nasal aperture, internal nasal fossa, and nasopharynx) that displays an eco-geographic pattern of variation consistent with adaptation to climatic conditions. Because European Neanderthals lived during periods characterized by glacial conditions, many aspects of their morphology, including facial skeletal traits (e.g., nasal cavity and paranasal sinuses), have been interpreted as adaptations to a cold climate [18]. However, it has been shown that genetic drift can account for several of these traits [19]. Consequently, the significance of Neanderthal skeletal morphology is still debated.

The NC is a negative space delimited by bones housing the nasal airways (NA). As such, the NC is the gateway to the respiratory system [20] and indirectly participates in inspired and expired air conditioning. The NC displays a variable and complex morphology based on the shape and size of the aspects of the bones forming that negative space – the maxilla, nasal, palatine, vomer, sphenoid, frontal, ethmoid and lachrymal bones. The upper, middle and lower nasal turbinates or conchae contribute to the complexity of the NC morphology. The quantity of inspired air depends on NC size, shape and particularly on its height and width, especially at its entrance and exit points (i.e., piriform aperture and the choanae, respectively) [21,22]. Consequently, it is likely that NC morphology influences respiratory energetics. The effectiveness of air conditioning is also related, at least partially, to NC morphology, and particularly to NC length (e.g., [8]) and SA/V (e.g., [9]).

However, the functional negative space primarily responsible for air conditioning is represented by the NA. The NA are delimited by mucosa and housed within the NC. Because of its dense vascularization, NA mucosa vary in thickness depending on several possibly interrelated factors, including blood pressure, temperature, humidity and the nasal cycle [9,23,24]. This results in fluctuations in the level of congestion (reduced volume), or the opposite, i.e., decongestion, exhibited by the NA. Obviously, only studies based on living individuals allow NA morphology to be analyzed and quantified; computed tomography (CT) images offer appropriate material for that purpose. Very few studies quantifying NA morphology have been published to date. One such study is that of Yokley [9], in which the author uses a two-dimensional approach for *in vivo* CT images to compute

the ratio between the perimeter and the area of one coronal section through the nasal passages. These measurements were done twice per specimen, one with NA partially congested by the nasal mucosa and another with nasal airways fully decongested after virtually removing the nasal mucosa. Only the measurements of the fully decongested NA were found to correlate with eco-geographic variables. However, the results obtained with fully decongested NA are somewhat artificial since they are based on the hypothesis that the thickness of the mucosa is null, which effectively produces a measurement of NC.

The following question therefore remains: what does NC size (i.e., volume, V) tell us about functional NA? In other words, what are the differences between NC and NA size when the mucosa is taken into account? The aim of the present study is to quantify NC size and air-conditioning potential (i.e., SA/V) and compare them with those of NA. Since NC volume is often approximated by the centroid size (square root of the sum of squared distances of a set of landmarks from their centroid, CS) of a set of anatomical landmarks measured on the bones forming the NC, we also explore whether CS is a reliable proxy for NC volume. Three working hypotheses were tested throughout the present study: (H1) NC V, surface area (SA) and SA/V are proportional to NA counterparts; (H2) because of larger body and lean mass, males display larger NC and NA than females; (H3) the CS of a set of anatomical landmarks measured on the bones forming the NC provides a reliable proxy for NC volume.

Materials and methods

For the purposes of this study, head CT angiogram images (slice thickness: 0.625 mm) of adult patients examined at the emergency ward of the University Hospital of Bordeaux were selected. The following patients were systematically excluded: those less than 18 and more than 59 years of age and those with major facial skeletal dysmorphology, under respiratory assistance, or with obstructed nasal airways. Patients imaged with their mouth open were also excluded to avoid potential bias linked to mouth breathing. Fifteen men and fifteen women were included in the sample (mean age = 31.8 years; SD = 11.0 years). There were no significant age differences between males and females ($t = -0.0652$, $p = 0.9502$). All images were collected retrospectively and anonymized. Only the sex and exact age on examination were kept. This study has been reviewed and approved by the Univ. of Bordeaux IRB (*Comité de Protection des Personnes Sud-Ouest et Outre Mer III*).

First, the NA were defined by segmenting the lumen corresponding to the airways' functional volume and delimited anteriorly by the nasal aperture and posteriorly by the

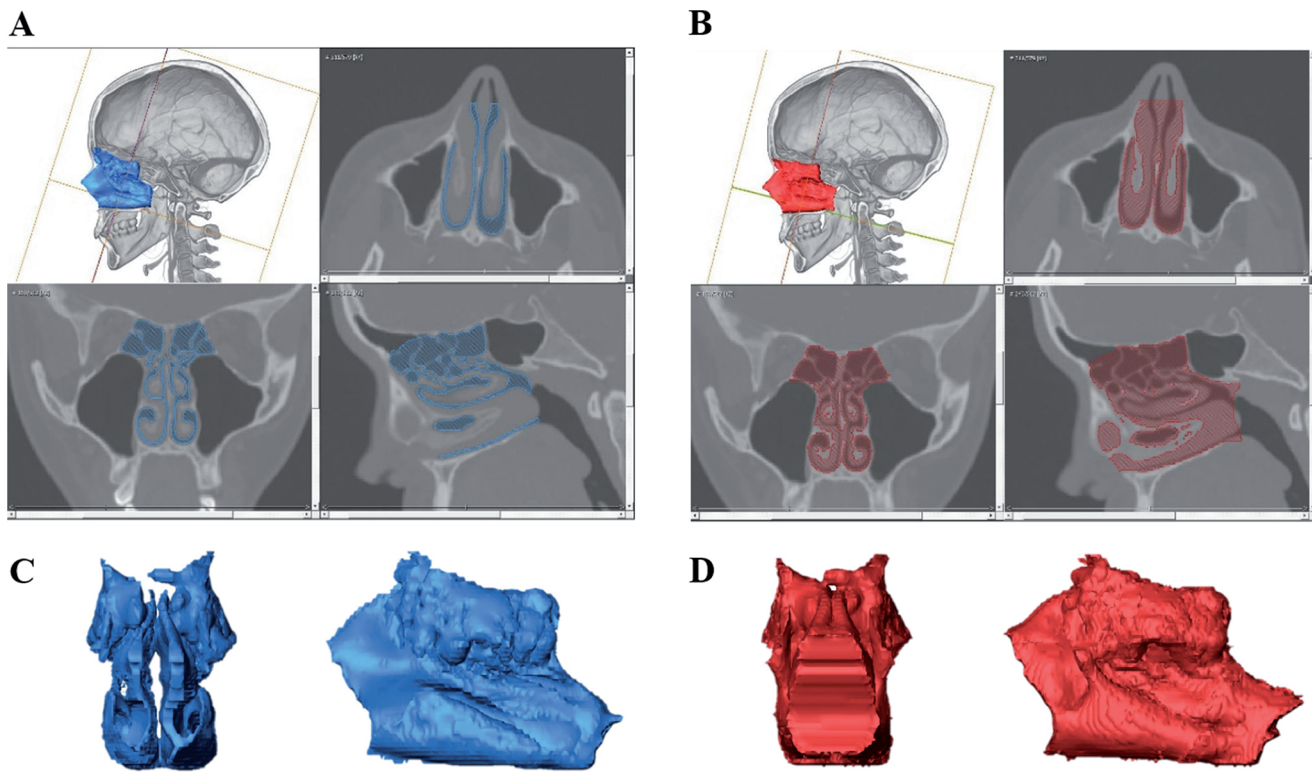


Fig. 1 Segmentation of the nasal airways (NA) (A) and nasal cavity (NC) (B). NA and NC are delimited anteriorly by the nasal aperture and posteriorly by the choanae. They were segmented in the transverse plane (upper right) and inspected in the coronal and sagittal planes (lower left and lower right, respectively). Anterior and lateral views of three-dimensional reconstructions of NA (C) and NC (D). / Segmentation des voies aériennes nasales (NA, A) et de la cavité nasale (NC, B). NA et NC sont délimitées antérieurement par l'ouverture nasale et postérieurement par les choanes, et ont été segmentées dans le plan transverse (en haut à droite) et inspectées dans les plans coronal et sagittal (respectivement en bas à gauche et en bas à droite). Vues antérieure et latérale des reconstructions 3D de NA (C) et NC (D)

choanae (Figs 1A, 1C). Because of the difficulty of objectively determining where the NA end and where the ethmoidal cells begin, the latter were included in what is defined as NA in the present study. Then, the NC was defined by segmenting both the lumen (i.e. NA) and the soft tissues covering the bones forming the NC (from anterior nasal aperture to choanae) (Figs 1B, 1D). Though segmenting nasal conchae can sometimes be challenging (e.g., [25]), they were segmented as bone and not included in the computation of NC measurements. NA and NC were segmented in the transverse plane and inspected in the coronal and sagittal planes (Fig. 1). Both NC and NA were closed on each transverse slice anteriorly by a line joining the two aspects of the maxilla or the nasal bones forming the nasal aperture, and posteriorly by a line joining the distal walls of the choanae formed by the sphenoid and passing through the most posterior aspect of the vomer (Fig. 1). For NA and NC, both left and right sides were considered to avoid potential nasal cycle effects. The nasal cycle is characterized by a recurrent variation in air mass flow partitioning between the right and left airways, which alternatively display different degrees of

mucosa congestion, enabling the passageways to alternate between predominantly fulfilling their air-conditioning and mucus clearance roles [24]. Because of the central aspect of the segmentation process in the present study, the repeatability of the protocol was quantified by measuring five individuals twice (one set of measurements at the start of data collection, one set at the end). The results are given in Table 1 and show that intra-observer error is negligible.

In addition, 16 three-dimensional landmarks were measured on bone (Fig. 2). The three-dimensional coordinates of the landmarks were then analyzed by geometric morphometrics using generalized Procrustes superimposition [26,27]. Centroid size (CS, the square root of the summed squared distances of each landmark to the centroid) was used as a proxy for NC size.

Next, because it has been shown that airflow in the lower and middle meatus account for over 80% (50% and 30% respectively) of the total nasal airflow [28], the hormion and the most anterior point on the left and right nasomaxillary sutures were selected to define a plane that was subsequently used to separate the upper meatus from the middle

Table 1 Repeatability of the segmentation process of the nasal airways including ethmoidal cells (NA) and nasal cavity (NC) with corresponding volume and surface area^a; each individual was segmented twice / Répétabilité de la segmentation des voies aériennes nasales incluant les cellules ethmoidales (NA) et de la cavité nasale (NC) avec les volumes et aires surfaciques correspondants. Chaque individu a été segmenté deux fois

	NA V	NC V	NA SA	NC SA
Ind. A_round#1	22.95	59.79	22.83	18.35
Ind. B_round#1	29.10	58.57	27.04	23.63
Ind. C_round#1	28.32	54.32	23.77	18.34
Ind. D_round#1	29.13	48.76	20.60	14.59
Ind. E_round#1	18.28	61.48	25.12	21.46
Ind. A_round#2	23.03	59.48	23.20	18.65
Ind. B_round#2	29.08	57.92	26.93	21.84
Ind. C_round#2	28.31	53.97	23.63	17.94
Ind. D_round#2	29.38	48.52	20.78	14.38
Ind. E_round#2	18.95	60.96	25.82	21.17
% diff. Ind. A	0.34%	0.51%	1.62%	1.68%
% diff. Ind. B	0.07%	1.11%	0.40%	7.58%
% diff. Ind. C	0.02%	0.65%	0.56%	2.14%
% diff. Ind. D	0.85%	0.49%	0.87%	1.46%
% diff. Ind. E	3.66%	0.84%	2.78%	1.35%

^a Values are in cm³ for volumes and mm² for surface areas / Les valeurs sont exprimées en cm³ pour les volumes et en mm² pour les aires surfaciques.

and lower meatus. Only the latter portion was then studied. Though this plane might not be ideal, among the several planes tested passing through the measured landmarks, this was the one that produced the most satisfactory results for the separation of the upper meatus from the middle and lower meatus.

The SA/V ratio was computed for both the NC and NA as it is a relevant proxy for air-conditioning potential.

Finally, to broadly describe relative NC dimensions, linear measurements of NC length (from nasomaxillary suture, left to choanal roof, left) and NC width (mean between inter-lower turbinate base and inter-alare distances) were recorded (Fig. 2). NC height was measured from, superiorly, the most anterior point of the lower surface of the cribriform plate taken on a slice parallel to the mid-sagittal plane (passing through the nasal, anterior nasal spine and posterior nasal spine), and inferiorly to the perpendicular projection of the uppermost point onto the nasal surface of the maxilla. This slice was the closest to the mid-sagittal plane, on which the vomer was no longer visible, to avoid any artificial reduction of NC height (Fig. 2). Greater NC height and width were expected to facilitate volumetric air intake, while NC length has no influence. However a longer NC was expected to facilitate air conditioning by increasing air residence time.

T-tests with Monte Carlo permutations ($n = 9999$) and Pearson's correlation coefficients with Monte Carlo permu-

tations ($n = 9999$) were used to test the hypotheses. For these tasks, the PAST software package was used [29].

Results

H1: NC V, SA and SA/V are proportional to NA counterparts

When considering the entire NC and NA, including the ethmoidal cells, there was no significant correlation between NA V and NC V ($R^2 = 0.0445$, $p = 0.2625$), although there was a significant correlation between NA SA and NC SA ($R^2 = 0.2305$, $p = 0.0075$) (Table 2). There was no significant correlation between NA SA/V and NC SA/V ($R^2 = 0.0065$, $p = 0.7066$) (Table 2). NA SA/V was characterized by greater dispersion (coefficient of variation: $c_v = 0.223$) than NC SA/V ($c_v = 0.144$). When considering only the lower two-thirds of NA and NC, a significant though relatively low correlation was found between NA V and NC V ($R^2 = 0.1408$, $p = 0.0349$) and another between NA SA and NC SA ($R^2 = 0.7066$, $p = 0.0001$) (Table 2). There was no significant correlation between NA SA/V and NC SA/V ($R^2 = 0.0078$, $p = 0.6234$) (Table 2). NA SA/V was characterized by greater dispersion ($c_v = 0.313$) than NC SA/V ($c_v = 0.131$).

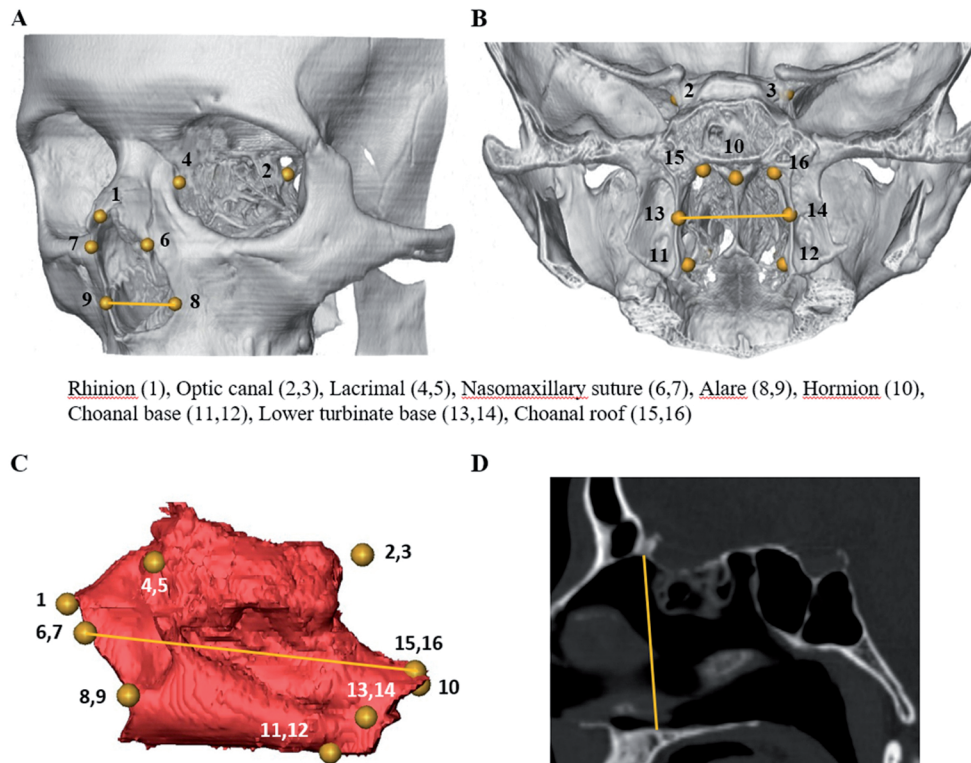


Fig. 2 Landmarks ($n = 16$) were measured on bone to compute the centroid size of the nasal cavity (NC) (anterior-lateral view, A; posterior-inferior view, B). Lateral view of the reconstructed NC with projected landmarks (C). Sagittal slice used to measure NC height, from, superiorly, the most anterior point of the lower surface of the cribriform plate to, inferiorly, the perpendicular projection of the uppermost point onto the nasal surface of the maxilla (D). The four linear distances measured are represented on the corresponding images / Les landmarks ont été mesurés sur les os afin de calculer la taille centroïde de la cavité nasale (NC) (vue antéro-latérale, A ; vue postéro-inférieure, B). Vue latérale de NC une fois reconstruite avec les landmarks projetés (C). Coupe sagittale utilisée pour mesurer la hauteur de NC, du point le plus antérieur de la surface inférieure de la plaque cribiforme (point supérieur) au point correspondant à la projection orthogonale du point supérieur sur le maxillaire (point inférieur) (D). Les quatre distances linéaires mesurées sont représentées sur les vues correspondantes

H2: Males display larger NC and NA than females

When considering the entire NA and NC, no significant differences were found between males and females for NA V ($t = 1.2721, p = 0.2144$), NA SA ($t = -0.1336, p = 0.8982$), NA SA/V ($t = -2.0569, p = 0.0510$), NC V ($t = -1.8106, p = 0.0792$), NC SA ($t = -0.1429, p = 0.2599$) or NC SA/V ($t = 0.1149, p = 0.9613$) (Table 3). When considering only the lower two-thirds of NA and NC, there were no significant differences between male and female NA V ($t = 1.1018, p = 0.2736$), NA SA ($t = -0.1778, p = 0.8584$), NA SA/V ($t = -1.4302, p = 0.1575$), NC V ($t = -1.4307, p = 0.1656$), NC SA ($t = -0.5453, p = 0.5925$) or NC SA/V ($t = 0.9974, p = 0.3319$) (Table 3). While measurements taken on males were larger overall than on females, the latter displayed larger NA V, both for the entire NA and for only the lower two-thirds.

Although males displayed larger NC linear measurements overall, no significant differences between male and female NC height ($t = 1.2981, p = 0.2024$), NC width ($t = 0.8589, p = 0.3950$) and NC length ($t = 0.9827, p = 0.3301$) were found (Table 4).

H3: CS of NC provides a reliable proxy for NC volume

There was a significant though rather low correlation between NC V and NC CS, both when considering the entire NC ($R^2 = 0.3597, p = 0.0005$) or only the lower two-thirds of the NC ($R^2 = 0.1944, p = 0.0147$). Male NC CS was significantly larger than female NC CS only when considering the entire NC ($t = 2.5138, p = 0.0180$). When considering the lower two-thirds of NC, there were no significant differences between male and female NC CS ($t = 1.9556, p = 0.0606$).

Table 2 Comparison of volume (V), surface area (SA) and surface-area-to-volume ratio (SA/V) between nasal airways (NA) and nasal cavity (NC)^a / *Comparaison des volumes (V), aire surfacique (SA) et ratio aire surfacique sur volume (SA/V) entre les voies aériennes nasales (NA) et la cavité nasale (NC)*

	NA V vs. NC V	NA SA vs. NC SA	NA SA/V vs. NC SA/V
NC and NA with ethmoidal cells	0.0445 (0.2625)	0.2305 (0.0075)	0.0065 (0.7066)
NC and NA lower two-thirds	0.1408 (0.0349)	0.7066 (0.0001)	0.0078 (0.6234)

^a Values are coefficients of determination (R^2) and significance after Monte Carlo permutations (p , in parenthesis) / *Les valeurs correspondent à des coefficients de détermination (R^2) et à la significativité après simulations de Monte Carlo (p, entre parenthèses)*

Table 3 Nasal airways (NA) and nasal cavity (NC) volume (V), surface area (SA), and surface-area-to-volume ratio (SA/V) by sex^{a,b} / *Volume (V), aire surfacique (SA) et ratio aire surfacique sur volume (SA/V) des voies aériennes nasales (NA) et de la cavité nasale (NC) selon le sexe*

	NA V	NC V	NA SA	NC SA	NA SA/V	NC SA/V
<i>Entire nasal airways (NA) and nasal cavity (NC)</i>						
M	22.55	63.38	24.86	21.5	1.17E-03	3.40E-04
F	25.37	59.21	24.70	20.20	9.98E-04	3.42E-04
M vs. F	1.27 (0.2144)	-1.81 (0.0792)	-0.13 (0.8982)	-0.14 (0.2599)	-2.06 (0.0510)	0.11 (0.9613)
<i>Lower two-thirds of nasal airways (NA) and nasal cavity (NC)</i>						
M	9.90	32.85	10.82	10.69	1.20E-03	3.27E-04
F	11.33	30.39	10.69	10.36	1.02E-03	3.43E-04
M vs. F	1.10 (0.2736)	-1.4307 (0.1656)	-0.18 (0.8584)	-0.55 (0.5925)	-1.43 (0.1575)	1.00 (0.3319)

^a Values are means in cm^3 for volumes and mm^2 for surface areas / *Les valeurs correspondent à des moyennes en cm^3 pour les volumes et en mm^2 pour les aires surfaciques.*

^b Values are Student *t*-values (*t*) and significance after Monte Carlo permutations (p , in parenthesis) / *Les valeurs correspondent à des valeurs de test *t* de Student (*t*) et à leur significativité après simulations de Monte Carlo (p, entre parenthèses).*

Table 4 Nasal cavity linear measurements by sex^{a,b} / *Mesures linéaires de la cavité nasale selon le sexe*

	NC height	NC width	NC length
M	49.2	25.8	71.2
F	47.8	25.3	69.8
M vs. F	1.2981 (0.2024)	0.8589 (0.3950)	0.9827 (0.3301)

^a Values are means in mm / *Les valeurs correspondent à des moyennes exprimées en mm.*

^b Values are Student *t*-values (*t*) and significance after Monte Carlo permutations (p , in parenthesis) / *Les valeurs correspondent à des valeurs de test *t* de Student (*t*) et à leur significativité après simulations de Monte Carlo (p, entre parenthèses).*

Discussion

Based on our results, H1, stating that NC V, SA and SA/V are proportional to NA counterparts, can only be supported with some limitations, since only the volume of the lower two-

thirds of NC was significantly correlated with that of NA. However, this correlation seemed relatively low ($R^2 = 0.1408$). Although the correlation was high for SA between NA and NC, this was not the case for SA/V, which is commonly used as a proxy for air-conditioning potential. Consequently, it might be more appropriate to consider only the lower and middle meatus when measuring NC. This is consistent with the fact that the lower two-thirds of NA account for over 80% of the total nasal airflow [28]. However, it appeared that interpolation made on air-conditioning potential on the basis of NC SA/V could be problematic.

This study revealed no significant differences between male and female NA V, NC V, NA SA, NC SA, NA SA/V, or NC SA/V, either considered as a whole or for only the lower two-thirds. Consequently, H2, stating that males display larger NC and NA than females, should be rejected. Because NC height and width primarily constrain volumetric air intake, both were expected to be significantly larger in males. However, neither was significantly larger in males than in females. Overall, these results offer little support to the hypothesis that, due to larger body size and lean mass,

male NC and NA are larger than female NC and NA. However, these results are based on a rather small sample size ($n = 30$) and it is expected that with a larger sample, some of these differences might exceed the significance threshold.

The 16 anatomical landmarks measured in this study on NC correspond to the measurable landmarks on CT images from a list of landmarks conventionally measured on dry skulls in comparable studies [e.g., 8,10,11,22]. Based on our results, the CS of such a landmark configuration appears to be a relatively poor proxy for NC volume, especially when considering the lower two-thirds of NC ($R^2 = 0.1944$). Thus, H3, stating that the CS of NC provides a reliable proxy for NC volume, should be rejected. It is unlikely that the rather complex geometry of NC could be captured in an optimal manner by these external landmarks that might over-simplify NC complex geometric properties. Consequently, measuring NC volume might be the only reliable way of quantifying NC size.

NA appears to be much more variable than NC. One obvious explanatory factor of this inter- and intra-individual variation is the mucosa itself, which varies in volume and consequently contributes to variation in NA volume as well. In contrast, for the same individual, the NC volume remains constant. This study attempted to control for a maximum of factors influencing mucosa congestion/decongestion. First, only patients breathing through the nose, without respiratory assistance and with their mouth closed during the CT exam were selected. Second, a relative rest state was assumed at the time of imaging (i.e., no engagement in significant physical activities), as well as relatively homogeneous environmental conditions, as temperature and humidity levels were controlled by air conditioning. Third, the nasal cycle was taken into account by measuring the right and left NA rather than just one side. Since this study focused on the state of rest, considering a fully decongested NA did not seem relevant. Note that during physical exercise, the nasal mucosa decongests almost to the same level as after using a topical decongestant [30], although a significant part of respiration occurs through the mouth. The level of stress experienced by the patients could not be controlled for, however. Despite all these precautions, NA SA/V was twice to three times more variable than NC SA/V. This result agrees with that obtained by Yokley [9] in two dimensions and showing that, when the mucosa was taken into account (i.e., not fully decongested), variation in SA/V was too substantial to observe any significant difference in SA/V between individuals of European and African descent.

Another explanatory factor for the overall low correlation between NA and NC measurements is the anatomical complexity of the nasal conchae and the acknowledged difficulty of segmenting them on CT images. This difficulty is linked to the complex geometry of the nasal conchae and the surrounding soft tissues and fluids [25]. While the nasal conchae were

segmented as bone and consequently not taken into consideration when computing NC measurements, it is possible that for some individuals, imperfect segmentation resulted in the inclusion of small parts of the nasal conchae in NC measurements. The fact that males displayed larger mean NC volumes but smaller mean NA volumes compared to females (Table 3) could suggest that males have larger nasal conchae potentially associated with larger mucosa volumes.

The results of this preliminary study seem to challenge the validity of the often assumed or implied correlation between NA and NC size/volume. Because of our relatively small sample size and methodological limitations (e.g., segmentation of the conchae, variation in mucosa thickness), these preliminary results should still be validated by future studies that could provide a more robust description of the relationship between NA and NC. If these preliminary results were to be confirmed by future studies, results produced by studies based on dry skull materials focusing on air-conditioning and respiratory energetics using NC as a proxy for NA might need to be re-interpreted. This would also apply to studies on these topics involving fossils such as Neanderthals, for which the NC is rarely fully preserved. Such future studies would need to use larger *in vivo* samples, as well as possibly samples from different regions of the world, to provide more in-depth results on the nature of the relationship between NA and NC morphological variation and co-variation and their implications for air-conditioning and respiratory energetics. One key aspect for future work will be to use imaging parameters optimized for nasal conchae visualization and segmentation in order to investigate the potential role of the nasal conchae and the overlying mucosa in the differences observed between NC and NA measurements.

Acknowledgements Y.H. is supported by the French National Research Agency's (ANR) LaScArBx research program and its "Investments for the Future" program [ANR-10-LABX-52]. The author is grateful to Drs. Andrej Evteev, Sébastien Villotte, Lauren Butaric, Christina Nicholas, Jessica Joganic and Christine Couture for interesting discussions on previous versions of this work. Comments from the two reviewers (Drs. Scott Maddux and Philipp Gunz, anonymity waived) helped to improve the overall quality of the manuscript.

Conflict of interest: The author declares no conflict of interest.

References

- Thomas A, Buxton L (1923) Man's nasal index in relation to certain climatic conditions. *J R Anthropol Inst* 53:92–122

2. Davies A (1932) A re-survey of the morphology of the nose in relation to climate. *J R Anthropol Inst* 62:337–59
3. Weiner JS (1954) Nose shape and climate. *Am J Phys Anthropol* 12:615–8
4. Carey JW, Steegmann AT (1981) Human nasal protrusion, latitude, and climate. *Am J Phys Anthropol* 56:313–9
5. Franciscus RG, Long JC (1991) Variation in human nasal height and breadth. *Am J Phys Anthropol* 85:419–27
6. Roseman CC (2004) Detecting interregionally diversifying natural selection on modern human cranial form by using matched molecular and morphometric data. *Proc Natl Acad Sci USA* 101:12824–9
7. Hubbe M, Hanihara T, Harvati K (2009) Climate signatures in the morphological differentiation of worldwide modern human populations. *Anat Rec* 292:1720–33
8. Noback ML, Harvati K, Spoor F (2011) Climate-related variation of the human nasal cavity. *Am J Phys Anthropol* 145:599–614
9. Yokley TR (2009) Ecogeographic variation in human nasal passages. *Am J Phys Anthropol* 138:11–22
10. Evteev A, Cardini AL, Morozova I, et al (2014) Extreme climate, rather than population history, explains mid-facial morphology of Northern Asians. *Am J Phys Anthropol* 153:449–62
11. Fukase H, Ito T, Ishida H (2016) Geographic variation in nasal cavity form among three human groups from the Japanese Archipelago: Ecogeographic and functional implications. *Am J Hum Biol* 28:343–51
12. Churchill SE, Shackelford LL, Georgi JN, et al (2004) Morphological variation and airflow dynamics in the human nose. *Am J Hum Biol* 16:625–38
13. Doorn DJ, Taylor DJ, Gambaruto AM, et al (2008) Nasal architecture: Form and flow. *Philos Transact A Math Phys Eng Sci* 366:3225–46
14. Holton NE, Yokley TR, Franciscus RG (2011) Climatic adaptation and Neandertal facial evolution: A comment on Rae et al (2011). *J Hum Evol* 61:624–7
15. Holton N, Yokley T, Butaric L (2013) The morphological interaction between the nasal cavity and maxillary sinuses in living humans. *Anat Rec* 296:414–26
16. Maddux SD, Yokley TR, Svoma BM, et al (2016) Absolute humidity and the human nose: A reanalysis of climate zones and their influence on nasal form and function. *Am J Phys Anthropol* 161:309–20
17. Maddux SD, Butaric LN, Yokley TR, et al (2017) Ecogeographic variation across morphofunctional units of the human nose. *Am J Phys Anthropol* 162:103–19
18. Steegmann AT, Cerny FJ, Holliday TW (2002) Neandertal cold adaptation: Physiological and energetic factors. *Am J Hum Biol* 14:566–83
19. Weaver TD (2009) Out of Africa: modern human origins special feature: the meaning of neandertal skeletal morphology. *Proc Natl Acad Sci USA* 106:16028–33
20. Enlow DH (1990) Facial growth 3 Sub edition. Saunders WB Co, Philadelphia, p. 572
21. Swift D, Proctor D (1977) Access of air to the respiratory tract. In: Brain J, Proctor D, Reid L (ed) Respiratory defense mechanisms. Dekker M, New York, pp. 63–91
22. Bastir M, Rosas A (2013) Cranial airways and the integration between the inner and outer facial skeleton in humans. *Am J Phys Anthropol* 152:287–93
23. Cauna N (1982) Blood and nerve supply of the nasal lining. In: Proctor D, Andersen I (ed) The nose: Upper airways physiology and the atmospheric environment. Elsevier Biomedical Press, New York, pp. 45–69
24. White DE, Bartley J, Nates RJ (2015) Model demonstrates functional purpose of the nasal cycle. *Biomed Eng OnLine* 14
25. Uosyte R, Shaw DJ, Gunn-Moore DA, et al (2015) Effects of fluid and computed tomographic technical factors on conspicuity of canine and feline nasal turbinates. *Vet Radiol Ultrasound* 56:494–502
26. Rohlf F, Slice D (1990) Extensions of the Procrustes method for the optimal superimposition of landmarks. *Syst Zool* 39:40–59
27. Dryden IL, Mardia KV (1998) Statistical shape analysis. Wiley, Chichester, p. 347
28. Xiong G, Zhan JM, Jiang HY, et al (2008) Computational fluid dynamics simulation of airflow in the normal nasal cavity and paranasal sinuses. *Am J Rhinol* 22:477–82
29. Hammer Ø, Harper DAT, Ryan PD (2001) PAST: Paleontological Statistics software package for education and data analysis. *Palaeontol Electron* 4:1–9
30. Hilberg O (2002) Objective measurement of nasal airway dimensions using acoustic rhinometry: Methodological and clinical aspects. *Allergy* 57 Suppl 70:5–39

Social Characterization of the Medieval and Modern Population from Joué-lès-Tours (France): Contribution of Oral Health and Diet

Caractérisation sociale de la population médiévale et moderne de Joué-lès-Tours (France) : apports de l'état sanitaire bucco-dentaire et de l'alimentation

V. Miclon · M. Gaultier · C. Genies · O. Cotté · F. Yvernault · E. Herrscher

Reçu le 10 juillet 2017 ; accepté le 03 octobre 2017
© Société d'Anthropologie de Paris et Lavoisier SAS 2017

Abstract The social and cultural changes that occurred between the medieval and modern periods in urban contexts are well documented; however, those in rural contexts are less well understood. This research aims to bridge this gap by analysing changes in dietary practices and oral health conditions between the medieval and modern eras, and by identifying their relationship with the social status of individuals buried at the rural site of the church of Saint-Pierre and Saint-Paul in Joué-lès-Tours (Indre-et-Loire, France). The objectives of this study are to jointly analyse the isotopic data concerning the diet of 37 individuals and the osteological and archaeological data, and to tie these results in with local historical and archaeozoological data. While the burial

practices identified between the thirteenth and eighteenth centuries suggest social distinctions between groups of individuals, the study of diet ($\delta^{13}\text{C}$ and $\delta^{15}\text{N}$) and the state of oral health point to a homogeneous social group characterized by the preferential consumption of pig meat, poultry and freshwater resources, and a degraded state of health. The available parochial registers and regional archaeozoological knowledge tend to confirm this hypothesis. This study confirms the relevance of the isotopic tool, which supplies dietary information to reinforce the archaeo-anthropological framework of interpretation, and also provides a critical examination of some of the criteria used to discuss the social composition of a set.

Keywords Social status · Oral health · Collagen · Carbon · Nitrogen · Historical

V. Miclon (✉) · M. Gaultier · O. Cotté
Université de Tours, CNRS, CITERES UMR 7324,
37200 Tours, France
e-mail : valentin.miclon@etu.univ-tours.fr

M. Gaultier
Service de l'archéologie du département d'Indre-et-Loire,
hôtel du département, place de la préfecture,
F-37927 Tours cedex 9, France

C. Genies
Éveha Tours, 13, rue des Granges-Galand,
F-37550 Saint-Avertin, France

O. Cotté
Institut national de recherches archéologiques préventives,
32, rue Delizy, F-93500 Pantin, France

F. Yvernault
Institut national de recherches archéologiques préventives,
148, avenue Maginot, F-37100 Tours, France

E. Herrscher
Aix-Marseille université,
CNRS, ministère de la Culture
et de la Communication, LAMPEA,
13094 Aix-en-Provence, France

Résumé Si les modifications sociales et culturelles entre la société médiévale et moderne en contexte urbain sont bien documentées, celles en contexte rural le sont nettement moins. Cette recherche se propose de combler cette lacune, en analysant les modifications des pratiques alimentaires et des états de santé entre le Moyen Âge et l'époque moderne et en cernant ses relations avec le statut social des individus inhumés sur le site de l'église rurale Saint-Pierre-et-Saint-Paul de Joué-lès-Tours (Indre-et-Loire). Les objectifs visent une analyse conjointe des données isotopiques relatives à l'alimentation de 37 individus et des données ostéologiques et archéologiques et une mise en perspective des résultats avec les données archivistiques et archéozoologiques locales. Si les pratiques funéraires identifiées entre le XIII^e et le XVIII^e siècle laissent supposer des distinctions sociales entre les groupes d'individus, l'étude de l'alimentation ($\delta^{13}\text{C}$ et $\delta^{15}\text{N}$) et de l'état sanitaire bucco-dentaire plaide en faveur d'un groupe social homogène caractérisé par une consommation préférentielle de viande de porc, de volaille et de ressources d'eau douce, avec un

état sanitaire dégradé. Les registres paroissiaux disponibles et les connaissances archéozoologiques régionales tendent à accréditer cette hypothèse. Cette étude confirme la pertinence de l'outil isotopique qui permet *via* l'alimentation de renforcer la grille de lecture archéoanthropologique, tout en apportant un regard critique sur certains critères utilisés pour discuter de la structuration sociale d'un ensemble.

Mots clés Statut social · État sanitaire · Collagène · Carbone · Azote · Historique

Introduction

The social characterization of individuals discovered in an archaeological context often comes up against different problems, making the exercise particularly delicate. Indeed, while the development of archaeological and anthropological methods improves our understanding of the management of funerary areas, and reveals clusters of deceased individuals within the population [1], the analysis and understanding of these phenomena, in relation to the reality experienced by the population, are confronted with the perception and cultural norms of society and of the people who had to face death individually and collectively [2].

The integration of aspects linked to the world of the living, rather than to the world of the dead, and especially to aspects with close connections to the social structure, such as dietary practices, can now provide essential information for the characterization of archaeological populations. In fact, they are the result of the close relationship between biological imperatives, resource availability, individual preferences and social norms [3,4]. Although textual, iconographic and archaeological sources provide ample insights into the dietary practices of medieval populations, these archives leave some aspects in the dark, including the dietary habits of rural populations [5–8]. The development of methods to study diet at an individual level offered the opportunity to improve our knowledge of the food practices of past societies using a comparative intra- and inter-site approach [9]. The analysis of the isotopic ratios of bone collagen carbon and nitrogen is invaluable as it reveals the dietary habits of the last 10 years of life of each of the subjects [10], thus expanding their archaeological identity. Surprisingly, the application of this method to the study of medieval and modern populations remains marginal in France [11–13]:

The use of these analyses therefore presents a twofold challenge:

- documenting food practices neglected by textual sources;

- integrating these data with existing data for different scales of analysis between the individual and the region in order to better characterize the population under study.

Using a sample of 37 individuals from a well-documented archaeological context, this study proposes to compare osteological data, including age and sex estimation and an assessment of dental health, to diet, by analysing the isotopic ratios of carbon and nitrogen in bone collagen. The results obtained will then be linked to the archeozoological data of Touraine and the study of parish registers.

Medieval diet in Touraine, the contribution of archeozoology

Several archeozoological studies have been carried out on the animal remains from the city of Tours as part of academic work, but also during preventive archeology excavations. Based on archaeological sources, the meat-based food of the inhabitants of Tours is well known since at least the Gallo-Roman period [14]. Despite several preventive excavations in rural areas, the rural diet is less well understood due to a deficient *corpus*. The analysis of the bone remains from medieval and modern Tours does not show a particularly marked regional character. As in most other cities across the kingdom, beef is largely dominant. Like in the rest of Europe during the medieval and modern periods, there is a gradual decrease in pork in favour of beef and sheep due to a new interest in speculative breeding [15,16]. Although major trends can be identified, the proportions of this triad (cattle, pig and sheep), and the composition of the wildlife *spectrum* vary, sometimes to a large degree, depending on the context and period in question. The social environment has a major impact on meat supply choices. The use of pig meat, particularly that of piglets, is a characteristic feature of the richest social groups. Indeed, the count's residency of the 11th and 12th centuries [7] and Saint-Julien's Abbey in the 14th century [8] are marked by a quantitatively and qualitatively high supply of pork. The kitchens of the count's residence also yielded a wide diversity and a slightly higher proportion of game birds, characteristic of seigneurial food. While lay lords preferred large game (deer and wild boar) and large birds (e.g., swans, cranes), ecclesiastical circles preferred small game, such as the hare [8]. It is also important to note that, for these privileged environments, the most meat-rich pieces are quantitatively the most important. Most of them come from animals raised specifically for meat and slaughtered when they reached their *optimum* weight. Besides these very specific contexts, more modest sites, such as the house of a craftsman or merchant in the 16th century, show a much simpler and much less varied food profile. For this kind of

habitat, most of the meat supply is beef and the consumed pieces are of *medium* to low quality for the period [8].

Materials and methods

The site

The site of the church of Saint-Pierre and Saint-Paul is located in the town of Joué-lès-Tours, 5 km southwest of the historical centre of the city of Tours, in the department of Indre-et-Loire (Fig. 1). It was discovered during preventive excavations carried out by a team comprising members of the archaeological service of the Indre-et-Loire department (Sadi) and the French National Institute for Preventive Archaeological Research (INRAP), under the direction of Pierre Papin. The aim of the excavation was to study a rural Christian sanctuary that became the centre of a parish town during the medieval period. This excavation revealed the evolution of the sanctuary and the management of the dead over a long period of time, as the chronology of the site extends from the 7th to the 18th centuries. The archaeological operation revealed three periods of funerary occupation (Fig. 2):

- the first period (7th–11th centuries) is defined by the existence of a building with a nave surrounded by a funerary area. During this period, the building was not intended to accommodate the deceased, as only one individual from this chronological phase was discovered in *ecclesia*, suggesting that this man benefitted from special status within the community;

- the period between the end of the 11th and the beginning of the 13th centuries is marked by major architectural (the addition of an apse, a north chapel and a south transept) and funerary changes, since no burial from this period was discovered, suggesting a restructuring of the cemetery topography beyond the boundaries of the excavation;
- from the second half of the 13th century, within the limits of the excavation, burials were installed in different sections of the building. No burial from this period was discovered outside the church due to the restriction of the cemetery to the west, outside the excavated area. This phase is also characterized by a diversification of funerary practices, with the appearance of well-ordered tombs (anthropomorphic formations, funerary stone, stretcher), alongside more modest tombs. Grave goods also appear in some cases, such as the presence of precious metal rings (copper alloy, silver and gold) and funerary pots. The analysis of the impregnations on the internal surfaces of the funerary pots suggests the use of incense probably from India or Ceylon. An initial anthropological study of the subjects from this period revealed that almost 80 % of them were adults and that out of the 30 individuals whose sex could be determined, the presence of 16 men and 14 women showed no marked disparity in sex distribution [17].

The analysis of burial frequency revealed a much lower rate in the northern chapel, which, together with the presence of an individual buried with its head pointing towards the east (potentially a priest [18]), suggests that the area was reserved for a particular group of the population. Elsewhere in the edifice privileged burials (described above) contrast with more modest burials.

Sample

As part of this research, a new osteological study, as well as an analysis of the isotopic ratios of carbon and nitrogen of bone collagen, was carried out on 37 individuals from this site. The selection of these individuals was based on a set of archaeological factors: topographical (specific location in the building, orientation of the deceased), material (funerary architecture, presence of special grave goods: funerary pots, gold or copper rings, rosary beads), chronological (known and precise dating of individuals covering the period) and osteological (good representation of the number of observable teeth; adult individuals whose sex can be reliably estimated).

Three groups were defined as follows:

- the first encompasses seven individuals present in a space that seems reserved for a small number of subjects: “the northern chapel”. In this study, these individuals will be grouped under this name;

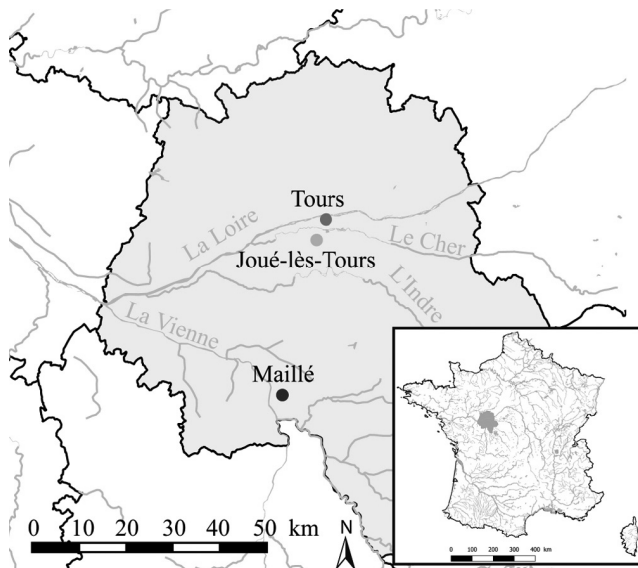


Fig. 1 Location of the studied archaeological site / Localisation du site étudié

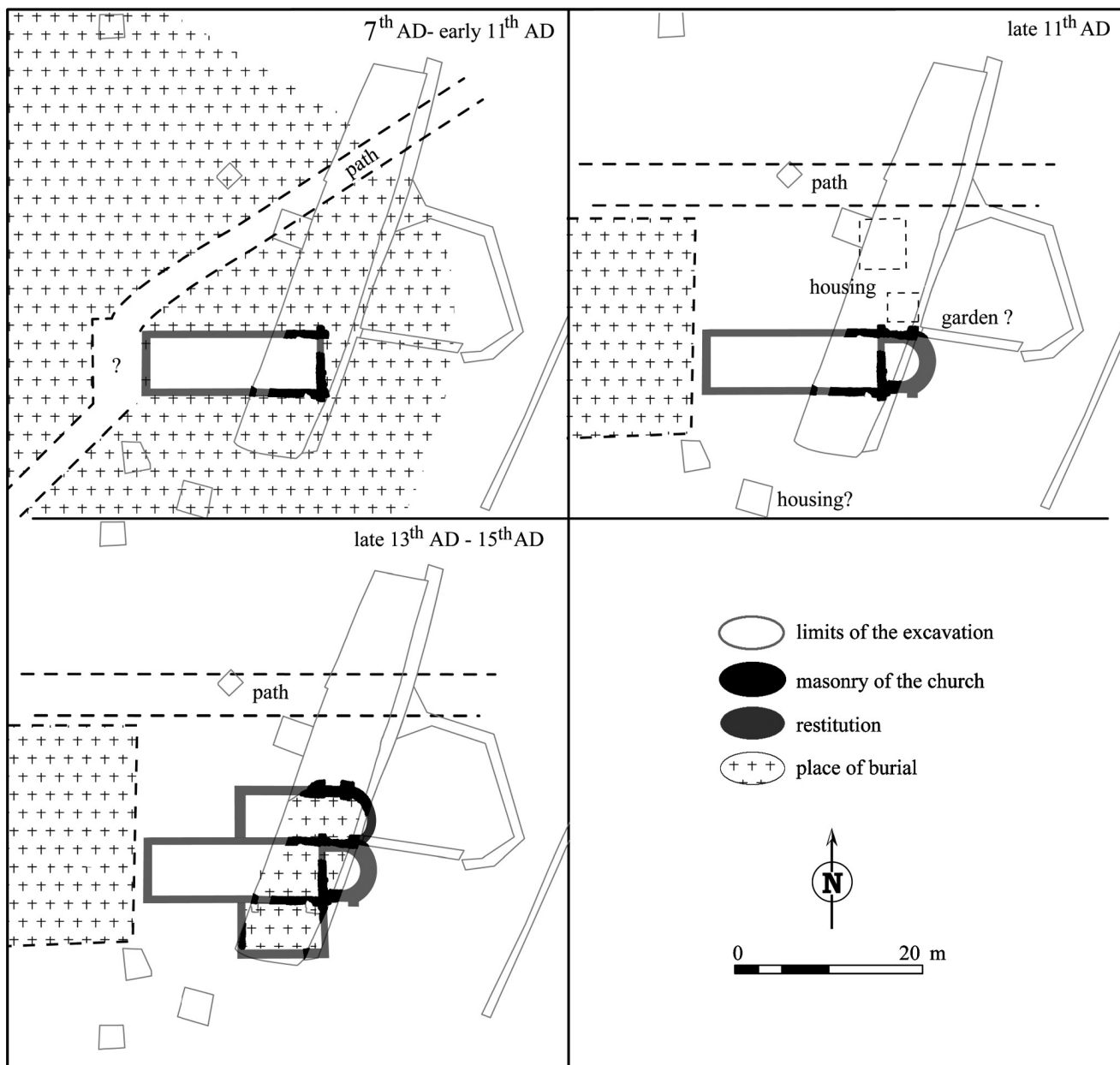


Fig. 2 Maps showing an overview of the topographic evolution of the site of Joué-lès-Tours from the 10th to the 15th centuries, modified from Papin et al. [17] / Plans synthétiques de l'évolution topographique du site de Joué-lès-Tours du x^e au xv^e siècle, modifiés d'après Papin et al. [17]

- the second consists of individuals buried outside the northern chapel. Their funerary treatment suggests a privileged status (anthropomorphic formations, funerary stone, stretcher, funerary pots or precious metal rings). The adjective “privileged” will be used here to indicate the fourteen individuals belonging to this group;
- the last includes 16 subjects buried in “simple” tombs within the nave or the southern transept, which contrast with those of the two preceding groups as no particular funeral treatment was reserved for them. In this work, this group will be labelled as “Others”.

These 37 individuals can be divided into three distinct chronological groups. A “Medieval” group including the 11 individuals from between the 13th and 15th centuries. Another “Modern” group encompasses the 22 subjects attributed with precision to the period between the 16th and the 18th centuries. A third set “Imprecise dating” includes four individuals who could not be reliably assigned to either of these periods (Table 1).

Measurements of the isotopic carbon and nitrogen ratios of these individuals were compared with those obtained from a group of animals (six cattle, five goats, seven pigs,

three fowl and one horse) from the Maillé sites of “Villiers” and “La Roche” (Table 2). This site was chosen as the source of the archeozoological *corpus* as it provides well-dated structures and presents the most similarities with the Joué-lès-Tours site: rural context, chronological contemporaneity, geographical proximity.

Osteological methods

Sex estimation was based on probabilistic sex diagnosis [19]. A probability threshold of 0.95 was required for validation of the diagnosis.

The age-at-death estimation of the individuals was made by studying the morphology of the auricular surface of the

ilium according to the method elaborated by Schmitt [20]. These estimations were occasionally complemented by observations of distinctive ossification characteristics, such as the sternal end of the clavicle and the iliac crest [21], and those related to dental development.

Dental health

Teeth are very resistant to diagenetic processes, which means that they are conserved where bones are generally not preserved. They are also the only hard and mineralized elements of the skeleton exposed to the environment through contact with food, and their structure is strongly dependent on genetics [22]. Different health indicators of the buccal

Table 1 Chronological and social distribution of the studied individuals / Distribution chronologique et sociale des individus étudiés				
Groups	Medieval (13th–15th)	Imprecise dating (13th–18th)	Modern (16th–18th)	Total
The northern chapel	2	4	1	7
Privileged	2	0	12	14
Others	7	0	9	16
Total	11	4	22	37

Table 2 Taxonomic, chronological, and biogeochemical data of 22 bones from the archeozoological corpus / Données taxinomiques, chronologiques et biogéochimiques des 22 ossements animaux de Maillé

Sample	Species	Period	Yield (mg/g)	%C	%N	C/N	$\delta^{13}\text{C}$ (‰)	$\delta^{15}\text{N}$ (‰)
MA_F01	Cattle	Medieval	64.1	39.5	14.4	3.2	-21.9	7.6
MA_F02	Cattle	Medieval	187.7	41.8	15.4	3.2	-21.4	4.5
MA_F03	Cattle	Medieval	180.0	42.0	15.4	3.2	-21.7	10.2
MA_F04	Cattle	Medieval	50.9	42.7	15.6	3.2	-21.5	6.2
MA_F05	Cattle	Modern	145.3	42.0	15.3	3.2	-21.3	7.2
MA_F06	Cattle	Modern	54.0	40.1	14.6	3.2	-21.7	5.3
MA_F07	Goat	Medieval	35.5	40.3	14.6	3.2	-21.0	4.6
MA_F08	Goat	Medieval	183.3	42.2	15.4	3.2	-21.5	5.7
MA_F09	Goat	Medieval	33.9	40.0	14.5	3.2	-21.5	6.5
MA_F10	Goat	Modern	35.1	34.3	11.4	3.5	-22.0	8.2
MA_F11	Goat	Modern	55.3	39.9	14.3	3.3	-21.2	6.9
MA_F12	Horse	Medieval	27.1	36.8	13.2	3.2	-22.3	6.1
MA_F13	Domestic fowl	Medieval	162.5	42.3	15.4	3.2	-20.1	8.7
MA_F14	Domestic fowl	Medieval	172.6	42.4	15.2	3.2	-20.3	8.7
MA_F15	Domestic fowl	Medieval	172.4	41.2	14.9	3.2	-20.4	7.1
or goose								
MA_F16	Pig	Medieval	24.4	36.9	13.5	3.2	-21.3	8.1
MA_F17	Pig	Medieval	155.9	35.9	13.0	3.2	-21.1	6.1
MA_F18	Pig	Medieval	168.1	43.1	15.8	3.2	-20.8	8.7
MA_F19	Pig	Medieval	71.8	42.1	15.3	3.2	-20.7	7.5
MA_F20	Pig	Medieval	50.4	41.5	15.3	3.2	-21.2	10.6
MA_F21	Pig	Modern	49.0	38.4	14.0	3.2	-20.6	7.3
MA_F22	Pig	Medieval	154.1	41.0	15.0	3.2	-20.4	5.6

Medieval period: 13th–15th centuries; Modern period: 16th–18th centuries

sphere are related to diet and are also relatively easy to observe. They are assessed using various well-established evaluation methods. In this study, the caries and *ante mortem* losses were counted and wear, tartar and periodontosis were evaluated using a rating system derived from that proposed by Brothwell [23]. For each of these criteria, an index was established, corresponding either to the number of teeth or dental sites showing the feature relative to the total number of teeth, or dental sites for which the criterion is observable (caries and *ante mortem* losses), or relative to the average of the stages of each tooth for which the criterion is observable per individual (wear, tartar and periodontosis). These individual indices were used if, and only if, at least eight observations were possible, that is, eight teeth for caries, wear, dental calculus, periodontosis or eight observable dental sites (*ante mortem* losses) per individual (Table 3).

A non-specific stress indicator: linear enamel hypoplasia

Amelogenesis may be disturbed by stress resulting in defects in consistency or color in the form of lines or bands on the tooth surface [24]. These markers are “non-specific stress markers” [25] because they reflect various disturbances (e.g., physiological, environmental, dietary) experienced by the individual during childhood while the tooth is forming. These disturbances can be very informative for determining intra-population differences in order to assess whether they are correlated with particular socioeconomic groups [26].

During this work, hypoplasias were observed under low-angled light and macroscopically counted on the vestibular surface of each tooth. An index was then established corresponding to the number of hypoplasias observed relative to the number of teeth in a suitable state of preservation for recording these marks (Table 3).

Isotopic analysis

This study builds on research carried out over the last 30 years on the evolution of stable isotope ratios of carbon and nitrogen ($^{13}\text{C}/^{12}\text{C}$ and $^{15}\text{N}/^{14}\text{N}$, respectively) in the biological tissues of organisms from different environments [27]. The $\delta^{13}\text{C}$ and $\delta^{15}\text{N}$ values of plants are reflected in those of consumers from the upper trophic levels, accompanied by heavy isotope enrichment at each level of the food web [28]. The increase in the isotopic ratios between plant-based food and bone collagen in herbivores is estimated to be ~5‰ for carbon and 3–5‰ for nitrogen [28]. There is also an enrichment of ~1‰ for $\delta^{13}\text{C}$ and of 3–5‰ for $\delta^{15}\text{N}$ [29,30] between the bone collagen of prey and that of consumers. Collagen enrichment in ^{15}N depends mainly on the length of the food chain. In aquatic environments, food chains are longer than on land, leading to higher ^{15}N enrich-

ment, and hence higher $\delta^{15}\text{N}$ values for high-trophic consumers. This is also true for $\delta^{13}\text{C}$ values.

Different factors can modify the local isotopic values of plants at the bottom of the trophic network and are reflected in the tissues of organisms of successive trophic levels [31], even within a radius of < 100 km [32]. Insofar as the isotopic approach consists in evaluating which food poles are closest to the isotopic values of human subjects, it is essential to take into consideration a local and contemporary faunal reference system for the human population studied.

The isotopic ratios of carbon and nitrogen in bone collagen largely reflect the protein content of the diet due to its polypeptide nature. Protein synthesis is, in fact, a result of the reuse of the ingested amino acids [29]. It is generally accepted that these relationships provide information about the average diet during the last 10 years of an individual's life [10].

In this study, collagen extraction was carried out at the UMR 7269 LAMPEA in Aix-en-Provence. The protocol used was defined by Longin [33] and modified by Bocherens [34]. The collagen samples were analysed by the Iso-Analytical laboratory (Crewe, Cheshire, UK), which carried out the elemental and isotopic measurements with an isotopic mass spectrometer (EA-IRMS). The equipment used was a Europa Scientific 20-20 isotope mass spectrometer coupled with an automated elemental analyser. An internal beef liver standard (IA-R042) was used for which the isotopic content was calibrated from standards provided by the international atomic energy agency: IAEA-CH-6 (sucrose, $\delta^{13}\text{C} = -10.43\text{\textperthousand}$) and IAEA-N-1 (ammonium sulfate, $\delta^{15}\text{N} = 0.40\text{\textperthousand}$). The analytical accuracy obtained from the repeated analysis of the internal laboratory standard was 0.11‰ for the $\delta^{13}\text{C}$ values and 0.04‰ for the $\delta^{15}\text{N}$ values.

Statistical tests were carried out using R software (3.2.3). The nonparametric Wilcoxon and Kruskal-Wallis tests were used: the former for comparing two series and the latter for series of three (Table 4).

Results

Osteological data

We were able to estimate the sex on 23 of the 37 individuals studied. This sample is composed of 12 men and 11 women, along with 14 individuals of undetermined sex (Table 3). The estimation of the age at death of all the individuals in our *corpus* covers a period of several decades. The relationship between this factor and food and health could not be evaluated (Table 3).

No statistically significant differences were found in distributions of the different oral health indicators, sex, socioeconomic groups or chronological periods (Table 4).

Table 3 Osteological, chronological, and biogeochemical data of 37 individuals from Joué-lès-Tours / Données ostéologiques, chronologiques et biogéochimiques des 37 individus de Joué-lès-Tours

Sample	Period	“Social status”	Age (90%)	Sex	Bone	Yield (mg/g)	‰C	‰N	C/N	Usable dental indices							
										δ ¹³ C (‰)	δ ¹⁵ N (‰)	Caries	Periodontitis	Calculus	Wear	AML	LEH
JLT_515	Modern	Other	[20+]	I	MTT5 L foot	113.1	40.2	14.7	3.2	-19.1	13.0	0.13	1.81	1.40	2.20	0.03	1.00
JLT_518	Modern	Other	[20-39]	M	Phalanx prox R hand	82.2	40.2	14.8	3.2	-19.5	13.6	0.40	1.25	0.63	2.50	0.11	2.93
JLT_531	Modern	Privileged	[20+]	I	MTT3 R foot	179.2	42.5	15.7	3.2	-19.1	13.5	-	-	-	-	0.94	-
JLT_541	Modern	Other	[30+]	M	MTT 2 L foot	57.3	41.4	15.2	3.2	-19.4	12.4	-	-	-	-	-	-
JLT_556	Modern	Privileged	[20-59]	F	Phalanx prox L hand	132.6	43.1	15.8	3.2	-19.9	12.2	-	-	-	-	-	-
JLT_560	Modern	Other	[20+]	I	Phalanx prox R hand	46.5	39.9	14.9	3.1	-19.2	12.6	0.11	1.17	1.22	2.61	0.00	1.65
JLT_561	Modern	Privileged	[20+]	I	L fibula diaphysis	97.8	40.7	15.3	3.1	-19.0	10.6	-	-	-	-	-	-
JLT_576	Imprecise	The northern chapel	[20-59]	M	MTT 4 R foot	59.8	42.5	15.8	3.1	-19.4	12.2	0.00	-	1.56	2.89	0.08	0.00
JLT_583	Modern	The northern chapel	[20+]	I	Phalanx prox R hand	59.5	39.9	15.1	3.1	-19.3	13.0	0.75	1.00	0.78	2.92	0.11	0.88
JLT_591	Modern	Privileged	[20+]	I	MTC 3 L Hand	48.6	42.4	15.8	3.1	-19.4	11.8	0.62	1.00	0.55	3.43	0.27	2.05
JLT_593	Modern	Privileged	[20-49]	F	Phalanx prox R hand	131.5	42.5	16.0	3.1	-19.6	11.5	-	-	-	-	-	-
JLT_604	Modern	Other	[20+]	I	MTT 5 L Foot	26.3	36.8	13.7	3.1	-18.8	12.2	0.38	2.67	1.48	2.76	0.09	0.52
JLT_611	Modern	Other	[20-39]	F	Phalanx prox R hand	120.1	41.8	15.5	3.1	-20.0	11.9	-	-	-	-	-	-
JLT_613	Medieval	Other	[20-49]	M	Phalanx prox L hand	72.7	41.2	15.3	3.1	-19.2	11.7	-	-	-	-	-	-
JLT_620	Modern	Privileged	[20-49]	M	Phalanx prox L hand	172.5	43.4	16.3	3.1	-19.5	13.3	-	-	-	-	-	-
JLT_636	Medieval	Other	[20-39]	F	MTT5 L foot	32.2	38.8	14.3	3.2	-19.1	11.1	0.07	0.29	0.55	0.97	0.03	0.77
JLT_680	Modern	Other	[30+]	M	MTT5 L foot	85.4	39.9	14.5	3.2	-19.3	12.2	-	-	-	-	-	-
JLT_681	Modern	Privileged	[20-39]	F	MTT5 L foot	52.6	42.3	15.7	3.2	-18.9	12.9	-	-	-	-	-	-
JLT_693	Imprecise	The northern chapel	[20+]	I	MTT5R foot	68.6	41.9	15.2	3.2	-19.3	11.8	-	-	-	-	-	-
JLT_698	Medieval	Privileged	[20-59]	M	Phalanx prox L hand	35.7	38.6	14.1	3.2	-19.1	13.0	-	-	-	-	-	-
JLT_703	Modern	Privileged	[15-29]	F	Phalanx prox L hand	99.6	39.4	14.5	3.2	-19.9	11.7	-	-	-	-	-	-

(Suite page suivante)

Sample	Period	“Social status”	Age (90%)	Sex	Bone	Yield (mg/g)	$\delta^{13}\text{C}$ (‰)	$\delta^{15}\text{N}$ (‰)	Usable dental indices					
									C/N	C/N	Caries	Periodontitis	Calculus	Wear
JLT_704	Inprecise	The northern chapel	[30+]	I	MTT5 L foot	39.2	37.8	13.7	3.2	-18.9	11.0	-	-	-
JLT_709	Modern	Other	[30+]	F	MTT5 R foot	63.1	41.0	15.1	3.2	-19.1	12.3	-	-	-
JLT_710	Modern	Other	[30+]	M	Phalanx prox R	41.2	39.7	14.2	3.3	-19.5	11.3	-	-	-
JLT_716	Modern	Privileged	[50+]	M	Phalanx prox L	58.0	40.1	14.6	3.2	-19.3	12.3	0.33	-	0.58
JLT_732	Medieval	Other	[20–39]	F	MTT5 R foot	45.1	39.9	14.8	3.1	-19.6	12.0	-	-	-
JLT_744	Modern	Privileged	[20–49]	I	Phalanx prox R	61.8	41.3	15.4	3.1	-19.9	12.4	-	-	-
JLT_758	Medieval	Other	[15–29]	F	Phalanx prox L	19.8	35.0	12.9	3.2	-19.9	11.6	0.24	-	0.64
JLT_765	Medieval	The northern chapel	[20+]	I	Phalanx prox R	74.9	40.5	15.1	3.1	-19.4	12.0	0.08	1.50	1.00
JLT_767	Modern	Privileged	[20–39]	F	MTT5 L foot	27.3	33.0	12.2	3.1	-19.6	13.0	0.27	1.20	0.70
JLT_786	Medieval	The northern chapel	[20+]	I	R fibula diaphysis	35.1	42.0	15.7	3.1	-19.4	12.8	-	-	-
JLT_827	Medieval	Other	[30+]	M	MTT5 R foot	50.0	40.8	14.3	3.3	-20.2	11.0	-	-	2.40
JLT_828	Medieval	Other	[20+]	I	Phalanx prox L	56.2	39.8	14.9	3.1	-19.5	12.5	0.45	-	0.09
JLT_844	Medieval	Other	[30+]	I	Phalanx prox R	45.6	37.6	13.9	3.2	-19.9	12.5	0.28	2.60	0.50
JLT_862	Medieval	Privileged	[20+]	F	MTT2 R foot	23.9	30.6	11.2	3.2	-19.5	12.9	0.03	0.96	0.80
JLT_868	Modern	Privileged	[30+]	M	MTT5 R foot	35.0	39.4	14.4	3.2	-19.7	12.2	0.00	1.42	1.31
JLT_942	Inprecise	The northern chapel	[20–39]	M	MTT5 L foot	38.8	40.9	15.2	3.1	-19.6	12.6	0.07	0.22	0.33

Medieval period: 13th–15th centuries; Imprecise period: 13th–18th centuries

Sex: I, indeterminate; F, female; M, male

Bone: MTT, Metatarsal; MTC, Metacarpal; Prox, Proximal; R, Right; L, Left

Usable dental indices: AML, *Ante mortem* losses; LEH, Linear enamel hypoplasia

Table 4 Distribution of different oral health and isotopic indicators by sex, chronological series and socio-economic groups / Distributions des différents indicateurs sanitaires bucco-dentaires et isotopiques selon le sexe, les périodes chronologiques et les groupes socio-économiques

Indicator	Sex			Period			“Social status” groups			
	nM	nF	p ^a	nMed	nMod	p ^a	nPrivileged	nNorthern	nOthers	p ^b
Calculus	4	4	0.886	6	9	0.637	5	4	8	0.841
AML	4	4	0.642	6	10	0.358	6	4	8	0.845
Periodontitis	2	3	1.000	4	8	0.671	4	3	6	0.349
Wear	4	4	0.114	6	9	0.456	5	4	8	0.759
Caries	4	4	0.559	6	9	0.272	5	4	8	0.614
LEH	4	4	0.343	5	9	0.112	5	4	7	0.511
δ ¹³ C	11	11	0.409	11	22	0.442	14	7	16	0.679
δ ¹⁵ N	11	11	0.598	11	22	0.358	14	7	16	0.577

AML, *Ante mortem* losses; LEH, Linear enamel hypoplasia; nM, Number of males; nF, Number of females; nMed, Number of individuals from the medieval period; nMod, Number of individuals from the modern period; nPrivileged, Number of individuals in the “privileged” group; nNorthern chapel, Number of individuals from the northern chapel; nOthers, Number of individuals in the “Others” group

^a: p-value from a Wilcoxon–Mann–Whitney test; ^b: p-value from a Kruskal–Wallis test

The number of decayed teeth in relation to the total number of teeth, for which this criterion is observable, is comparable to those of various historical European populations. The rate of carious lesions in the Joué-lès-Tours sample (23.2%) falls within the observed range for these periods, but is towards the upper limits (Fig. 3) [9,11,22,35,36].

Therefore, the studied sample shows a degraded health status compared to other contemporaneous populations, at least with regard to these lesions. It appears likely, given the high frequency of caries in the Joué-lès-Tours population, that individuals regularly consumed carbohydrates.

Only 1 of the 16 individuals, for whom the index was established on at least 8 teeth, was free of linear enamel hypoplasia. Thus, for the *corpus* studied, the prevalence of these lesions is 93.8%. This is particularly high when compared to the medieval and modern adult populations described in the literature (Fig. 4) [9,11,25,37]. Despite the small number of studied individuals, this result suggests that the individuals in our *corpus* experienced a set of non-specific intense stresses, and is indicative of difficult living conditions during all the periods considered, irrespective of sex or social status.

Isotopic data

The atomic C/N ratio is a tool used to verify the preservation of the collagen of a sample. DeNiro [38] has shown that this ratio must be between 2.9 and 3.6 for archaeological bones. The relative amounts of carbon and nitrogen in each sample can also be used as a control. It is generally accepted that for

archaeological remains, these must be greater than 30% and 11%, respectively [39]. Finally, the extracted yield of collagen must be > 10 mg/g [39].

The 59 analysed (human and faunal) samples satisfied the criteria for the validation of collagen preservation. All the indicators fell within the limits indicating that all the samples are neither degraded nor contaminated (Tables 2, 3, extraction yield > 10 mg/g, %C > 30, %N > 11 and C/N between 2.9 and 3.6) [38,39].

δ¹³C values for fauna (*n* = 22) range from −22.3 to −20.1‰, and those of δ¹⁵N, from 4.5 to 10.6‰ (Table 2, Fig. 5). The δ¹³C values for fauna correspond to the expected values for terrestrial animals in a temperate environment dominated by C₃ type plants [27]. There is ¹³C and ¹⁵N enrichment between herbivores and omnivores (+0.9‰ in ¹³C and +1.2‰ in ¹⁵N), which the Wilcoxon test shows to be statistically significant (*p* < 0.05 and *p* = 0.05, respectively). Heavy isotope enrichment, although significant, is less than that observed between two consecutive trophic levels, indicating a low assimilation of animal proteins in the diet of omnivorous animals [12].

The human δ¹³C values (*n* = 37) range from −20.2 to −18.8‰ (mean ± SD = −19.4 ± 0.3‰), and those of δ¹⁵N between 10.6 and 13.6‰ (12.2 ± 0.7‰) (Table 3, Fig. 5). The results appear to be homogeneous within the human population ($\Delta(\delta^{13}\text{C}_{\max} - \delta^{13}\text{C}_{\min}) = 1.4\text{‰}$ and $\Delta(\delta^{15}\text{N}_{\max} - \delta^{15}\text{N}_{\min}) = 3.0\text{‰}$). The δ¹³C values for humans also correspond to the expected values for an environment dominated by C₃ plants [27]. Individuals from the northern chapel (*n* = 7) show δ¹³C values between −19.6 and −18.9‰

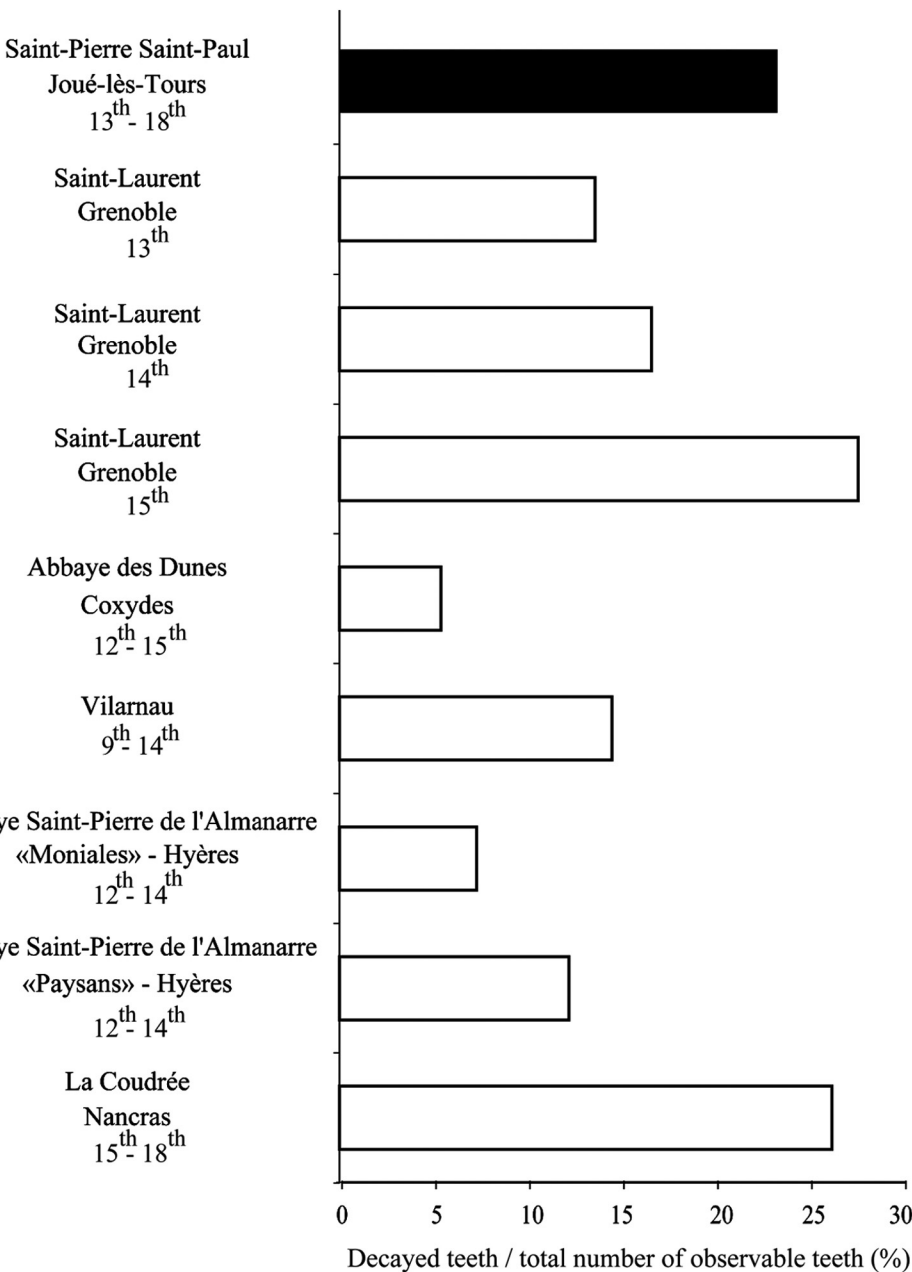


Fig. 3 Proportion (%) of decayed teeth per total number of observable teeth for various historical populations: SPSP: Saint-Pierre-et-Saint-Paul de Joué-lès-Tours; SLT: Saint-Laurent de Grenoble [11]; AbD: abbaye des Dunes de Coxydes [9]; Vil: Vilarnau [22]; SPAm: Saint-Pierre de l'Almanarre — “Nuns” [35]; SPAp: Saint-Pierre de l'Almanarre — “Peasants” [35]; LCou: La coudrée à Nancras [36]; Proportion (%) de dents cariées par rapport au nombre total de dents observables de différentes populations historiques : SPSP : Saint-Pierre-et-Saint-Paul de Joué-lès-Tours ; SLT : Saint-Laurent de Grenoble [11] ; AbD : abbaye des Dunes de Coxydes [9] ; Vil : Vilarnau [22] ; SPAm : Saint-Pierre de l'Almanarre — « Moniales » [35] ; SPAp : Saint-Pierre de l'Almanarre — « Paysans » [35] ; LCou : La coudrée à Nancras [36]

($-19.3 \pm 0.2\text{‰}$) and $\delta^{15}\text{N}$ values between 11.0 and 13.0‰ ($12.2 \pm 0.6\text{‰}$). The individuals from the “privileged” group ($n = 14$) have $\delta^{13}\text{C}$ values between -19.9 and -18.9‰ ($-19.5 \pm 0.3\text{‰}$) and $\delta^{15}\text{N}$ values between 10.6 and 13.5‰ ($12.4 \pm 0.8\text{‰}$). Finally, individuals in the “others” group

($n = 16$) have $\delta^{13}\text{C}$ values ranging from -20.2 to -18.8‰ ($-19.4 \pm 0.4\text{‰}$) and $\delta^{15}\text{N}$ values ranging from 11.0 to 13.6‰ ($12.1 \pm 0.7\text{‰}$). Individuals from the medieval period ($n = 11$) have $\delta^{13}\text{C}$ values between -20.2 and -19.1‰ ($-19.5 \pm 0.3\text{‰}$) and $\delta^{15}\text{N}$ values between 11.0 and 13.0‰

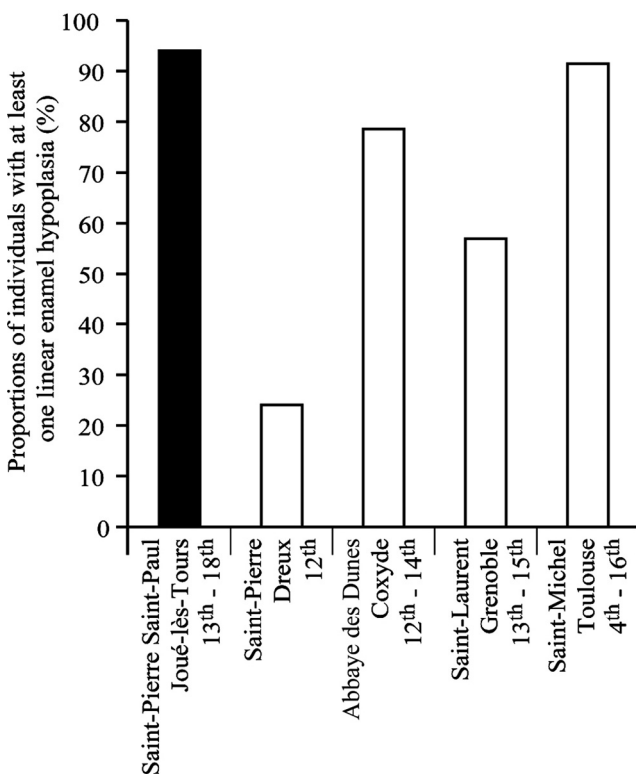


Fig. 4 Proportions of individuals with at least one linear enamel hypoplasia from various historical populations [9,11,25,37] / Proportions des individus porteurs d'au moins une hypoplasie linéaire de l'email dentaire au sein de différentes populations historiques [9,11,25,37]

($12.1 \pm 0.7\text{‰}$). Those from the modern period ($n = 22$) have $\delta^{13}\text{C}$ values ranging from -20.0 to -18.8‰ ($-19.4 \pm 0.3\text{‰}$) and $\delta^{15}\text{N}$ values between 10.6 and 13.6‰ ($12.4 \pm 0.7\text{‰}$).

Discussion

Diet reconstitution

The comparison of the isotopic data of human subjects with those obtained for the fauna from Maillé shows that a human diet consisting exclusively of herbivores is incompatible with the results obtained, as $\Delta^{13}\text{C}_{\text{Humans-Herbivores}} = 2.2\text{‰}$ and $\Delta^{15}\text{N}_{\text{Humans-Herbivores}} = 5.6\text{‰}$ (Fig. 5). On the other hand, a human diet composed mainly of omnivores could theoretically explain the values obtained within the population as a whole because $\Delta^{13}\text{C}_{\text{Humans-Omnivores}} = 1.3\text{‰}$ and $\Delta^{15}\text{N}_{\text{Humans-Omnivores}} = 4.4\text{‰}$ (Fig. 5). While this is the most parsimonious explanation, it is not the only possible hypothesis. Indeed, the consumption of young unweaned herbivores [40], or of herbivores fed with plants fertilized with manure [41], and the consumption of aquatic resources [28], could also explain the values obtained for humans.

Indeed, data from the literature indicate that medieval marine fish (whiting, skate, ling, haddock, herring and pleuronectiformes) discovered in a Dominican priory in East Yorkshire (probably from the North Sea) have $\delta^{13}\text{C}$ values between -16.1 and -11.8‰ and $\delta^{15}\text{N}$ values between 10.1 and 17.2‰ ($n = 19$; [42]). Given the isotopic values of these species, the combined consumption of marine resources and herbivore meat could explain the significant isotopic enrichments calculated solely on the basis of a difference between herbivores and humans.

Although freshwater fish have $\delta^{13}\text{C}$ values that are generally closer to terrestrial values, these species display very wide variability, even within the same hydrographic set. For instance, Katzenberg and Weber [43] obtained (eight taxa, $n = 21$) $\delta^{13}\text{C}$ values between -24.6 and -12.9‰ and between 7.3 and 13.7‰ for $\delta^{15}\text{N}$ for the same lake. Similarly, Dufour et al [44] showed that high variations exist between different hydrographic sets for $\delta^{13}\text{C}$ and $\delta^{15}\text{N}$ values, including those for the same taxon. These authors revealed that for seven different taxa from four lakes, $\delta^{13}\text{C}$ values varied from -32.2 to -19.8‰ and from 7.0 to 14.9‰ for $\delta^{15}\text{N}$.

Thus, in Joué-lès-Tours, the consumption of aquatic resources, whether marine or freshwater, is consistent with the results obtained for the isotopes under investigation. Moreover, considering the fact that lifestyles were strongly dictated by the Church during this period, it seems plausible that these individuals would have consumed fish. Indeed, the village is located at the heart of a river system known to have been exploited, as examples of contemporaneous fisheries in the region have been previously described [45]. A study of the archival sources carried out before this work also indicates the presence, at least during the modern period, of a fishpond within the presbytery adjoining the church, which attests to the availability and proximity of this resource in the landscape [17]. Finally, the presence of fish during the High Middle Ages on the site of Joué-lès-Tours was revealed fortuitously by carpological analysis [17]. Although the fish remains have not been taxonomically determined, archival data tend to support the hypothesis of the consumption of freshwater resources. Mixed consumption of pork, poultry and freshwater resources is the most likely scenario to account for the distribution of the isotopic ratios obtained for the 13th–18th centuries. The isotopic characterization of the archaeological freshwater fish of the region will make it possible to verify this hypothesis.

Diet and health

The state of oral health appears degraded for the observed criteria compared to other contemporaneous populations, and homogeneous within our *corpus* for all the studied parameters. This observation is consistent with individuals

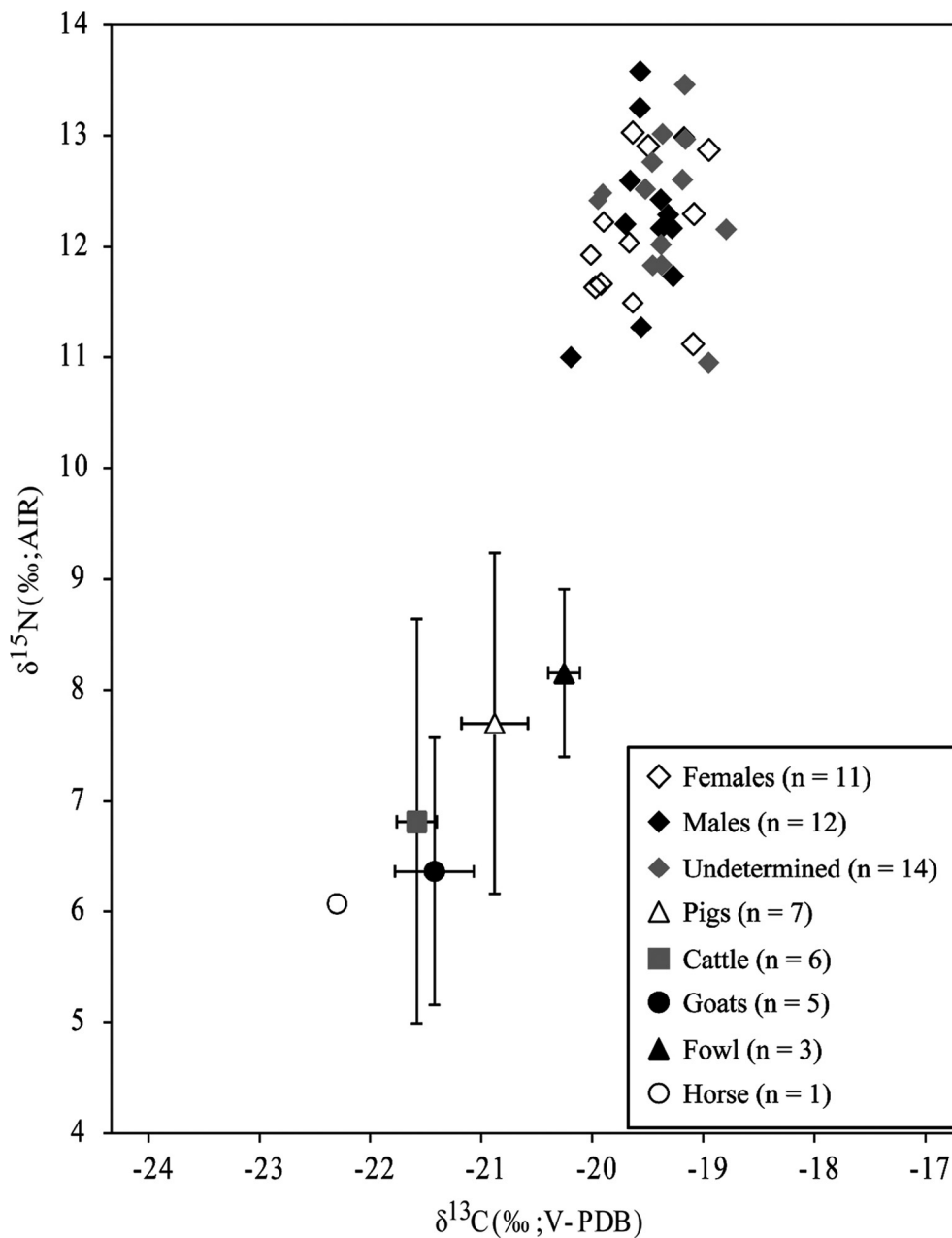


Fig. 5 Isotope ratios ($\delta^{15}\text{N}$ and $\delta^{13}\text{C}$) of humans and local contemporaneous animal corpus ($\pm 1\sigma$) / Rapports isotopiques ($\delta^{15}\text{N}$ et $\delta^{13}\text{C}$) des humains et de la faune régionale ($\pm 1\sigma$)

belonging to a group within a close-knit social and cultural context, as is the marked similarity observed between the subjects with regard to non-specific stress markers, such as linear enamel hypoplasia.

The isotopic and health data resulting from this study, and the invariability of the results obtained for the different chronological periods considered here, calls into question the previously accepted postulate that there was a rupture between the medieval and modern periods in terms of food-related behaviour. Our results also raise questions concerning the relationship between the social status and health

of medieval and modern populations, as in Joué-lès-Tours the likelihood of belonging to an affluent group is not inconsistent with poor health.

Diet and social status

The Kruskal-Wallis test comparing the isotopic values for the different proposed social groups did not reveal any significant differences between them (Table 4). As the proposed social groups have similar isotopic signatures, the comparison of the alimentary resources consumed by men and

women was carried out on the whole *corpus* (a set of 23 individuals of known sex, all periods combined). The Wilcoxon test also confirmed the homogeneity of the isotopic values of carbon and nitrogen with regard to sex ($p > 0.05$).

The social groups studied here were proposed on the basis of archaeological criteria. However, our results, concerning food or health, showed no difference between these groups (Table 4). Two hypotheses should thus be considered; either the proposed criteria do not correspond to a real social structure, or these groups do not have distinct dietary practices (perceptible by biochemical analysis) or different health status.

Diet and chronological phases

In the absence of differences in isotopic signatures between men and women, as well as between the proposed social groups (Table 4), well-dated individuals from our *corpus* were compared and divided into two major chronological phases: the medieval period (13th–15th) and the modern period (16th–18th), in order to determine whether changes occurred over time.

According to the Wilcoxon test carried out for the $\delta^{13}\text{C}$ and $\delta^{15}\text{N}$ variables ($p > 0.05$), the isotopic values do not differ significantly between these two periods for the individuals buried at the site of the Saint-Pierre-et-Saint-Paul

Church in Joué-lès-Tours. Therefore, there would be no change in protein intake between the two chronological phases considered.

Study of the parochial registers of Joué-lès-Tours

The parochial registers of Joué-lès-Tours contain 7,452 death certificates from 1670 to 1792, which represents an average of 61 burials per year in the parish. The study of these documents makes it possible to compare the recruitment of each funerary area and thus to analyse whether they conform to biological or social criteria. The last mention of a burial inside the building dates from 1775.

In the registers, the profession of the deceased or of their parents is indicated for 3,086 individuals. To compare the representation of the different social groups within the funerary areas, the different professions were divided into different social categories: “highest” (noble, clergy, bourgeois), “medium+” (master craftsman, merchant, member of the army, clerk, etc.), “medium” (husbandman), “medium” (winegrower, craftsman), “lowest” (domestic, daily worker).

For individuals for whom the burial site and the occupation (their own or their relatives) are known (Fig. 6), only 1% of the total cemetery population belongs to the highest social category, that is, 55 individuals, as opposed to 12.5% in the church (77 people). The highest social

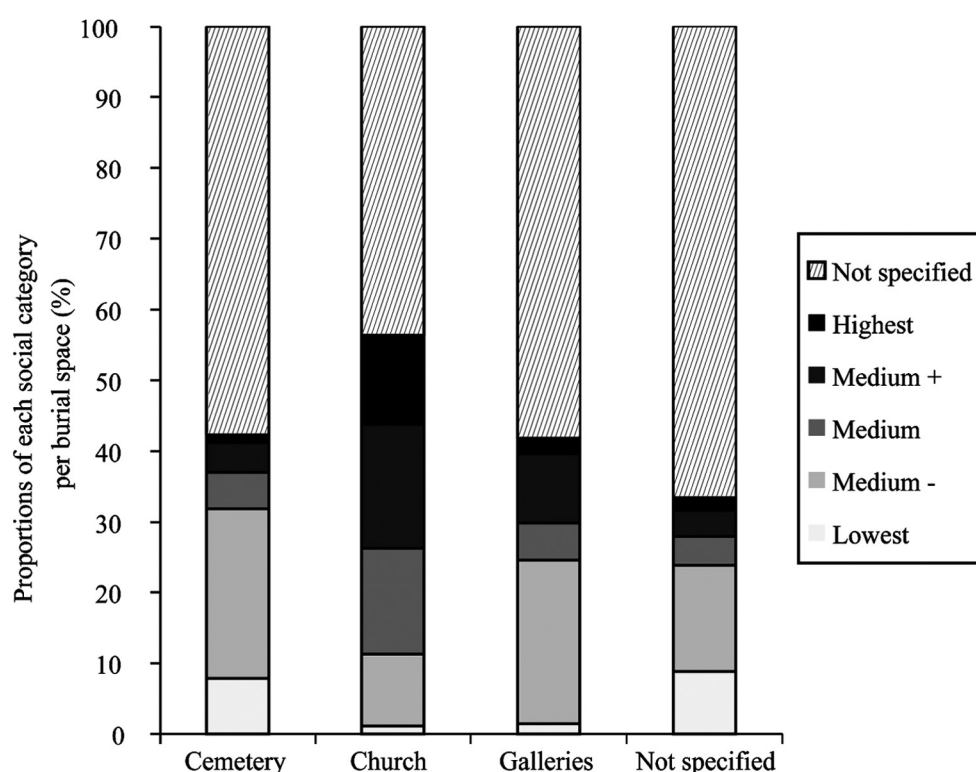


Fig. 6 Proportions of death certificates in the parish registers (1670–1792) according to social class and place of burial / Proportions des actes de décès dans les registres paroissiaux (1670–1792) selon la catégorie sociale et le lieu d’inhumation

categories are preferentially buried inside the church. Nevertheless, this is not an exclusive rule and the majority of burials inside the church belong to the middle classes. Thus, of the 532 burials in the church, there are 80 labourers, 39 merchants, and 25 winegrowers. Yet, nothing rules out the presence of a certain number of representatives from “important families” of local proprietors and farmers among the intermediate categories. Categories considered to be inferior are also mentioned, such as six domestic servants. However, these individuals were in the service of those with an influence over the community (lord, lieutenant of the king, etc.).

With regard to age distribution, the registers were very informative (Fig. 7). Children from birth to 10 years old represent about 20% of the burials within the church (36.5% in the cemetery). The 10- to 19-year-old group represents 3% of the burials in the church, compared with 5.8% in the cemetery. The presence of adults between the ages of 20 and 49 years is almost constant for the church (25.8%) and the cemetery (27.6%). On the other hand, people over 50 represent 30.6% of those buried in the church, compared to 22.8% of those buried in the cemetery. Therefore, the adult age groups, especially those over the age of 50 years, are better represented within the church.

For the church population, the average age at death for those over 20 years is 51.2 years. This is within the range proposed by Maillard [46], who established that the “norm” in Touraine for this period was between 50 and 55 years of age. Nevertheless, it is relatively low within this range. It is important to recall that this range is based on parishes in their entirety and not only on the privileged groups studied here. In addition, Joué’s parochial registers indicate that for the entire population, the average age at death for individuals who have reached 20 years is 48 years, which is below this “norm” [17]. Consequently, these documents seem to support the hypotheses proposed on the basis of archaeological, osteological and isotopic findings; namely, that the population buried in the church had a privileged status within the community and a lower life expectancy compared to other parishes in the region — a fact that could be related to the observed degraded health of the individuals.

Conclusion

Joué-lès-Tours holds a prominent place in the knowledge and understanding of medieval and modern rural societies. This site, with its high density and long duration of funerary

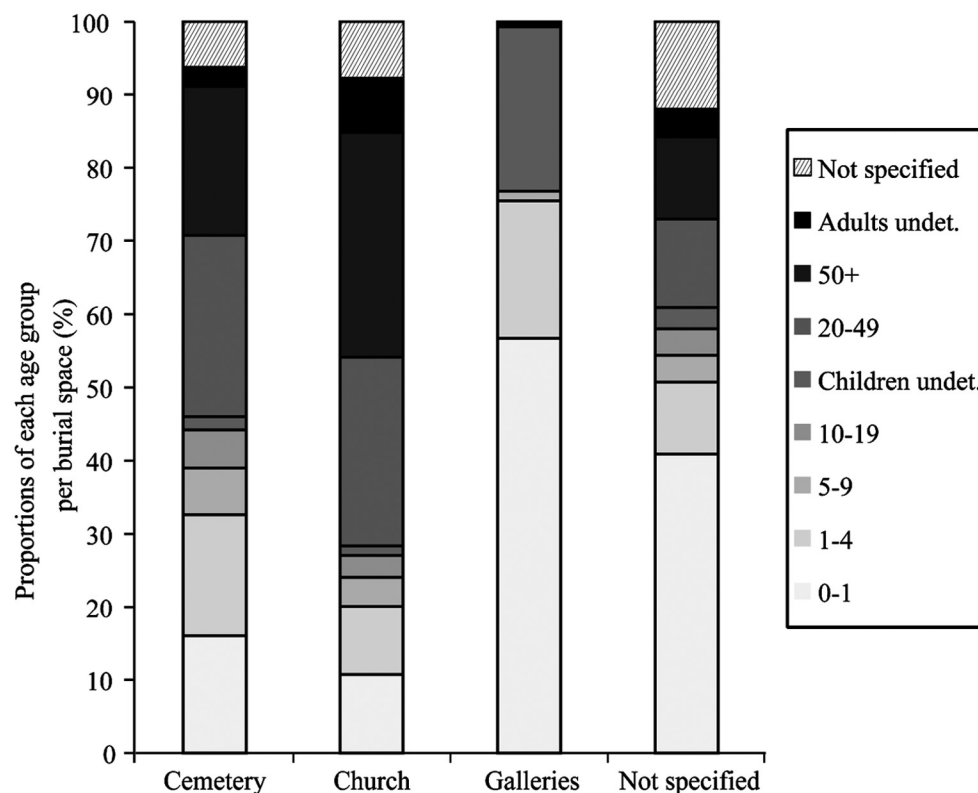


Fig. 7 Proportions of death certificates in the parish registers (1670–1792) according to age and place of burial / Proportions des actes de décès dans les registres paroissiaux (1670–1792) selon l’âge et le lieu d’inhumation

practices, underwent a multidisciplinary study and provided a foundation of knowledge on which this work could be based. The objective was to clarify the complex relationship between the diet, social status and health of a rural medieval population by reducing the scale of analysis down to the level of the individual.

The biochemical and anthropological analyses applied here clarified this relationship by using a sample of 37 individuals buried between the 13th and 18th centuries in the church of Saint-Pierre-et-Saint-Paul of Joué-lès-Tours, and comparing them with a set of 22 contemporaneous animals from Maillé. The human *corpus* was based on the ability of each individual to provide maximum information about social status, oral health, age and sex. It was also essential that the *corpus* included individuals from various time frames across the whole studied period.

The isotopic study of the medieval and modern humans of Joué-lès-Tours and the contemporaneous local fauna showed that the population presents an unexpected diet for this period compared to information from textual sources about rural dietary practices [5]. It seems that the meat component of the diet focused mainly on pork and poultry, in addition to aquatic resources, probably freshwater. Within our sample, this diet appears to be very homogeneous, at least with regard to the protein content, which is similar for men and women, and for all the chronological periods and groups studied. Indeed, our *corpus* is composed of individuals predominantly buried in a privileged space inside the church. In addition, the community is located near Tours, and certainly had strong links with the city. Pork consumption was the main marker of social distinction in this city during these periods [7,8], and it is possible that this model was reproduced by the surrounding communities.

This study provides new elements for our understanding of medieval and modern society in Touraine, but also raises other questions in relation to the site, and the region. Thus, for Joué-lès-Tours, only new analyses of the population buried outside the building can confirm or invalidate the model that we propose—namely, the presence inside the church of a homogeneous group of socially privileged individuals with a specific diet.

At a regional level, similar analyses of different sites would improve our understanding of medieval and modern food practices, including the impact of the availability of resources on different scales, social and religious practices, and the type of human settlement, on the diet of these periods.

Acknowledgments The authors thank Pierre Papin of the archaeological service of the department of Indre-et-Loire and Gwenael Roy of the French National Institute for Preventive Archaeological Research (INRAP) for providing archaeological material. The authors also thank Steve Broo-

kes from IsoAnalytical Ltd. for the spectrometric analyses, and Guy André and Leïa Mion from UMR 7269 LAMPEA for their valuable assistance in sample preparation. The authors also thank Inga Topolnicki from the University of Sydney, Isabelle Josseau-Montagne from the University of Tours and Louise Byrne for editing the English version of the manuscript. The authors thank the anonymous reviewers for their careful reading and their valuable comments and suggestions to improve the quality of the paper.

Conflict of interest: None.

References

- Castex D, Courtaud P, Duday H (2011) Le regroupement des morts : genèse et diversité archéologique. Maison des sciences de l'homme d'Aquitaine, Bordeaux, France, 306 p
- Ariès P (1977) L'homme devant la mort. Éditions du Seuil, Paris, France, 642 p
- Lévi-Strauss C (1964–1971) Mythologiques. Plon, Paris, France, 4 vol.
- Poulain JP (2008) Manger aujourd'hui : attitudes, normes et pratiques. Privat, Toulouse, France, 235 p
- Lauriou B (2002) Manger au Moyen Âge : pratiques et discours alimentaires en Europe aux XIV^e et XV^e siècles. Hachette, Paris, France, 299 p
- Meyzie P (2010) L'alimentation en Europe à l'époque moderne. Armand Colin, Paris, France, 288 p
- Genies C (2014) Le régime carné. In: Galinié H (éd) Des thermes de l'Est de Caesarodunum au château de Tours : le site 3. FERACF, Tours, pp 143
- Cotté O (2008) La société urbaine à Tours et l'animal (XIV^e–XVII^e s.) : approche archéozoologique. Thèse de doctorat, université François-Rabelais de Tours, 2 vol, 830 p
- Polet C (1996) Essai de paléonutrition appliquée à trois populations médiévales belges. Thèse de doctorat, Université libre de Bruxelles, 182 p
- Hedges REM, Clement JG, Thomas CDL, et al (2007) Collagen turnover in the adult femoral mid-shaft: modeled from anthropogenic radiocarbon tracer measurements. Am J Phys Anthropol 133:808–16
- Herrscher E (2001) Contribution de l'analyse paléoépidémiologique et paléobiogéochimique à la connaissance de la santé et de l'alimentation à la fin du Moyen Âge, église Saint-Laurent de Grenoble (XIII^e–XV^e s., Isère, France). Thèse de doctorat, Muséum national d'histoire naturelle, Paris, France, 335 p
- Herrscher E (2003) Alimentation d'une population historique, analyse des données isotopiques de la nécropole Saint-Laurent de Grenoble (XIII^e–XV^e siècle, France). Bull Mem Soc Anthropol Paris 15:149–269
- Carlier A, Hervieu P, Herrscher E (2014) Les habitudes alimentaires à l'époque moderne : contributions des analyses isotopiques. In: Nin N (éd) Aix en archéologie : 25 ans de découvertes. Snoeck, Heule, pp 457–9
- Galinié H, Lorans É, Husi P, et al (2007) Tours antique et médiéval : lieux de vie, temps de la ville : 40 ans d'archéologie urbaine, FERACF, Tours, France, 440 p + 1 CD-Rom
- Audoin-Rouzeau F (1995) Compter et mesurer les os animaux. Pour une histoire de l'élevage et de l'alimentation en Europe de l'Antiquité aux temps modernes. Histoire Mesure 10:277–312

16. Clavel B (2001) L'animal dans l'alimentation médiévale et moderne en France du Nord (xii^e–xvii^e siècles). *Rev Archeol Picardie* 19:9–204
17. Papin P, Livet J, Vanhove C, et al (2013) Joué-lès-Tours (37). Places Victor-Hugo et François-Mitterrand. Origine et évolution d'un centre paroissial rural. Conseil général d'Indre-et-Loire, Inrap, DRAC/SRA Centre, Orléans, France, 4 vol., 1830 p
18. Lorans É, Husi P, Theureau C, et al (2006) Saint-Mexme de Chignon, V^e–XX^e siècles. Éditions du CTHS, Paris, France, 598 p
19. Murail P, Bruzek J, Houët F, et al (2005) DSP: a tool for probabilistic sex diagnosis using worldwide variability in hip-bone measurements. *Bull Mem Soc Anthropol Paris* 17:167–76
20. Schmitt A (2005) Une nouvelle méthode pour estimer l'âge au décès des adultes à partir de la surface sacropelvienne iliaque. *Bull Mem Soc Anthropol Paris* 17:89–101
21. Webb PAO, Suchey JM (1985) Epiphyseal union of the anterior iliac crest and medial clavicle in a modern multiracial sample of American males and females. *Am J Phys Anthropol* 68:457–66
22. Esclassan R (2012) Étude des caries dentaires en fonction du sexe au sein d'individus adultes de la population médiévale (ix^e–xv^e siècles) de Vilarnau (Pyrénées-Orientales) et synthèse sur l'usure. Thèse de doctorat, université Toulouse-III-Paul-Sabatier, 249 p
23. Brothwell DR (1981) Digging up bones: the excavation, treatment, and study of human skeletal remains, Cornell University Press, Ithaca, New York, 208 p
24. Goodman AH, Armelagos GJ (1985) Factors affecting the distribution of enamel hypoplasias within the human permanent dentition. *Am J Phys Anthropol* 68:479–93
25. Castex D (1994) Mortalité, morbidité et gestion de l'espace funéraire au cours du haut Moyen Âge, contribution spécifique de l'anthropologie biologique. Thèse de doctorat, université Bordeaux-I, 2 vol, 500 p
26. Lewis M, Roberts C (1997) Growing pains: the interpretation of stress indicators. *Int J Osteoarchaeol* 7:581–6
27. Schoeninger MJ, DeNiro MJ (1984) Nitrogen and carbon isotopic composition of bone collagen from marine and terrestrial animals. *Geochim Cosmochim Acta* 48:625–39
28. Bocherens H (1999) Isotopes stables et reconstitution du régime alimentaire des hominidés fossiles : une revue. *Bull Mem Soc Anthropol Paris* 11:261–87
29. Ambrose SH, Norr L (1993) Experimental evidence for the relationship of the carbon isotope ratios of whole diet and dietary protein to those of bone collagen and carbonate. In: Lambert JB, Grupe G (eds) Prehistoric human bone. Springer, Berlin, Heidelberg, pp 1–37
30. Bocherens H, Drucker D (2003) Trophic level isotopic enrichment of carbon and nitrogen in bone collagen: case studies from recent and ancient terrestrial ecosystems. *Int J Osteoarchaeol* 13:46–53
31. Goude G, Fontugne M (2016) Carbon and nitrogen isotopic variability in bone collagen during the Neolithic period: influence of environmental factors and diet. *J Archaeol Sci* 70:117–31
32. Herrscher E, Le Bras-Goude G (2010) Southern French Neolithic populations: isotopic evidence for regional specificities in environment and diet. *Am J Phys Anthropol* 141:259–72
33. Longin R (1971) New method of collagen extraction for radiocarbon dating. *Nature* 230:241–2
34. Bocherens H, Fizet M, Mariotti A, et al (1991) Isotopic biogeochemistry (¹³C, ¹⁵N) of fossil vertebrate collagen: application to the study of a past food web including Neanderthal man. *J Hum Evol* 20:481–92
35. Aubry M, Mafart B, Cherid A, et al (2001) Pathologie dentaire d'une population de moniales cisterciennes de l'abbaye Saint-Pierre de l'Almanarre (xii^e–xvi^e s.). In: Hadjouis D, Mafart B (éds) La paléo-odontologie : analyses et méthodes d'étude. Paléoanthropologie et paléopathologie osseuse. ART-COM', Paris, pp 138–51
36. Bédécarrats S, Souquet-Leroy I, Leroy F (2016) Caractérisation biologique et comportements funéraires d'une population rurale moderne — La « Coudrée », Nancras, Charente-Maritime (17). *Bull Mem Soc Anthropol Paris* 28(1 Suppl):8
37. Garcin V, Velemínský P, Trefný P, et al (2010) Dental health and lifestyle in four early mediaeval juvenile populations: comparisons between urban and rural individuals, and between coastal and inland settlements. *HOMO* 61:421–39
38. DeNiro MJ (1985) Postmortem preservation and alteration of in vivo bone collagen isotope ratios in relation to palaeodietary reconstruction. *Nature* 317:806–9
39. Van Klinken GJ (1999) Bone collagen quality indicators for palaeodietary and radiocarbon measurements. *J Archaeol Sci* 26:687–95
40. Hedges REM, Reynard LM (2007) Nitrogen isotopes and the trophic level of humans in archaeology. *J Archaeol Sci* 34:1240–51
41. Bogaard A, Heaton THE, Poulton P, et al (2007) The impact of manuring on nitrogen isotope ratios in cereals: archaeological implications for reconstruction of diet and crop management practices. *J Archaeol Sci* 34:335–43
42. Müldner G, Richards MP (2005) Fast or feast: reconstructing diet in later medieval England by stable isotope analysis. *J Archaeol Sci* 32:39–48
43. Katzenberg MA, Weber A (1999) Stable isotope ecology and palaeodiet in the Lake Baikal region of Siberia. *J Archaeol Sci* 26:651–9
44. Dufour E, Bocherens H, Mariotti A (1999) Palaeodietary implications of isotopic variability in Eurasian lacustrine fish. *J Archaeol Sci* 26:617–27
45. Noizet H (2007) La fabrique de la ville : espaces et sociétés à Tours, IV^e–XIII^e siècle. Publications de la Sorbonne, Paris, France, 504 p
46. Maillard B (1992) Les campagnes de Touraine au XVIII^e siècle : étude d'histoire économique et sociale. PU Rennes, Rennes, France, 500 p

Liste des thèses et habilitations à diriger les recherches (HDR) en anthropologie soutenues en 2018

Muséum national d'Histoire naturelle

Lou Albessard : *Covariation morphologique du crâne et de l'endocrâne au cours de l'évolution du genre Homo.*

Thèse de doctorat soutenue le 17 décembre 2018.

Directeurs : A. Balzeau, S. Durrelman, D. Grimaud-Hervé ;

Rapporteurs : J. Braga, K. Harvati ;

Examinateurs : P. Gunz, B. Maureille, S. Prima.

Bérénice Alard : *Étude génétique des populations de langue austro-asiatique : de la famille linguistique au groupe de parenté.*

Thèse de doctorat soutenue le 22 novembre 2018.

Directeurs : R. Chaix, E. Heyer ;

Rapporteurs : E. Génin, S. Mazières ;

Examinateurs : G. van Driem, D. Higuet.

Cécile Buquet-Marcon : *De l'analyse ostéologique à la reconstitution du programme funéraire. Gestes mortuaires et populations du Baloutchistan pakistanais proto-historique, V^e–III^e millénaires av. J.-C.*

Thèse de doctorat soutenue le 5 décembre 2018.

Directeur : P. Sellier ;

Rapporteurs : D. Castex, A. Coppa ;

Examinateurs : J. Bendezu-Sarmiento, P. Butterlin, P. Chambon, U. Franke.

Hemmamuthe Goudiaby : *Pratiques funéraires et statut des morts dans les ensembles résidentiels mayas classiques (250–950 apr. J.-C.).*

Thèse de doctorat soutenue le 14 février 2018.

Directeur : G. Pereira ;

Rapporteurs : P. Chambon, V. Tiesler ;

Examinateurs : D. Michelet, P. Nondédéo, E. Weiss-Krejci.

Sandrine Prat : *Les Hominines plio-pléistocènes et les Hommes anatomiquement modernes : histoire évolutive, biodiversité et modalités d'expansion. Le crâne dans tous ses états.*

HDR soutenue le 7 septembre 2018.

Rapporteurs : Z. Alemseged, J.-J. Hublin ;

Examinateurs : E. Gilissen, D. Grimaud-Hervé, M. Patou-Mathis, P. Tassy.

Université Aix-Marseille

Estelle Herrscher : *Entre terre et mer : les pratiques alimentaires à l'épreuve du temps.*

HDR soutenue le 22 mai 2018.

Directeur : R. Chenorkian ;

Rapporteurs : E. Cunha, F. Le Mort, I. Ribot ;

Examinateur : O. Dutour.

Alexia Lattard : *Défunt, pratiques et espaces funéraires au sein de la civitas de Forum Iulii au cours du Haut-Empire.*

Thèse de doctorat soutenue le 12 décembre 2018.

Directeurs : A. Schmitt, J.-C. Sourisseau ;

Rapporteurs : D. Castex, W. Van Andringa ;

Examinateurs : V. Bel, J.-P. Brun.

Enguerran Macia : *Anthropologie du vieillissement et écologie de la santé*

HDR soutenue le 22 mai 2018.

Rapporteurs : S. Blanc, A. Guerci, P. Le Coz, M. Signoli ;

Examinateurs : G. Boëtsch, L. Gueye, J.L. Mège.

Florence Petit : *Polymorphisme érythrocytaire : approche anthropologique et interprétation de patterns de diversité génétique, entre peuplement et sélection.*

Thèse de doctorat soutenue le 22 juin 2018.

Directeurs : J. Chiaroni, C. Costedoat ;

Rapporteurs : H. Naya, F. Noizat-Pirenne ;

Examinateurs : M. Baragatti, S. Mazières.

Université de Bordeaux

Frédérique Blaizot : *Contribution de la typologie funéraire à l'étude des systèmes de représentation et d'autodéfinition des sociétés aux dix premiers siècles de notre ère.*

HDR soutenue le 8 octobre 2018.

Rapporteurs : I. Cartron ; C. Knüsel, L. Tranoy ;
 Examinateurs : B. Boissavat-Camus, E. Boucharlat, H. Dudy, P. Pion, W. Van Andringa.

Caroline Partiot : *Diversité biologique des enfants décédés en période périnatale et traitements funéraires au Kerma classique — Les exemples de la nécropole 8B-51 (Kerma classique, Soudan) et des cimetières de Blandy-les-Tours (X^e–XII^e siècles, France) et de Provins (XIII^e–XVIII^e siècles, France)*.

Thèse de doctorat soutenue le 28 novembre 2018.

Directeurs : D. Castex, M. Guillon, B. Maureille ;
 Rapporteurs : P. Adalian, T. Holliday ;
 Examinateurs : I. Crevecoeur, P. Tallet, A. Thomas.

Mathilde Samsel : *Microévolution et bioarchéologie des groupes humains de la fin du Pléistocène et du début de l'Holocène en Europe occidentale : apports de l'anthropologie biologique aux connaissances sur le Paléolithique final et le Mésolithique*.

Thèse de doctorat soutenue le 29 mai 2018.

Directeurs : C. Knüsel, S. Villotte ;
 Rapporteurs : C. Meiklejohn, H.C. Petersen ;
 Examinateurs : I. Crevecoeur, G. Marchand, B. Maureille, F. Valentin.

Université Toulouse-III-Paul-Sabatier

Cazenave Marine : *Caractérisation multisite de la distribution osseuse corticale et de l'organisation du réseau*

trabéculaire du squelette postcrânien de Paranthropus robustus : implications taxonomiques, fonctionnelles et paléobiologiques.

Thèse de doctorat soutenue le 15 octobre 2018.

Directeurs : J. Braga, R. Macchiarelli, A.C. Oettle ;
 Rapporteurs : F.E. Grine, E. Pouydebat ;
 Examinateurs : D. Marchi, N. Telmon.

Rozenn Colleter : *Pratiques funéraires, squelettes et inégalités sociales. Étude d'un échantillon des élites bretonnes à l'Époque moderne*.

Thèse de doctorat soutenue le 25 octobre 2018.

Directeurs : E. Crubézy, N. Telmon ;
 Rapporteurs : D. Garcia, M. Signoli ;
 Examinateurs : E. Cunha, D. Rougé.

Guillaume de Bonnecaze : *Variation morphologique du cornet inférieur chez l'Homme : analyse du polymorphisme et application pratique en pathologie rhinosinusienne*.

Thèse de doctorat soutenue le 27 septembre 2018.

Directeurs : F. Savall, N. Telmon ;
 Rapporteurs : J. Michel, V. Prulière-Escabasse ;
 Examinateurs : G. Captier, E. Serrano.

Vincent Zvenigorodsy-Durel : *Étude des parentés génétiques dans les populations humaines anciennes : estimation de la fiabilité et de l'efficacité des méthodes d'analyse*.

Thèse de doctorat soutenue le 13 novembre 2018.

Directeurs : C. Keyser, X. Mata ;
 Rapporteurs : E. Génin, J. Goudet ;
 Examinateurs : E. Crubézy, E. Rivals, A. Sabbagh.

Les espaces funéraires de l'habitat groupé des Ruelles à Serris (Seine et Marne), Frédérique Blaizot, Thanat'Os, Maison des Sciences de l'Homme de Bordeaux, 2017, 573 p.

B. Bizot

Reçu le 25 juillet 2018 ; accepté le 28 août 2018
© Société d'Anthropologie de Paris et Lavoisier SAS 2018

Ce volumineux ouvrage est la publication de la thèse soutenue par Frédérique Blaizot en décembre 2011 à l'université de Bordeaux I. Le sujet de cette thèse étant consacré à un seul site, la publication peut dans une certaine mesure s'apparenter à une monographie. Le plan de l'ouvrage reprend celui de la thèse, il comprend sept chapitres auxquels il faut ajouter de nombreux tableaux en annexe disponibles sur le site de l'institut Ausonius (<http://ausoniuseditions.u-bordeaux-montaigne.fr>).

L'introduction est consacrée à la présentation du site archéologique des Ruelles fouillé entre 1989 et 1997 sous la responsabilité de B. Foucray puis de F. Gentili. Une surface d'environ 24 ha a été entièrement explorée, ce qui a permis de mettre en évidence un ensemble complexe de six unités d'habitation associées aux VII-VIII^e siècles à un habitat aristocratique. Au centre de l'emprise prenaient place une église bâtie en pierre et une seconde construite sur charpente. Ces édifices ont constitué l'épicentre d'un vaste ensemble funéraire ceint de fossés. Deux bâtiments à vocation domestique ou agricole sont présents dans cet espace. Des petits groupes d'inhumations ont également été exhumés à proximité des habitats disséminés dans l'emprise. L'habitat aristocratique est abandonné à la fin du VIII^e siècle et, aux X-XI^e siècles, d'importants changements sont apportés dans la position et l'organisation des différentes unités d'habitation. Les établissements sont abandonnés dans le courant du XI^e siècle. Les objectifs de cette recherche, également développés dans l'introduction, sont : « la restitution des dispositifs funéraires, la caractérisation des pratiques funéraires et sociales, et l'organisation et la dynamique des espaces funéraires dans l'unité du site ».

B. Bizot
Ministère de la Culture et de la Communication,
Direction régionale des affaires culturelles de Provence Alpes
Côtes d'Azur, Service régional de l'archéologie

UMR 7268-ADES, Aix-Marseille Université, CNRS, EFS,
Marseille, France

Le corpus est constitué de 682 sépultures primaires soit 982 individus. L'analyse prend également en compte les sites de même nature fouillés dans un rayon de 2,5 km. Le matériel anthropologique n'a pu être revu dans le cadre de cette thèse car la collection a été vandalisée en 2005 et est depuis inaccessible. Ces faits ont lourdement handicapé l'approche archéo-anthropologique et ont contraint F. Blaizot à baser son analyse sur des données anthropologiques acquises avec des méthodes parfois révolues et en tout cas moins fiables qu'il n'avait été supposé dans les années 1990. Cette difficulté qui, pour beaucoup, aurait été rédhibitoire constitue une contrainte dont F. Blaizot s'est accommodée grâce notamment à un enregistrement de terrain précis qui lui a permis de fonder son analyse sur une typochronologie très élaborée supplémentant au mieux l'absence de datations radiocarbone.

Les trois chapitres suivants sont consacrés aux dispositifs de dépôt des corps. Ils proposent une analyse rigoureuse des données archéo-anthropologiques en vue de dégager des critères typologiques. Les sépultures mal documentées sont écartées. La définition de chaque type s'appuie sur l'analyse détaillée de nombreux cas illustrés par des relevés et photographies donnant à apprécier toute la variabilité des critères entrant dans la typologie. Aucun indice n'est négligé, que ce soit la forme initiale de la fosse, les effondrements postérieurs qu'elle a pu subir ou les déplacements causés par la circulation de l'eau. L'incidence de l'ordre de décomposition des différents éléments constituant la tombe – corps et contenu – est évaluée. Cette analyse détaillée oblige à recourir à un vocabulaire parfois imagé pour définir au mieux les éléments récurrents de la typologie. Certains termes, comme l'« encagement des corps » pour qualifier les blocs disposés au plus près du squelette paraissent propres à l'auteur. La nomenclature choisie (type 3-B, type 3-A/B-D, etc.) devient vite pesante et sujet à confusion mais il n'y a sans doute guère d'autres solutions compte tenu du nombre important de paramètres traités.

Le chapitre II traite des tombes en fosses. Définies par l'absence de parois construites, elles peuvent comporter un

plancher ou un couvercle. Trois grands sous-types sont définis, ceux-ci se déclinent en plusieurs variantes. Une présentation détaillée du comportement du squelette soumis à l'effondrement des dispositifs de plancher avec des « effets de plaque caractérisés par le déplacement de régions anatomiques maintenues en connexion » apporte des précisions sur des dislocations dont la cause était jusqu'alors rarement expliquée.

Le chapitre III, consacré aux contenants de bois, revient sur le distinguo cercueil/coffre souvent discuté par les archéologues. Selon l'auteur, cette discussion est stérile car les arguments archéologiques permettent rarement de trancher. Il lui paraît préférable de parler de contenant de bois. Selon la même méthode que précédemment, toutes les variantes – sept sous-types – de contenants et leurs avatars taphonomiques sont passés en revue avec de nombreuses descriptions à l'appui.

Le chapitre IV aborde la question des os en situation secondaire en différenciant ce qui relève de rites codifiés, de pratiques funéraires aux modalités techniques aléatoires et de circulations d'ossements totalement déconnectés de leur origine. La représentation de chaque pièce anatomique est quantifiée par un ratio nombre de pièces présentes/nombre de pièces attendues en fonction du NMI de l'ensemble étudié. Cet outil simple permet de qualifier efficacement les différents modes de réduction des corps et de les mettre en relation avec la typologie des sépultures et les pratiques telles que l'empilement de certains contenants périssables ou la reprise de fosses. Les réductions individuelles de corps apparaissent ainsi surtout pratiquées dans les sépultures dotées d'un plancher. Lors de réutilisations volontaires des tombes, les crânes sont le plus souvent placés au chevet et les os rangés. Le constat est fait que, à partir de la troisième réinhumation, la quantité d'os pour chaque individu diminue significativement, ce qui soulève la question de la valeur symbolique de la réduction comme « pars pro toto ». Pour l'auteur, « l'ensemble constitue alors très probablement un lieu de mémoire ».

Le chapitre V aborde la question de la chronologie. Celle-ci est établie sur la base des données obtenues sur l'ensemble funéraire groupé. Treize tombes seulement ont livré du mobilier. Les chronologies relatives entre types de tombes sont examinées. Ces relations ne restituent pas une chronologie tranchée entre les différents types mais il se dessine des tendances. La construction de contenants mettant en œuvre des blocs n'apparaît pas dans les secteurs les plus récents. La surélévation du plancher ou du corps touche tous les types de sépultures et apparaît aux phases les plus anciennes jusqu'au IX^e siècle. La tombe en fosse, présente dès la fin du VIII^e, adopte dans le courant du siècle suivant un plan anthropomorphe. Celui-ci se simplifie rapidement, la logette céphalique est abandonnée, ne subsiste qu'un rétrécissement au niveau des épaules. Aux périodes les plus anciennes sont

pratiquées de véritables réductions de corps. Dans les phases moyennes et récentes, la réintégration d'ossements prend diverses formes et résulte de recoulements ou réappropriations d'espaces. La présence d'amas d'os dans la fosse de la dernière sépulture constituée est surtout rencontrée aux VIII-IX^e siècles.

Ces premiers éléments aboutissent à une restitution des dynamiques en œuvre dans la constitution de l'espace funéraire. L'exercice est compliqué par le fait que 16% des tombes n'ont pu être attribuées à une phase et 59 % sont à cheval sur plusieurs phases. « Les données ne montrent pas de rupture dans la durée de l'occupation de l'espace, mais plutôt des extensions avec des zones plus densément occupées que d'autres selon les phases : autour des bâtiments du VII^e jusqu'au moins la fin du VIII^e siècle, importante expansion vers l'est, début du développement vers le nord durant le IX^e s., développement vers l'ouest dès le début du X^e siècle et poursuite de l'extension vers le nord ; à la charnière des IX-X^e siècle et sans doute jusque dans la première partie du X^e siècle, le cimetière est occupé sur une surface maximale ». Durant toute cette période, des fosses disséminées sur l'ensemble de la zone funéraire principale, ainsi que l'abandon d'un bâtiment puis la construction d'un séchoir, montrent que cet espace n'est pas exempt d'activités domestiques ou agricoles. La question de « concessions familiales » à proximité de l'église en pierre est discutée à propos d'agrégiations de sépultures présentant de nombreuses caractéristiques communes. Les profondeurs d'enfouissement sont également passées en revue. Les cotes indiquées sont celles, en mètres NGF, des fonds de fosse. L'auteur ne précise pas l'épaisseur du recouvrement ni si les éventuels pendages du terrain naturel ont été pris en compte. Les enfants sont inhumés moins profondément que les adultes.

La question bien particulière des espaces funéraires dispersés dans les habitats est traitée dans le chapitre VI. 97 sépultures primaires ont été examinées dans un périmètre de 500 m autour de l'habitat. Il apparaît que la typologie des tombes est identique à celle du cimetière, manquent seulement les cercueils monoxyles surélevés et deux catégories de tombes en fosse. A l'inverse de la zone funéraire, les tombes présentant un contenant ou un plancher sont majoritaires. Les relations stratigraphiques sépultures/habitat sont difficiles à établir ; la typochronologie suggère que les tombes sont contemporaines des habitats. Dans une discussion, F. Blaizot s'interroge sur la notion de cimetière à l'époque mérovingienne. Les habitants des Ruelles considéraient-ils les tombes regroupées près des églises comme un cimetière ? « L'enclos et les fossés qui entourent les tombes et les églises pourraient très bien être liés aux seuls sanctuaires sans fournir aucunement un cadre délimitant les inhumations ». Il est également constaté que l'espace accordé à ces inhumations est limité, les recoulements ne sont pas rares.

L'ensemble des données acquises est synthétisé dans le chapitre VII consacré aux pratiques funéraires. La question du recrutement souffre évidemment de l'absence de données anthropologiques actualisées. L'auteur a tenté au mieux de limiter les erreurs en intégrant par exemple l'âge des immatures déterminé avec des méthodes jugées peu fiables dans deux classes d'âge contigües. Malgré leurs faiblesses, les données démographiques constituent l'un des socles de l'analyse. Diverses courbes de mortalité sont générées à partir des âges au décès des immatures et en fonction de différents critères typologiques, topographiques, etc. Les immatures indéterminés sont redistribués dans les classes d'âge au prorata de la représentation de chaque classe d'âge estimée à partir des sujets d'âge déterminé. Les combinaisons présentant les meilleurs rapports $D(5-9)/D(10-14)$ et $D(5-14)/D(\geq 20)$ sont prises en compte. Si la méthode employée fait parfois débat, le recours à un schéma de mortalité de référence permettant de mettre en exergue les anomalies est adapté aux objectifs de cette étude. Mais la restitution des résultats s'avère, à certains moments, difficile à suivre dans le texte comme sur les tableaux. Les quotients de mortalité obtenus à partir des individus en situation primaire et ceux trouvés en position secondaire font ressortir quelques particularités. Le rapport de masculinité s'avère aussi très instructif. Dans la zone funéraire, il est équilibré à l'est et autour des églises, les femmes sont deux fois plus nombreuses que les hommes au nord ; ces derniers dominent à l'ouest. « Les tombes dispersées dans l'habitat, isolées ou en groupes de 2 à 3 unités, renferment plus de femmes et plus d'individus décédés entre 5 et 19 ans que celles qui sont réunies en groupes de 15 à 50 sépultures, caractérisées par une plus forte proportion d'individus masculins et un recrutement équilibré et conforme sur les trois classes d'âges de 5 à 19 ans. » Diverses hypothèses sont évoquées à propos du rapport de masculinité déséquilibré. Parmi celles-ci l'incidence d'une domesticité féminine ou d'une petite communauté de moniales est évoquée. Dans la zone funéraire, le déséquilibre est en effet dû à une forte dominance de sépultures féminines au nord et à l'est de l'église construite sur charpente.

Une réflexion approfondie est également menée sur le rôle possible de chaque espace funéraire, sur les traitements des corps et les architectures funéraires ainsi que sur la valeur sociale que chacun de ces éléments pourrait revêtir. L'architecture des tombes n'apparaît pas constituer à elle seule un indicateur de statut mais « certains individus réunissent plusieurs éléments [...] pour exprimer leur position sociale. » La sépulture est considérée comme témoin de « l'idéologie funéraire » ; l'architecture funéraire participe de la mise en scène des funérailles. Se manifeste également la volonté d'entretenir la relation avec le défunt précédent à travers la réduction du corps. La mise en scène des crânes dans les réductions n'est observée qu'au sein de ce que F. Blaizot qualifie de « groupe aristocratique ». Isoler le défunt

du contact avec la terre semble être également une préoccupation récurrente. Ces pratiques disparaissent progressivement au IX^e siècle. Au siècle suivant, la moindre importance accordée à la sépulture est concomitante du statut sacré que la consécration confère au cimetière. L'« organisation des morts » est passée d'un modèle polynucléaire où chaque espace d'inhumation a une signification dans la société à une organisation communautaire. Cette évolution accompagne les mutations fondamentales que connaît la société rurale aux X-XI^e siècles. Dans le cas des Ruelles, la disparition de l'église construite en pierres que F. Blaizot associe à la classe aristocratique et la conservation de celle construite sur charpente qui, à la même époque, semble polariser les sépultures dans une répartition complexe selon les sexes et âges témoigneraient, avec la disparition concomitante de l'habitat aristocratique, de ces mutations. Ces évolutions n'abolissent pas certaines constantes, « la dimension identitaire » s'exprime par l'emplacement, des contenants en bois, la réutilisation de tombes, une « micro-organisation du cimetière » matérialise les liens ou différences entre les groupes sociaux.

Pour conclure, F. Blaizot revient sur les difficultés d'exploiter les données issues de grandes opérations archéologiques. Les moyens ont manqué lors de la fouille dans les années 1990. L'inexpérience a joué également. La volonté d'exhaustivité dans l'étude post-fouille est sans doute l'une des causes de l'inachèvement de ce travail. L'auteur insiste sur le fait que, si la reprise des données de terrain a été possible, c'est en grande partie grâce au caractère systématique et exhaustif de l'enregistrement de terrain. Pour les contextes funéraires médiévaux, la typochronologie des tombes et le recrutement sont considérés comme les éléments incontournables de toute étude. Et, au stade actuel de la recherche, la publication de catalogues analytiques apparaît comme une étape essentielle.

Cet ambitieux travail apporte, si besoin en était encore, la démonstration du haut niveau d'expertise de son auteur. Centré sur la caractérisation des architectures et des traitements funéraires des défunts selon les grands principes de l'archéo-anthropologie enseignés par H. Duday, il constitue à bien des égards une ressource. Chaque type d'inhumation est ainsi envisagé dans toutes ses variantes possibles et, d'un point de vue pratique, le lecteur peut aborder les chapitres consacrés à la typologie des tombes comme un référentiel à plusieurs entrées. Cette monographie replace au premier plan la typologie des sépultures en lui conférant une valeur heuristique dépassant la nécessité prosaïque de nommer un objet. C'est bien en effet le souci d'une mise en perspective sociale et historique des données qui sous-tend cette recherche qui ne manquera pas, j'en suis certain, d'inspirer certains travaux à venir. La terminologie imagée qui a été choisie pour qualifier certains types de tombes ou effets taphonomiques sera sans doute reprise. Comme à l'accoutumé, le

risque est grand que l'emploi de ce vocabulaire à forte valeur évocatrice connaisse des dérives. Pour lever toute ambiguïté sur certains vocables (par ex. tombe en chambre, engagement) on ne saurait trop recommander qu'il soit toujours employé en référence au site des Ruelles. Enfin, l'inachèvement de l'étude des contextes domestiques au moment où

cette thèse a été soutenue aurait pu constituer un frein à la parution de cet ouvrage. L'auteur et l'éditeur ont choisi de ne pas attendre plus et, malgré les incertitudes pesant encore sur la datation ou la qualification de certains contextes domestiques, il faut se féliciter de la publication de cet ensemble funéraire incomparable pour le haut Moyen-Age.

Jean-Pierre Bocquet-Appel (1949–2018)

J.-J. Hublin

© Société d'Anthropologie de Paris et Lavoisier SAS 2019

La taille des populations humaines du passé, leur distribution spatiale et leur fluctuation en relation avec des facteurs environnementaux ou économiques sont des facteurs déterminants de leur évolution biologique et culturelle. C'est ce vaste champ d'études qui a passionné Jean-Pierre Bocquet-Appel tout au long de sa vie professionnelle. Il s'y est investi avec fougue, en explorant de nombreux aspects de l'anthropologie démographique, et il a apporté ainsi une contribution essentielle à leur compréhension. Ses thématiques de recherche ont couvert un large spectre, allant de la paléodémographie proprement dite à la démographie contemporaine, avec d'importants apports théoriques et méthodologiques. Jean-Pierre Bocquet-Appel est mort à Paris le 13 août 2018 des suites d'une maladie qui ne lui a accordé que peu de chance dans cet ultime combat. Il laisse derrière lui une brique essentielle dans le mur sans cesse reconstruit de la connaissance. Au-delà du chercheur de premier plan, c'était un homme remarquable dont l'intelligence ne tolérait ni la compromission ni la médiocrité.

Né le 25 octobre 1949, dans le 12^e arrondissement de Paris, Jean-Pierre Bocquet-Appel a connu une enfance troublée et il en fut longtemps tourmenté. Mal à l'aise dans son environnement familial comme dans son environnement scolaire, il quittera l'école à 16 ans pour devenir employé dans une banque et plus tard brièvement chez Renault. Ce n'est qu'adulte qu'il retrouvera la famille d'un père biologique disparu. Il s'en fera reconnaître et, adopté par sa grand-mère paternelle, rejoindra au début des années 1980 le nom de « Appel » à celui de son état civil de naissance. Pour ceux qui furent proches de lui, il ne fait pas de doute que bien des ressorts de sa personnalité trouvent leurs racines dans ce chemin de vie hors du commun. Jean-Pierre Bocquet-Appel a toujours été à la recherche des vérités cachées. Passionnément attaché à l'exactitude des faits, il



Fig. 1 Portrait de Jean-Pierre Bocquet-Appel

développa dans la vie comme dans la science une approche exigeante et hyperrationnelle des êtres et des choses.

Dans l'après-1968, il retrouve le chemin des études académiques en découvrant la possibilité que lui offre l'École pratique des hautes études (EPHE) de passer un diplôme d'enseignement supérieur. Il l'obtiendra en 1974 sous la direction d'Annette Laming-Emperaire, alors investie dans l'étude des sites archéologiques de l'Amérique du Sud. Mais c'est surtout son travail de thèse de troisième cycle intitulé « Perspectives paléodémographiques » sous la direction de Denise Ferembach et Jean-Marie Pesez qui l'oriente vers ses futures recherches. Jean-Pierre Bocquet-Appel est un autodidacte infatigable qui, pour mener à bien ses travaux, s'immerge dans l'étude des méthodes statistiques, ainsi que dans

J.-J. Hublin (✉)
Collège de France, 11 place Marcelin-Berthelot,
F-75231 Paris cedex 05, France
e-mail : hublin@eva.mpg.de

Department of Human Evolution,
Max-Planck Institute for Evolutionary Anthropology,
6 Deutscher Platz, D-04103 Leipzig, Germany

celle de l'anglais et de l'espagnol. À la suite de sa soutenance, il trouvera son premier emploi scientifique en tant que « préparateur », au sein du laboratoire d'anthropologie biologique de l'EPHE (troisième section). Il travaille à Juvisy, auprès de Denise Ferembach qui jouera un grand rôle dans sa formation et dont la générosité l'impressionne beaucoup. C'est de cette époque que datent ses premières publications avec Claude Masset qui lui aussi rédige une thèse sur les indicateurs paléodémographiques. De travées osseuses des épiphyses du fémur et de l'humérus en sutures crâniennes, les deux chercheurs n'en finissent pas de buter sur les difficultés de reconstruction de la pyramide des âges dans les séries archéologiques. En 1982, ils publient ensemble dans le *Journal of Human Evolution* l'article qui reste à ce jour le plus cité parmi les très nombreux que Jean-Pierre Bocquet-Appel a produits. C'est un éclatant *Farewell to Paleodemography* qui sonne le glas des approches traditionnelles de la discipline. À l'évidence, le choix des échantillons de référence biaise la distribution par âges d'un ensemble de squelettes que l'on veut étudier. Après cette remise en cause, les deux chercheurs s'emploieront à proposer de nouvelles approches pour estimer l'âge moyen au décès de tels ensembles et en tirer d'autres paramètres démographiques.

En 1981, Jean-Pierre Bocquet-Appel et moi-même nous retrouvons en concurrence directe pour un poste de chercheur au CNRS. Je le rencontre pour la première fois, hors contexte académique, et, malgré les circonstances, nous sympathisons immédiatement, car nous avons déjà beaucoup à partager. Abandonnant une séquence monotone de recrutement disciplinaire qui devait condamner l'un ou l'autre, cette année-là, le Comité national ne trancha pas et nous recruta tous les deux. Jean-Pierre Bocquet-Appel est d'abord rattaché au LA 184 L'Homme préhistorique où il ne restera guère. En 1984, il rejoint le laboratoire d'informatique pour les sciences de l'homme (LISH) où il a accès à des moyens de calcul performants pour réaliser sa thèse d'État qu'il soutiendra à 34 ans sous la direction de Jean Hiernaux et Jean-Marc Lalouel, deux grands scientifiques qu'il admire. Son parcours professionnel au CNRS passera en 1991 par URA 49 (Centre de recherches anthropologiques du musée de l'Homme) devenu plus tard UMR152 (laboratoire d'anthropologie) où il me retrouvera. Finalement, en 1998, il appartiendra aux membres fondateurs d'une unité propre du CNRS (EP 1781, puis UPR 2147) : « *Dynamique de l'évolution humaine : Individus, Populations, Espèces* » que j'ai eu l'honneur de diriger. Jean-Pierre Bocquet-Appel regrettera souvent que cette unité soit structurellement dissociée du milieu universitaire et de la formation. Devenu directeur de recherche en 1995, il s'est cependant toujours attaché à diriger des travaux d'étudiants et de postdoctorants. C'est avec son retour vers l'EPHE qu'il peut pleinement s'investir dans l'enseignement et la formation de jeunes chercheurs. D'abord chargé de conférences, invité

en 1995, il devient finalement directeur d'études cumulant dans la troisième section à partir de 2008, poste qu'il occupera jusqu'à sa retraite.

Sur le plan de la recherche, Jean-Pierre Bocquet-Appel a fait preuve d'une curiosité et d'une créativité peu commune dans le vaste domaine de l'anthropologie. Il a été capable de s'intéresser aussi bien à la taille des armures du XVI^e siècle pour reconstituer le format corporel de la classe féodale qu'à l'influence du climat, de l'alimentation et de la démographie sur la morphologie squelettique de séries portugaises du XIX^e siècle. Après la déconstruction de la paléodémographie qui a suivi l'article de 1982 est venu ensuite le temps de sa reconstruction. Après plusieurs séjours à l'université de Stony-Brook (États-Unis) où il a collaboré avec Robert R. Sokal, il est au début des années 1990 un des précurseurs de la démographie spatiale, celle qui a jeté les bases conceptuelles de l'analyse de la Transition démographique contemporaine. Jean-Pierre Bocquet-Appel comprend que c'est le croisement des méthodes de datations, des données spatiales et, plus tard, celui des données paléogénétiques avec les données paléodémographiques, qui permettent de pleinement saisir la dynamique des peuplements humains du passé. Cette approche intégrative lui ouvre des voies d'investigation nouvelles, et elle lui permettra d'apporter des résultats scientifiques majeurs.

Il s'intéresse aux populations paléolithiques et collabore avec Pierre-Yves Demars pour analyser les données fournies par les sites archéologiques du Paléolithique supérieur sur une vaste aire géographique eurasienne pour reconstituer densité des peuplements et géographie humaine de ces chasseurs-collecteurs. La question du remplacement des Néandertaliens par les hommes modernes le passionne aussi et motive au plus haut point ses recherches. C'est un problème sur lequel il travaillait encore à la veille de sa disparition. Poursuivant ses analyses des nécropoles néolithiques, il met surtout en évidence, en 2002, la Transition démographique néolithique (ou Transition démographique agricole) marquée, en Europe, par une explosion de la fécondité féminine au passage d'une économie de collecte à une économie agricole. Cette révolution démographique, qui a précédé de plusieurs millénaires la Transition démographique contemporaine, a été ensuite reconnue dans la quasi-totalité des foyers de néolithisation. C'est une découverte majeure qui a donné lieu à des publications devenues incontournables et à la tenue de réunions scientifiques comme Jean-Pierre Bocquet-Appel aimait à les organiser. Elle lui valut une reconnaissance internationale renouvelée dont peu de chercheurs de sa génération peuvent se prévaloir.

Il faut enfin souligner l'intérêt constant de Jean-Pierre Bocquet-Appel pour l'histoire de l'Anthropologie et les questions épistémologiques et éthiques parfois épineuses qui l'entourent. En témoignent ses entretiens avec Henri-Victor Vallois, figure dominante de l'Anthropologie d'une

époque, et avec Gustave Malécot, internationalement reconnu comme théoricien de génétique des populations. Il s'y est employé avec une radicalité sans doute en partie héritée de sa jeunesse syndicaliste et de son ardeur à rétablir une vérité qu'il considérait comme masquée par une historiographie trop lisse. Certes, au quotidien, Jean-Pierre Bocquet-Appel pouvait être rugueux. Il n'avait que peu de tolérance pour les approximations méthodologiques et la petitesse intellectuelle. Mais pour qui savait l'écouter, une discussion scientifique avec lui était toujours une expérience des plus enrichissantes. Ses éclats, ses réflexions parfois acides, mais toujours pertinentes, sur le monde de la recherche et des chercheurs, les échanges plus personnels que nous avons pu avoir, tout cela reste à jamais gravé en moi. *Farewell* Jean-Pierre...

Remerciements Mes vifs remerciements à Eugénie Bocquet-Appel, Dominique Vincent, Claude Masset, Pierre Darlu, Estelle Herrscher et Anna Degioanni pour leur assistance dans la réalisation de ce texte.

Bibliographie

1. Balabdaoui F, Bocquet-Appel JP, Lajaunie C, Irudaya Rajan S (2001) Space-time evolution of the fertility transition in India, 1961–1991. *Int J Popul Geogr* 7:129–48. <https://doi.org/10.1002/ijpg.213>
2. Bergot C, Bocquet JP (1976) Étude systématique, en fonction de l'âge, de l'os spongieux et de l'os cortical de l'humérus et du fémur. *Bull Mem Soc Anthropol Paris* 3:215–42. <https://doi.org/10.3406/bmsap.1976.1852>
3. Blondiaux J, Naji S, Bocquet-Appel JP, et al (2016) The leprosarium of Saint-Thomas d'Aizier: the cementochronological proof of the medieval decline of Hansen disease in Europe? *Int J Paleopathol* 15:140–51. <https://doi.org/10.1016/j.ijpp.2015.02.005>
4. Bocquet JP (1977) Paléodémographie : ce que nous apprend la Nubie soudanaise. *Annales* (Paris, France : 1946) 32:54–69
5. Bocquet JP, Masset C (1977) Estimateurs en paléodémographie : l'Homme. *Rev Fr Anthropol* 17:65–90
6. Bocquet JP (1979) Sjovold (T.), 1977 — Non-metrical divergence between skeletal populations. The theoretical foundation and biological importance of C.A.B. Smith's mean measure of divergence. *Ossa*, 4. *Bull Mem Soc Anthropol Paris* 6-3:351–2
7. Bocquet JP (1979) Une approche de la fécondité des populations inhumées. *Bull Mem Soc Anthropol Paris* 6:261–8. <https://doi.org/10.3406/bmsap.1979.1965>
8. Bocquet JP (1989) Muller-Hill (Benno) — Science nazie, science de mort. L'extermination des Juifs, des Tziganes et des malades mentaux de 1933 à 1945. *Bull Mem Soc Anthropol Paris* 1-1-2: 158–60
9. Bocquet JP, Bergot C (1977) Évolution de l'os cortical de l'humérus en fonction de l'âge. *Bull Mem Soc Anthropol Paris* 4:359–69. <https://doi.org/10.3406/bmsap.1977.1888>
10. Bocquet JP, Reverseau JP (1979) Estimation de la stature de la classe féodale d'après les armures du XVI^e siècle. *Ethnol Fr* 9:85–94
11. Bocquet-Appel J (2002) Paleoanthropological traces of a Neolithic Demographic Transition. *Curr Anthropol* 43:637–50. <https://doi.org/10.1086/342429>
12. Bocquet-Appel J (2009) The demographic impact of the agricultural system in human history. *Curr Anthropol* 50:657–60. <https://doi.org/10.1086/605552>
13. Bocquet-Appel JP (2005) The archaeological and genetic foundations of the European population during the Late Glacial: implications for “agricultural thinking” (Comment on C. Gamble, W. Davies, P. Pettitt, L. Hazelwood, M. Richard). *Cambridge Archaeol J* 15:212–3
14. Bocquet-Appel J, Naji S (2006) Testing the hypothesis of a worldwide Neolithic Demographic Transition: corroboration from American cemeteries. *Curr Anthropol* 47:341–65. <https://doi.org/10.1086/498948>
15. Bocquet-Appel JP (1985) Small populations: demography and paleoanthropological inferences. *J Hum Evol* 14:683–91
16. Bocquet-Appel JP (1989) L'anthropologie physique en France et ses origines institutionnelles. *Gradhiva* 6:23–34
17. Bocquet-Appel JP (1991) Réponse à Jean Anthony. *Gradhiva* 7:96–7
18. Bocquet-Appel JP (1996) Interview de Gustave Malécot (mai 1993, avril 1994). *Bull Mem Soc Anthropol Paris* 8:105–14. <https://doi.org/10.3406/bmsap.1996.2431>
19. Bocquet-Appel JP (1996) Interview de Henri-Victor Vallois (le 15 février 1981). *Bull Mem Soc Anthropol Paris* 8:81–103. <https://doi.org/10.3406/bmsap.1996.2430>
20. Bocquet-Appel JP (2004) A regional biological approach to the spread of farming in Europe, Anatolia, the Levant, South-Eastern Europe, and the Mediterranean (comment on R. Pinhasi, M. Pluciennik). *Curr Anthropol* 45:S75–S6. <https://doi.org/10.1086/422085>
21. Bocquet-Appel JP (2005) The closest route to a stable population: fitting a distribution to deaths by age with application to paleodemography (comment on N. Bonneuil). *Curr Anthropol* 46:S38–S9. <https://doi.org/10.1086/422085>
22. Bocquet-Appel JP (2008) What's mother to do? A hypothesis about the division of labor among Neandertals and modern humans in Eurasia (comment on S.L. Kuhn, M.C. Stiner). *Curr Anthropol* 47:965. <https://doi.org/10.1086/422085>
23. Bocquet-Appel JP, Bacrot JN (1993) Isolation by distance, trend surface analysis, and spatial autocorrelation. *Hum Biol* 65:11–27
24. Bocquet-Appel JP, Bacrot JN (1994) Generalized wombling. *Syst Biol* 43:442. <https://doi.org/10.2307/2413680>
25. Bocquet-Appel JP, Bacrot JN (1997) Brief communication: estimates of some demographic parameters in a Neolithic rock-cut chamber (approximately 2000 BC) using iterative techniques for aging and demographic estimators. *Am J Phys Anthropol* 102:569–75. [https://doi.org/10.1002/\(SICI\)1096-8644\(199704\)102:4<569::AID-AJPA11>3.0.CO;2-Z](https://doi.org/10.1002/(SICI)1096-8644(199704)102:4<569::AID-AJPA11>3.0.CO;2-Z)
26. Bocquet-Appel JP, Demars PY (2001) The blind leading the lame. Responses to PB Pettitt and AWG Pike. *Antiquity* 75:418–9
27. Bocquet-Appel JP, Jakobi L (1990) Familial transmission of longevity. *Ann Hum Biol* 17:81–95
28. Bocquet-Appel JP, Jakobi L (1993) A test of a path model of biocultural transmission of fertility. *Ann Hum Biol* 20:335–47
29. Bocquet-Appel JP, Masset C (1996) Paleodemography: expectancy and false hope. *Am J Phys Anthropol* 99:571–83. [https://doi.org/10.1002/\(SICI\)1096-8644\(199604\)99:4<571::AID-AJPA4>3.0.CO;2-X](https://doi.org/10.1002/(SICI)1096-8644(199604)99:4<571::AID-AJPA4>3.0.CO;2-X)
30. Bocquet-Appel JP, Rajan IS, Bacrot JN, Lajaunie C (2002) The onset of India's fertility transition. *Eur J Popul / Rev Eur Demogr* 18:211–32. <https://doi.org/10.1023/A:1019721310893>
31. Bocquet-Appel JP (1996) Note sur l'origine de deux interviews : Henri-Victor Vallois et Gustave Malécot. *Bull Mem Soc Anthropol Paris* 8:115–23. <https://doi.org/10.3406/bmsap.1996.2432>

32. Bocquet-Appel JP (2011) The agricultural demographic transition during and after the agriculture inventions. *Curr Anthropol* 52: S497–S510. <https://doi.org/10.1086/659243>
33. Bocquet-Appel JP (2011) When the world's population took off: the springboard of the Neolithic Demographic Transition. *Science* (New York, NY) 333:560–1. <https://doi.org/10.1126/science.1208880>
34. Bocquet-Appel JP (2012) Commentary on Sokal's "ancient movement patterns determine modern genetic variances in Europe" (1991). *Hum Biol* 84:553–4. <https://doi.org/10.3378/027.084.0505>
35. Bocquet-Appel JP, Arsuaga JL (1999) Age distributions of hominid samples at Atapuerca (SH) and Krapina could indicate accumulation by catastrophe. *J Archaeol Sci* 26:327–38. <https://doi.org/10.1006/jasc.1998.0370>
36. Bocquet-Appel JP, Degioanni A (2013) Neanderthal demographic estimates. *Curr Anthropol* 54:S202–S13. <https://doi.org/10.1086/673725>
37. Bocquet-Appel JP, Demars PY (2000) Neanderthal contraction and modern human colonization of Europe. *Antiquity* 74:544–52. <https://doi.org/10.1017/S0003598X00059901>
38. Bocquet-Appel JP, Demars PY (2000) Population kinetics in the Upper Paleolithic in Western Europe. *J Archaeol Sci* 27:551–70. <https://doi.org/10.1006/jasc.1999.0471>
39. Bocquet-Appel JP, Demars PY, Noiret L, Dobrowsky D (2005) Estimates of Upper Palaeolithic meta-population size in Europe from archaeological data. *J Archaeol Sci* 32:1656–68. <https://doi.org/10.1016/j.jas.2005.05.006>
40. Bocquet-Appel JP, Dubouloz J (2003) Traces paléoanthropologiques et archéologiques d'une transition démographique néolithique en Europe. *Bull Soc Prehist Fr* 100:699–714. <https://doi.org/10.3406/bspf.2003.12905>
41. Bocquet-Appel JP, Dubouloz J (2004) Expected palaeoanthropological and archaeological signal from a Neolithic Demographic Transition on a worldwide scale. *Documenta Praehistorica* 31:25–33. <https://doi.org/10.4312/dp.31.2>
42. Bocquet-Appel JP, Formoso B, Stépanoff C (2017) Pour une anthropologie générale. Crise et renouveau du partenariat scientifique et institutionnel de l'anthropologie biologique, l'anthropologie sociale et la préhistoire. *L'Homme* 223–224:221–46
43. Bocquet-Appel JP, Jakobi L (1991) La transmission familiale de la longévité à Arthez d'Asson (1685–1975). *Population* (French Edition) 46:327. <https://doi.org/10.2307/1533239>
44. Bocquet-Appel JP, Jakobi L (1993) Transmission familiale de la fécondité : le test d'un modèle (Arthez d'Asson, 1744–1890). *Population* (French Edition) 48:771. <https://doi.org/10.2307/1534106>
45. Bocquet-Appel JP, Jakobi L (1997) Diffusion spatiale de la contraception en Grande-Bretagne, à l'origine de la transition. *Population* (French Edition) 52:977–1003. <https://doi.org/10.2307/1534621>
46. Bocquet-Appel JP, Jakobi L (1998) Evidence for a spatial diffusion of contraception at the onset of the fertility transition in Victorian Britain. *Population* (An English Selection) 10:181–204
47. Bocquet-Appel JP, Masset C (1982) Farewell to paleodemography. *J Hum Evol* 11:321–33. [https://doi.org/10.1016/S0047-2484\(82\)80023-7](https://doi.org/10.1016/S0047-2484(82)80023-7)
48. Bocquet-Appel JP, Naji S, Linden MV, Kozlowski JK (2009) Detection of diffusion and contact zones of early farming in Europe from the space-time distribution of 14C dates. *J Archaeol Sci* 36:807–20. <https://doi.org/10.1016/j.jas.2008.11.004>
49. Bocquet-Appel JP, Naji S, Vander Linden M, Kozlowski J (2012) Understanding the rates of expansion of the farming system in Europe. *J Archaeol Sci* 39:531–46. <https://doi.org/10.1016/j.jas.2011.10.010>
50. Bocquet-Appel JP, Sokal RR (1989) Spatial autocorrelation analysis of trend residuals in biological data. *Syst Biol* 38:333–41. <https://doi.org/10.2307/2992399>
51. Bocquet-Appel JP, Tuffreau A (2009) Technological responses of Neanderthals to macroclimatic variations (240,000–40,000 BP). *Hum Biol* 81:287–307. <https://doi.org/10.3378/027.081.0310>
52. Bocquet-Appel JP, Ery K (1988) Une analyse spectrale de la distribution de la stature dans une nécropole. *Rev Archeometr* 12:35–9. <https://doi.org/10.3406/arsci.1988.1246>
53. Darlu P, Bocquet-Appel JP (1987) Une méthode de reconnaissance des apparentés fondée sur des mesures quantitatives. *Bull Mem Soc Anthropol Paris* 4:191–200. <https://doi.org/10.3406/bmsap.1987.1635>
54. Hiernaux J, Bocquet-Appel JP (1987) Physique and personality. *Curr Anthropol* 28:566–7. <https://doi.org/10.1086/203563>
55. Hiernaux J, Bocquet-Appel JP (1988) La liaison entre la personnalité et le physique. *Psychométrie et Psychologie* 8:52–63
56. Bocquet-Appel JP, Tavares da Rocha MA, Xavier de Morais MH (1980) Peut-on estimer l'âge au décès à l'aide du remaniement osseux ? *Biom Hum Paris* 15:51–6
57. Kohler TA, Glaude MP, Bocquet-Appel JP, Kemp BM (2008) The Neolithic Demographic Transition in the US Southwest. *American Antiquity* 73:645–69. <https://doi.org/10.1017/S0003598X08000473>
58. Naji S, Colard T, Blondiaux J, et al (2016) Cementochronology, to cut or not to cut? *Int J Paleopathol* 15:113–9. <https://doi.org/10.1016/j.ijpp.2014.05.003>
59. Tran TNN, Aboudharam G, Gardeisen A, et al (2011) Classification of ancient mammal individuals using dental pulp MALDI-TOF MS peptide profiling. *PLoS One* 6:e17319. <https://doi.org/10.1371/journal.pone.0017319>

Ouvrages

60. Bocquet-Appel JP (2008) La paléodémographie : 99,99 % de l'Histoire démographique des êtres humains. Éditions Errance, Paris, 192 p
61. Bocquet-Appel JP, Xavier de Morais MH (1987) Anthropologie et histoire : un essai de reconstitution de la variation de la population portugaise au XIX^e siècle. Fontes Documentais Portuguesas, Foundation Calouste Gulbenkian, avec le concours du CNRS, 184 p

Direction d'ouvrages

62. Bocquet-Appel JP, Bar-Yosef O (eds) (2008) The Neolithic Demographic Transition and its consequences. Springer, New York, 544 p (Comptes rendus dans : American Journal of Physical Anthropology 143:327; Canadian Studies in Population 37:613–15; Human Biology 83:645–50; Hum Ecol 37:675–76)
63. Bocquet-Appel JP (ed) (2008) Recent advances in Paleodemography: Data, Techniques, Patterns. Springer, New York, 294 p
64. Bocquet-Appel JP, Courgeau D, Pumain D (eds) (1996) Spatial analysis of biodemographic data. Eurotext, John Libbey Ed, Londres, Paris, 367 p

Bulletins et Mémoires de la Société d'Anthropologie de Paris (BMSAP)

Recommandations aux auteurs

La Société d'Anthropologie de Paris publie dans ses Bulletins et Mémoires des articles originaux, des revues de synthèse ou des notes concernant le champ disciplinaire de l'anthropologie biologique, depuis la paléoanthropologie jusqu'à l'écologie humaine, en passant par la génétique des populations et l'histoire de la discipline. Tous les manuscrits soumis à la revue font l'objet d'un processus d'évaluation (reviewing). Pour être publié, chaque article doit :

- recueillir les avis favorables des membres du Comité de lecture auquel ils sont soumis
- obéir aux normes de présentation exposées ci-dessous

1 - Soumission électronique du manuscrit

Le **manuscrit** doit être soumis en un seul fichier au format DOC comprenant successivement texte, légendes des tableaux et des figures, tableaux, illustrations (300 DPI), par e-mail à l'adresse suivante : redacchef@sapweb.fr

La **version acceptée du manuscrit** devra être envoyée en plusieurs fichiers distincts : un unique fichier Word (DOC) correspondant au texte, aux tableaux et aux légendes d'une part, et les figures sous la forme de fichiers JPEG, EPS ou TIFF séparés d'autre part.

Il est explicitement convenu que tout manuscrit soumis aux **Bulletins et Mémoires de la Société d'Anthropologie de Paris** est un travail original qui n'a pas été publié et qui n'est pas en cours d'évaluation par une autre revue.

2 - Préparation du manuscrit

Le manuscrit sera rédigé en français ou en anglais. Il devra comporter successivement : un **titre** en anglais **et** en français, les **nom, prénom et adresse des auteurs**, l'**adresse e-mail** du contact, des **mots clés** (6 maximum) en français **et** en anglais, un **résumé** en anglais **et** en français (1500 caractères maximum espaces compris), une **version abrégée** facultative (4000 caractères maximum espaces compris) en anglais **ou** en français (dans la langue non utilisée pour l'article), le texte du manuscrit, la liste des références bibliographiques, la liste des tableaux, la liste des figures, les tableaux et les figures. Les pages et les lignes du manuscrit seront numérotées de façon continue dès la page de titre.

Le **texte** du manuscrit (texte, titres et intertitres, notes infrapaginaires, abréviations ou sigles, références bibliographiques, légendes des tableaux et figures) n'excédera pas 50 000 caractères (espaces compris) pour un article et 20 000 caractères (espace compris) pour une note. Il sera de préférence rédigé avec la police Times New Roman, 12 pt, en double interligne, et mis en page au format A4 avec des marges de 25 mm.

Titres et intertitres. Le titre principal de l'article n'excédera pas 200 caractères (espaces compris). En outre, le corps du texte de chaque article comportera

au maximum 2 niveaux de titres que l'auteur veillera à bien rendre distincts sur son manuscrit. Ceux-ci ne seront pas numérotés.

Les **notes infrapaginaires** sont appelées dans le texte par un numéro en chiffres arabes et en exposant, sans crochets ni parenthèses. Elles seront rejetées en bas de page et devront être limitées en nombre et en longueur.

Les **abréviations ou sigles** doivent être explicités lorsqu'ils apparaissent pour la première fois. Les termes scientifiques et techniques, ainsi que les unités de mesures et les symboles statistiques, doivent être conformes aux normes internationales.

Les **références bibliographiques** sont signalées entre [crochets] et numérotées par ordre d'apparition.
• Dans le corps du texte, seul le premier auteur est mentionné suivi de « et al. » lorsqu'il y a plusieurs auteurs (par exemple : « Fisher a montré que... [1] ; Cette hypothèse due à Jablonski et al... [2] ; Deux articles de paléoanthropologie... [3] et [4] »). Dans la mesure du possible, les numéros des références seront placés en fin de phrase.

• Dans la liste des références, celles-ci seront agencées par ordre d'apparition dans le texte. S'il y a quatre auteurs ou plus, seuls les trois premiers seront mentionnés, suivis d'une virgule et de la mention « et al ». Seules les références appelées dans le texte doivent figurer dans la liste de références en fin d'article. Les titres des périodiques sont écrits en respectant les abréviations standard (List of Serial Title Word Abbreviations).

Le **modèle de présentation** est illustré par les exemples suivants :

- Pour un article dans un périodique : Hershkovitz I, Smith P, Sarig R, et al (2011) Middle pleistocene dental remains from Qesem Cave (Israel). Am J Phys Anthropol 144(4):575-92
- Pour un ouvrage : Scheuer JL, Black S (2000) Developmental Juvenile Osteology, Academic Press, San Diego, California, 587 p
- Pour un article dans un ouvrage collectif : Gomila J (1980) L'Afrique subsaharienne. In: Hiernaux J (ed) La diversité biologique humaine. Masson, Paris, pp 107-196

Les **légendes des tableaux et figures** seront portées en fin de manuscrit, sur une feuille séparée du texte avec leur traduction en anglais ou en français. Chaque légende doit être suffisamment explicite par elle-même, sans qu'il soit nécessaire de se référer au texte. Les auteurs veilleront toutefois à limiter leur longueur. La numérotation des tableaux (en chiffres arabes) et des figures (en chiffres arabes) se fait selon leur ordre d'apparition dans le texte.

Les **tableaux** seront fournis au format word, présentés sur des pages séparées et placés à la fin du document texte.

Les **illustrations** seront fournies aux formats JPEG, AI ou EPS, avec une résolution minimale de 600 dpi et doivent être composées avec une largeur correspondant à une colonne (8,5 cm), une colonne et demi (12 cm) ou deux colonnes (17,5 cm) de l'article imprimé ; les textes des illustrations sont écrits en police Times New Roman, 10 pt (taille d'impression) et 11 pt pour les titres.

Les images seront reproduites par défaut en couleur dans la version électronique et en noir et blanc dans la version imprimée. Les images couleur devront être fournies dans une qualité permettant le transfert en niveaux de gris.

Rappel des points à vérifier avant de soumettre votre article :

- Titres, résumés et mots clés en français et en anglais
- Affiliation et coordonnées complètes de chacun des auteurs, auteur correspondant et co-auteurs
- Références citées dans le texte, numérotées par ordre d'apparition dans le texte et mises en forme selon les règles
- Appels dans le texte entre crochets du numéro des références citées
- Titres des tableaux et appellations des tableaux dans le texte
- Légendes des figures et appellations des figures dans le texte
- Attention spéciale à la qualité de la langue utilisée, français et/ou anglais

Bulletins et Mémoires de la Société d'Anthropologie de Paris (BMSAP)

Guidelines to authors

The Société d'Anthropologie de Paris publishes in its Bulletins et Mémoires original articles, reviews of works or notes in the field of biological anthropology, from the palaeoanthropology to the human ecology and population genetics, and the history of the discipline. All submitted manuscripts are evaluated during a reviewing process. Publication of articles is subject to the following conditions:

- approval by members of the Review Committee to which it is submitted;
- adherence to the standards of presentation set out below.

1 - Electronic submission of Manuscript

The manuscript including text, tables, illustrations (300 DPI) and their captions must be submitted as a single DOC file by e-mail to redacchef@sapweb.fr

The accepted version of the manuscript will be sent as separate files: a single Word text file (DOC) including the text, tables and captions on the one hand, and the illustrations as separate JPEG, EPS or TIFF files on the other hand.

The author guarantees that his/her contribution is original. It is assumed that all manuscripts sent to the *Bulletins et Mémoires de la Société d'Anthropologie de Paris* is an original paper which has not been published before and which is not evaluated in another Journal.

2 - Preparation of manuscript

The manuscript must be written in either English or French. It must include successively: the **title** in both English **and** French, the **name, surnames** and **address of the authors**, the **email** address of the corresponding author, keywords (maximum of 6) in both English **and** French, an **abstract** in both English **and** French (1,500 characters including spaces), a facultative **abridged version** (4,000 characters including spaces) in either English **or** French (depending on the language of the manuscript), the text of the manuscript, the list of bibliographic references, the list of tables, the list of figures, the tables and the figures. Each page and line of the manuscript must be sequentially numbered from the title page.

The **text** of the manuscript (text, titles and headings, footnotes, abbreviations, bibliographical references, captions for tables and figures) should not exceed 50,000 characters (including spaces) for an article and 20,000 characters (including spaces) for a note. It will be preferentially written using the font Times New Roman 12 pt, double spaced, A4 page size with margin of 25 mm.

Titles and headings. The main title of the article will not exceed 200 characters (including spaces). In addition, the text of each article will contain a maximum of 2 clearly distinct title levels. They will not be numbered.

Footnotes are noted in the text by Arabic numerals and in superscript, without brackets or parenthesis. They are to be placed at the bottom of the page and should be limited in number and in length.

Abbreviations or initials must be explained when they appear for the first time. Scientific and technical terms, as well as units of measurement and statistical symbols, must conform to international norms.

Bibliographical references are indicated using [brackets] and numbered in their order of appearance in the text.

- In the text, only the first author is listed. It is followed by a comma and the words "et al." When there are many authors (example: "Fisher showed that... [1]; This hypothesis formulated by Jablonski et al... [2]; Two articles in paleoanthropology... [3] and [4]"). Wherever possible, the numbers of references are to be placed at the end of the sentence.
- The reference list is organised in alphabetical order of the authors cited and in chronological order of the publications for each author. All authors are listed if there are three or less. If there are more than three, only three are listed first, followed by a comma and the words "et al". The titles of journals should be abbreviated according to standard abbreviations (List of Serial Title Word Abbreviations).

The **presentation model** is illustrated by the following examples:

- For an article in a journal: Hershkovitz I, Smith P, Sarig R, et al (2011) Middle pleistocene dental remains from Qesem Cave (Israel). Am J Phys Anthropol 144(4):575-592
- For a book: Scheuer JL, Black S (2000) Developmental Juvenile Osteology, Academic Press, San Diego, California, 587 p
- For an article in a collective work: Gomila J (1980) L'Afrique subsaharienne. In: Hiernaux J (ed) La diversité biologique humaine. Masson, Paris, pp 107-196

The **captions for tables and figures** will be presented on a separate page at the end of the manuscript, with a French or English translation. Each caption must be explicit enough in itself, so that reference to the text is not necessary. The numbering

of the tables (in Arabic numerals) and figures (in Arabic numerals) must follow the order in which they appear.

The **tables** must be presented in Word format, on separated pages, and provided at the end of the text document.

The **illustrations** must be provided in JPEG, AI or EPS format, with a minimum resolution of 600 DPI. Illustrations must be composed with a width of one column (8,5cm), one column and half (12cm) or two columns (17,5cm) of the printed paper. The text of illustrations must be written in police Times New Roman, 10 pt (printed size) and 11pt for titles.

Color art is free of charge for online publication. If black and white will be shown in the print version, make sure that the main information will still be visible. Many colors are not distinguishable from one another when converted to black and white. A simple way to check this is to make a xerographic copy to see if the necessary distinctions between the different colors are still apparent. If the figures will be printed in black and white, do not refer to color in the captions. Color illustrations should be submitted as RGB (8 bits per channel).

Items to verify before manuscript submission:

- Title, keywords and abstract in both French and English
- Full contact details of each author, corresponding author and co-authors
- References numbered alphabetically and formatted following the guidelines
- Quotations in the text of the reference number in square brackets
- Title of tables and call for tables in the text
- Caption of figures and call for figures in the text
- Special attention to the quality of the language used, French and/or English.